



UNIVERSITAT ROVIRA I VIRGILI

COMPUTATIONAL MODELING TO EXPLORE UNCONVENTIONAL REACTIVITY PATTERNS IN C-H ACTIVATION AND BORON CHEMISTRY

Diego García López

ADVERTIMENT. L'accés als continguts d'aquesta tesi doctoral i la seva utilització ha de respectar els drets de la persona autora. Pot ser utilitzada per a consulta o estudi personal, així com en activitats o materials d'investigació i docència en els termes establerts a l'art. 32 del Text Refós de la Llei de Propietat Intel·lectual (RDL 1/1996). Per altres utilitzacions es requereix l'autorització prèvia i expressa de la persona autora. En qualsevol cas, en la utilització dels seus continguts caldrà indicar de forma clara el nom i cognoms de la persona autora i el títol de la tesi doctoral. No s'autoritza la seva reproducció o altres formes d'explotació efectuades amb finalitats de lucre ni la seva comunicació pública des d'un lloc aliè al servei TDX. Tampoc s'autoritza la presentació del seu contingut en una finestra o marc aliè a TDX (framing). Aquesta reserva de drets afecta tant als continguts de la tesi com als seus resums i índexs.

ADVERTENCIA. El acceso a los contenidos de esta tesis doctoral y su utilización debe respetar los derechos de la persona autora. Puede ser utilizada para consulta o estudio personal, así como en actividades o materiales de investigación y docencia en los términos establecidos en el art. 32 del Texto Refundido de la Ley de Propiedad Intelectual (RDL 1/1996). Para otros usos se requiere la autorización previa y expresa de la persona autora. En cualquier caso, en la utilización de sus contenidos se deberá indicar de forma clara el nombre y apellidos de la persona autora y el título de la tesis doctoral. No se autoriza su reproducción u otras formas de explotación efectuadas con fines lucrativos ni su comunicación pública desde un sitio ajeno al servicio TDR. Tampoco se autoriza la presentación de su contenido en una ventana o marco ajeno a TDR (framing). Esta reserva de derechos afecta tanto al contenido de la tesis como a sus resúmenes e índices.

WARNING. Access to the contents of this doctoral thesis and its use must respect the rights of the author. It can be used for reference or private study, as well as research and learning activities or materials in the terms established by the 32nd article of the Spanish Consolidated Copyright Act (RDL 1/1996). Express and previous authorization of the author is required for any other uses. In any case, when using its content, full name of the author and title of the thesis must be clearly indicated. Reproduction or other forms of for profit use or public communication from outside TDX service is not allowed. Presentation of its content in a window or frame external to TDX (framing) is not authorized either. These rights affect both the content of the thesis and its abstracts and indexes.



UNIVERSITAT
ROVIRA I VIRGILI

Computational Modeling to Explore Unconventional Reactivity Patterns in C–H Activation and Boron Chemistry

Diego García López



DOCTORAL THESIS
2018

UNIVERSITAT ROVIRA I VIRGILI
COMPUTATIONAL MODELING TO EXPLORE UNCONVENTIONAL REACTIVITY PATTERNS IN C-H ACTIVATION
AND BORON CHEMISTRY
Diego García López

PhD Thesis

Computational Modeling to Explore Unconventional Reactivity Patterns in C–H Activation and Boron Chemistry

Diego García López

Supervised by

Dr. Jorge Juan Carbó Martín

Departament de Química Física i Inorgànica
Grup de Química Quàntica



UNIVERSITAT
ROVIRA i VIRGILI

Tarragona 2018

UNIVERSITAT ROVIRA I VIRGILI
COMPUTATIONAL MODELING TO EXPLORE UNCONVENTIONAL REACTIVITY PATTERNS IN C-H ACTIVATION
AND BORON CHEMISTRY
Diego García López



UNIVERSITAT ROVIRA I VIRGILI

Jorge Juan Carbó Martín, Professor Agregat del Departament de Química Física i Inorgànica de la Universitat Rovira i Virgili.

FAIG CONSTAR que aquest treball, titulat

“Computational Modeling to Explore Unconventional Reactivity Patterns in C–H Activation and Boron Chemistry”

que presenta Diego García López per a l’obtenció del títol de Doctor, ha estat realitzat sota la meva direcció al Departament de Química Física i Inorgànica d’aquesta universitat.

Tarragona, 27 d’Abril del 2018

El director de la tesi doctoral

Jorge Juan Carbó Martín

UNIVERSITAT ROVIRA I VIRGILI
COMPUTATIONAL MODELING TO EXPLORE UNCONVENTIONAL REACTIVITY PATTERNS IN C-H ACTIVATION
AND BORON CHEMISTRY
Diego García López

Overview of the Thesis

The rapid progress that computational power has undergone during recent years has emerged as a valuable tool for helping to solve the experimental chemistry aspirations, such as unraveling reactions mechanism, predict the activity of compounds or describe microscopic interactions throughout time. In this context, this thesis attempts to combine both computational and synthetic chemistry domains since is largely based on collaborations with experimental groups in order to unveil the ultimate forces governing particular processes, but also employs modeling techniques to predict the outcome of yet untested chemical phenomena.

After the introduction and goals of this thesis (Chapters 1, 2 and 3), the first part deals with the activation of inert C–H bonds (Chapters 4 and 5). This field of inquire has been one of the main topics in organometallic chemistry during last years since transition-metal-based systems are able to cleave the C–H linkage under mild conditions and in the absence of oxidant agents. Activation and posterior functionalization of the omnipresent C–H bond may allow the conversion of cheap and abundant organic compounds into valuable molecules while providing synthetic shortcuts to desirable products. Despite the great challenge displayed by this reactivity, many efforts are devoted in understand this chemical transformation and design new process to overcome its inherent difficulties.

In Chapter 4, we determined computationally the mechanism of remote C–H activation on titanium dinuclear complexes ($[\{\text{Ti}(\eta^5\text{-C}_5\text{Me}_5)\text{R}_2\}_2(\mu\text{-O})]$, $\text{R} = \text{CH}_2\text{SiMe}_3$, CH_2CMe_3 , and CH_2Ph) that has been observed by the group of Dr. Santamaría at the University of Alcalá. DFT calculations show that the mechanism involves a first α -hydrogen abstraction to generate a transient titanium alkylidene, which enables it to activate β - and γ -C(sp^3)–H bonds on the adjacent titanium center. The calculations also establish a reactivity order for the different type of γ -H abstractions, trimethylsilyl > neopentyl \cong benzyl, allowing us to explain the experimental selectivity.

In Chapter 5, we interpreted the rare Ni–(C_{Ph}–H) interaction in solid state structure of $[\text{NiBr}(\kappa^3\text{-P,N,C(H)-L}^{\text{H}})]\text{BF}_4$ observed by the group of Prof. van der Vlugt at the University of Amsterdam. This structure can be directly related to a fast and facile C–H cyclometalation at the Ni^{II} center. The theoretical study includes the quantum theory of atoms in molecules (QTAIM) and electron localization function (ELF) analysis which characterize the nature of the Ni–(C_{Ph}–H) bond as a bona fide albeit weak (an)agostic coordinative interaction, with predominant Ni–($\eta^1\text{-C}_{\text{Ph}}$) character.

The second part concerns boron chemistry and it was performed in collaboration with Dr. Elena Fernández at the Universitat Rovira i Virgili (Chapters 6, 7 and 8). This atom typically comprises three linkages forming trivalent compounds that have been traditionally regarded

as electrophilic agents. However, boryl synthons can change their electrophilic character towards a nucleophilic behavior depending on the nature of the substituents attached to the boron atom. Indeed, suitable ligands are capable of supplying enough electron density so that yield the boron nucleus unable to stabilize the excess of negative charge and seeks for other atoms to bond with. This recent discovery of the nucleophilic performance of these species represents a milestone in organic synthesis. Furthermore, non-conventional routes for the functionalization of unsaturated bonds in organic molecules under metal-free conditions by diboron compounds are beginning to appear. Concerning boron-interelement reagents, the reactivity might offer a wider scope via push-pull effect. Hence, the versatility and reaction conditions offered by boryl synthons make them attractive for the construction of carbon-carbon and carbon-heteroatom bonds.

In Chapter 7, we described the development of quantitative structure-activity relationships (QSAR) for the nucleophilic activity of trivalent boron compounds, covering boryl fragments bonded to alkali and alkaline-earth metals, to transition metals, and to sp^3 boron units in diboron reagents. Multivariate regression techniques were carried out for determining a quantitative relationship between ground-state properties and nucleophilic activity. The descriptors chosen were the charge of the boryl fragment ($q[B]$) and the boron p/s orbital population ratio (p/s) to describe the electronic structures of boryl moieties, whereas the distance-weighted volume (V_w) descriptor was used to evaluate the steric effects. The resulting three-term easy-to-interpret QSAR model showed statistical significance and predictive ability ($r^2 = 0.88$, $q^2 = 0.83$). The use of chemically meaningful descriptors has allowed identification of the factors governing the boron nucleophilicity and indicates that the most efficient nucleophiles are those with enhanced the polarization of the B-X bond towards the boron atom and reduced steric bulk. Also, we used the QSAR model to make a priori predictions of experimentally untested compounds. Finally, we built specific QSAR models for the nucleophilicity of transition metal-free boron reagents including symmetric and asymmetric diboron reagents activated by Lewis bases, as well as boron-interelement compounds.

In Chapter 7, the heterolytic cleavage of the mixed diboron reagent, pinB-Bdan, and the formation of two *geminal* C-Bpin and C-Bdan bonds was rationalised based on DFT calculations to occur via a concerted yet asynchronous mechanism. Diastereoselection is attained on substituted cyclohexanones and such computational studies provide understanding on the origin of the selectivity. We also studied the observed alkoxide-assisted, selective deborylation of Bpin from multisubstituted sp^3 -carbon *via* generation of a Bdan stabilized carbanion that easily conducts to a selective protodeboronation sequence.

In Chapter 8, theoretical calculations rationalized the observed regio- and stereoselectivity of the *anti*-3,4-selenoboration of α,β - acetylenic esters and ynamides using catalytic amounts of PCy_3 . Interestingly, in the absence of phosphine the selenoboration switched from the formation of α -vinyl selenides to β -vinyl selenides. The computational study discovered a novel mechanism which differs from previous mechanistic proposals for analogous *anti*-

selective carboration, silaboration and diboration. The phosphine adds to the β position of the alkynoate switching the polarity of the triple bond and favoring the 1,3-selenoboration which produces the α -addition of selenyl group. Then, the autocatalytic action of a second selenoborane reagent, which coordinates to the phosphorus ylide intermediate, determines the stereoselectivity and completes the catalytic process.

Finally, a summary of the conclusions is presented in Chapter 9.

Contents

1. INTRODUCTION	
1.1. A Chemical perspective	3
1.2. Activation of C–H bonds	4
1.2.1. The C–H reactivity	4
1.2.2. Classification of C–H bond activation	6
1.2.3. The agostic concept: C–H as a ligand	11
1.2.4. Remarks and perspectives	14
1.3. Trivalent boron reagents in organic synthesis	15
1.3.1. Tunable reactivity of boryl moieties	15
1.3.2. Metal-containing nucleophilic boron compounds	16
1.3.3. Metal-free nucleophilic boron compounds	21
1.3.4. Unconventional additions of boron compounds	27
1.3.5. Transition-metal-free B–interelement reactions	30
1.3.6. Remarks and perspectives	33
1.4. References	34
2. MODELING WITH COMPUTATIONAL CHEMISTRY	
2.1. Evolution of computational chemistry	45
2.2. Density Functional Theory	46
2.3. Modeling reactivity	52
2.4. Electronic structure analysis	59
2.4.1. Natural Bond Orbitals (NBO)	60
2.4.2. Quantum Theory of Atoms in Molecules (QTAIM)	63
2.4.3. Electron Localization Function (ELF)	67
2.5. References	69
3. OBJECTIVES	
3.1. Objectives	75

4. MECHANISTIC INSIGHTS INTO C-H ACTIVATION INVOLVING DIMETALLIC TITANIUM SPECIES	
4.1. Introduction	81
4.2. Experimental background	82
4.3. Results and Discussion	84
4.4. Computational Details	94
4.5. Conclusions	95
4.6. References	95
5. UNRAVELING THE AGOSTIC INTERACTIONS OF ARENE C(sp²)-H AT NICKEL PINCER COMPLEXES	
5.1. Introduction	99
5.2. Experimental background	100
5.3. Results and Discussion	103
5.4. Computational Details	107
5.5. Conclusions	108
5.6. References	108
6. TRACING A NUCLEOPHILIC MAP FOR THE USE OF TRIVALENT BORON COMPOUNDS	
6.1. Introduction	117
6.2. Results and discussion	118
6.2.1. QSAR model for the nucleophilicity of trivalent boron compounds	118
6.2.2. Specific structure-nucleophilicity relationships in transition-metal-free B-B and B-interelement	135
6.3. Computational details	144
6.4. Conclusions	145
6.5. References	146
7. GEMINAL-ADDITIONS OF UNSYMMETRICAL DIBORANES TO KETONES AND ALDEHYDES	
7.1. Introduction	155

7.2. Experimental background	157
7.3. Results and discussion	161
7.4. Computational details	167
7.5. Conclusions	168
7.6. References	168
8. UNRAVELING THE MECHANISM OF SELENOBORANE ANTI-ADDITION TO ALKYNES	
8.1. Introduction	171
8.2. Experimental background	173
8.3. Results and discussion	178
8.4. Computational details	186
8.5. Conclusions	186
8.6. References	187
9. CONCLUSIONS	
9.1. Conclusions	191

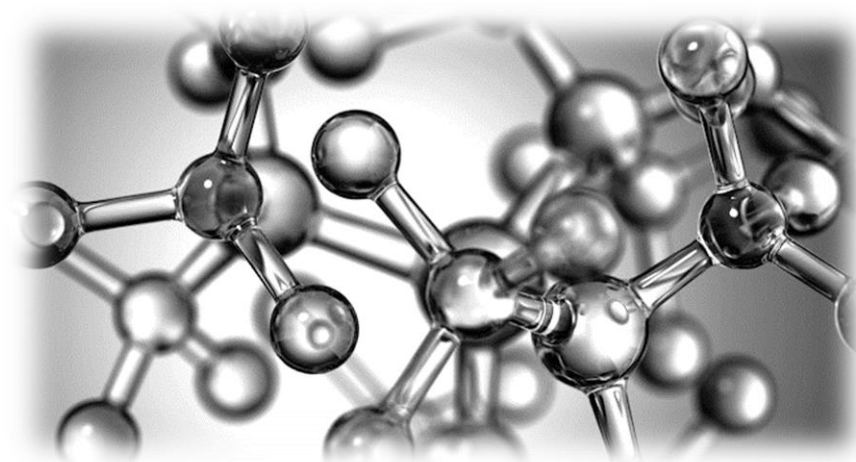
ACKNOWLEDGEMENTS

LIST OF PUBLICATIONS

COLLABORATIONS

UNIVERSITAT ROVIRA I VIRGILI
COMPUTATIONAL MODELING TO EXPLORE UNCONVENTIONAL REACTIVITY PATTERNS IN C-H ACTIVATION
AND BORON CHEMISTRY
Diego García López

Introduction



*Chemistry began by saying it would change the baser metals into gold.
By not doing that it has done much greater things.*

— Ralph Waldo Emerson —

*You don't need to be a genius to do chemistry;
you just need to be smarter than molecules.*

— John Anthony —

UNIVERSITAT ROVIRA I VIRGILI

COMPUTATIONAL MODELING TO EXPLORE UNCONVENTIONAL REACTIVITY PATTERNS IN C-H ACTIVATION
AND BORON CHEMISTRY

Diego García López

1. Introduction

1.1. A chemical perspective

Humankind has always been curious to understand nature of the phenomena involving in our daily life. Our questioning mind is responsible for this need for comprehension. Over the centuries we have been acquiring tons of knowledge, so we came to a point where scientists had to specialize. This is how different areas of study, such as chemistry, physics or biology, hatched out from a common ancient science. In turn, during the last decades the diverse disciplines of science have evolved –and are still evolving– into more detailed and specified topics. For instance, concerning in chemistry there exists the organic branch, which is focused in studying substances related to living organisms, namely those that have carbon atoms as a molecular skeleton. Hence, it is not surprising that organic chemistry has been one of the most active disciplines of science since it has allowed the study and development of new ways to synthesize molecules for our own interest and welfare.^[1,2]

Although in the past the areas of chemistry had clear boundaries dividing each specialized region, the frontiers are blurred nowadays as one can complement others and vice versa. A good example can be found in organometallic chemistry which, by definition, studies those molecules containing a metal-carbon bond. However, this discipline also heeds in entities lacking this required linkage but that can be considered organometallic species as well. In fact, this formalism is disregarded when a particular molecule has a reactivity behavior that derives from or could lead to an organometallic compound. In other words, the domain of organometallic chemistry belongs to those molecules that have an existent metal-carbon bond before or while reacting, which can also be transient or temporary.

In principle, organometallic chemistry was thought to be a subset of inorganic coordination chemistry. Nevertheless, this point of view have changed due to the crucial role that organometallic compounds play in organic chemistry by catalyzing the synthesis of a great amount of molecules.^[3,4] Moreover, this interplay between organic frameworks and metal entities is also fundamental for biological systems as they are present in proteins and cofactors.^[5] Some well-known examples illustrating this can be rendered in iron reversibly binding dioxygen in hemoglobin, cobalt found in vitamin B12 or molybdenum proteins catalyzing the reduction of nitrogen and nitrate.

The connection established by organic and organometallic chemistry endowed experimental chemists the capability to synthesize molecules of growing complexity.^[6] Consequently, we have reached such a sophistication level that nowadays they are more concerned in efficiency

rather than feasibility. This means that synthesis has incorporated an engineering philosophy in terms of optimizing the process. Certainly, if nature is able to produce large amounts of complex molecules in a difficult but highly efficient way, organic chemistry must be aware of that in order to understand and emulate its synthetic routes. Therefore, we should feel obligated to provide large quantities of complex natural products with a minimum amount of labor and material expense.^[7]

The rapid progress in computational power during recent years has emerged as a mighty tool for helping to solve the organic chemistry aspirations. Indeed, it has enabled such a good partnership between synthetic and quantum chemistry that molecular modelling turns out to be almost indispensable nowadays. It is now possible to go even deeper into the microscopic world and understand the basics of atomic interactions, molecular forces and reaction mechanisms. Taking advantage of this alliance, two avant-garde and pioneering topics of organic and organometallic chemistry fields are introduced here in order to elucidate and unveil the ultimate effects governing some processes concerning C–H bond activation and unconventional boron reactivity.

1.2. Activation of C–H bonds

1.2.1. The C–H reactivity

Alkyl compounds are not only the building blocks of living organisms, they are also present in diverse important materials, such as crude petroleum, pharmaceuticals and plastics. They consist of chains or rings of consecutive carbon atoms, each capped with one or more hydrogen atoms. However, this scaffolding can be interrupted with occasional “heteroatoms”, mainly oxygen, nitrogen, phosphorus, sulfur, and the halogens, that form the so-called functional groups, which can be attached to or contained within the skeleton of carbon atoms. Over the centuries, generations of organic chemists have been gaining expertise in preparing new molecular structures from other basic and abundant molecules in an increasing efficient manner, traditionally by the interconversion of those existing functional groups or by matching nucleophiles with electrophiles. However, during the recent years, the scientific community has been witnessing the emergence of a truly revolutionary trend in organic synthesis (especially caused by environmental and economic requirements): the activation and functionalization of inactive C–H bonds.^[8–11] This historically latent reactivity has nowadays become feasible, popular and trendy.

The importance of this chemical process can be better understood if it is beard in mind that alkane's main characteristic is inertness. This trait arises from its constituent atoms all being held together by strong and localized C–C and C–H bonds, so that there are no filled orbitals of high energy neither empty orbitals of low energy that could readily participate in a reaction. This characteristic is not present in unsaturated hydrocarbons, where delocalized π -electrons can be easily excited to more accessible virtual orbitals (Figure 1.1). Therefore, olefins and alkynes are prone to facile and widely diverse functionalizations that make them a high valuable starting material for synthetic and industrial purposes.^[12] Despite their inactivity towards lots of molecules, alkanes are known to be extremely good candidates for combustion reactions producing carbon dioxide and water. Although these reaction products are thermodynamically stable and economically unattractive molecules, such processes are principally exploited for their energy content and not for their considerable potential as valuable precursors for more important and expensive chemicals. Thus, the large abundant of hydrocarbon frameworks make them one of the best energy feedstocks.

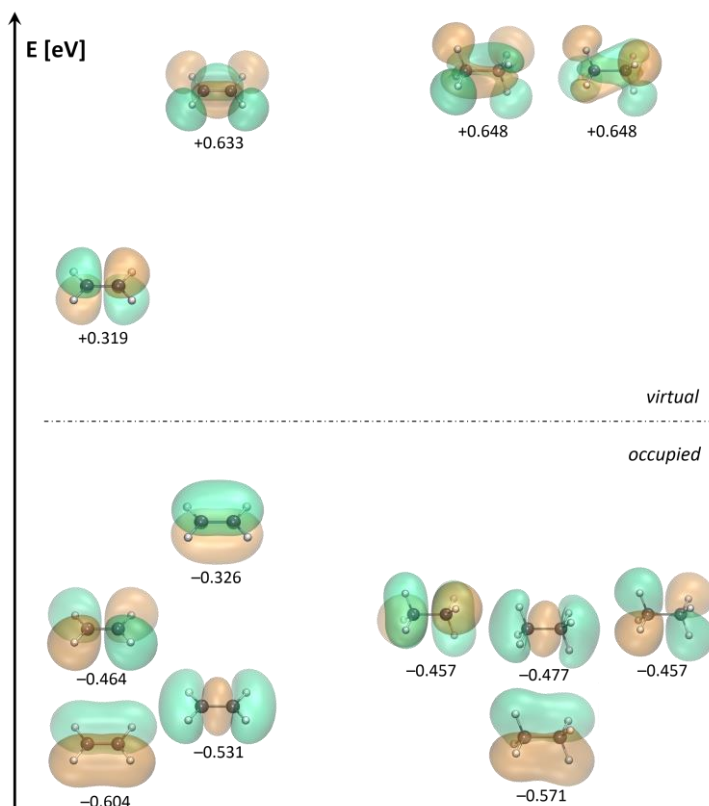


Figure 1.1. Frontier Molecular Orbital diagram of energy for ethene (left) and ethane (right); energies in eV.

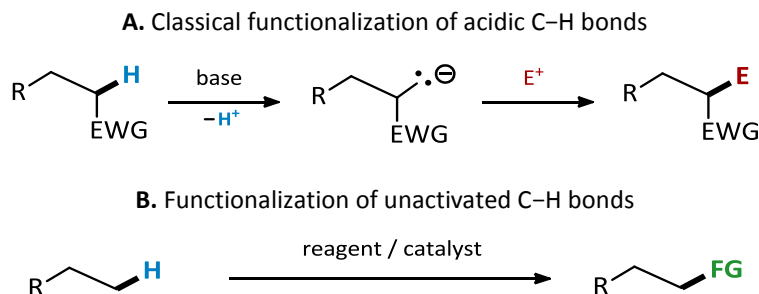
Putting aside the powerful energetic impact of burning alkanes, the discovery and characterization of reactions that enable direct functionalization of the omnipresent C–H bond have become an undeniably step forward. The direct transformation of these linkages creates a wormhole into the vast universe of organic synthesis, providing shortcuts to more atom-economical and more straightforward routes to desirable products. The relevance of such finding can be seen in the high number of processes aimed to directly create carbon-carbon or carbon-heteroatom bonds.^[13–23] Its degree of significance is so relevant that has been incorporated into the synthesis of complex natural products and biological active molecules.^[24–26] Nevertheless, nature has been using its own way to employ inert C–H bonds as latent functional groups for hundreds of years in chemoselective enzymatic reactions prior to their discovery. The paradigm system is the cytochrome P450s,^[27,28] but other proteins have also been studied and even *in silico* enzymes were also constructed.^[29]

The achievement of selective transformations of alkanes under mild conditions becomes feasible with the presence of a transition metal. The binding of small and relatively inactive molecules to a metal center alters the relative energy of their orbitals or even their polarity. This enhanced reactivity induced the appearance of the first examples of C–H activations in the 1970's, but only assisted through participation of π orbitals of aromatic hydrocarbons^[30] or involving intramolecular reactions.^[31] Although these transformations were not promising by the time they were discovered, soon after that more and more examples began to appear to expand the scope of this process, which rapidly started to grow importance.^[32]

1.2.2. Classification of C–H bond activation

- **Acidic vs. non-acidic hydrogens**

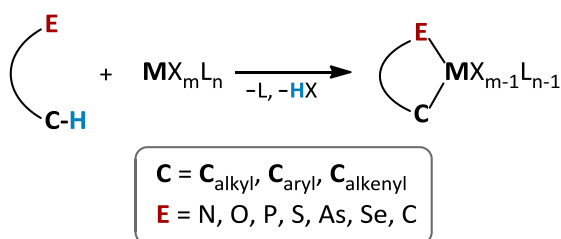
Before going into deep, it is worthwhile to define what modern C–H activation is about in order to avoid misleading concepts. In classical organic chemistry some functional groups, namely electro-withdrawing groups (EWD), make nearby C–H bonds acidic and therefore prone sites for the classical deprotonation. The resulting nucleophilic species are then quenched with electrophilic reagents to form carbon-carbon and carbon-heteroatom bonds (Scheme 1.1A). Likewise, in another type of acidic C–H bonds reactivity, electrophilic aromatic substitutions install functional groups or form a carbon-carbon bond at the position of a C–H bond as well. Undoubtedly, these chemical conversions belong to a C–H bond activation process, although modern “C–H bond functionalization” generally refers to reactions that introduce functional groups at C–H bonds that lack the activating influence of nearby pre-existing functional groups (Scheme 1.1B). Up to now, a major effort is focused on the addition of new groups at typically unreactive C–H bonds in molecules containing existing functionality, thus trying to minimize the number of steps that a chemical conversion may need.



Scheme 1.1. Functionalization of the C–H bond.

▪ **Activation by directive groups vs. undirected activation**

Not only is C–H bond functionalization challenging because of the difficulty of modify these bonds over other more reactive type of linkages in organic molecules, but also the regioselectivity aspect represents an additional hurdle since such molecules contain several and diverse C–H bonds. To deal with both reactivity and selectivity issues it is of common practice to use substrates with functional groups in order to bind them first with a transition metal. Sometimes it is necessary to modify this already existing functionality to another one than can serve as a ligand for a transition-metal complex. This process is called *directed functionalization* due to the fact that C–H activation occurs when such bond is driven towards the metal promoted by the initial binding of the existing functional group. This procedure involves the C–H bond cleavage to form a cyclic product with a metal-carbon bond in a reaction termed *cyclometallation* (Scheme 1.2).^[33]



Scheme 1.2. Directed C–H functionalization involves cyclometallation.

Since its discovery in the early 1960s,^[34,35] cyclometallation has become one of the most popular organometallic reactions, since it enables the formation of a metal-carbon σ -bond. One of the reasons for the considerable attention this reaction received could be because it is probably the mildest route for activating strong C–H bonds. The cyclometallated species formed, or *metallacycles*, have been successfully applied in the traditional domains of organometallic chemistry, comprising organic transformations and catalysis (especially the

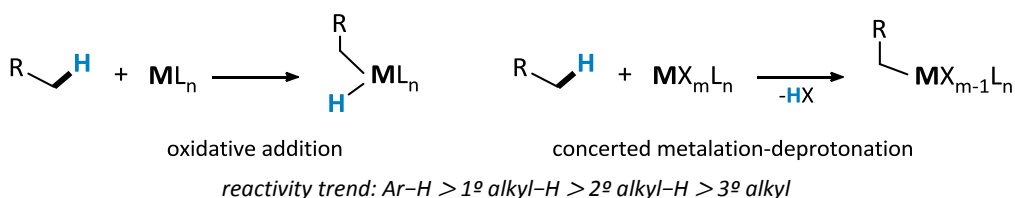
catalytic activation of C–H bonds in unreactive alkanes), as well as the stabilization of reactive intermediates.^[33] This process typically consists on the two consecutive steps previously outlined: initial coordination of the metal center via an electron donor group present in the substrate and subsequent intramolecular activation of the C–H bond driven by the union of that donor group, which closes the metallacycle. The effective bond activation is thus most often a heteroatom-assisted process, involving classical donors such as N, O, P, S, Se, and As, although cases of carbon-assisted C–H bond activation are known as well. This precoordination of the substrate as a ligand modifies the electron density at the metal center, and furthermore, provides steric constraints favoring the bond-activation step. In fact, it is assumed that the arrangement of the chain of atoms from elements E to C (Scheme 1.2) in the neighborhoods of the metal center coordination sphere is essential for reducing the entropic and enthalpic costs of the subsequent C–H bond-activation step and in the ring closing process. Actually, these two parameters reveal the ease of intramolecular bond activation as compared to intermolecular processes. In addition, it must be pointed out that deprotonation of the activated C–H junction might result from an anionic ligand binded to the metal (Scheme 1.2) or from a base present in the solvent. The increased acidity of the hydrogen prior its scission from the carbon suggests that some weak interaction might be present (*vide infra*).

Despite the fact that the first reported cyclometalated complex involved the reaction of nickelocene with azobenzene,^[34] C–H metalation has been more commonly observed in second- and third-row metal-based systems. Among the different ligand structures promoting C–H metalation, pyridine has proven very efficient as a directing group. Within this context, the group of Prof. van der Vlugt has been recently studying the unusual reactivity of C–H bonds with Ni-complexes. To that end, they have introduced reversible cyclometalation as manoeuvre for cooperative catalysis, using a strongly chelating (P,N)-ligand that features a flanking phenyl arm.^[36] This emerging methodology, also referred as synergistic catalysis, consist on a synthetic strategy wherein two different substrates (a potential nucleophile and electrophile) are both simultaneously activated by a multifunctional catalyst or two separate catalysts to afford a single chemical transformation.^[37,38] Hence, reversible cyclometallation involving C–H bonds is an appealing approach to store hydrogen or proton present in the medium. In addition, these processes motivate further interest regarding the kind of stabilizing interactions that can be present in metallacycles.^[36,39,40] Chapter 5 of this thesis presents a detailed analysis of these interplays that are rather uncommon for nickel complexes.

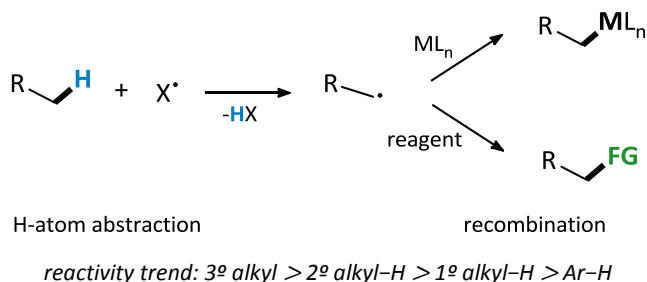
Alternatively, *undirected functionalization* implies an even greater challenge on C–H bond activation.^[41] The dare is either to install a functional group at a position that cannot be reached by chelation to a transition metal center, or that lacks functional groups altogether. The absence of a directing group in the substrate disables the possibility of a previous interaction with a reagent or a catalyst, and therefore makes the regioselectivity less

controllable. Consequently, if a reactive agent is employed, it would have to break and functionalize the C–H bond without any assistance. In the absence of a cyclometalation, the C–H bond cleavage step is mostly intermolecular and often slower than with the presence of such chelation. Thus, several limitations must be surpassed before undirected functionalizations become affordable synthetic methods to be used widely. Despite these obstacles, undirected synthetic strategies have extensively been reported.^[41] Nonetheless, mechanistic general rules leading to the disclosed selective functionalization of C–H bonds in alkyl chains are difficult to rationalize due to the wide variety of different reactions associated with this so-outstanding chemical conversion; even so, some possible guidelines have been suggested (Scheme 1.3).^[41]

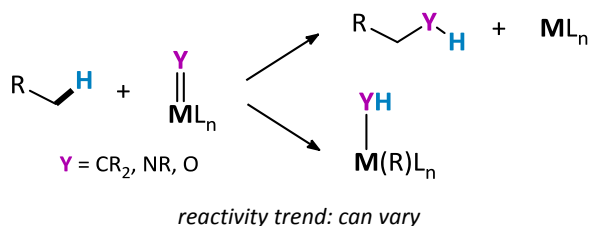
A. Concerted formation of M–C bond:



B. Stepwise formation of M–C bond or functionalization through a radical intermediate:



C. Insertion of carbene or alkylidene, nitrene or imido, and oxene functional groups into C–H bond:



Scheme 1.3. Possible mechanisms for a selective C–H bonds functionalization.

Reactions that construct a metal-carbon bond by C-H bond cleavage tend to occur by concerted pathways (Scheme 1.3A), rather than do it through in a stepwise radical manner (Scheme 1.3B). The selectivity of the former reactions is often dictated by the strength of the metal-carbon linkage in the potential organometallic intermediates, relative to the strength of the C-H bonds.^[42] For this reason, concerted C-H bond functionalization occur by formation of a metal-carbon bond at aryl over alkyl C-H bonds. Furthermore, steric hindrance is also important since reactions forming metal-carbon bonds tend to occur at primary over secondary C-H bonds, and at secondary over tertiary C-H bonds. This reactivity has been extensively reviewed due to its paramount importance in the organometallic domain, giving rise to a large amount of catalytic processes.^[43]

Functionalization of C-H junctions occurring without formation of a metal-carbon bond can take place by stepwise pathways (Scheme 1.3B, down). In this case, reactions can result from the formation of alkyl radicals and recombination of such radical with a metal complex or a reagent that delivers a functional group (Scheme 1.3B). The C-H bond reactivity evading a metal-carbon junction formation tends to be favored at the position where such C-H bond is weaker, which usually coincides with an electron rich zone.^[44] However, steric factors also play a role by influencing the position of hydrogen atom abstraction, and hindered reagents have been developed in order to privilege an abstraction of a secondary C-H bond over a tertiary C-H bond.^[45] In addition, the presence of a heteroatom can modify the site of reaction. The most influencer atoms are nitrogen and oxygen, which promote the alpha C-H bond activation.

Analogously to the previous stepwise mechanism, in metal-carbenoid-induced C-H activation the metal does not need to interact directly with the alkane C-H bond in order to form a C-C linkage (Scheme 1.3C, up).^[46] Metal-nitrenoid complexes have also been shown to be capable reagents for C-H functionalization, a reaction that is usually called C-H amination.^[47-49] Insertions carried out by oxenes are more difficult to encounter,^[50,51] but hopefully future synthetic routes will be developed by mimicking nature's way to introduce atomic oxygen into C-H junctions.^[52] Interestingly, reported examples of arene and alkane C-H σ -bond activation, *via* addition across metal-nitrogen multiple bonds by early transition metal complexes, have been known since long time ago.^[53,54] The reactivity of titanium-imido compounds performing C-H cleavages has been theoretically investigated by the groups of Prof. Cundari and Prof. Sakaki.^[55,56] Regarding metal-carbon multiple bonds, the first documented C-H bond activation was performed intramolecularly in a titanium complex.^[57] The use of such type of compounds has been explored by Prof. Mindiola as a tool for activating C-H bonds,^[58-61] but other metal centers have been disclosed as well.^[62-66]

In principle, transition metals capable to achieve high oxidation states (early- and middle-transition metals) are prone to form stable multiple metal-carbon bonds.^[67] Those unions combined with a d^0 metal in high oxidation state, lacking available electrons from its ligands,

cannot activate C–H junctions by following oxidative additions. Instead, activation is undergone *via* σ -bond metathesis in a concerted four-center mechanism, without any change in the oxidation state of the metal, and resembling [2+2] cycloadditions.^[68] Hence, the key role for determining the triggering mechanism of C–H bonds is related to the holding of d -electrons in the metal involved.^[69] Within this mechanistic context, Chapter 4 of this thesis examines computationally the intramolecular C–H activation in dimetallic titanium-alkyl complexes *via* formation of a transient titanium-alkylidene species, which acts as a Lewis base activating different type of remote C–H bonds.

1.2.3. The agostic concept: C–H as a ligand

Soon after the discovery of transition metal-alkyl compounds, it became clear that the presence of metals imparted properties to the alkyl group that were unprecedented. Traditional coordination chemistry considered that a ligand could only interact with a transition metal center either in an ionic fashion or via a relatively strong donor-acceptor bond. Leaving aside anionic ligands (which often make strong bonds), it was believed that neutral ligands would bind the metal center establishing a HOMO-LUMO interaction. Although there is no correlation between the M–L bond dissociation energy and the HOMO energy of the ligand, it was always rationalized that ligands with very low lying occupied orbitals would be unlikely to interact with a metal center. Taking into account this premise, a poor Lewis base would thus be incapable of acting as a ligand to a Lewis acidic metal center. However, experimental evidences of compounds with weak interaction between the metal and the hydrogen began to appear, and advances in characterization techniques (such as crystal structure determination and nuclear magnetic resonance spectra) supported the idea that in suitable circumstances the C–H bond could act as a ligand to a transition metal center by forming a 3-center-2-electron covalent bond.^[70] This novel interplay was named “*agostic*”, from the Greek “*αγοστός*”, and may be translated as to clasp, to draw towards, or to hold close to oneself. Back in 1983, the first definition stated:^[70]

“We propose the term ‘agostic’ which will be used to discuss the various manifestations of covalent interactions between carbon-hydrogen groups and transition metal centers in organometallic compounds. The word agostic will be used to refer specifically to situations in which a hydrogen atom is covalently bonded simultaneously to both a carbon atom and a transition metal atom.”

The coinage of a specific term that describes this phenomenon highlights the importance of such finding. Although the situation was originally delimited to C–H bonds, this has been extended to other binding scenarios embracing B–H, Si–H, or even C–C, yet they will not be taken in consideration henceforth.^[71,72] The magnitude of agostic interactions discovery is

reflected in the large number of organometallic complexes wherein it has been detected. For example, they are suggested to play a crucial role in controlling olefin polymerization processes since they are frequently found in key intermediates and transition states for chain growth and termination.^[73–76] Agostic interactions are also present in two related pathways of central relevance in organometallic reactivity: concerted oxidative addition^[77] and heterolytic cleavage by reductive elimination.^[78] Furthermore, it was proposed that agostic interactions might play a decisive role in cyclometallations using d-block transition metals, by either favoring or preventing some of such processes.^[79] Thus, a thorough understanding of this phenomenon may help in designing new reagents for a more specific C–H functionalization.

Agostic interactions concerning C–H junctions are usually described nowadays in terms of the Dewar-Chat-Duncanson (DCD) model as a charge transfer process.^[80,81] The pivotal idea laying behind is an orbital picture in which there is σ charge donation from the C–H linkage to empty orbitals of suitable symmetry on the metal while π back-donation occurs from filled d-based molecular orbitals on the metal to the virtual C–H antibonding orbital, weakening the bond. This simple model has been corroborated over the years by means of a wide range of computational tools and provides a framework to discuss experimental observables related to the nature of agostic interactions.^[71,72] Nevertheless, although the usefulness of the DCD model has been proven in a large variety of cases,^[82–84] its general applicability in the context of agostic interactions has been questioned.^[85] In addition, it has been suggested very recently that its simplicity might have limited consideration of other factors contributing to the structural stability of agostic complexes.^[86] More specifically, the role of London forces (dispersion interactions between transient dipoles of nonpolar but polarizable bodies)^[87,88] has been proposed to carry great importance in those bonding situations,^[86] yet this hypothesis has not been explored despite the fact that dispersion affects various structural features of molecular species.^[89–92] However, for the concerns of this work, we will consider that agostic interactions obey the DCD model since we are focused on their identification instead of disentangle their origins.

Analysis of the different types of agostic interactions requests a need for a classification. They are generally grouped according to the connectivity between the last interacting atom (mainly hydrogen) and the metal along covalent bonds (Figure 1.2). This method implies that there is no closer look at the nature of the metal-carbon-hydrogen interaction but at the structure of the ligand which chelates the metal. Nonetheless, the simplicity of this approach makes it the most common categorization used in the literature.

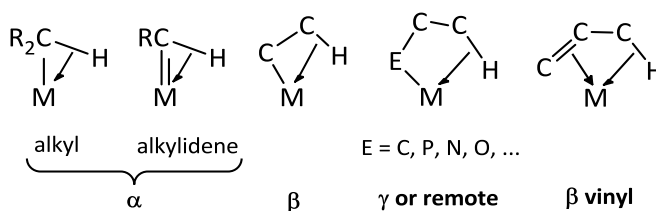


Figure 1.2. The agostic bond situations.

This classification does not reflect that the specific electronic interactions present in each of the previous subgroups might rely on the compound considered. In other words, there is no general rule for the orbital interaction attending the previous categorization of agostic interactions since it is based on geometric criteria. Therefore, compounds belonging to a given subset must be examined independently. Regarding α -agostic interactions, the rationalization for the stabilization lies in the engagement between the empty metal atom orbitals and the HOMO of the ligand, which determines if the tilted geometry is energetically favorable or not.^[93] It is noteworthy to point out that agostic geometries can take place in more sterically hindered complexes and be absent in less sterically crowded compounds, which highlights the electronic origin of such interaction.^[93–95] Geometrical distortions in β -agostic cases are less noticeable, although many of the interplays observed in α -agostic examples may also be valid for β -agostic counterparts.^[96,97] Remote γ -, δ -, and ϵ -agostic interactions are rare but not unknown.^[98–104] However, potential evidences (based on new available crystallographic data) that could imply the formation of these latter features are sometimes not correlated with an electron density exploration from a computational point of view.^[105,106]

Identification of an agostic situation is not always straightforward, since there are some nuances and there are also several interpretations. In fact, there is a fair amount of available techniques and methods that are capable to reveal some clues about this phenomenon. Nonetheless, this might not be sufficient and boundary cases could remain unclear.

Before the rapid progress that computational chemistry has deployed within the last decades, in the past the determination of agostic interactions was solely experimental by employing molecular spectroscopy techniques (although crystallographic data has been a traditionally powerful characterization technique, since it directly provides information about the three dimensional structure of a compound). For instance, one of the tell-tale signs of an agostic interaction is a significantly lower value of the NMR spin-spin coupling constant of the C–H bond. Interestingly, whereas the $^1J_{\text{C-H}}$ can decrease around 50% of its value the bond length is only marginally elongated.^[107]

Another experimental technique frequently used is the IR spectroscopy. Since agostic bonds are usually slightly elongated compared to normal C–H bonds the associated stretching frequency is lower than that of a bond with no additional interactions present. In addition, it

has been demonstrated a correlation of the IR analysis with NMR spectroscopy technique,^[108] thus there is a relationship between the stretching frequency of the agostic C–H bond and the $^1J_{C-H}$ coupling constant. This can be of particular interest, especially when one of these experimental measurements is difficult to carry out.

From a theoretical point of view, it is also possible to identify an agostic interaction on the basis of electron density with topological analysis.^[71,72,82,85,109,110] Two methodologies that have been traditionally used are the *Quantum Theory of Atoms in Molecules* (QTAIM)^[111] and the *Electron Localization Function* (ELF).^[112] The former approach provides an atomic subdivision of the molecular space where each atom localizes a certain number of electrons whereas the latter one enables the localization of regions in the molecular space where electrons concentrate, leading to chemically significant regions like bonds or lone pairs (*vide infra*). While the first one is a widespread used theory, the second is not so popular. However, both of them are analogous and well-complemented tools with supported evidences to be highly effective. This mutual support is essential, because it appears that even after many years of increasing experimental examples of agostic situations in molecular systems, the jury is still out on what is the best way to probe such interactions.

1.2.4. Remarks and perspectives

Activation and functionalization of C–H bonds was once exotic, but nowadays it has entered into mainstream research topics in chemistry. Nevertheless, this extremely challenging reactivity keeps this field of inquire ahead of the curve. One of the difficulties to deal with have always concerned the control for a site selectivity. Indeed, since if a C–H bond is likely to react, other C–H junctions might be prone to react as well, which would lead to a mixture of products. In relation with this, in most of the cases it would be attractive to achieve monofunctionalization, and this might also represent a hurdle. Another difficulty arises from the fact that the reactivity of a compound outcoming a C–H bond functionalization is greater than the starting material, which would lead again to a mixture of products. And not only that, in general, reagents destined to functionalize the C–H linkage tend not to be compatible with the alkane binding to the metal center, because such union is usually labile and may be displaced by the entering functionalizing agent. Finally, the last obstacle to overcome derives from the previously mentioned effect of existing functional groups in close proximity of C–H linkages and weakening the bond, therefore making them more reactive than the desired alkyl C–H junction. However, all these hindrances are easily surpassed if one looks into nature's strategy to cleave C–H bonds. Although, trying to mimic the selectivity displayed by enzymes reactivity would need the introduction of molecular recognition at a very sophisticated level. Thus, in spite of the important progress achieved to date,^[113–115] much work therefore still remains.

1.3. Trivalent boron reagents in organic synthesis

1.3.1. Tunable reactivity of boryl moieties

In 1904, Richard Abegg formulated what is now known as “Abegg’s rule”, which states that the difference between the maximum positive and negative valences of an element is frequently eight.^[116] This rule was used later in 1916 in perhaps one of the most successful and simple models to explain the chemical bond: the electron pairing model developed by Gilbert Lewis, which gave rise to the famous octet rule displayed in a cubical atom theory.^[117] Essentially, it proclaimed that a stable arrangement is attended when an atom is surrounded by eight electrons. In addition, this octet can be comprised by own electrons and some electrons of others atoms, which are shared. When atoms have fewer than eight electrons, they tend to react and form more stable compounds. Thus, an atom continues to form bonds until an octet of electrons is achieved. However, it must be pointed out that this rule is only valid when s and p electrons are involved, making it useful for the main group elements (transition metal or inner-transition metal blocks do not obey this rule). At the same time, atoms tend to maintain a neutral charge as far as possible. Only the noble gases have zero charge with filled valence octets, so all of the other elements have an intrinsic charge when they have eight electrons surrounding them. The consequence of these two guiding principles is that atoms seek to share electrons in a way that minimizes their charge while fulfilling an octet in the valence shell. Nevertheless, it is always difficult to rationalize patterns in chemistry without having some exceptions, and boron is one of them in the octet rule. This fact might be the source for the wide variety of reactivity patterns in boron molecules.

Following the principles of the Lewis bonding model, boron would form three linkages to other atoms with the three outer and unpaired electrons of its valence shell. In principle, this situation is not adequate to satisfy the octet rule, so boron is forced in some occasions to form aggregates comprising electro deficient binding.^[118,119] As a consequence, the majority of trivalent boron compounds are electrophiles due to the lack of two electrons to populate their outer orbital by themselves. The first confirmation to the previous statement came with the addition of a borane reagent to an alkene, which was performed in 1954 by diboron tetrachloride to ethylene,^[120] but soon after that other unsaturated hydrocarbons such as propene, cyclopropane, acetylene, allyl halides and many others were also explored.^[121] This reactivity proceeds via electron donation of the unsaturated substrate to the vacant p-type orbitals of the adjacent diboron, thus breaking the B–B bond and promoting a *cis* addition. Despite the effectivity of this reaction, diboron dihalides present an inherent instability that became a strong drawback towards the development of this reactivity.^[122,123]

Alternatively, the parent $B_2(NR_2)_4$ and $B_2(OR)_4$ compounds were easier to handle since they are more stable compared to diboron dihalides. The explanation for that needed an upgrade in the theory of bonding and to evolve into the *molecular orbital theory*.^[124] The justification lies in the negative charge density transfer from the substituents' highest occupied orbitals into boron's empty p-orbital. However, as a consequence, the more stable the boryl fragments the less reactive they become. The activity decrease displayed by these compounds laid the foundations for catalytic borylation of hydrocarbons through transition metal complexes.^[125,126] Regarding hydroboration, catalytic processes were found to alter the chemoselectivity of reactions of multifunctional substrates while provide alternatives for manipulating regio-, stereo-, and chemoselectivity.^[127] Concerning diboron reagents, the initial addition of bis(pinacolato)diboron to alkynes was developed in 1993 by Miyaura, Suzuki and co-workers,^[128] while the first diboration of alkenes was exemplified with bis(catecholato)diboron by Marder, Baker, Westcott and co-workers, in 1995.^[129]

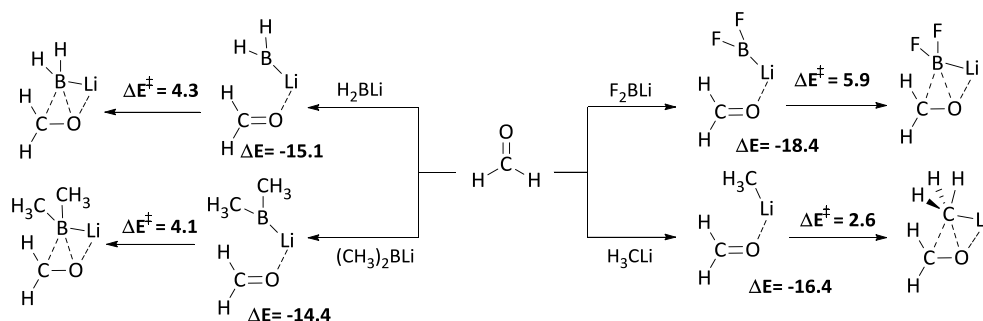
Undeniably, since its discovery,^[130–132] electrophilic reactivity of trivalent boron compounds towards organic molecules have been of great usefulness,^[125,133] especially because of the ease to afterwards refunctionalize selectively C–B bonds.^[134,135] However, despite the aforementioned reactivity of such boron units, they can change their electrophilic character towards a nucleophilic behavior depending on the nature of the substituents attached to the boron atom.^[136–138] Indeed, suitable ligands are capable of supplying enough electron density so that yield the boron nucleus unable to stabilize the excess of negative charge and seeks for other atoms to bond with. This recent discovery of the nucleophilic performance of these species represents a milestone in organic synthesis, which has developed routes to exploit this novel property in two principal ways: firstly by using diverse metals with a direct linkage to the boron moiety,^[139] and secondly in a green-way metal-free context within the last years.^[139,140]

1.3.2. Metal-containing nucleophilic boron compounds

Boryl-transition-metal complexes have stimulated the synthesis of organoboron compounds since their discovery.^[141–143] The first crystal structure analyses of boryl-metal complexes were not published until 1990, when borabicyclo[3.3.1]nonyl (BRR') was linked to an iridium(III) center to form a trigonal-planar boryl ligand (sum of angles about 359° and Ir–B bond distance equal to 2.093(7) Å).^[144] Even in this early example it was suggested that $d\pi-p\pi$ backbonding from iridium to boron to compensate the electronic deficiency on boron was weak. Therefore, boryl-transition-metal complexes have largely been regarded as reagents that contain an electrophilic –BRR' moiety to react with nucleophiles in a stoichiometric and catalytic way. However, the nature of the d-block metals might switch the reactivity of the boryl moiety from electrophilic to nucleophilic character. Moreover, the nature of the boron substituents

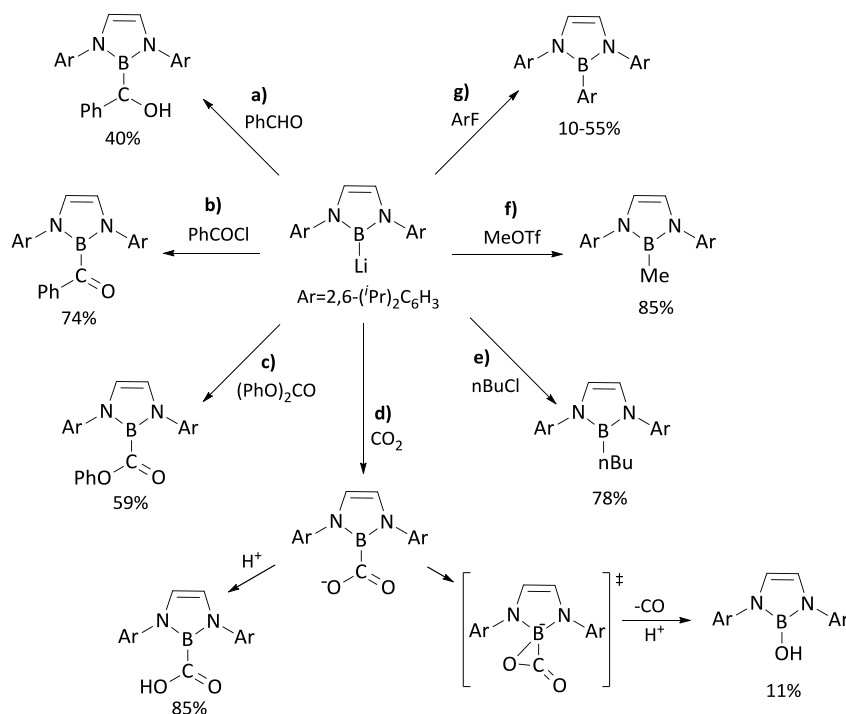
may also affect the σ interaction between the boron and the metal and therefore the potential nucleophilicity of boron.^[137] It is a question of a balance between the intrinsic Lewis acidity of the boron, due to its empty p orbital perpendicular to the molecular plane, and the accumulated electron density in the polarized σ bonds.

Oddly enough, the case of lithioboranes, LiBR_2 , combine a formal negative charge located on the boryl moiety with a vacant p orbital on boron, generating an unusual reactivity. The first studies of the reactivity of these compounds were theoretical ones due to the difficulty in isolating these species.^[145] The addition of lithioboranes to formaldehyde was shown to proceed in a similar way as methyl lithium reacts with such molecule (Scheme 1.4). Model species $\text{LiB}(\text{CH}_3)_2$, H_2BLi , and F_2BLi were selected in order to analyze its reactivity behavior and it was found that they initially interact with the substrate to form precursor complexes with the carbonyl oxygen coordinated side-on to lithium. After overcoming low activation barriers, these intermediates yield three-membered B-C-O ring structures with a dative boron-oxygen bond. Despite this, no umpollung occurs on boron atom and it still bears a positive charge (with the exception of H_2BLi), so the predicted reactivity proceeds via nucleophilic attack of the boryl anion moiety. The computed activation barriers are 4.1, 4.3 and 5.9 kcal·mol⁻¹ for $(\text{CH}_3)_2\text{BLi}$, H_2BLi and F_2BLi , respectively, indicating that the nucleophilicity trend of boryl fragments follows the order: $(\text{CH}_3)_2\text{B} > \text{H}_2\text{B} > \text{F}_2\text{B}$.



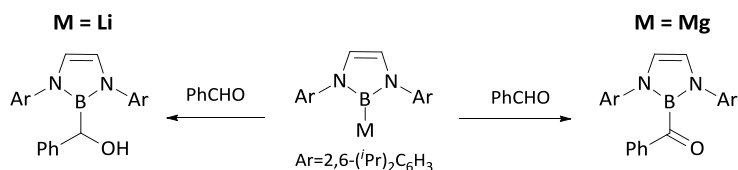
Scheme 1.4. Computed reaction energies (kcal·mol⁻¹) for the addition of lithioboranes and methyl lithium to formaldehyde.

Analogously, the first isolated diamino-substituted boryllithium compound was shown to react with a variety of organic electrophiles (Scheme 1.5).^[146,147] In general, the reactivity of such compound with carbonyl groups gives the same corresponding products as a carbanion would do. These evidences demonstrate undoubtedly the nucleophilic character of boryllithium compounds, which react with organic electrophiles via a wide range of mechanisms such as nucleophilic substitution ($\text{S}_{\text{N}}2$ -type), nucleophilic addition, nucleophilic addition/elimination, and nucleophilic aromatic substitution ($\text{S}_{\text{N}}\text{Ar}$ -type).^[146,147]



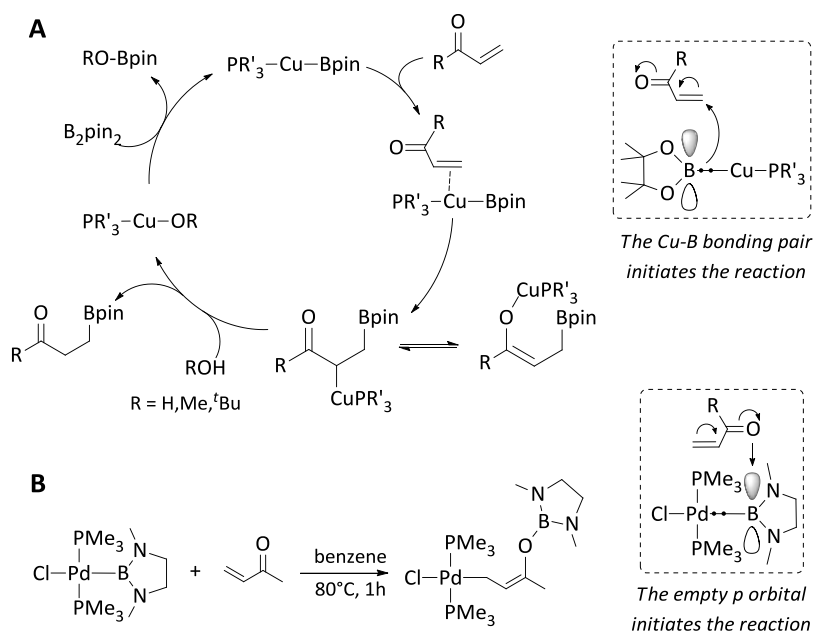
Scheme 1.5. Reactivity of the diamino-substituted boryllithium compound with various organic electrophiles.

The strongly remarked nucleophilic character of boryllithium compounds allowed the synthesis of its borylmagnesium counterparts by transmetalation.^[148] Interestingly, such a change in the metallic counterion (from lithium to magnesium) of boryl moieties alters considerably its reactivity towards electrophile agents. A clear example can be found in the product that both compounds produce when reacting with benzaldehyde: whereas boryllithium gives the α -borylbenzyl alcohol in high yield, borylmagnesium bromide affords a mixture of products, of which, unexpectedly, benzoylborane is formed as the main product (Scheme 1.6). The different product delivered by each of these two compounds was tried to be rationalized by means of theoretical calculations, leading to the conclusion that larger the amount of p orbital character in the M–B σ bond, the more reactive as a nucleophile the boryl fragment can be.^[149]



Scheme 1.6. Reactivity of boryllithium and borylmagnesium towards benzaldehyde.

While the character of boryl moieties bonded to alkali and alkaline-earth metals is clearly nucleophilic, the tendency with transition metals might depend strongly on the metal. For instance, borylcopper complexes react in a complementary manner as borylpalladium compounds would do (Scheme 1.7). Experimentally, it was found that copper mediated the β -boration to α,β -unsaturated carbonyl compounds,^[150–152] and from a theoretical point of view evidences of a nucleophilic boryl moiety attack were provided (Scheme 1.7.A).^[153] In stark contrast, the analogous reaction of a palladium complex suggested the insertion of the α,β -unsaturated ketone into the Pd–B bond with a reversed regioselectivity, thereby providing the 1,4-addition product in which the palladium was bonded to the β -carbon atom and the boryl fragment was bonded to the oxygen atom (Scheme 1.7.B).^[154]

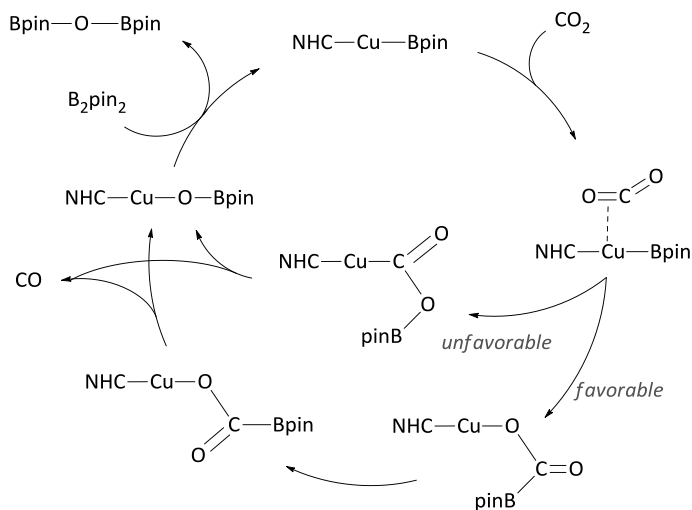


Scheme 1.7. Reactivity of α,β -unsaturated carbonyl compounds with (A) a borylcopper complex and (B) a borylpalladium.

Nevertheless, not only the metal plays an important role in the nucleophilicity of trivalent boron units, substituents attached to boron are also a variable to take into account (M-BR_2). This was evidenced in the theoretical analysis of several types of boryl fragments on a series of square-planar platinum(II) complexes to measure the *trans*-effect (i.e. the labilization of ligands that are *trans* to one another) which were inducing to other substituents in the metal.^[155] The computational study shows that the more p character of the sp -hybridized orbital of the boryl ligand ($-\text{BR}_2$), the greater σ -donating ability of such ligand and the more covalent character the interaction, resulting in a larger *trans* effect. Substituents on the boryl ligands also tune the hybrid used for that bonding situation. More electronegative

substituents prefer having hybrid orbitals with less s-type character. Therefore, the boron center links those substituents with a high s-type character, resulting in a boryl fragment ($-BR_2$) with less s-donor ability.

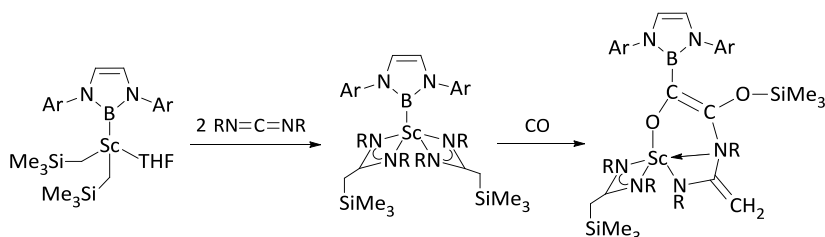
The synthesis of boryllithium compounds also enabled the construction of other electron-rich metal complexes different from the previous ones and comprising as well a M-B junction.^[156,157] In this context, the nucleophilic behavior of a boryldibromozincate was also tested, affording the same results as the aforementioned borylcopper when reacting towards α,β -unsaturated ketones.^[158] Also borylmetal complexes of group eleven were described to interact with diboranes to catalyze both the diboration and hydroboration of alkenes and alkynes,^[159–163] but copper complexes have focused much more attention and its reactivity has been widely explored. For instance, it was experimentally and theoretically proven that such complexes catalyze the reduction of CO_2 to CO in the presence of B_2pin_2 (Scheme 1.8).^[164,165] Computational studies have demonstrated that reduction occurs through CO_2 insertion into a Cu-B bond to give a Cu-O-C-B framework, in accordance with a nucleophilic attack of the boryl ligand at the C=O carbon. In principle, the electronic density concentration at the Cu-B bond is responsible for giving rise to a small CO_2 insertion barrier.^[165] The well documented reactivity of borylcopper complexes with nucleophilic boryl synthons can therefore be the base of efficient synthetic routes towards organoborane compounds.^[166–172]



Scheme 1.8. Borylcopper modified with NHC ligand (NHC = 1,3-bis(2,6-diisopropyl)phenyl imidazole-2-ylidene) mediated CO_2 reduction to CO.

Transmetalation with lithioboranes also made possible the construction of boryl moieties coordinated to early transition metals and rare earth metals.^[173–175] Among all those compounds, just some of them have been tested against electrophilic agents. In the case of

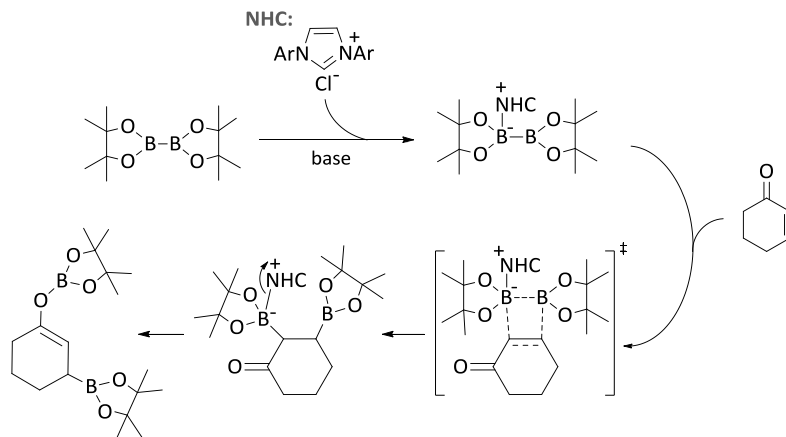
hafnium complex it was shown an activity for polymerization of ethylene and hex-1-ene, but it did not reflect a clear nucleophilic reactivity.^[173] On the other hand, borylscandium compounds were proven to undergo insertion reactions into the Sc–B bond with carbodiimide and subsequent carbon monoxide to give new boron containing rare earth metal complexes (Scheme 1.9).^[175]



Scheme 1.9. Reactions of scandium boryl complexes with carbodiimide and carbon monoxide

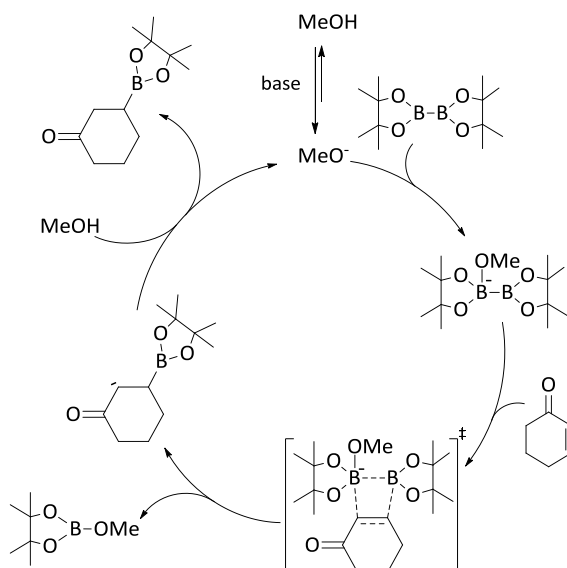
1.3.3. Metal-free nucleophilic boron compounds

In spite of the interesting and novel properties of transition-metal complexes, organic synthesis is currently moving towards methods without using such metal species in order to avoid elimination of these highly toxic products in posterior purification processes.^[176,177] Hence, since organoboranes are very important in organic synthesis and biomedicine,^[135,178] the metal-free approach might be a very appealing alternative to generate them. Indeed, it has been not long ago demonstrated that diboron reagents can perform nucleophilic reactivity processes under appropriate conditions, representing the very first metal-free approach towards the application of trivalent nucleophilic boron atoms.^[179,180] The activation of one of the boryl fragments is possible by the sole addition of electron donor reagents, such as amines, *N*-heterocyclic carbenes and alkoxides. The interaction of these molecules with a boron atom polarizes the B–B bond, and facilitates its heterolytic cleavage towards an electrophilic agent. For instance, *N*-heterocyclic carbenes generated *in situ* by deprotonation of imidazolium salts with Brønsted bases activated the bis(pinacolato)diboron reagent *via* Lewis acid-base interaction and catalyzed the β -boration of electron deficient olefins (Scheme 1.10).



Scheme 1.10. Catalytic β -boration of α,β -unsaturated conjugated compounds with bis(pinacolato)diboron activated by NHC.

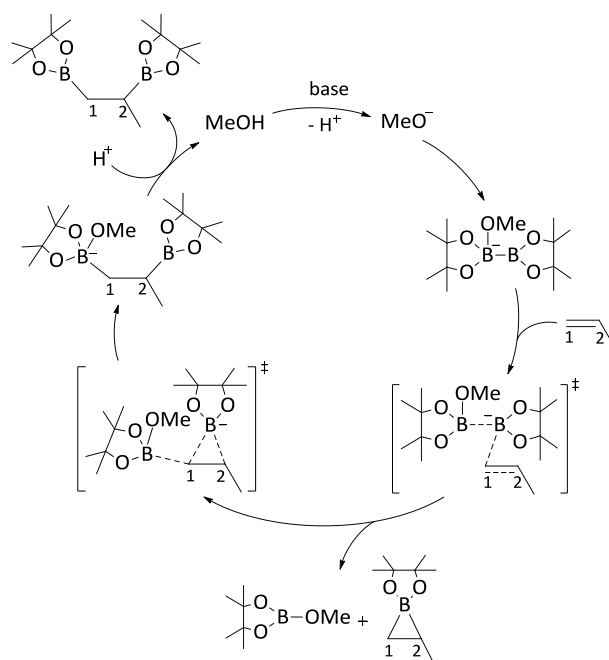
Despite the great advance in boron chemistry exhibited in the previous example, it is possible to simplify even more this novel reactivity. In fact, only with the use of methanol and a Brønsted base both acyclic and cyclic activated olefins can be efficiently transformed into the corresponding β -borated products in the presence of a series of diborons (Scheme 1.11).^[180,181]



Scheme 1.11. Catalytic β -boration of α,β -unsaturated conjugated compounds with bis(pinacolato)diboron activated by methoxide.

The base deprotonates the methanol and the resulting methoxide interacts with the diboron reagent to form an intermediate that consists on a Lewis acid-base adduct (Scheme 1.11). As a consequence, the other boron which keeps an sp^2 hybridization gains a pronounced nucleophilic character and is able to attack electro deficient olefins involving the interaction between the polarized σ_{B-B} and the $\pi^*_{C=C}$ molecular orbitals.^[180,181] The second anionic intermediate is formed directly *via* the heterolytic cleavage of the $B(sp^2)-B(sp^3)$ bond, the formation of the new C-B bond, and the release of a single boronic species. Protonation of such anionic intermediate with methanol furnishes the product and generates another methoxide anion, converting the reaction into a catalytic process (Scheme 1.11).

It is noteworthy to emphasize the change in the chemoselectivity produced in this reaction when replacing electro-deficient olefins by electro-localized ones. This modification leads to a diborated olefin as the main product, and only traces of the hydroborated product can be observed.^[182] A new plausible catalytic cycle mechanism was proposed to explain this different reactivity. Theoretical calculations supported the assumption, in which a model propylene was used as a model olefin substrate and a $MeO^- \rightarrow bis(pinacolato)-diboron$ reagent was selected (Scheme 1.12).^[182] The two transition states suggested therein can explain the formation of the product and the hydroborated by-product. In the first one the sp^2 boron atom of the activated diboron adduct interacts with the unsubstituted carbon atom (C_1) of the $C=C$ double bond, while the B-B bond weakens, and the negative charge density on the adjacent carbon (C_2) increases. It was proposed that the interaction leading to this transition state is the overlap between the strongly polarized B-B σ bond (HOMO) of the activated diboron reagent and the antibonding π^* orbital (LUMO) of the olefin, clearly suggesting a nucleophilic attack of the reagent towards the substrate. The excess of negative charge density on C_2 cannot be stabilized by an electro-accepting functional group and results in considerable kinetic lability due to the positive inductive effect of the alkyl substituent. Hence, the negatively charged C_2 atom is prone to attack any electrophilic site, and the closest one is the boron atom which is losing the B-B bond as a result of nucleophilic attack to C_1 . The distribution of the negative charge density among C_1 , C_2 , and the boron atom, might explain the connection between the first transition state and the "hydroborated" by-product, which protonation has still to occur. Finally, the interaction of a negatively charged olefin and an electrophilic $Bpin(Ome)$ moiety can be described with the second transition-state structure, which directly leads to the methoxide adduct of the diborated main product. This intermediate yields the final diborated product after protonation.



Scheme 1.12. Suggested catalytic cycle for the organocatalytic diboration of olefins.

An interesting feature of this mechanism is that although the nucleophilic boron atom attacks at the C₁ atom, it will be in the product bonded to C₂. Another peculiarity about this reactivity sequence is that connects two transition states without an intermediate species in between. This type of potential energy surface describes a reaction mechanism that is different from stepwise or concerted and has been referred to as a two-step-no-intermediate mechanism.^[183] Conversely, there is just one transition state furnishing the by-product. This bifurcation of the reaction path arise when sequential transition states with no intervening local energy minimum are found.^[184] Such phenomena is surprisingly general to encounter and affect experimental observables like kinetic isotope effects and product distributions. Beside this, electronic effects seem to be involved in determining a diborated or hydroborated as a final product. Indeed, if an electro-attracting group is placed in the terminal carbon of the olefin the first transition state becomes more stabilized (due to a higher degree of delocalization of the negative charge) and the hydroborating side-reaction emerges as a competitive alternative to achieve the final product. That is the case of α,β -unsaturated carbonyl compounds as substrates (activated olefins), for which the hydroborated (β -borated) substrate is the only product of the reaction.

The activation energies in the nucleophilic attack of the boryl adduct and thermodynamic stabilities of the anionic intermediate were calculated for a wide range of substrates to provide some insights into the scope of this reactivity (Figure 1.4).^[181] In all cases, the

electronic energy barrier is considerably smooth due to the fact that the negative charge in the adduct becomes more delocalized in the transition state species. However, the relative high values of the free energy barriers are induced by the entropy effects derived from an associative process, which tend to overestimate the energetics of the involved reactions. The lowest activation energy and greatest thermodynamic stability of the intermediate have been observed in the case of acrylaldehyde, followed by the ketone and the ester. Interestingly, the boryl nucleophilic attack seemed to be feasible for all substrates, even towards non-activated olefins such as styrene and propylene, as shown experimentally and theoretically in the diboration of nonactivated olefins (Figure 1.4).^[181]

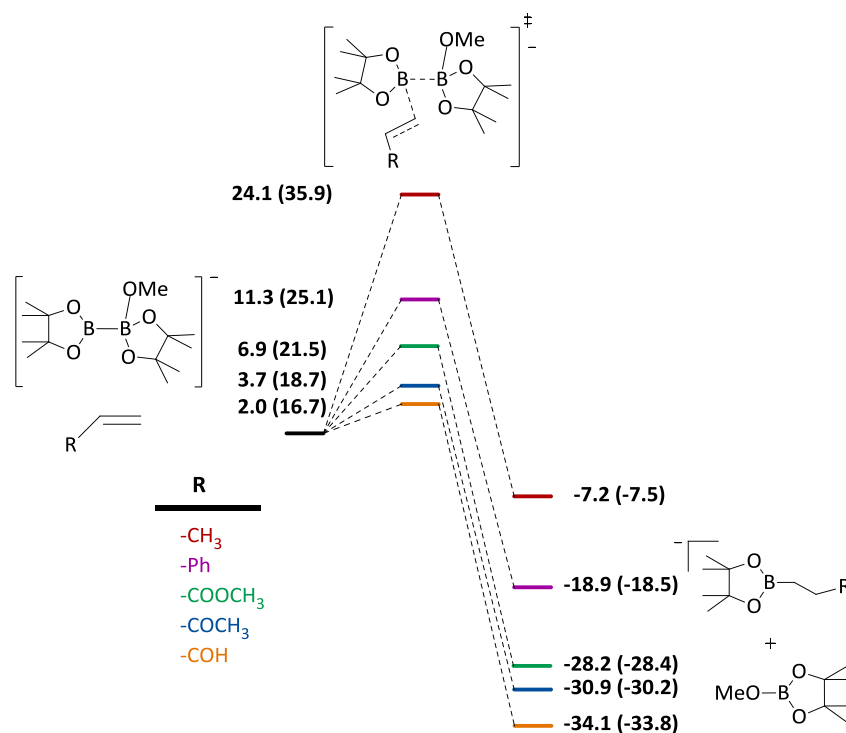
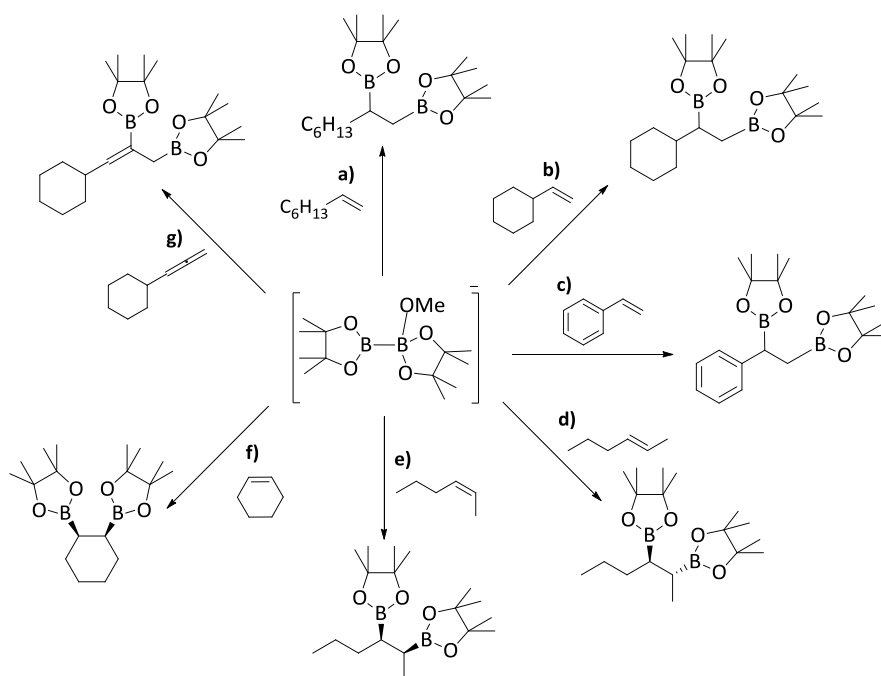


Figure 1.4. Energy profile for several monosubstituted alkenes. Values for energy barrier and reaction energy are given in kcal mol⁻¹ for electronic energy and Gibbs free energy (in parenthesis), relative to the diborane adduct plus the respective alkene.

All these precedents prove that trivalent boron can act as nucleophilic synthons in a proper organocatalytic context. Even so, the scope of this reactivity was extended to a variety of non-activated olefins yielding the diborated product in all cases and therefore confirming the power of this synthetic route (Scheme 1.13).^[182] For instance, bis(pinacolato)diboron can be added quantitatively to 1-octene in the presence of MeOH and Cs₂CO₃ as a base (Scheme 1.13a). Changing the n-hexyl substituent to cyclohexyl does not influence the reactivity of the

C=C double bond significantly, and conversion of vinylcyclohexane into the desired diborated product can be achieved (Scheme 1.13b). The diboration of styrene requires milder reaction conditions than that of the aliphatic alkenes to obtain high selectivity (Scheme 1.13c). Interestingly, the diboration of internal alkenes provided crucial information since diboration of *trans*-hex-2-ene gives the diborated product in a 3:97 (*syn:anti*) ratio (Scheme 1.13d), while *cis*-hex-2-ene 26at the corresponding diborated product in a 95:5 (*syn:anti*) ratio (Scheme 1.13e). Similarly, the diboration of cyclohexene exclusively gives the *cis* diborated product (Scheme 1.13f). Another interesting finding is that nucleophilic diboration of allenes favours the formation of the 1,2-diborated product (Scheme 1.13g), in contrast to most transition metal catalyzed diborations of allenes which usually provide the 2,3-diborated isomers as primary products.^[185,186] The generality of the methodology has been proved by the successful use of different diborons, which all have been efficiently activated by the MeOH/base system (base = Cs₂CO₃) providing a similarly powerful boryl nucleophilic unit.^[182]



Scheme 1.13. Scope of organocatalytic diboration of alkenes mediated by MeO⁻→bis(pinacolato)diboron.

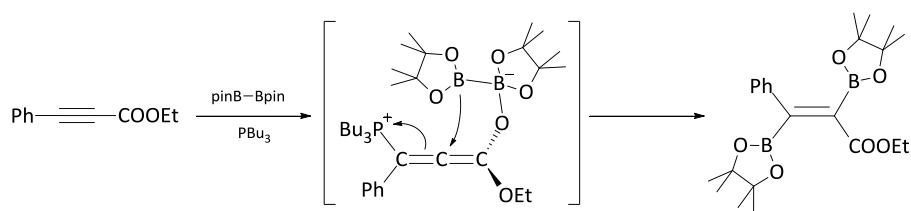
The former two subsections regarding the nucleophilicity of trivalent boron compounds are put into study in Chapter 6. Because the outlined reactivity carried out by boryl units represents a milestone in the synthesis of organoboron species, we examined the nucleophilic activity of some of those boryl fragments in order to establish quantitative relationships between the structures of trivalent boron compounds and their nucleophilicity. To that end,

we employed ground state molecular descriptors and used the computed nucleophilic energy barrier to a model substrate as a response variable. Trends extracted from structure *versus* nucleophilic activity relationships might be used for a priori evaluation of untested trivalent boron compounds, and for deriving guidelines for novel agent design.

1.3.4. Unconventional additions of boron compounds

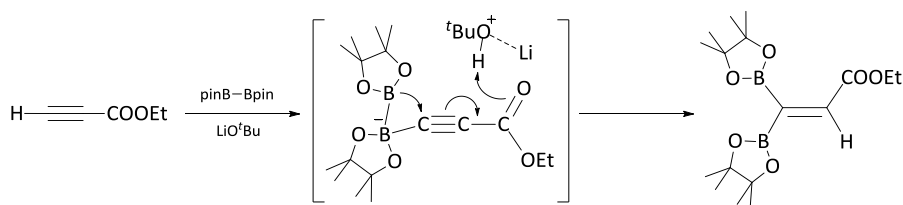
Before the former exposition, traditional organic chemistry established a guideline for the reactivity of trivalent boron molecules in the absence of metals, which consisted on the simple electrophilic interaction to potentially nucleophilic substrates facing each other in a *syn* geometrical disposition and delivering a 1,2-product. This pattern can be seen even in nucleophilic additions of Lewis-base activated diboron compounds to alkenes, where the stereospecific *syn*-mechanism has been fully addressed from theoretical calculations and empirical data.^[182,187,188] The 1,2-diboration of olefins through base-mediated activation is also feasible to occur in an intramolecular *syn*-manner for both alkenyl and propargylic alcohols, via deprotonation of the OH group, with the consequent assisted delivery of the boryl units to the unsaturated fragment of the substrate.^[189,190]

However, alongside with the previously detailed behavior of the activated diboron compounds, novel reactivity different from the *syn* additions have been observed. In particular, a phosphine-mediated organocatalytic process for the diboration of alkynoates has been reported to occur in an *anti*-selective fashion (Scheme 1.14).^[191] The vicinal disposition of the two boryl moieties installed allows their posterior functionalization in a stepwise manner, which can be advantageous for the synthesis of a diverse array of unsymmetrical tetrasubstituted alkenes, such as (*Z*)-tamoxifen analogues, that represent key antiestrogenic anticancer drugs. The role of the phosphine as a catalyst was suggested to be as the initiator of a conjugate addition to the triple bond enabling the Lewis base character of the carbonyl group and forming a zwitterionic allenolate intermediate. Then, the sp^2 boryl moiety might migrate to the central carbon atom of the allene in a nucleophilic attack to construct a phosphorus ylide, from where a cyclic boronate and a concomitant release of the phosphine catalyst could yield the final product.^[191]



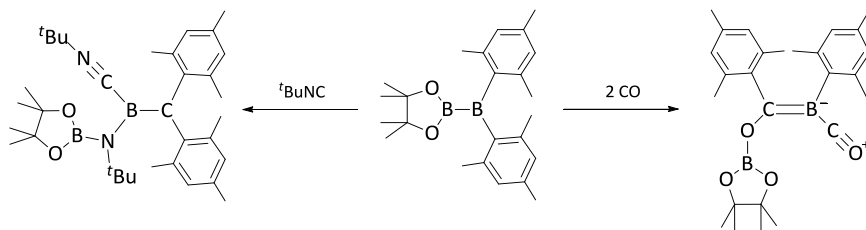
Scheme 1.14. Selective *anti*-diboration of alkynoates.

Another reactivity pattern different from both *syn*- and *anti*-1,2-additions can take place in terminal alkynes such as propiolates and propiolamides to generate *gem*-additions. In those substrates, a facile deprotonation of the terminal hydrogen in the triple bond by Brønsted bases is able to promote the synthesis of functionalized 1,1-diborylakenes (Scheme 1.15).^[192] The proposed initial hydrogen abstraction to form the acetylide could lead to the attack of one boron atom of the B₂pin₂, and the subsequent alkynyl borate might afford the migration of the terminal boryl moiety to the sp-hybridized carbon atom of the alkyne with a simultaneous protonation of the carbonyl oxygen atom. Alternatively, lithium carbenoids have also been shown to react with B₂pin₂ to yield 1,1-diborylakenes.^[193]



Scheme 1.15. Selective 1,1-diboration of propiolates.

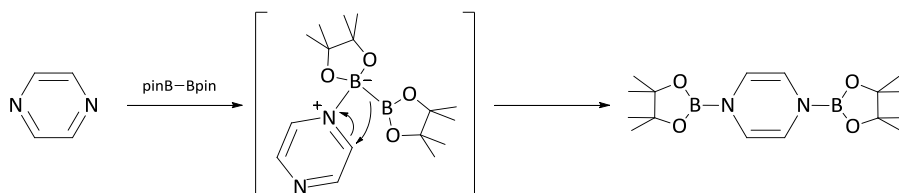
Exploration of unsymmetrical diborane compounds reactivity also conducted to novel outcomes when made them react with carbon monoxide and *tert*-butyl isonitrile at room temperature (Scheme 1.16).^[194] In the first case, a solution of Bpin-BMes can react with CO to insert such molecule into the B-B bond, with a subsequent migration of the Mes fragment to the carbon atom and the incorporation of a second CO molecule. For the second case, when an excess of the isonitrile agent is made react with the diboron compound, also two molecules are enclosed in the final product. Surprisingly, in one of the *tert*-butyl isonitrile molecules incorporated, the carbon-nitrogen triple bond can be completely splintered in absence of any transition-metal complex.



Scheme 1.16. Reaction of unsymmetrical Bpin-BMes diborane compound with carbon monoxide and *tert*-butyl isonitrile at room temperature in a metal-free context.

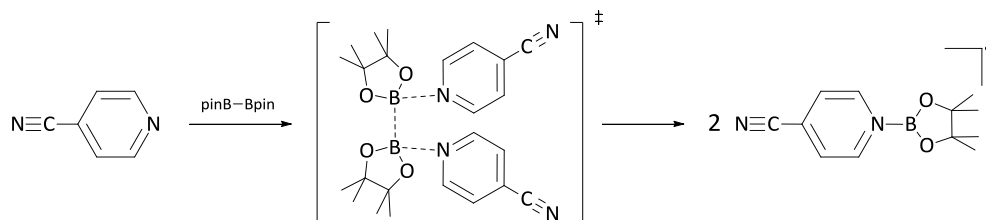
Moreover, other type of additions different from the former ones can render the cleavage of the B-B bond to be functionalized afterwards. In particular, it has been reported that the

reaction of pyrazine with B_2pin_2 can promote a 1,4-addition of the boryl units on the nitrogen atoms at room temperature (Scheme 1.17).^[195] The suggested mechanism consists on a dearomatization process based on the coordination of one of the nitrogen atoms of pyrazine to one of the Bpin moieties to generate a four coordinate boron intermediate, conferring a nucleophilic character to the vicinal boryl unit. A subsequent attack of such boryl fragment follows to form a transient bond with the C₂ carbon atom of the pyrazine providing a momentary 1,2-addition intermediate that ends up in a *N,N'*-diboryl-1,4-dihydropyrazine product *via* rearrangement of the α -boryl unit.



Scheme 1.17. Addition of B_2pin_2 to pyrazine substrates.

Previous additions had in common an heterolytic fracture of the B–B bond to display different type of additions to unsaturated species. However, it has been proven that 4-cyanopyridine is able to promote an homolytic cleavage of the symmetrical B_2pin_2 compound *via* the cooperative coordination to the two boron atoms of the diborane to create pyridine boryl radicals (Scheme 1.18).^[196] This novel reactivity has been found both experimentally and computationally to proceed through a cooperative Lewis base mechanism, being the captodative effect (i.e. a synergistic phenomenon consisting on the stabilization of a radical species by an electron-withdrawing substituent and an electron-donating substituent through multiple resonant structures)^[197] responsible for the holding of the generated boryl radical. With this novel activation mode, 4-cyanopyridine and B_2pin_2 under mild conditions were proven to achieve feasibly catalytic reduction of azocompounds and quinones, and deoxygenation of sulfoxides to sulphides.^[196]



Scheme 1.18. Homolytic cleavage of the B–B bond with 4-cyanopyridine.

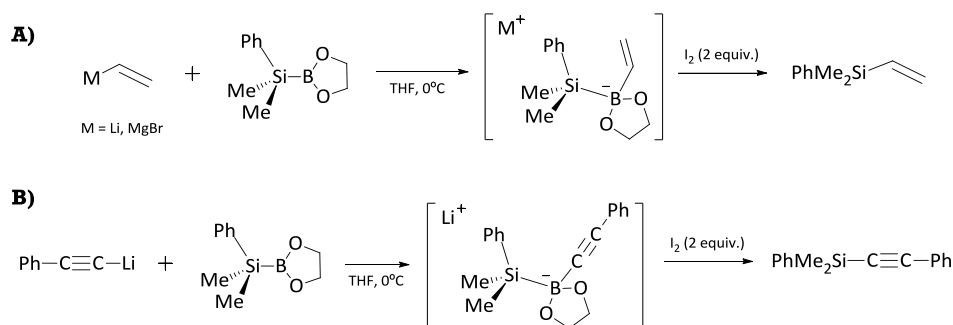
Metal-free borylative processes have shown to be a versatile manner to functionalize unsaturated bonds, which can be in turn selectively transformed into other groups after the

former functionalization. Hence, further exploration is crucial for the synthesis of organoboranes of growing complexity. Chapter 7 of this thesis examines the unsymmetrical 1,1-diboration of diazo compounds, formed *in situ* from aldehydes and cyclic and non-cyclic ketones in the absence of any metal.

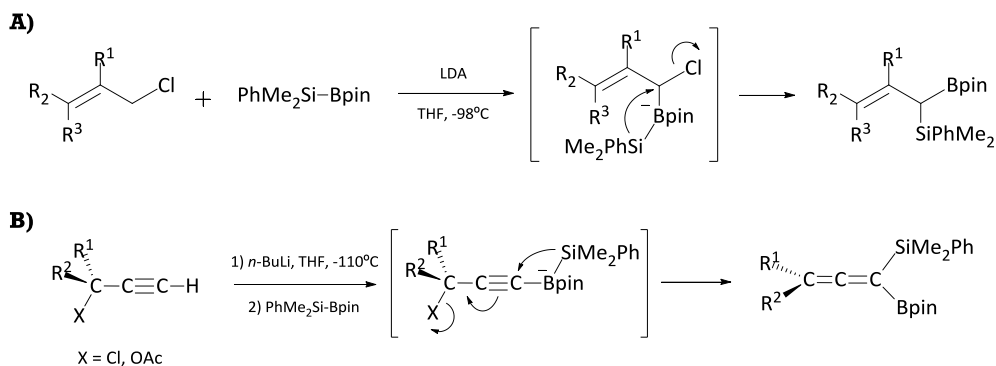
1.3.5. Transition-metal-free B–interelement reactions

A new class of synthetic methodologies can be explored from the substitution of the B–B linkage by a B–interelement binding, being that element a non-metal atom. Depending on the intrinsic nature of such element and its ligands attached, plus the substituent groups belonging to the boron, the chemistry displayed by these type of junctions may be diverse.^[140] The justification for that seems to be related with a “push-pull” effect, which involves an internal charge transfer coming from an electron donor and an electron acceptor within the same molecule.^[198] This interaction is responsible for reducing the HOMO-LUMO energy gap, thus makes the system prone to react with certain substrates. If those donor-acceptor groups are directly bonded, such as the case of some B–interelement systems, the coordination of a Lewis-base to the boron atom enhances nucleophilic character of the interelement fragment.

Regarding the B–Si junctions, in 1995 seminal studies on the reaction of silylboranes with alkenyl and alkynyllithium were reported to conduct to alkenyl- and alkynylsilanes after an appropriate treatment with iodine, respectively (Scheme 1.19).^[199] Some years later, it was described the reaction of PhMe₂Si–Bpin silylboranes with *in situ* generated carbenoid species to yield 1-boryl-1-silyl-1-alkenes *via* 1,2-migration rearrangement of the silyl moiety.^[193] This type of reorganization can also be found in the synthesis of 1-boryl-1-silyl-2-alkenes and 1-boryl-1-silylallenes through reaction between the same PhMe₂Si–Bpin silylborane and *in situ* generated α -chloroallyllithiums and 3-chloro- or 3-alkoxy-1-alkynes, respectively (Scheme 1.20).^[200,201]

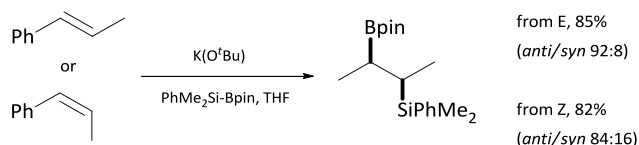


Scheme 1.19. A) Reaction of a silylborane with alkenyl metals and posterior 1,2-migration of the borate complex, B) Reaction of a silylborane with an alkynyllithium compound and their subsequent 1,2-migration.



Scheme 1.20. A) Synthesis of 1-boryl-1-silyl-2-alkenes from PhMe₂Si-Bpin silylborane and *in situ* generated α -chloroallyllithiums, B) Synthesis of 1-boryl-1-silylallenes from PhMe₂Si-Bpin silylborane and *in situ* generated 3-chloro- or 3-alkoxy-1-alkynes.

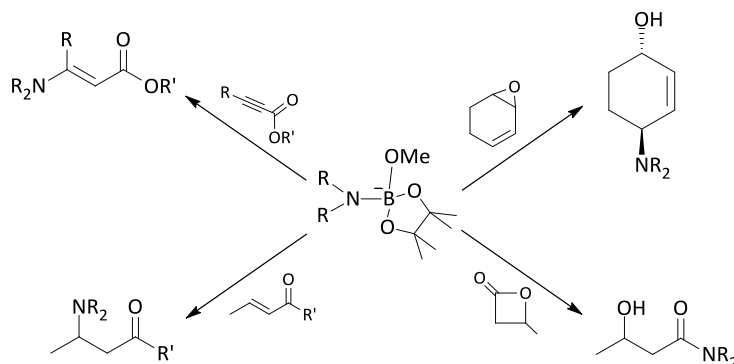
In general, reactions of silylboranes tend to occur with a 1,2-migration to afford *gem*-additions.^[202–204] However, likewise with the B–B linkage, there exist other types of additions for the B–Si case. For instance, the phosphine-catalyzed reaction of alkynoates with PhMe₂SiBpin silylborane was also developed and suggested to take place in the same manner as the B₂pin₂ counterpart (Scheme 1.14).^[191] This *anti*-1,2-addition produced (*Z*)-3-boryl-2-silylalkenoate in high yield and stereoselectivity. Also an alkoxy base-catalyzed silaboration of aromatic alkenes was reported to provide mostly the same *anti*-product even using (*E*)- or (*Z*)-1,2-disubstituted alkenes (Scheme 1.21).^[205] Similar patterns of reactivity between B–B and B–Si can be found as well in the insertion of isocyanides into their bond, or in the dearomatization of pyrazine.^[195,206] Interestingly, even photo-induced reactions of silylborane might be employed to functionalize unsaturated bonds with a silicon moiety, although the conversion is not high enough to consider it a synthetic methodology.^[207]



Scheme 2.21. Alkoxy base-catalysed silaboration of aromatic alkenes.

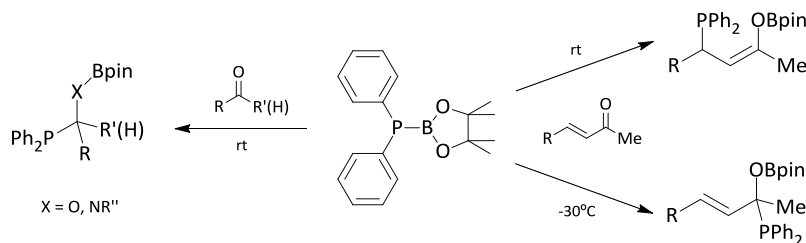
Aminoboranes have also become useful reagents for addition reactions with organic molecules in order to provide efficient heterofunctionalization protocols. Initial attempts were originally limited to insert the corresponding B–N bond into isocyanates, isothiocyanates and carbodiimides.^[208–210] Another approach consisted on a [4+2] cycloaddition from the direct aminoboration of a carbon-carbon triple bond to create simultaneously a C–N and a C–B bond to generate a six-member ring.^[211] However, a breakthrough came through the alkoxy ions

activation of pinB–NR₂ for the selective addition of the amine group into activated unsaturated substrates (Scheme 1.22).^[212] The formation of a Lewis acid-base adduct was confirmed experimentally by the shift in the ¹¹B NMR spectra observed. Since a transition-metal-free aminoboration of non-activated unsaturated hydrocarbons has not yet been described, this synthetic route seems to be the launching pad to enhance the nucleophilic attack of amino moieties towards electro-deficient olefins.



Scheme 2.22. Amination reactivity of alkoxy-activated aminoboranes towards transition-metal-free.

For phosphinoborane compounds the interaction between the phosphorus lone pair and the boron empty orbital in diazaborole compounds was shown to be best described as a pure σ -bond by means of crystallographic and computational data.^[213] The lack of any $\pi_{P \rightarrow B}$ overlap favors a single bond scenario and therefore the nucleophilic reactivity of the phosphine unit through its lone pair. Thus, their reaction towards aldehydes, ketones and aldimines generates 1,2-products at room temperature,^[214] just as observed for diboron reagents (Scheme 1.23).^[215] Interestingly, when employing α,β -unsaturated ketones the afforded 1,2- and 1,4-products depend on the reaction conditions (solvent and temperature).^[214] Moreover, the electrophilic addition of pinB–PPh₂ to acridine and pyridine can be performed at room temperature to afford a 1,4-product,^[214] resembling again the behavior of diboron compounds (Scheme 1.17).^[195]



Scheme 2.23. Transition-metal-free addition of pinB–PPh₂ to ketones, imines and α,β -unsaturated ketones.

The first addition of thioboranes to unsaturated bonds in a transition-metal-free context took place at room temperature employing α,β -unsaturated ketones and aldehydes as substrates.^[216] As observed for the B–P case,^[214] the reaction proceeds without the need of any additive due to the donor-acceptor electron interaction of the boron of the boryl unit and the oxygen of the carbonyl group. Consequently, the thiolate fragment enhances its nucleophilic character and is able to promote the 1,4- *versus* 1,2-addition, as function of the involved substrate.^[216] The analogous reaction employing ynones was also achieved in absence of transition metal complexes or additives and yielded the synthesis of vinylsulphides.^[217] Finally, the insertion of the diazo derivative $\text{Me}_3\text{SiCHN}_2$ into the B–S bond was proved to allow for the formation of the multisubstituted $\text{H-C}(\text{SR})(\text{Bpin})(\text{SiMe}_3)$ series of compounds.^[218] The proposed mechanism might involve an initial interaction of the nucleophilic diazo carbon with the electron deficient boron of the Bpin moiety, followed by 1,2-migration of the adjacent thiolate fragment to generate the α,α -substituted product and the concomitant release of dinitrogen. The interest in these multisubstituted compounds can be illustrated by their consecutive base-assisted transformations to afford a variety of modifications leading to other functionalities.^[218]

Activated olefins, such as α,β -unsaturated ketones and aldehydes, also reacted with phenylselenium borane in a similar way that its sulphur counterpart.^[219] This process furnishes β -(phenylseleno) substituted ketones and aldehydes as products at room temperature without any metal or organocatalytic assistance. Theoretical calculations on this system proposed a plausible mechanism and also explained the selectivity towards the 1,4-addition *versus* the 1,2-adduct. Moreover, a reliable route to stereodefined (*Z*)-alkenyl selenides can be guaranteed employing α,β -acetylenic ketones.^[217]

Regarding the importance of forming C–heteroatom bonds, the metal-free B–interelement strategy seems an appealing approach. In Chapter 8 we studied the regio- and stereoselectivity of the *anti*-3,4-selenoboration of α,β -acetylenic esters and ynamides using catalytic amounts of a basic phosphine. Curiously, in the absence of the phosphine the selenoboration switched from the formation of α -vinyl selenides to β -vinyl selenides. A possible mechanistic path is proposed in order to elucidate the origin of this opposite reactivity trend.

1.3.6. Remarks and perspectives

The concept of boron reagents has changed drastically during the recent last years due to the amount of publications that changed our vision of such species. The currently quotidian idea of synthesize and employ trivalent nucleophilic boron compounds for their applicability in the field of organic chemistry would have been inconceivable a few years ago. Nevertheless, by

now, the scientific community not only has been able to demonstrate the umpolung of trivalent boranes, but also has generated a great number of examples wherein the boron attacks organic molecules while bearing a nucleophilic behavior. Furthermore, it has been demonstrated that B–B and B–interelements compounds are able to perform reactivity patterns different from classic 1,2-*syn*-additions. If there is any weak point on the use of boryl synthons, it would be the lack of synthetic methods capable to provide asymmetric induction under a transition-metal-free context for this reagents. On the other hand, looking behind to see the improvements achieved in a so-short period of time, there are evidences to feel confident about a further progress that has still yet to come.

1.4. References

- [1] K. C. Nicolaou, T. Montagnon, *Molecules That Changed the World*, Wiley-VCH, **2008**.
- [2] E. J. Corey, L. Kürti, B. Czakó, *Molecules and Medicine*, John Wiley & Sons, **2007**.
- [3] H. Alper, *Transition Metal in Organic Synthesis*, Elsevier, **1976**.
- [4] S. E. Gibson, *Transition Metals in Organic Synthesis: A Practical Approach*, Oxford University Press, **1997**.
- [5] G. Jaouen, W. Beck, M. J. McGlinchey, *Bioorganometallics*, WILEY-VCH, **2006**.
- [6] J. F. Hartwig, *Nature* **2008**, *455*, 314–322.
- [7] T. Hudlicky, J. W. Reed, *The Way of Synthesis: Evolution of Design and Methods for Natural Products*, Wiley-VCH, **2007**.
- [8] R. H. Crabtree, *J. Chem. Soc. Dalt. Trans.* **2001**, 2437–2450.
- [9] J. A. Labinger, J. E. Bercaw, *Nature* **2002**, *417*, 507–514.
- [10] F. Kakiuchi, N. Chatani, *Adv. Synth. Catal.* **2003**, *345*, 1077–1101.
- [11] K. Godula, S. Sames, *Science* **2006**, *312*, 67–73.
- [12] K. Weissmermel, H.-J. Arpe, *Industrial Organic Chemistry*, WILEY-VCH, **2008**.
- [13] X. Chen, K. M. Engle, D. H. Wang, Y. Jin-Quan, *Angew. Chemie - Int. Ed.* **2009**, *48*, 5094–5115.
- [14] D. A. Colby, R. G. Bergman, J. A. Ellman, *Chem. Rev.* **2010**, *110*, 624–655.
- [15] T. W. Lyons, M. S. Sanford, *Chem. Rev.* **2010**, *110*, 1147–1169.
- [16] L. Ackermann, *Chem. Rev.* **2011**, *111*, 1315–1345.
- [17] C. S. Yeung, V. M. Dong, *Chem. Rev.* **2011**, *111*, 1215–1292.
- [18] J. Wencel-Delord, T. Droge, F. Liu, F. Glorius, *Chem. Soc. Rev.* **2011**, *40*, 4740–4761.
- [19] P. B. Arockiam, C. Bruneau, P. H. Dixneuf, *Chem. Rev.* **2012**, *112*, 5879–5918.
- [20] B.-J. Li, Z.-J. Shi, *Chem. Soc. Rev.* **2012**, *41*, 5588–5598.

- [21] J. Wencel-Delord, F. Glorius, *Nat Chem* **2013**, *5*, 369–375.
- [22] L. Yang, H. Huang, *Chem. Rev.* **2015**, *115*, 3468–3517.
- [23] T. Gensch, M. N. Hopkinson, F. Glorius, J. Wencel-Delord, *Chem. Soc. Rev.* **2016**, *45*, 2900–2936.
- [24] J. Yamaguchi, A. D. Yamaguchi, K. Itami, *Angew. Chemie - Int. Ed.* **2012**, *51*, 8960–9009.
- [25] D. Y.-K. Chen, S. W. Youn, *Chem. - A Eur. J.* **2012**, *18*, 9452–9474.
- [26] L. McMurray, F. O'Hara, M. J. Gaunt, *Chem. Soc. Rev.* **2011**, *40*, 1885–1898.
- [27] M. Sono, M. P. Roach, E. D. Coulter, J. H. Dawson, *Chem. Rev.* **1996**, *96*, 2841–2888.
- [28] B. Meunier, S. P. de Visser, S. Shaik, *Chem. Rev.* **2004**, *104*, 3947–3980.
- [29] G. Kiss, N. Çelebi-Ölçüm, R. Moretti, D. Baker, K. N. Houk, *Angew. Chemie Int. Ed.* **2013**, *52*, 5700–5725.
- [30] M. L. Green, P. J. Knowles, *J. Chem. Soc. D Chem. Commun.* **1970**, 1677.
- [31] P. Foley, G. M. Whitesides, *J. Am. Chem. Soc.* **1979**, *101*, 2732–2733.
- [32] L. Jiang, E. A. Althoff, F. R. Clemente, L. Doyle, D. Röthlisberger, A. Zanghellini, J. L. Gallaher, J. L. Betker, F. Tanaka, C. F. Barbas, et al., *Science* **2008**, *319*, 1387–1391.
- [33] M. Albrecht, *Chem. Rev.* **2010**, *110*, 576–623.
- [34] J. P. Kleiman, M. Dubeck, *J. Am. Chem. Soc.* **1963**, *85*, 1544–1545.
- [35] A. C. Cope, R. W. Siekman, *J. Am. Chem. Soc.* **1965**, *87*, 3272–3273.
- [36] L. S. Jongbloed, B. de Bruin, J. N. H. Reek, M. Lutz, J. I. van der Vlugt, *Catal. Sci. Technol.* **2016**, *6*, 1320–1327.
- [37] A. E. Allen, D. W. C. MacMillan, *Chem. Sci.* **2012**, *3*, 633–658.
- [38] D.-S. Kim, W.-J. Park, C.-H. Jun, *Chem. Rev.* **2017**, *117*, 8977–9015.
- [39] Y. Gloaguen, L. M. Jongens, J. N. H. Reek, M. Lutz, B. de Bruin, J. I. van der Vlugt, *Organometallics* **2013**, *32*, 4284–4291.
- [40] S. Oldenhof, F. G. Terrade, M. Lutz, J. I. van der Vlugt, J. N. H. Reek, *Organometallics* **2015**, *34*, 3209–3215.
- [41] J. F. Hartwig, M. A. Larsen, *ACS Cent. Sci.* **2016**, *2*, 281–292.
- [42] J. N. Harvey, *Organometallics* **2001**, *20*, 4887–4895.
- [43] S. Niu, M. B. Hall, *Chem. Rev.* **2000**, *100*, 353–406.
- [44] T. Newhouse, P. S. Baran, *Angew. Chemie Int. Ed.* **2011**, *50*, 3362–3374.
- [45] V. A. Schmidt, R. K. Quinn, A. T. Brusoe, E. J. Alexanian, *J. Am. Chem. Soc.* **2014**, *136*, 14389–14392.
- [46] H. M. L. Davies, R. E. J. Beckwith, *Chem. Rev.* **2003**, *103*, 2861–2904.
- [47] P. Müller, C. Fruit, *Chem. Rev.* **2003**, *103*, 2905–2920.
- [48] H. M. L. Davies, J. R. Manning, *Nature* **2008**, *451*, 417.
- [49] S. H. Cho, J. Y. Kim, J. Kwak, S. Chang, *Chem. Soc. Rev.* **2011**, *40*, 5068–5083.
- [50] K. Yoshizawa, *Coord. Chem. Rev.* **2002**, *226*, 251–259.
- [51] P. P.-Y. Chen, R. B.-G. Yang, J. C.-M. Lee, S. I. Chan, *Proc. Natl. Acad. Sci.* **2007**, *104*, 14570–14575.

- [52] P. Hlavica, *Eur. J. Biochem.* **2004**, *271*, 4335–4360.
- [53] C. C. Cummins, S. M. Baxter, P. T. Wolczanski, *J. Am. Chem. Soc.* **1988**, *110*, 8731–8733.
- [54] J. L. Bennett, P. T. Wolczanski, *J. Am. Chem. Soc.* **1994**, *116*, 2179–2180.
- [55] T. R. Cundari, T. R. Klinckman, P. T. Wolczanski, *J. Am. Chem. Soc.* **2002**, *124*, 1481–1487.
- [56] N. Ochi, Y. Nakao, H. Sato, S. Sakaki, *J. Am. Chem. Soc.* **2007**, *129*, 8615–8624.
- [57] H. van der Heijden, B. Hessen, *J. Chem. Soc. Chem. Commun.* **1995**, 145–146.
- [58] B. C. Bailey, H. Fan, E. W. Baum, J. C. Huffman, M.-H. Baik, D. J. Mindiola, *J. Am. Chem. Soc.* **2005**, *127*, 16016–16017.
- [59] J. A. Flores, V. N. Cavaliere, D. Buck, B. Pinter, G. Chen, M. G. Crestani, M.-H. Baik, D. J. Mindiola, *Chem. Sci.* **2011**, *2*, 1457–1462.
- [60] M. G. Crestani, A. K. Hickey, X. Gao, B. Pinter, V. N. Cavaliere, J.-I. Ito, C.-H. Chen, D. J. Mindiola, *J. Am. Chem. Soc.* **2013**, *135*, 14754–14767.
- [61] T. Kurogi, M. E. Miehlich, D. Halter, D. J. Mindiola, *Organometallics* **2018**, *37*, 165–167.
- [62] M. P. Coles, V. C. Gibson, W. Clegg, M. R. J. Elsegood, P. A. Porrelli, *Chem. Commun.* **1996**, 1963–1964.
- [63] E. Tran, P. Legzdins, *J. Am. Chem. Soc.* **1997**, *119*, 5071–5072.
- [64] C. B. Pamplin, P. Legzdins, *Acc. Chem. Res.* **2003**, *36*, 223–233.
- [65] J. G. Andino, U. J. Kilgore, M. Pink, A. Ozarowski, J. Krzystek, J. Telsner, M.-H. Baik, D. J. Mindiola, *Chem. Sci.* **2010**, *1*, 351–356.
- [66] K. Nomura, B. K. Bahuleyan, K. Tsutsumi, A. Igarashi, *Organometallics* **2014**, *33*, 6682–6691.
- [67] R. R. Schrock, *Chem. Rev.* **2002**, *102*, 145–180.
- [68] R. Waterman, *Organometallics* **2013**, *32*, 7249–7263.
- [69] F. Roudesly, J. Oble, G. Poli, *J. Mol. Catal. A Chem.* **2017**, *426*, 275–296.
- [70] M. Brookhart, M. L. H. Green, *J. Organomet. Chem.* **1983**, *250*, 395–408.
- [71] E. Clot, O. Eisenstein, in *Struct. Bond.*, Springer-Verlag, Berlin, **2004**, pp. 1–36.
- [72] M. Lein, *Coord. Chem. Rev.* **2009**, *253*, 625–634.
- [73] P. Cossee, *Tetrahedron Lett.* **1960**, *1*, 12–16.
- [74] R. B. Cracknell, A. G. Orpen, J. L. Spencer, *J. Chem. Soc. Chem. Commun.* **1984**, 326–328.
- [75] W. Kaminsky, R. Steiger, *Polyhedron* **1988**, *7*, 2375–2381.
- [76] L. H. Shultz, D. J. Tempel, M. Brookhart, *J. Am. Chem. Soc.* **2001**, *123*, 11539–11555.
- [77] R. H. Crabtree, *J. Organomet. Chem.* **2004**, *689*, 4083–4091.
- [78] B. Rybtchinski, L. Konstantinovskiy, L. J. W. Shimon, A. Vigalok, D. Milstein, *Chem. - A Eur. J.* **2000**, *6*, 3287–3292.
- [79] I. Omae, in *J. Organomet. Chem.*, Elsevier, **2011**, pp. 1128–1145.
- [80] M. J. S. Dewar, *Bull. Soc. Chim. Fr.* **1951**, *18*, C71–C79.
- [81] J. Chatt, L. A. Duncanson, *J. Chem. Soc.* **1953**, 2939–2947.

- [82] G. Frenking, N. Fröhlich, *Chem. Rev.* **2000**, *100*, 717–774.
- [83] B. Giovanni, B. Leonardo, T. Francesco, *Angew. Chemie Int. Ed.* **2013**, *52*, 11599–11602.
- [84] G. Bistoni, S. Rampino, N. Scafuri, G. Ciancaleoni, D. Zuccaccia, L. Belpassi, F. Tarantelli, *Chem. Sci.* **2016**, *7*, 1174–1184.
- [85] W. Scherer, G. S. McGrady, *Angew. Chemie - Int. Ed.* **2004**, *43*, 1782–1806.
- [86] Q. Lu, F. Neese, G. Bistoni, *Angew. Chemie Int. Ed.* **2018**, DOI 10.1002/anie.201801531.
- [87] F. London, *Zeitschrift für Phys.* **1930**, *63*, 245–279.
- [88] R. Eisenschitz, F. London, *Zeitschrift für Phys.* **1930**, *60*, 491–527.
- [89] G. Stefan, S. P. R., *Angew. Chemie Int. Ed.* **2011**, *50*, 12639–12642.
- [90] W. J. Philipp, S. P. R., *Angew. Chemie Int. Ed.* **2015**, *54*, 12274–12296.
- [91] S. Rosel, C. Balestrieri, P. R. Schreiner, *Chem. Sci.* **2017**, *8*, 405–410.
- [92] D. J. Liptrot, P. P. Power, *Nat. Rev. Chem.* **2017**, *1*, 4.
- [93] O. Eisenstein, Y. Jean, *J. Am. Chem. Soc.* **1985**, *107*, 1177–1186.
- [94] G. Ujaque, A. C. Cooper, F. Maseras, O. Eisenstein, K. G. Caulton, *J. Am. Chem. Soc.* **1998**, *120*, 361–365.
- [95] A. C. Cooper, E. Clot, J. C. Huffman, W. E. Streib, F. Maseras, O. Eisenstein, K. G. Caulton, *J. Am. Chem. Soc.* **1999**, *121*, 97–106.
- [96] A. Demolliens, Y. Jean, O. Eisenstein, *Organometallics* **1986**, *5*, 1457–1464.
- [97] A. Haaland, W. Scherer, K. Ruud, G. S. McGrady, A. J. Downs, O. Swang, *J. Am. Chem. Soc.* **1998**, *120*, 3762–3772.
- [98] H. C. Brown, *Tetrahedron* **1961**, *12*, 117–138.
- [99] K. H. Den Haan, J. L. De Boer, J. H. Teuben, A. L. Spek, B. Kojic-Prodic, G. R. Hays, R. Huis, *Organometallics* **1986**, *5*, 1726–1733.
- [100] S. H. Yang, W. H. Jo, S. K. Noh, *J. Chem. Phys.* **2003**, *119*, 1824–1837.
- [101] E. D. Brady, D. L. Clark, J. C. Gordon, P. J. Hay, D. W. Keogh, R. Poli, B. L. Scott, J. G. Watkin, *Inorg. Chem.* **2003**, *42*, 6682–6690.
- [102] D. L. Davies, S. M. A. Donald, O. Al-Duaij, J. Fawcett, C. Little, S. A. Macgregor, *Organometallics* **2006**, *25*, 5976–5978.
- [103] M. Roger, N. Barros, T. Arliguie, P. Thuéry, L. Maron, M. Ephritikhine, *J. Am. Chem. Soc.* **2006**, *128*, 8790–8802.
- [104] V. Montiel-Palma, M. A. Munoz-Hernandez, T. Ayed, J.-C. Barthelat, M. Grellier, L. Vendier, S. Sabo-Etienne, *Chem. Commun.* **2007**, 3963–3965.
- [105] D. L. Clark, J. C. Gordon, P. J. Hay, R. L. Martin, R. Poli, *Organometallics* **2002**, *21*, 5000–5006.
- [106] L. Perrin, L. Maron, O. Eisenstein, M. F. Lappert, *New J. Chem.* **2003**, *27*, 121–127.
- [107] X. Solans-Monfort, O. Eisenstein, *Polyhedron* **2006**, *25*, 339–348.
- [108] A. Poater, X. Solans-Monfort, E. Clot, C. Coperet, O. Eisenstein, *Dalt. Trans.* **2006**, 3077–3087.

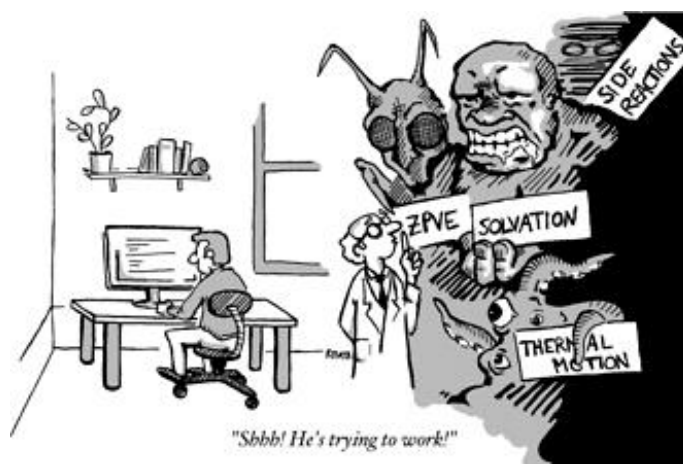
- [109] P. L. A. Popelier, G. Logothetis, *J. Organomet. Chem.* **1998**, *555*, 101–111.
- [110] E.-L. Zins, B. Silvi, M. E. Alikhani, *Phys. Chem. Chem. Phys.* **2015**, *17*, 9258–9281.
- [111] R. F. W. Bader, *Atoms in Molecules A Quantum Theory*, **1995**.
- [112] A. D. Becke, K. E. Edgecombe, *J. Chem. Phys.* **1990**, *92*, 5397–5403.
- [113] J. F. Hartwig, *J. Am. Chem. Soc.* **2016**, *138*, 2–24.
- [114] B. G. Shul'pin, *Catal.* **2016**, *6*, DOI 10.3390/catal6040050.
- [115] H. M. L. Davies, D. Morton, *J. Org. Chem.* **2016**, *81*, 343–350.
- [116] R. Abegg, *Zeitschrift für Anorg. Chemie* **1904**, *39*, 330–380.
- [117] G. N. Lewis, *J. Am. Chem. Soc.* **1916**, *38*, 762–785.
- [118] G. Rayner-Canham, T. Overton, *Descriptive Inorganic Chemistry*, W. H. Freeman & Co, **2015**.
- [119] D. Hnyk, M. L. Mckee, *Boron: The Fifth Element*, Springer, **2015**.
- [120] G. Urry, T. Wartik, R. E. Moore, H. I. Schlesinger, *J. Am. Chem. Soc.* **1954**, *76*, 5293–5298.
- [121] P. Ceron, A. Finch, J. Frey, J. Kerrigan, T. Parsons, G. Urry, H. I. Schlesinger, *J. Am. Chem. Soc.* **1959**, *81*, 6368–6371.
- [122] A. K. Holliday, A. G. Massey, *Chem. Rev.* **1962**, *62*, 303–318.
- [123] J. A. Morrison, *Chem. Rev.* **1991**, *91*, 35–48.
- [124] R. S. Mulliken, *Science* **1967**, *157*, 13–24.
- [125] I. A. I. Mkhalid, J. H. Barnard, T. B. Marder, J. M. Murphy, J. F. Hartwig, *Chem. Rev.* **2010**, *110*, 890–931.
- [126] J. F. Hartwig, *Chem. Soc. Rev.* **2011**, *40*, 1992–2002.
- [127] K. Burgess, M. J. Ohlmeyer, *Chem. Rev.* **1991**, *91*, 1179–1191.
- [128] T. Ishiyama, N. Matsuda, N. Miyaura, A. Suzuki, *J. Am. Chem. Soc.* **1993**, *115*, 11018–11019.
- [129] R. T. Baker, P. Nguyen, T. B. Marder, S. A. Westcott, *Angew. Chemie Int. Ed. English* **1995**, *34*, 1336–1338.
- [130] H. C. Brown, S. K. Gupta, *J. Am. Chem. Soc.* **1971**, *93*, 4062–4063.
- [131] E. Negishi, H. C. Brown, *Synthesis (Stuttg)*. **1972**, 197–199.
- [132] H. C. Brown, S. K. Gupta, *J. Am. Chem. Soc.* **1975**, *97*, 5249–5255.
- [133] C. M. Vogels, S. A. Westcott, *Curr. Org. Chem.* **2005**, *9*, 687–699.
- [134] N. Miyaura, A. Suzuki, *Chem. Rev.* **1995**, *95*, 2457–2483.
- [135] D. S. Matteson, *Stereodirected Synthesis with Organoboranes*, Springer, **1995**.
- [136] H. Braunschweig, *Angew. Chemie Int. Ed.* **2007**, *46*, 1946–1948.
- [137] L. Dang, Z. Lin, T. B. Marder, *Chem. Commun.* **2009**, 3987–3995.
- [138] M. Yamashita, *Angew. Chemie Int. Ed.* **2010**, *49*, 2474–2475.
- [139] J. Cid, H. Gulyas, J. J. Carbo, E. Fernandez, *Chem. Soc. Rev.* **2012**, *41*, 3558–3570.
- [140] A. B. Cuenca, R. Shishido, H. Ito, E. Fernández, *Chem. Soc. Rev.* **2017**, *46*, 415–430.
- [141] H. Nöth, G. Schmid, *Angew. Chemie Int. Ed. English* **1963**, *2*, 623.

-
- [142] H. Braunschweig, *Angew. Chemie Int. Ed.* **1998**, *37*, 1786–1801.
- [143] G. J. Irvine, M. J. G. Lesley, T. B. Marder, N. C. Norman, C. R. Rice, E. G. Robins, W. R. Roper, G. R. Whittell, L. J. Wright, *Chem. Rev.* **1998**, *98*, 2685–2722.
- [144] R. T. Baker, D. W. Ovenall, J. C. Calabrese, S. A. Westcott, N. J. Taylor, I. D. Williams, T. B. Marder, *J. Am. Chem. Soc.* **1990**, *112*, 9399–9400.
- [145] M. Wagner, N. J. R. van Eikema Hommes, H. Noeth, P. v. R. Schleyer, *Inorg. Chem.* **1995**, *34*, 607–614.
- [146] Y. Segawa, M. Yamashita, K. Nozaki, *Science* **2006**, *314*, 113–115.
- [147] Y. Segawa, Y. Suzuki, M. Yamashita, K. Nozaki, *J. Am. Chem. Soc.* **2008**, *130*, 16069–16079.
- [148] M. Yamashita, Y. Suzuki, Y. Segawa, K. Nozaki, *J. Am. Chem. Soc.* **2007**, *129*, 9570–9571.
- [149] J. Cid, J. J. Carbó, E. Fernández, *Chem. - A Eur. J.* **2012**, *18*, 12794–12802.
- [150] K. Takahashi, T. Ishiyama, N. Miyaura, *Chem. Lett.* **2000**, *29*, 982–983.
- [151] K. Takahashi, T. Ishiyama, N. Miyaura, *J. Organomet. Chem.* **2001**, *625*, 47–53.
- [152] H. Ito, H. Yamanaka, J. Tateiwa, A. Hosomi, *Tetrahedron Lett.* **2000**, *41*, 6821–6825.
- [153] L. Dang, Z. Lin, T. B. Marder, *Organometallics* **2008**, *27*, 4443–4454.
- [154] S. Onozawa, M. Tanaka, *Organometallics* **2001**, *20*, 2956–2958.
- [155] J. Zhu, Z. Lin, T. B. Marder, *Inorg. Chem.* **2005**, *44*, 9384–9390.
- [156] Y. Segawa, M. Yamashita, K. Nozaki, *Angew. Chemie Int. Ed.* **2007**, *46*, 6710–6713.
- [157] M. Yamashita, K. Nozaki, *Pure Appl. Chem.* **2008**, *80*, 1187–1194.
- [158] T. Kajiwara, T. Terabayashi, M. Yamashita, K. Nozaki, *Angew. Chemie Int. Ed.* **2008**, *47*, 6606–6610.
- [159] J. Ramirez, R. Corberan, M. Sanau, E. Peris, E. Fernandez, *Chem. Commun.* **2005**, 3056–3058.
- [160] L. Dang, H. Zhao, Z. Lin, T. B. Marder, *Organometallics* **2008**, *27*, 1178–1186.
- [161] V. Lillo, M. R. Fructos, J. Ramírez, A. A. C. Braga, F. Maseras, M. M. Díaz-Requejo, P. J. Pérez, E. Fernández, *Chem. - A Eur. J.* **2007**, *13*, 2614–2621.
- [162] H. R. Kim, I. G. Jung, K. Yoo, K. Jang, E. S. Lee, J. Yun, S. U. Son, *Chem. Commun.* **2010**, *46*, 758–760.
- [163] H. Jang, A. R. Zhugralin, Y. Lee, A. H. Hoveyda, *J. Am. Chem. Soc.* **2011**, *133*, 7859–7871.
- [164] D. S. Laitar, P. Müller, J. P. Sadighi, *J. Am. Chem. Soc.* **2005**, *127*, 17196–17197.
- [165] H. Zhao, Z. Lin, T. B. Marder, *J. Am. Chem. Soc.* **2006**, *128*, 15637–15643.
- [166] C. Kleeberg, L. Dang, Z. Lin, T. B. Marder, *Angew. Chemie Int. Ed.* **2009**, *48*, 5350–5354.
- [167] D. S. Laitar, E. Y. Tsui, J. P. Sadighi, *J. Am. Chem. Soc.* **2006**, *128*, 11036–11037.
- [168] H. Zhao, L. Dang, T. B. Marder, Z. Lin, *J. Am. Chem. Soc.* **2008**, *130*, 5586–5594.
- [169] J.-E. Lee, J. Kwon, J. Yun, *Chem. Commun.* **2008**, 733–734.
- [170] H. Ito, C. Kawakami, M. Sawamura, *J. Am. Chem. Soc.* **2005**, *127*, 16034–16035.
-

- [171] H. Ito, Y. Sasaki, M. Sawamura, *J. Am. Chem. Soc.* **2008**, *130*, 15774–15775.
- [172] C.-T. Yang, Z.-Q. Zhang, H. Tajuddin, C.-C. Wu, J. Liang, J.-H. Liu, Y. Fu, M. Czyzewska, P. G. Steel, T. B. Marder, et al., *Angew. Chemie Int. Ed.* **2012**, *51*, 528–532.
- [173] T. Terabayashi, T. Kajiwara, M. Yamashita, K. Nozaki, *J. Am. Chem. Soc.* **2009**, *131*, 14162–14163.
- [174] L. M. A. Saleh, K. H. Birjkumar, A. V Protchenko, A. D. Schwarz, S. Aldridge, C. Jones, N. Kaltsoyannis, P. Mountford, *J. Am. Chem. Soc.* **2011**, *133*, 3836–3839.
- [175] S. Li, J. Cheng, Y. Chen, M. Nishiura, Z. Hou, *Angew. Chemie Int. Ed.* **2011**, *50*, 6360–6363.
- [176] P. I. Dalko, L. Moisan, *Angew. Chemie Int. Ed.* **2004**, *43*, 5138–5175.
- [177] A. Berkessel, H. Gröger, *Asymmetric Organocatalysis: From Biomimetic Concepts to Applications in Asymmetric Synthesis*, WILEY-VCH, **2005**.
- [178] D. G. Hall, *Boronic Acids. Preparation and Applications in Organic Synthesis and Medicine*, Wiley-VCH, **2005**.
- [179] K. Lee, A. R. Zhugralin, A. H. Hoveyda, *J. Am. Chem. Soc.* **2009**, *131*, 7253–7255.
- [180] A. Bonet, H. Gulyás, E. Fernández, *Angew. Chemie* **2010**, *122*, 5256–5260.
- [181] C. Pubill-Ulldemolins, A. Bonet, C. Bo, H. Gulyás, E. Fernández, *Chem. - A Eur. J.* **2012**, *18*, 1121–1126.
- [182] A. Bonet, C. Pubill-Ulldemolins, C. Bo, H. Gulyás, E. Fernández, *Angew. Chemie Int. Ed.* **2011**, *50*, 7158–7161.
- [183] D. A. Singleton, C. Hang, M. J. Szymanski, M. P. Meyer, A. G. Leach, K. T. Kuwata, J. S. Chen, A. Greer, C. S. Foote, K. N. Houk, *J. Am. Chem. Soc.* **2003**, *125*, 1319–1328.
- [184] D. H. Ess, S. E. Wheeler, R. G. Iafe, L. Xu, N. Çelebi-Ölçüm, K. N. Houk, *Angew. Chemie Int. Ed.* **2008**, *47*, 7592–7601.
- [185] N. F. Pelz, A. R. Woodward, H. E. Burks, J. D. Sieber, J. P. Morken, *J. Am. Chem. Soc.* **2004**, *126*, 16328–16329.
- [186] A. R. Woodward, H. E. Burks, L. M. Chan, J. P. Morken, *Org. Lett.* **2005**, *7*, 5505–5507.
- [187] N. Miralles, J. Cid, A. B. Cuenca, J. J. Carbó, E. Fernández, *Chem. Commun.* **2015**, *51*, 1693–1696.
- [188] A. B. Cuenca, N. Zigon, V. Duplan, M. Hoshino, M. Fujita, E. Fernández, *Chem. – A Eur. J.* **2016**, *22*, 4723–4726.
- [189] T. P. Blaisdell, T. C. Caya, L. Zhang, A. Sanz-Marco, J. P. Morken, *J. Am. Chem. Soc.* **2014**, *136*, 9264–9267.
- [190] Y. Nagashima, K. Hirano, R. Takita, M. Uchiyama, *J. Am. Chem. Soc.* **2014**, *136*, 8532–8535.
- [191] K. Nagao, H. Ohmiya, M. Sawamura, *Org. Lett.* **2015**, *17*, 1304–1307.
- [192] A. Morinaga, K. Nagao, H. Ohmiya, M. Sawamura, *Angew. Chemie Int. Ed.* **2015**, *54*, 15859–15862.
- [193] T. Hata, H. Kitagawa, H. Masai, T. Kurahashi, M. Shimizu, T. Hiyama, *Angew. Chemie* **2001**, *113*, 812–814.
- [194] H. Asakawa, K.-H. Lee, Z. Lin, M. Yamashita, *Nat. Commun.* **2014**, *5*, 4245.

- [195] K. Oshima, T. Ohmura, M. Suginome, *Chem. Commun.* **2012**, *48*, 8571–8573.
- [196] G. Wang, H. Zhang, J. Zhao, W. Li, J. Cao, C. Zhu, S. Li, *Angew. Chemie Int. Ed.* **2016**, *55*, 5985–5989.
- [197] H. G. Viehe, Z. Janousek, R. Merenyi, L. Stella, *Acc. Chem. Res.* **1985**, *18*, 148–154.
- [198] F. Bures, *RSC Adv.* **2014**, *4*, 58826–58851.
- [199] J. D. Buynak, B. Geng, *Organometallics* **1995**, *14*, 3112–3115.
- [200] M. Shimizu, H. Kitagawa, T. Kurahashi, T. Hiyama, *Angew. Chemie Int. Ed.* **2001**, *40*, 4283–4286.
- [201] M. Shimizu, T. Kurahashi, H. Kitagawa, T. Hiyama, *Org. Lett.* **2003**, *5*, 225–227.
- [202] M. Shimizu, T. Kurahashi, H. Kitagawa, K. Shimono, T. Hiyama, *J. Organomet. Chem.* **2003**, *686*, 286–293.
- [203] M. Murakami, I. Usui, M. Hasegawa, T. Matsuda, *J. Am. Chem. Soc.* **2005**, *127*, 1366–1367.
- [204] V. K. Aggarwal, M. Binanzer, M. C. de Ceglie, M. Gallanti, B. W. Glasspoole, S. J. F. Kendrick, R. P. Sonawane, A. Vázquez-Romero, M. P. Webster, *Org. Lett.* **2011**, *13*, 1490–1493.
- [205] H. Ito, Y. Horita, E. Yamamoto, *Chem. Commun.* **2012**, *48*, 8006–8008.
- [206] M. Suginome, T. Fukuda, H. Nakamura, Y. Ito, *Organometallics* **2000**, *19*, 719–721.
- [207] A. Matsumoto, Y. Ito, *J. Org. Chem.* **2000**, *65*, 5707–5711.
- [208] R. H. Cragg, M. F. Lappert, B. P. Tilley, *J. Chem. Soc.* **1964**, 2108–2115.
- [209] R. Jefferson, M. F. Lappert, B. Prokai, B. P. Tilley, *J. Chem. Soc. A Inorganic, Phys. Theor.* **1966**, 1584–1590.
- [210] B. Singaram, *Heteroat. Chem.* **1992**, *3*, 245–249.
- [211] B. Thiele, P. Schreyer, U. Englert, P. Paetzold, R. Boese, B. Wrackmeyer, *Chem. Ber.* **1991**, *124*, 2209–2216.
- [212] C. Solé, E. Fernández, *Angew. Chemie Int. Ed.* **2013**, *52*, 11351–11355.
- [213] M. Kaaz, J. Bender, D. Forster, W. Frey, M. Nieger, D. Gudat, *Dalt. Trans.* **2014**, *43*, 680–689.
- [214] E. N. Daley, C. M. Vogels, S. J. Geier, A. Decken, S. Doherty, S. A. Westcott, *Angew. Chemie Int. Ed.* **2015**, *54*, 2121–2125.
- [215] C. Sole, H. Gulyas, E. Fernandez, *Chem. Commun.* **2012**, *48*, 3769–3771.
- [216] M. G. Civit, X. Sanz, C. M. Vogels, J. D. Webb, S. J. Geier, A. Decken, C. Bo, S. A. Westcott, E. Fernández, *J. Org. Chem.* **2015**, *80*, 2148–2154.
- [217] M. G. Civit, X. Sanz, C. M. Vogels, C. Bo, S. A. Westcott, E. Fernández, *Adv. Synth. Catal.* **2015**, *357*, 3098–3103.
- [218] M. G. Civit, J. Royes, C. M. Vogels, S. A. Westcott, A. B. Cuenca, E. Fernández, *Org. Lett.* **2016**, *18*, 3830–3833.
- [219] X. Sanz, C. M. Vogels, A. Decken, C. Bo, S. A. Westcott, E. Fernandez, *Chem. Commun.* **2014**, *50*, 8420–8423.

Modeling with computational chemistry



Reproduced with permission from: R. A. Mata and M. A. Suhm, *Angew. Chemie Int. Ed.*, 2017, 56, 11011–11018.

*Truth, in science, can be defined as the working hypothesis
best fitted to open the way to the next better one.*

— Konrad Lorenz —

A computer is like a horse, it will sense weakness.

— Greg Wettstein —

To err is human - and to blame it on a computer is even more so.

— Robert Orben —

UNIVERSITAT ROVIRA I VIRGILI
COMPUTATIONAL MODELING TO EXPLORE UNCONVENTIONAL REACTIVITY PATTERNS IN C-H ACTIVATION
AND BORON CHEMISTRY
Diego García López

2. Modeling with computational chemistry

2.1. Evolution of computational chemistry

Last century provided undeniably the greatest revolutions and breakthroughs in the way that humankind understands nature. Regarding the physics domain, in 1926 Erwin Schrödinger formulated an equation^[1] that profoundly shocked our vision of the microscopic world and laid the groundwork for the quantum mechanics theory development, which is extensively used in different modern science fields. Despite its initial detractors,^[2] quantum mechanics (QM) proved –and keeps on proving– to be a reliable and foolproof theory.^[3,4] In fact, just three years after the appearance of Schrödinger’s equation Paul Dirac wrote:^[5]

“The general theory of quantum mechanics is now almost complete, [...]. The underlying physical laws necessary for the mathematical theory of a large part of physics and the whole of chemistry are thus completely known, and the difficulty is only that the exact application of these equations leads to equations much too complicated to be soluble. It therefore becomes desirable that approximate practical methods of applying quantum mechanics should be developed, which can lead to an explanation of the main features of complex atomic systems without too much computation.”

Hence, because of the inherent problematic involved in dealing with a multiple body system, the generated equations cannot be solved analytically and iterative numerical calculations must be performed. Therefore, further improvements of quantum mechanics aimed to develop approximated solutions of the many-electron Schrödinger’s equation^[1] (or Dirac-Coulomb equation^[6,7] in the case when relativistic effects are considered) by simplifying the entailed mathematical treatment. Even though, the huge number of operations needed to achieve any result required the help of computers to endure such tiresome task. Unfortunately, since these calculations comprise complicated algorithms they demand high computing resources, so affordable systems to be studied have always been dependent on the available hardware.

Nowadays, electronic structure calculations have become omnipresent. The rapid progress undergone in computing technology allows theoretical chemists to carry more calculations per time fraction,^[8] which can be translated into the study of larger systems and longer timescales (in dynamic time-evolution processes) while preserving the accuracy displayed by high-performance quantum methods. However, it should be beard in mind that electronic structure proceedings are just a *modus operandi* to understand the microscopic world, instead

of consider them as quantitative-data providers. We tend to elucidate the intricate physical phenomena ruling the world by simplifying the problem into model systems that we can comprehend. Thus, in order to guarantee a fruitful interplay, this discipline always has to be benchmarked with experimental results to evolve into better working hypotheses.

2.2. Density Functional Theory

Since its formal conception in 1964-1965, *Density Functional Theory* (DFT)^[9] has become the most popular method for electronic structure calculations in computational chemistry and physics. This fact might be due to the elegant and simple hypothesis that lays the foundation of this framework (and the efficient computing implementation done). Indeed, its basic premise states that “*all the intricate motions and pair correlations in a many-electron system are somehow contained in the total electron density alone*”.^[10] To put it in a nutshell, if the electronic density function along the spatial coordinates is known, a functional can be applied to obtain the energy of the system. Although this idea may seem naive, the results offered against its low computational cost are surprisingly accurate. Still, many theoreticians continue on striving to improve some stumbling blocks of this methodology in order to broaden its applicability systems. In 1998, due to the enormous growing usage of this tool and the revolution that it caused to computational sciences, the Swedish academy decided to award Walter Kohn (considered the father of DFT) with the Nobel Prize for his contribution in developing this theory.^[11] Nevertheless, before reaching this point, many previous contributions paved the way for this success.

Just after the appearance of Schrödinger’s equation in 1926 (eq. 2.1),^[1] hypotheses to approximate and accelerate the calculation of the many-body systems energy began to emerge. One of the most employed by quantum chemistry is the Born-Oppenheimer approximation,^[12] which was proposed in 1927 by Max Born and Robert Oppenheimer and is still indispensable nowadays. This assumption considers that electrons instantly adjust to changes in nuclear positions due to the much greater mass of nuclei with respect to electrons, permitting the motion of them to be non-correlated. In mathematical terms, it enables the wave-function of a molecule to be split into its electronic and nuclear components (eq. 2.2). For general purposes, the Born-Oppenheimer approximation is considered valid and will be henceforward taken in consideration.

$$\hat{H}\Psi = E\Psi \quad (2.1)$$

$$\Psi(\mathbf{r},\mathbf{R}) = \psi_{el}(\mathbf{r}) \times \psi_{nuc}(\mathbf{R}) \quad (2.2)$$

The origins of DFT also accounted with the contributions of Llewellyn Thomas^[13] and Enrico Fermi,^[14,15] who in 1927 and 1928 created the Thomas-Fermi model. In this framework, the electrons are regarded as an homogeneous gas satisfying the Fermi statistics (called fermion particles) and the interaction energy between them is determined from the classical Coulomb potential. Unfortunately, this theory has severe deficiencies because of its poor description of the outer regions of an atom. For instance, the charge density decays as radius to the power of six (r^6) far from the nucleus, rather than exponentially as it is expected.

At the same time, in a second line of approach, a method for calculating the Schrödinger's wave-function of an atom was developed by Douglas Hartree,^[16,17] who introduced the idea of a *self-consistent field*. In this methodology, the wave-function of an electron (ψ_i) is determined from the external mean field of the nucleus and the other electrons in a self-consistent way. In other words, one starts with an approximate field (such as one derived using the Thomas-Fermi (TF) approximation) and iterates until input and output fields for all electrons are the same. The wave-function of the N -electron system can be approximated by the product of N single-particle functions, as follows:

$$\Psi(\mathbf{r}_1, \mathbf{r}_2, \dots, \mathbf{r}_N) = \psi_1(\mathbf{r}_1)\psi_2(\mathbf{r}_2)\cdots\psi_N(\mathbf{r}_N) \quad (2.3)$$

where each $\psi_i(\mathbf{r}_i)$ in eq. 2.3 satisfies a one-electron Schrödinger equation (eq. 2.1) with a potential term arising from the average field of the other electrons. A couple of years later, in 1930, Vladimir Fock^[18] and John Slater^[19] replaced eq. 2.3 by a determinant of such functions (eq. 2.4). This transformation led to equations accounting antisymmetric behavior of electrons while satisfying the exclusion principle formulated by Wolfgang Pauli.^[20] These determinantal functions, known today as *Slater determinants*, and the resulting *Hartree-Fock equations* form the basis of what is called the *Wave-Function Theory* (WFT).

$$\Psi(\mathbf{r}_1, \mathbf{r}_2, \dots, \mathbf{r}_N) = \frac{1}{\sqrt{N!}} \begin{vmatrix} \psi_1(\mathbf{r}_1) & \psi_2(\mathbf{r}_1) & \cdots & \psi_N(\mathbf{r}_1) \\ \psi_1(\mathbf{r}_2) & \psi_2(\mathbf{r}_2) & \cdots & \psi_N(\mathbf{r}_2) \\ \vdots & \vdots & \ddots & \vdots \\ \psi_1(\mathbf{r}_N) & \psi_2(\mathbf{r}_N) & \cdots & \psi_N(\mathbf{r}_N) \end{vmatrix} \quad (2.4)$$

Soon after that in the same year, Paul Dirac realized about the possibility of incorporating the exchange interaction of fermions into Thomas-Fermi model. That meant to refurbish Hartree-Fock theory in terms of a density function, without reference to a single-determinant many-electron wave-function. However, the resulting Thomas-Fermi-Dirac theory (TFD)^[21] failed qualitatively as consequence of adopting a local density approximation for the kinetic term of the total energy.

The breakthrough finally took place in 1964 when Pierre Hohenberg and Walter Kohn developed two theorems and proved that only electron density at spatial points is sufficient to fully characterize the ground state of a many-electron system.^[22] The first theorem states that *“for any system of interacting particles in an external potential $V_{ext}(\mathbf{r})$, the density is uniquely determined”*. In other words, the external potential is a unique functional of the density. The second theorem asserts that *“a universal functional for the energy $E[\rho]$ can be defined in terms of the density; the exact ground state is the global minimum value of this functional”*, which can be interpreted as a reformulation of the variational principle,^[23] that guarantees a solution of minimum energy for the ground state. Although these theorems confirm the existence of a functional having a one-to-one correspondence between the system energy and its electronic density, they do not provide any information about how this functional has to look like.

Nonetheless, the biggest attainment in DFT came in 1965 by Walter Kohn himself and Lu Sham.^[24] They described a practical formalism to calculate the exact many-body energy with a fictitious one-electron system whose energies are functionals of the electron density (eq. 2.5):

$$E[\rho(\mathbf{r})] = T_0[\rho(\mathbf{r})] + \int \rho(\mathbf{r})[v_{ext}(\mathbf{r}) + u_{el}(\mathbf{r})]d\mathbf{r} + E_{xc}[\rho(\mathbf{r})] \quad (2.5)$$

$$v_{ext}(\mathbf{r}) = \sum_i \frac{-Z_i}{|\mathbf{R}_i - \mathbf{r}|} \quad (2.6)$$

$$u_{el}(\mathbf{r}) = \frac{1}{2} \int \frac{\rho(\mathbf{r}')}{|\mathbf{r}' - \mathbf{r}|} d\mathbf{r}' \quad (2.7)$$

$$E_{xc}[\rho(\mathbf{r})] = E_x[\rho(\mathbf{r})] + E_c[\rho(\mathbf{r})] \quad (2.8)$$

The first term in eq. 2.5 refers to the kinetic energy of electrons in a system which has the same density ρ as the real system, but in which there is no electron-electron interactions. It is the so-called system of *non-interacting* electrons, but this concept may be misunderstood due to the fact that electrons still interact with nuclei. The second expression (eq. 2.6) regards the external potential coming from nuclei corresponding to the interaction energy between electron and nucleus, while the third equation (eq. 2.7) accounts for the classical coulombic electron-electron repulsion effect. Finally, the last addend in eq. 2.5 consists of the exchange-correlation functional (eq. 2.8), which is unknown and includes all the energy contributions which were not contemplated by the previous equations. Indeed, this term is concerned in correcting the previous approximations since a many-electron system pretends to be treated as a many-one-electron problem. In other words, this functional is aimed to correct all the things that were “swept under the carpet”. The phenomena that were not addressed and

have to be considered comprise: *i*) electron exchange (short-range repulsion between electrons with parallel spins); *ii*) electron correlation (non-interacting electrons do need to correlate their movements); *iii*) the portion of the kinetic energy needed to obtain the true kinetic energy of the system; *iv*) and the correction for the electron self-interaction introduced by the classical coulomb potential (the one-electron simplification mimics the electron-electron repulsion of the many-electron system, thus an electron interacts with itself in a repulsive manner).

The Kohn-Sham formalism (KS) also considered a single Slater determinant of orthonormal orbitals ψ_i with total density,

$$\rho(\mathbf{r}) = \sum_{i=1}^N |\varphi_i^{KS}(\mathbf{r})|^2 \quad (2.9)$$

Regrouping all potentials together (eq. 2.11) and minimizing eq. 2.10 with respect to the orbitals φ_i yields the Kohn-Sham orbital equation (eq. 2.12):

$$E[\rho(\mathbf{r})] = \quad (2.10)$$

$$= \sum_{i=1}^N \left\langle \varphi_i^{KS}(\mathbf{r}) \left| -\frac{1}{2} \nabla^2 \right| \varphi_i^{KS}(\mathbf{r}) \right\rangle + \int \rho(\mathbf{r}) v_{ext}(\mathbf{r}) d\mathbf{r} + \int \rho(\mathbf{r}) u_{el}(\mathbf{r}) d\mathbf{r} + E_{xc}[\rho(\mathbf{r})]$$

$$v_{eff} = v_{ext} + u_{el} + \frac{\delta E_{xc}[\rho(\mathbf{r})]}{\delta \rho(\mathbf{r})} \quad (2.11)$$

$$\left[-\frac{1}{2} \nabla_i^2 + v_{eff} \right] \varphi_i^{KS}(\mathbf{r}) = \epsilon_i \varphi_i^{KS}(\mathbf{r}) \quad (2.12)$$

The resulting Kohn-Sham equation (eq. 2.12) recasts the Schrödinger equation problem of interacting electrons moving in an *external* potential into a problem of non-interacting electrons moving in an *effective* potential. Such statement implies that every electron is affected by the same effective potential (v_{eff}), thus making a huge difference with respect to the Hartree-Fock formalism where the potential contained is *nonlocal*, which means that every electron is affected by a different potential. In addition, formally the Kohn-Sham orbitals and energies are artifacts with no real physical significance since the description of the system as a collection of single particles is incorrect. Curiously enough, however, Kohn-Sham orbitals have proven to give quite accurate descriptions of band structures and bonding characters. This fact led to an investigation to rationalize such finding and whether if those orbitals carry any significance.^[25] Interestingly, the shape and symmetry properties of the Kohn-Sham orbitals have been found to be very similar to those calculated by Hartree-Fock. Anyhow, it

has to be beard in mind that the Kohn-Sham framework features a one-unique-electron potential that carries all correlation information within it, and Kohn-Sham orbitals are one-electron orbitals that are *density* optimal (as opposed to Hartree-Fock orbitals, which are *energy* optimal).

If the exact form of the exchange-correlation functional was known, the Kohn-Sham approach would give the exact energy. Consequently, the development of DFT is oriented on the improvement of this functional to describe energetics and molecular structures more accurately within the framework of the Kohn-Sham method. This has resulted in a plethora of functionals currently available, but at the same time their degree of faithfulness is often dependent on the molecular system or electronic properties studied. This is why some theoreticians consider the DFT method a “semi-empirical” approach, because as the range of applications was increasing new functionals were being developed for handling new incoming problems. Despite of that, it is possible to classify the extensive number of functionals into five major groups.

Local Density Approximation (LDA):

The chronological first step towards the calculation of an exchange-correlation functional was the *Local Density Approximation* (LDA). Several different formulations for this functional have been developed. Probably, the most popular is the Vosko-Wilk-Nusair (VWN).^[26] This procedure constitutes the simplest approach, as essentially assumes implicitly that the exchange-correlation energy at any point of the space is a function of the electronic density at that unique point, and it can be obtained from the electronic density of an homogeneous electron gas of the same density. In addition, the *Local Spin Density Approximation* (LSDA) represents a more general application of this approach by introducing spin dependence into the exchange-correlation functional, thus solving several conceptual concepts. Despite its simplicity, the LDA can offer surprisingly good results. However, that simplicity usually tends to underestimate the atomic energies for the ground state and the ionization energies, while overestimates binding energies and favors high spin state structures. In general, it is a bad approximation for small systems, although results improve as bigger is the size of the system studied, and its performance turns better in systems that have little variations on their electronic density.

Generalized Gradient Approximations (GGA):

Typical molecular systems are generally very different from a homogeneous electron gas. In fact, any real system is non-homogeneous since its electronic density changes along the spatial coordinates. Methods based on the *Generalized Gradient Approximations* (GGA) take into account this phenomenon and correct the approach accordingly. In this perspective, both correlation and exchange energies not only depend on the electron density but also on the gradients of such density. For this reason, functionals belonging to this group are often called *nonlocal* because of the effects incorporated. There exist two different philosophies for the

construction and development of the exchange expression in GGA functionals. The first line of approach is based on numerical fitting procedures involving large molecular training sets, being the Becke 88 (B88)^[27] probably the most famous one. In stark contrast, the second philosophy is more rational-based and considers Quantum Mechanical principles for the generation of such functionals. Perhaps, the best well-established example is the Perdew-Burke-Ernzerhof (PBE).^[28,29] For the correlation functional, several different formulations have been developed. Among them, the most employed are the Perdew 86 (P86),^[30,31] Perdew-Wang 91 (PW91),^[32] and Lee-Yang-Parr (LYP).^[33] In general, GGA methods represent a significant improvement over the *local* methods previously mentioned. They tend to give better structural energy differences and energy barriers.^[34] Moreover, GGA methods tend to expand and soften bonds,^[35,36] compensating for the LDA tendency to overbind.^[37] However, despite the accuracy of GGA methods in giving reliable results for covalent, ionic, metallic, and hydrogen bridge bonds, they typically fail for van der Waals interactions.^[38]

Meta-Generalized Gradient Approximations (m-GGA):

Recently, a new class of functionals was developed by including additional *semilocal* information beyond the first-order density gradient contained in the GGAs. These methods, termed meta-GGA (m-GGA), depend explicitly on higher order density gradients and/or on the kinetic energy density, which involves derivatives of the occupied Kohn-Sham orbitals (*semilocal* interactions). Even the significant improvements displayed by this formulation, these functionals are more technically challenging, with several difficulties in terms of numerical stability. Two of the most used examples belonging to this category of functionals are the TPSS^[39] and the M06-L.^[40]

Hybrid Functionals:

This approach combines the exchange-correlation of a conventional GGA method with a percentage of Hartree-Fock *nonlocal* exchange. This is the reason why there are named *hybrid* functionals. The weight factor for the degree of substitution in the exchange functional is optimized by fitting several processes, such as atomization energies or ionization potentials, to experimental values for a representative set of small molecules.^[41] Undoubtedly, these functionals have become a popular choice for quantum chemistry and are widely used, yet they are not so successful in solid-state physics. Some examples include B3PW91,^[27,32,42] TPSSH,^[43] or the extremely popular B3LYP.^[27,33,42]

Range Separated Functionals:

Traditionally, the treatment of mid- and long-range interactions by DFT offered a poor description. Nevertheless, this class of functionals are aimed to solve this drawback by splitting the electron-electron correlation into two parts, one long-range and the other short-range, to then tackle each part in a different manner. One way to do so is based on the implicit parametrization including some dispersion interactions. Well known examples of this approach are the Minnesota density functionals family.^[44-46] However, it has been argued that

such highly parameterized functionals may lead to numerical instability and artificial minima accounting long-range interactions.^[47] Moreover, the general good description at longer distances displayed by these functionals might result in artifacts in the density picture at shorter distances, probably due to an overparametrization.^[48] On the other hand, there exists another way to deal with long range correlation by adding a dispersion term based on the Becke-Johnson equation,^[49] which includes a damping function for mid- and long-range interactions. The most popular formulation applied to DFT calculations was developed by Stefan Grimme.^[50–52]

In summary, the framework of DFT has undoubtedly marked a milestone in computational chemistry. The wide variety of applications provided by this methodology enables a comprehensive understanding and a detailed prediction of a broad range of chemical, physical, and biological phenomena of great importance. This has been possible due to a great commitment between the computational costs that this method offers against the efficiency displayed, and therefore is normally viewed as an excellent modeling technique for ground-state structures and vibrational frequencies. Nonetheless, when tackling spin-state energetics of open-shell transition metal complexes, DFT performance turns out to be a persistent issue since not known exchange-correlation functional provides a good description. For that purpose, computational chemists have to pay the fee of choosing a suitable functional for obtaining reasonable results in a logical scale of time. Furthermore, although DFT continues to produce ever more accurate energy values (thanks to ongoing method development and refinements), new functionals are failing at correctly predict electron densities.^[53] This drawback might not be a problem for some applications in chemistry and biology in the view of the fact that energies and geometries of molecules are sometimes the most important pieces of information; even though, some modern functionals “may be giving the correct energies for the wrong reason”.^[54] It has been argued that a viable strategy to move forward is a combinatorial approach to develop new functionals that use fewer adjustable parameters than some modern ones use.^[55] In conclusion, DFT is an extremely valuable tool but it must be handle with care.

2.3. Modeling reactivity

Beyond the energy determination of static spatial configuration of a molecule, it is of great usefulness to correlate the energy of the system according to the position of its nuclei. This information is stored in a function named *Hyperpotential Energy Surface*, or simply *Potential Energy Surface* (PES), and it is built by computing the electronic energy for each nuclei’s spatial configuration (Figure 2.1).^[56] Overall, the PES reveals the energy landscape of a particular

chemical system. However, the entire computation of this scenery is only feasible for small systems containing a few atoms. In practice, only key points are considered, named stationary points, featuring a first derivative of the energy with respect to spatial coordinates equal to zero. Among them, only some local minima and first order saddle points are usually taken into account. All second derivatives (collected in the Hessian matrix) are positive for the former, but one negative value is found in the latter. From a chemical perspective, the mathematical description of the PES corresponding to minima can be related to reactants, intermediates and products, which means that the close neighborhood of such regions are of higher energy. The minimum energy path interconnecting these species leads to a first order saddle point and has the singular property of being a minima in all directions of space except one, known as the reaction coordinate. Thus, the height difference between a first order saddle point and a low laying local minima is the amount of potential energy that a stable spatial conformation of a molecule has to overcome in order to reach another stable conformation.

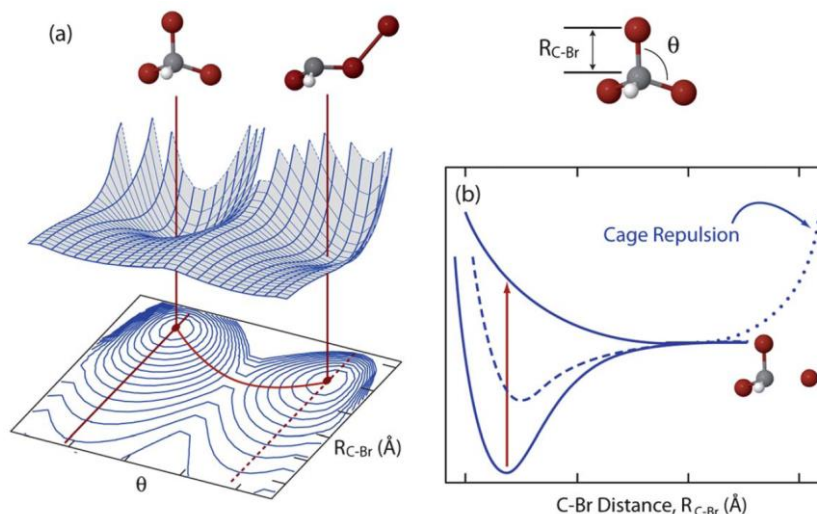


Figure 2.1. a) Sketch of the potential energy surface for ground state bromoform, CHBr₃. The structure in the upper right shows the coordinate system. There is a deep minimum for the bromoform (left) and a shallower minimum for the isomer, iso-bromoform (right). The barrier along the minimum energy path connecting the two lies below the dissociation asymptote. (b) Cuts through the ground-state surface for bromoform and iso-bromoform and through the excited-state surface for bromoform. The dotted curve qualitatively represents the repulsion by the surrounding molecules in solution. Adapted with permission of the publisher from reference [57].

The seek of the previously outlined stationary points is not straightforward,^[58] but its characterization is sufficient to establish a possible detailed route for the transformation of a particular system with no need to know the full shape of the PES. This is called a reaction

mechanism, and it consists on the definition of the elementary steps that take place during a chemical conversion.^[59,60] Recognition of these decisive stages can lead to rationalized design of processes, evading the trial-error approach. Hence, the effort aimed to elucidate and understand a mechanism can establish the guidelines to follow in order to improve a chemical reaction in terms of rate, yield or selectivity.

Nevertheless, despite the determination of suitable stationary points ruling a mechanism, the electronic energy parameter itself is not adequate to describe the chemical evolution in a proper manner. In addition, thermodynamic effects provided by free energy, and more precisely entropic terms, have to be considered since they account for the spontaneity of processes. Therefore, the traits of stationary points in the electronic PES have to be corrected concerning thermal effects, zero-point energies and entropic contributions. Even though, these refinements might not be enough when modeling with implicit solvent and there is a change in the molecularity of the process, due to the fact that associative reactions tend to overestimate free energy barriers whereas dissociative ones tend to underestimate them. Considering that Sackür-Tetrode equation states a situation with an ideal gas system for the calculation of the translational entropy,^[61-65] the accurate calculation of free energy activation barriers in solution is a challenging task so far. Some efforts to improve this nuance began from a tentative strategy, where the computed activation entropy was observed to be half of the experimental measurement.^[66,67] Some years later, in a step forward, the group of George Whitesides designed a free volume model in order to predict translational entropy in solution.^[68] This approach is based on considering the experimental density and the volume of solvent, regardless of the solute employed, thus limiting the space availability for the system to move freely. Since it still seems that there is no consensus to define the best way to correct these deviations in the free energy, it is at least worthwhile to consider the biased entropy values obtained along an energy profile as the upper or bottom limit associated to certain processes. In addition, besides this encumbrance when modeling chemical reactivity, some others obstacles such as an appropriate treatment of solvent effects or conformational mobility of isomers might remain. All in all, it seems that unmasking the principles governing a reaction mechanism by locating its most relevant stationary points is an arduous task, even assuming that the complete form of the PES does not need to be known. The effort and time-consuming resources required to significantly map the immense chemical space of small-to-medium size of organic molecules could make this strategy inefficient.^[69,70]

In conjunction to the former static exploration of the PES through its key points, dynamic methodologies involving time evolution are able to examine the energetic landscape of both atomic coordinates and momenta, offering a broader view of the chemical scenery. However, as a consequence, the sampling enlargement of big systems generally enforces the need to choose a former and less demanding computational method in order to ensure a reasonable time-consuming scale for the modeling process. Over the most popular and used techniques, there is classical *Molecular Dynamics* (MD)^[71] which studies the temporal evolution of systems

typically containing more than a thousand of atoms, for instance, the accommodation of a substrate into a protein active site. Classical MD simulations are exploited to describe noncovalent interactions, since atomic bonds are modeled as fastened albeit movable linkages. As drawback, the use of these methods translates into less accurate calculations but still extensively employed. Nevertheless, the rapid advance of technology and computing resources permitted a crucial improvement of this approach in 1976 by enabling the combination of those molecular mechanics calculations (MM) with *semiempirical* quantum mechanics methods (QM),^[72] giving rise to the hybrid QM/MM framework.^[73,74] Nowadays, the current computing power allows this modeling strategy to carry out more sophisticated QM calculations than those semiempirical ones. Moreover, QM/MM has established as a valuable tool not only for tackling biomolecular systems, but also for large inorganic and organometallic molecules, as well as processes with explicit solvent.^[75]

Alternative dynamic methodologies include quantum mechanics in the treatment of the system and are therefore highly computationally demanding simulations. Among them, *Car-Parrinello Molecular Dynamics* (CPMD) are extensively employed and can be described as the combination of static QM calculations, without fully convergence of the wave function, and classical MD simulations.^[76] Other modeling strategies can be found in *Monte Carlo* simulations, wherein (pseudo)randomly movements made to the configuration of a system generate states that are accepted or rejected in such a way as to obtain a chain of states that samples a well-defined probability distribution.^[77] Nonetheless, it must be pointed out that aforementioned techniques are mainly used when behavior of the system along time is fairly unknown, evading sampling all possible configurations.

Alongside to PES-exploratory techniques, there is an analogous methodology that postulates the existence of relationships between molecular structure and properties that can be derived from that atomic disposition, without the constrain of locating neither intermediates nor transition state species of the process associated. This approach, named *Quantitative Structure-Activity Relationship* (QSAR) or *Quantitative Structure-Property Relationship* (QSPR), was originally employed in biology based on the hypothesis of Corwin Hansch, which states that it is possible to obtain functions correlating numerical information of molecules (descriptors) with the activity or the property of such compounds (response variable).^[78] It is worth to mention that some years before, Hansch and co-workers had already proposed that biological processes could be treated like chemical reactions,^[79] inspired by the pioneering work of Louis Hammett in a quantitative description of substituent effects on organic reaction rates and equilibrium.^[80]

At those early stages, the calculation of descriptors was carried out with experimental techniques, but some years ago computation managed to complement this assignment.^[81] In addition, not only geometrical parameters can be calculated, but also quantities unachievable by experimental measurements such as the energy of the highest occupied molecular orbital; the dipole moment split into its x, y and z components; atomic charges; population of orbitals;

delocalizability; and so on. This fact led to an explosion in number of available descriptors, reaching to an amount over three thousands of different types.^[82] Despite of that, it seems that there is no generally accepted best set of parameters to use in quantitative molecular design, and each process might need its own and unique descriptors to be well-characterized.^[83]

Considering the three dimensional nature of reactivity and catalysis, descriptors traditionally employed have combined both electronic and steric factors (although they are generally somehow correlated). Comprehensive studies of parameters associated with the classic idea of a catalyst composed by a metal center surrounded by ligands have assisted the rationalization and improvement in the performance of such compounds. For instance, following initial and trailbreaking contributions in this field,^[84–86] Chadwick Tolman suggested the use of carbon monoxide as a probing ligand in metal center complexes to measure its stretching frequency, ν_{CO} , in order to estimate the electronic influence of other ligands on that metallic center.^[87] Nonetheless, it is important to highlight that steric effects can have important electronic consequences and vice versa. Therefore, the stretching frequency of carbon monoxide ligand might be affected by the steric crowdedness of the surrounding ligands. Analogously, it is also possible to use geometrical descriptors based on the steric size, which indirectly account for three-dimensionality and include easily-accessible parameters from classical physical organic chemistry, like those originally developed by Robert Taft^[88] and later modified by Marvin Charton.^[89–94] Another popular steric descriptor to gauge the size of a ligand was also proposed by Tolman based on the measure of a cone angle, ϑ , by defining the vertex at a metal center and the atoms at the curved face of the cone (Figure 2.2A).^[87] This descriptor was extensively applied, but the development of more structurally elaborated ligands, such as diphosphines or carbenes, could lead this steric parameter calculations to be meaningless since confinement of these novel ligands inside a cone overestimates their volume from a bad geometrical picture (in other words, the cone angle might be far apart from being homogeneous in all space directions).^[95]

On the road to better define the steric pressure brought about by bulky ligands, Luigi Cavallo and Steven Nolan proposed an alternate model to estimate atomic congestion, the percentage of buried volume, $\%V_{bur}$.^[96] This parameter measures the amount of volume of a sphere centered on the metal, buried by overlap with atoms of the ligand (Figure 2.2A). The volume of this sphere would represent the space around the metal atom that must be shared by the different ligands upon coordination. Therefore, the bulkier a specific ligand, the larger the amount of that sphere will be occupied by such ligand, implying a greater $\%V_{bur}$. This latter descriptor and Tolman's cone angle have been considered as equivalent measures of ligand steric size and used interchangeably in the literature.^[97] Despite this fact, discrepancies can be found, even for monodentate phosphines.^[98] The difference between these two steric parameters can be appreciated through an understanding of the distinct methods each uses to describe ligand size. The buried volume metric emphasizes steric hindrance proximal to the

metal by measuring the volume occupied by the ligand in a sphere of defined radius. By contrast, the cone angle parameter gauges a geometrical figure that encloses all groups of the ligand, regardless their distance from the metal, and is therefore sensitive to ligand size, even at large distances. Because the majority of ligand properties rely on the first coordination sphere, a correlation between the two parameters has been mostly observed; however, this correlation is not fulfilled by definition.

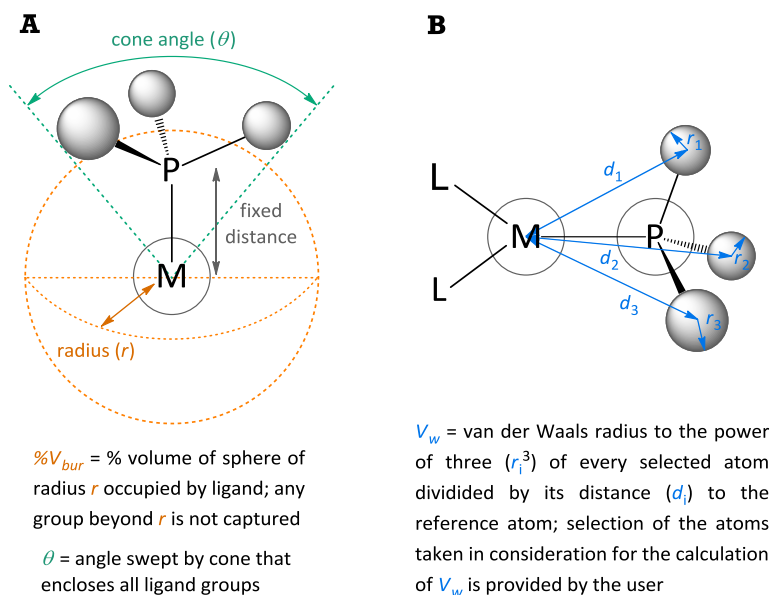


Figure 2.2. Scheme of the steric descriptors capable of measuring the steric impact of ligands attached to a metal center. A) The cone angle descriptor developed by Tolman (θ) and the percentage of buried volume proposed by Cavallo and Nolan ($\%V_{bur}$). B) The distance-weighted volume (V_w) designed by our research group.

As a step forward, we proposed a new molecular descriptor, the distance-weighted volume (V_w), to contribute to the quantification of steric effects (Figure 2.2B). Its calculation entails the selection of a central atom to be placed at the origin of coordinates and choose an element of the ligand to point z axis along that direction. Once the whole molecule is aligned it is possible to quantify the steric encumbrance of the ligand by considering three parameters: *i*) the number of atoms, excluding those which do not want to be taken into account, in the region defined by the alignment process, *ii*) the size of the atom (r = van der Waals radii in Å),^[99] and *iii*) the distance (d) from the atom to the origin of coordinates (in Å). The factor r^3 is divided by d for each atom and the sum is extended to all of the atoms in the given region (eq. 2.13).

$$V_w = \sum_{i=1}^N \frac{r_i^3}{d_i} \quad (2.13)$$

There is a very large variety of different types of molecular descriptors available to explain physicochemical properties and/or biological activities. The range of applications varies from set to set and the ease of interpretation of the different types of parameters might range from the obvious to intricate. However, if we pursue a good prediction of the response variable, if a good prediction of the response variable is pursued, the meaning of a descriptor can be put to the background as long as it provides good results. The need for interpretability of a descriptor depends on the application, but a mathematical model relating some target property to chemical features may be everything that comes into our minds. Of course it would be desirable to be able to attempt some explanation of the relationship between descriptors and response variable in chemical terms, but it is often not necessary, *per se*. Hence, a suitable group of descriptors for a particular study should be chosen considering their accessibility and the nature of the compounds in the data set.

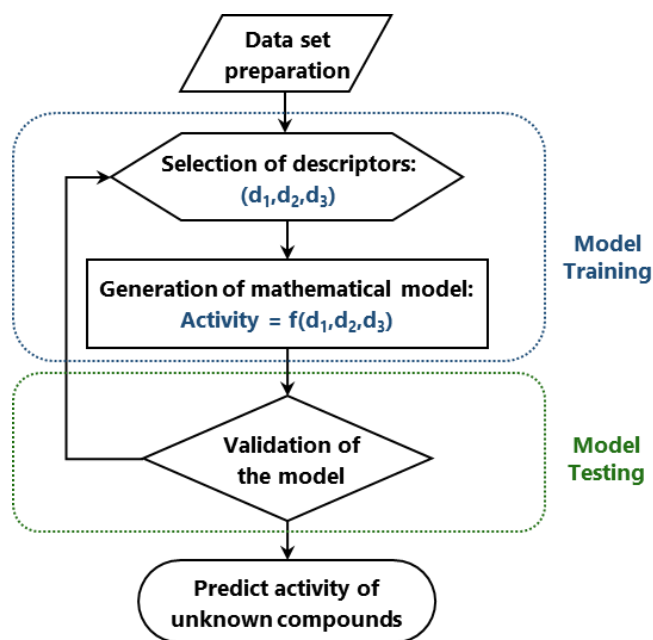


Figure 2.3. Scheme of a QSAR/QSPR development process.

A brief summary of a QSAR/QSPR process is depicted in Figure 2.3. The first stage consists on preparation of a data set of compounds based on the problem that wants to be tackled. Special care should be taken in this part, because a model is as good as the training set used to derive it (this is an inherent feature when modeling, but QSAR/QSPR approach is a tool

conceived for predicting). The second stage comprises the selection of descriptors, which has to account for the size of the training data set in order to avoid overfitting. This error is produced when the model adjusts in high level of agreement with existing data but fails in predicting new results. It is also essential to emphasize that a suitable set of descriptors is crucial for establishing a trustworthy relationship between them and the response variable. The next step of the process deals with the implementation of an appropriate statistical method to derive a robust mathematical correlation involving small to large number of variables. Various techniques are used for this purpose:^[100,101] regression-based techniques are employed when the response data of chemicals are quantitative (entirely numerical), enabling a quantitative prediction of the response (activity/property), while qualitative or semiquantitative chemical responses are modeled using classification-based techniques, allowing categorization (clusterization) of the data points into several groups or classes (such as highly or less active). Finally, the last part includes the test of the mathematical model previously built with compounds that have not been used to construct it aiming to demonstrate its predicting ability (external validation).

In principle, any property of a substance which is dependent on the chemical features of one or more of its constituents could be modeled using the techniques of QSAR/QSPR. Once a correlation between structure and activity or property has been found, compounds can be readily screened on the computer in order to select structures with the desired activity or properties, including those not yet synthesized. Then, it is possible to decide over the most promising compounds to test its validity in the laboratory. Hence, this approach accelerates the process of development of new molecules for use as drugs, materials, additives, or other purposes saving much time and resources. Nowadays, methodologies to map the chemical space are starting to be employed in fields such as homogeneous catalysis for the design of *in silico* novel catalyst^[102–104] (in which a change in their ligands can promote different selectivity ratios) or in chemical synthesis for the evaluation and improvement of already established reactivity.^[105–107] Therefore, generation of databases can lead to a facile, cheap and clean screening. In summary, meaningful foresights can be made with QSAR/QSPR techniques, providing tools to progress into uncharted territory and permitting a full engagement in the procedure of understand, design, test, and predict.

2.4. Electronic structure analysis

Obtaining information about the energy landscape of a chemical or physical reaction through the modification of the involved species is of great importance. Certain transformations within molecules might change key features conducting to a different outcome of a measured

property. This process is not only crucial for optimizing chemical or physical phenomena but also exhibits the beneficial or detrimental influences of such modifications. However, the fact of stockpiling the information resulting from those transformations does not provide any direct answer to the paramount question underlying such changes: why does a given modification lead to particular changes in chemical or physical properties of a system? The reason for that seems to be hidden in the bonding scenario of the molecule, or more precisely, in the distribution of the electron density along the spatial coordinates. Thus, the effort aimed to comprehend and interpret the nature of a chemical structure might lead to qualitative predictions in the response of a system. Once again, theoretical and computational chemistry methods comprise a valuable tool to corroborate past bonding theories while giving deeper insights into the microscopic interactions between atoms. The techniques used for illustrating the electronic description of certain systems are briefly explained below.

2.4.1. Natural Bond Orbitals (NBO)

The ultimate goal of *Natural Bond Orbital* (NBO) theory^[108] is to connect the numerical content stored in either the electronic wave-function or the electronic density of a molecular system with the simple albeit effective concepts of classic Lewis-like bonding theory.^[109] Moreover, the electronic representation supplied by this framework, introduced by Frank Weinhold, is also consistent with semiempirical constructions such as hybridization, electronegativity or resonance. Hence, this formalism constitutes a bridge between former bonding principles and modern electronic analyses, rendering a robust and comprehensible model enhanced by the accuracy of computational calculations.

In the framework of DFT, the electron density ρ of a closed-shell system of N electrons is expressed as a sum of contributions of all the occupied Kohn-Sham molecular orbitals φ_i^{KS} (eq. 2.9), which are delocalized over the entire molecule through linear combinations of atomic-centered basis functions, χ , arising from atomic orbitals (LCAO-MO) (eq. 2.14). The ground state that minimizes the energy of a given geometry is thus associated with a set of optimal coefficients c_{ik} constituting the source of the information to be extracted from a system.

$$\rho(\mathbf{r}) = \sum_{i=1}^N |\varphi_i^{KS}(\mathbf{r})|^2 = \sum_{i=1}^N \sum_{p=1}^M \sum_{q=1}^M c_{ip} c_{iq} \chi_p(\mathbf{r}) \chi_q(\mathbf{r}) a_{pq} \quad (2.14)$$

$$\int \rho(\mathbf{r}) d\mathbf{r} = \sum_{p=1}^M \sum_{q=1}^M a_{pq} \int \chi_p(\mathbf{r}) \chi_q(\mathbf{r}) d\mathbf{r} = \sum_{p=1}^M \sum_{q=1}^M a_{pq} \underbrace{\langle \chi_p(\mathbf{r}) | \chi_q(\mathbf{r}) \rangle}_{S_{pq}} \quad (2.15)$$

The NBO methodology seeks to reinterpret the delocalized electron density of a system in terms of a confined electronic distribution provided by the arrangements of covalent bonds (two-center-two-electron) and lone pairs (one-center-two-electron), recalling the Lewis bonding structure for the molecule under study. Thus, it is necessary a partition scheme capable of switching a three-dimensional Cartesian coordinates into localized domains, each attached to a particular atom. This is achieved in a series of steps, the first of which involves the independent diagonalization of the electron matrix blocks (eq. 2.14) expressed on the atomic orbitals localized only on single atoms, evading contribution of two or more atoms. In other words, just atomic orbitals contributing to the electron density of an individual atom A are considered. This process yields set of *prenatural atomic orbital* (PNAO) with atomic occupation numbers (n_A for atom A) as eigenvalues. The second step transforms the set of PNAO into a set of mutually orthogonal *natural atomic orbitals* (NAO). The occupation numbers n_A of the NAO on a given atom A allow to estimate the charge of such atom following eq. 2.16, which is the basis of natural population analysis (NPA).^[110] Moreover, it is possible to write an effective electronic configuration for each atom in the molecule, including fractional numbers in the population of the atomic shells (for instance, $(1s)^2(2s)^{1.74}(2p)^{4.62}$ could correspond to a bonding situation of an oxygen).

$$q_A = Z_A - \int \rho_A d\mathbf{r} = Z_A - n_A \quad (2.16)$$

The next step splits the NAO on each atom in three distinct sets: the strongly occupied core orbitals ($n \cong 2$), the *natural minimal basis* (NMB) constituted by the valence orbitals, and the remaining strongly empty Rydberg (or virtual) orbitals ($n \cong 0$). The core orbitals are ignored since they are considered as inactive in the bonding scheme of a molecule, and only the valence orbitals of the natural minimal basis set are taken into account in order to describe the bonding scenario. By mixing the valence NAO on atoms A and B it is allowed an electron-density sharing between these two atoms, thus creating *prenatural bonding orbital* (PNBO) with occupation number n_{AB} . This procedure is performed in a loop sequence between any pair of atoms, reaching a final structure that leaves the lowest amount of electron density out of the partition corresponding to classical covalent bonds or lone pairs. The final set of NBO is obtained at last by orthogonalization of all the PNBO, while preserving their bonding characteristics.

For a σ -bond between two atoms A and B, the NBO σ_{AB} is obtained as a linear combination of valence NAO on A ($\phi_i(A)$) and B ($\phi_j(B)$) as expressed in eq. 2.17.

$$\sigma_{AB} = \sum_i c_i(A)\phi_i(A) + \sum_j c_j(B)\phi_j(B) \quad (2.17)$$

From this expression, it is easy to introduce natural hybrid orbital (NHO) on each atom and thus to express the σ -bond as a linear combination of one hybrid on A ($h(A)$) and one hybrid on B ($h(B)$), as follows in equations 2.18-2.21.

$$\sum_i c_i(A)\phi_i(A) = c_A h(A) \quad (2.18)$$

$$c_A = \left[\sum_i c_i(A)^2 \right]^{1/2} \quad (2.19)$$

$$h(A) = \sum_i \frac{c_i(A)}{c_A} \phi_i(A) \quad (2.20)$$

$$\sigma_{AB} = c_A h(A) + c_B h(B) \quad (2.21)$$

For an element of the second series, the relative weights of s and p-orbitals in the hybrid $h(A)$ gives access to the hybridization. Interestingly, despite the mathematical treatment involved in these transformations, the NBO formalism follows Henry Bent's rule of hybridization,^[111] which relates molecular structure, central atom hybridization, and substituent electronegativities. Essentially, in order to explain the slight deviations from ideal geometries of small molecules, it was proposed that hybridization of a central atom can result in orbitals with unequal weight of atomic orbitals depending on the electronegativity of the substituent.^[112] In addition, the respective weights of the NBO hybrids orbitals (the coefficients c_A and c_B in σ_{AB}) give access to the polarity of the bond. Furthermore, to every σ -bond between the atoms A and B, σ_{AB} , the NBO procedure also identifies a corresponding antibond σ^*_{AB} according to the out-of-phase combination of the hybrid (eq. 2.22).

$$\sigma^*_{AB} = c_A h(A) - c_B h(B) \quad (2.22)$$

The antibonding situation belongs to the NBO sets of orbitals that are almost empty (alongside with Rydberg orbitals). Thus, since there are orbitals populated by almost two electrons (core, bonding, and lone pair), there can be electron density transference from these latter occupied to the former vacant orbitals. Therefore, the occupied orbitals can behave as internal Lewis base transferring electron density into the empty ones acting as internal Lewis acids. This donor-acceptor electron flow is responsible for the resulting nonstrictly localized bonding description, and for this reason some occupation numbers differ from 2 and 0. A linear combination of donating and accepting NBO orbitals can be written and generalized to all donor-acceptor interactions to obtain a *natural localized molecular orbital* (NLMO), which are strictly occupied by two electrons (eq. 2.23).

$$\tilde{\sigma}_i = c_i \sigma_i + c_j \sigma_j^* \quad (2.23)$$

The expression of the NLMO in the NBO basis allows to estimate the extent of delocalization of the parent NBO σ_i and to identify the main contributors in the accepting NBO orbitals. A picture displaying the orbital shape of some of the orbitals previously mentioned is shown in Figure 2.4.

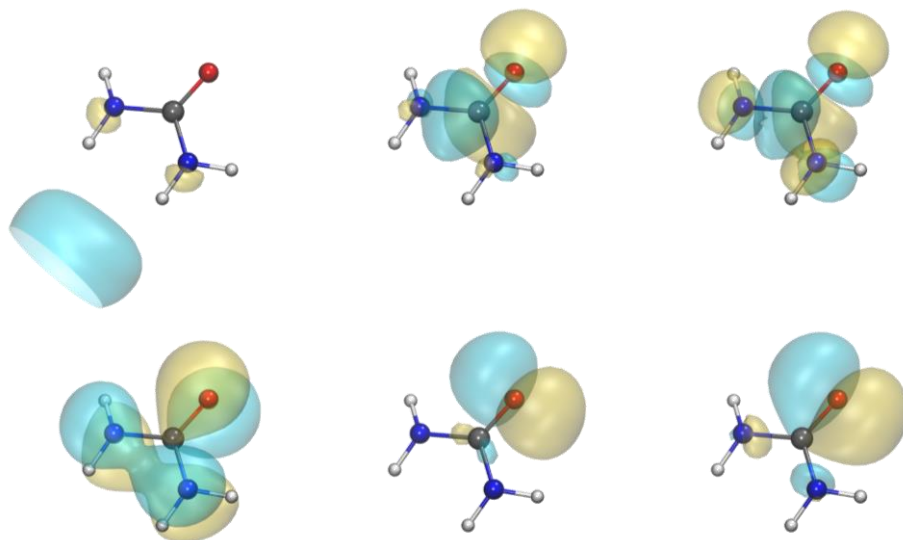


Figure 2.4. HOMO (down) and LUMO (up) of the urea molecule ($\text{H}_2\text{N-C(O)-NH}_2$). From left to right there are depicted the electronic representation corresponding to natural atomic orbitals (NAO), natural bond orbitals (NBO), and natural localized molecular orbital (NLMO).

Despite the above exposed, the bonding picture provided by the NBO formalism has not to be considered as an irrefutable truth. Instead, it should be viewed as a one of several partition schemes which deeply rooted in the description of molecules and is used by most chemists. This fact is due to the picture of the electronic density distribution that this methodology provides since it establishes a representation that becomes rational and intuitive while rendering the interaction trends of a molecule.

2.4.2. Quantum Theory of Atoms in Molecules (QTAIM)

Even though *Quantum Theory of Atoms in Molecules* (QTAIM)^[113] does not seem to be part of conventional theoretical chemistry, this theory is capable of furnishing a rigorous and elegant definition of two concepts that are used on a daily basis but are rather complicated to describe: the atom and the bond inside a molecule. Since everyone would undoubtedly agree that molecules are built by atoms, it can be concluded that these constructions are not novel

since molecules are based on atomic pre-organized entities. In fact, the preservation of atoms is what chemistry is about, it is a discipline of science concerned on the change produced when atoms interact to one another. Therefore, it is important for an atom to be well defined. However, there is no unique opinion of how to define an atom inside a molecule due to the lack of experimental measures capable of settle this dispute. Alternatively, this question can be tackled from a theoretical point of view.

The first appearance of a partitioning scheme of a molecule in its constituent atoms appeared in 1971.^[114] Richard Bader (considered the father of QTAIM) and co-workers proposed a model that revealed what was the base of the new theory they were going to develop:

“The prime reason for proposing any scheme which assigns some number of electrons to each nucleus in a molecule is to provide a measure of the charge transfer...”

Such partition consisted on using the point of minimum electron density between an internuclear axis of a pair of bonded nuclei as a definition for the partitioning surface. To illustrate this one-dimensional concept it is helpful to imagine two peaks in close proximity to each other. The existence of two summits directly implies a valley (minimum) between them. Thus, as no one would think in the possibility of overlapped mountains, there exists a sharp boundary separating these entities.

Although this example might seem clear, it is not straightforward how this definition can be extended to polyatomic molecules. The definition of an atom in a molecule is made by the gradient vector field, which is a collection of gradient paths, which in turn, can be seen as a succession of infinitely short gradient vectors (Figure 2.5). By definition, a gradient path is everywhere orthogonal to a contour line of constant electron density. This statement is equivalent to the fact that the gradient path traverses the electron density in the direction of maximum ascent. As a vector, it has a sense, and the origin and terminus of a gradient path have something in common: they are points where the gradient vanishes. Such points are called a critical points (CP), and their identification within the molecule is of great usefulness.

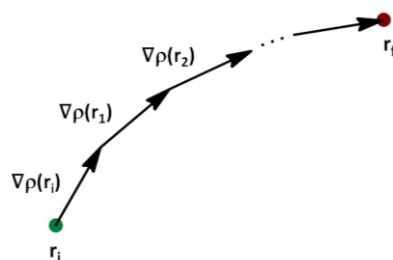


Figure 2.5. Construction of a gradient path.

The electronic density ρ is a three dimensional function, which implies that there are four types of (non-degenerate) critical points: maximums, minimums and two kind of saddle points. Its best characterization can be done by the eigenvalues λ_i ($i = 1, 2, 3$) of the Hessian matrix of ρ , evaluated at the CP. The most common way to express a CP is with its *rank* (r) and its *signature* (s). The former refers to the number of non-zero eigenvalues of a particular CP, whereas the latter is the sum of the sign of the eigenvalues. For example, a typical saddle point may have two negative and one positive eigenvalues. Thus, its rank is 3 and its signature is -1 , and the CP is denoted as $(3, -1)$. This particular type of critical point is called *bond critical point* (Figure 2.6 left, blue dotted) since it indicates the existence of a bond between two nuclei in an equilibrium geometry molecule. The bond critical point corresponds to a saddle point that has a maximum in only two directions and a minimum in the remaining one, which defines the course for the internuclear axis. Analogously, the opposite scenario is provided by a *ring critical point*, thus having a maximum in one direction and a minimum in the other two directions (Figure 2.6 right, green dotted).

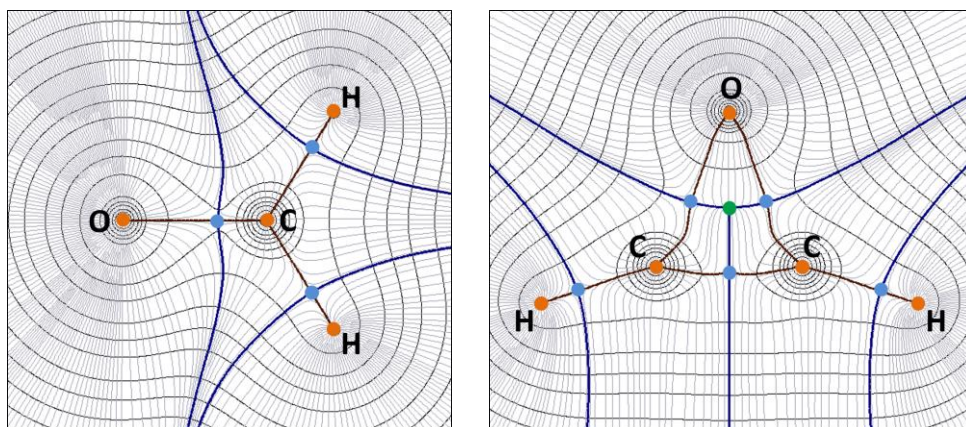


Figure 2.6. Electron density contour plot of formyl ($\text{H}_2\text{C}=\text{O}$, left) and oxirane ($\text{C}_2\text{H}_2\text{O}$, right) superimposed to a high number of gradient paths (an infinite multitude of gradient paths is called *gradient vector field*).

From Figure 2.6 it can be seen that gradient paths are originated at infinity (corresponding to a minima in the electron density) and terminating at the respective nuclei (maxima, orange dots). There is a special set of gradient paths that do not end at nuclei and terminate at *bond critical points* (blue lines). The main feature of bond critical points is linking two nuclei via an *atomic interaction line* (brown line). This means that from each bond critical point emerge two gradient paths, each of which is attracted to a different nucleus. It is also important to define the concept of *interatomic surface*, which delimitates two bonded atoms and is defined by all the gradient paths originating at infinity and terminating at a certain *bond critical point*. All this series of definitions lead to the most important idea of the QTAIM formalism: the

topological atom, also called *atomic basin*, which is defined by the set of gradient paths terminating at a nucleus.

Beyond the QTAIM framework of critical points localization and atom definition, this theory is also capable of supplying information about electron pair density. Traditionally, the pair density $\rho(\mathbf{r}_1, \mathbf{r}_2)$ has been the function that indicates the regions of space in which there is a probability of finding two electrons of opposite spin, and therefore a bonding situation. However, it has been shown that, in general, this density function mostly defines regions in space where atomic core in pairs of electrons are localized.^[115] Nevertheless, a correlation degree was observed between electron pairs and the Laplacian of the electron density,^[116] defined as $L(\mathbf{r}) = -\nabla^2\rho(\mathbf{r})$ for convenience. The differentiation of a function with respect its variables provides information about its degree of sharpness or broadness in the surroundings. Thus, when $\nabla^2\rho < 0$ at a given point, the electron density is locally concentrated, meaning that the value of ρ is locally higher than the neighboring points. Conversely, when $\nabla^2\rho > 0$ in a certain point, the electron density is locally depleted, which implies that the value of ρ will be higher in any point of the neighborhood (Figure 2.7). In summary, the fact that $L(\mathbf{r})$ can measure the concentration of the electron density suggested that it could be used to detect electron pair localization. Indeed, many studies proved the faithfulness of this agreement (although not perfect) thus supporting classical bonding theories such as Lewis model,^[109] and the later VSEPR model.^[117,118]

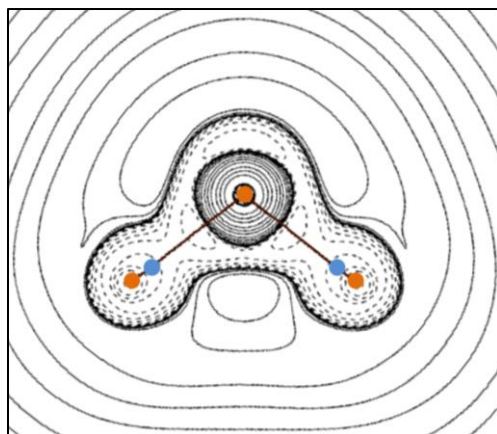


Figure 2.7. Laplacian contour map of a water molecule. The dashed contour lines correspond to positive $L(\mathbf{r})$ values (electronic charge concentration), whereas continuous lines correspond to negative $L(\mathbf{r})$ values (electronic charge depletion).

All these concepts lead to the conclusion that topological atoms are non-overlapping entities, totally crashing with the sharing idea of a covalent bond. However, the atom is completely defined within the molecule, and every property of the system (even those unable to be measured experimentally) can be split into its constituents. Another crucial consequence is

that there are no gaps between atoms, meaning that there is no empty space between them and every point in the space belongs to a topological atom. This might affect, for instance, the vision of self-assembly processes or the accommodation of a substrate in enzyme pockets. These phenomena are mostly related with steric hindrance, which should not be understood as a rigid conformation of atoms in space. Instead, these transformations could be seen as the deformation of a guest of topological atoms, each of which has an energy cost.

2.4.3. Electron Localization Function (ELF)

Localizing pairs of electrons, either bonded or non-bonded, is not an evident task in the topology of the electron density and it is possible to tackle this problem using different strategies. In fact, there is another approach called *Electron Localization Function* (ELF)^[119] capable of grapple with this issue. This framework has some similarities with QTAIM in the sense that it also addresses the topology of a function in order to analyze the molecular space, yet does not use the electron density itself. Instead, it deals with the conditional probability of same spin pairs, thereby giving a different vision to the chemical bonding in general. Indeed, the partition of the molecular space into basins described by ELF methodology features a decomposition that is not necessarily attached to a given atom but that might have some significance, like bonding regions or lone pairs. This analysis usually coincides and complements the QTAIM interpretation, as the former performs an atomic partition which generates, in turn, atomic domains, whereas ELF produces localization domains.

Introduced by Axel Becke and Kenneth Edgecombe from a Taylor series expansion of spherical averaged same-spin conditional pair probability,^[119] the ELF has become an essential and one of the most extensively used quantum mechanical methodologies to analyze electron localization. This might be due to the conditional probability term itself, which confers its main advantage over the pair density: it contains all relevant information about the motion of pairs of electrons (just as the pair density does), but it does not contain the irrelevant information concerning the position of the reference electron (eq. 2.24).

$$P_{\mathbf{r}_1, \mathbf{r}_2} = \frac{\gamma_{\mathbf{r}_1, \mathbf{r}_2}}{\rho_{\mathbf{r}_1}} \quad (2.24)$$

The analysis of ELF yields a partition into core and valence basins which “correspond to the qualitative electron pair domains of the VSEPR model and have the same geometry as the VSEPR domains”.^[120] It provides an intuitive picture by showing the regions of the molecular space where electrons localize. Actually, ELF topological analysis partitions the molecular space in so-called basins. These localization domains are defined by the local maxima, which can be classified in three different types: bonding and non-bonding valence basins (usually corresponding to bonding situations or lone pairs, respectively) and core basins. The latter,

labeled as $C(A)$ where A is the atomic symbol of the element, surrounds the nuclei with atomic charge $Z > 2$. For a given atom, this number varies with the number of core shell of such element and also with the local symmetry in the molecule. However, the reproduction of the shell number is not guaranteed in transition metal atoms. Conversely, the valence basins are organized around the core basins. The adopted nomenclature to label these domains is $V(A,B,...)$, where $A,B,...$ are the atomic symbols of the atomic cores having a boundary with the considered valence basin. It is necessary to highlight that a valence basin may belong to one or several atomic valence shells. Thus, a synaptic order of a valence basin is used to specify the number of atomic valence shell to which it belongs. Therefore, it can be found monosynaptic basins $V(A)$, corresponding to lone pairs; and disynaptic $V(A,B)$ and higher polysynaptic basins $V(A,B,C,...)$, corresponding to stabilizing interactions between atoms.

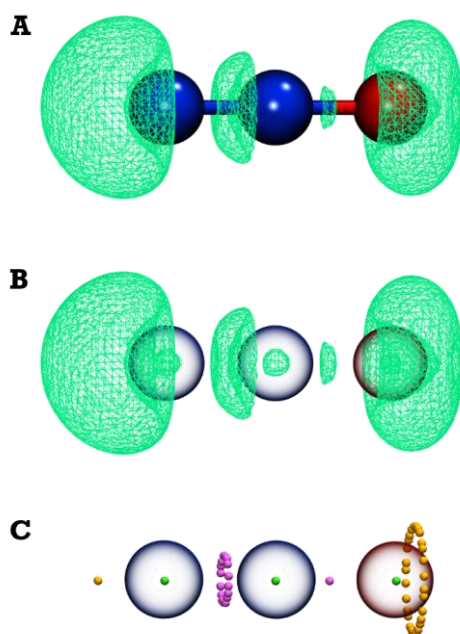


Figure 2.8. Different representations of the N_2O molecule (N in blue and O in red). A) ELF with $\rho = 0.77$ and opaque atoms displayed. B) ELF with $\rho = 0.77$ and empty atoms, C) Attractors colored in blue for non-paired electrons, yellow for bonding electrons and green for core electrons.

The ELF basins map of the N_2O molecule is displayed in Figure 2.8A. The valence basins are organized around the core basins where they share a boundary with (although the core basins cannot be seen in all the representations). There are two valence basins in the N_2O representation, one corresponding to the oxygen-nitrogen bonding situation, $V(N,O)$, and the other regarding to the nitrogen-nitrogen bond, $V(N,N)$. The valence shell of the oxygen atom is composed by an $V(N,O)$ basin and a non-pair electron basin, located at its right. In turn, the

valence shell of the central nitrogen is composed by a $V(N,O)$ and a $V(N,N)$. Finally, the other nitrogen's basin shell is formed by a $V(N,N)$ and another non-pair electron basin, placed at its left. In Figure 2.8C it can be seen the attractors corresponding to such basins.

2.5. References

- [1] E. Schrödinger, *Phys. Rev.* **1926**, *28*, 1049–1070.
- [2] A. Einstein, B. Podolsky, N. Rosen, *Phys. Rev.* **1935**, *47*, 777–780.
- [3] B. Espagnat d', *Sci. Am.* **1979**, *241*, 158–181.
- [4] A. Watson, *Science* **1997**, *277*, 481.
- [5] P. A. M. Dirac, *Proc. R. Soc. London. Ser. A* **1929**, *123*, 714–733.
- [6] P. A. M. Dirac, *Proc. R. Soc. London. Ser. A* **1928**, *117*, 610–624.
- [7] P. A. M. Dirac, *Proc. R. Soc. London. Ser. A* **1930**, *126*, 360–365.
- [8] H. Meuer, E. Strohmaier, J. Dongarra, H. Simon, M. Mauer, <https://www.top500.org/>.
- [9] R. G. Parr, W. Yang, *Density-Functional Theory of Atoms and Molecules*, Oxford University Press, **1994**.
- [10] A. D. Becke, *J. Chem. Phys.* **2014**, *140*, 18A301.
- [11] W. Kohn, *Rev. Mod. Phys.* **1999**, *71*, 1253–1266.
- [12] M. Born, R. Oppenheimer, *Ann. Phys.* **1927**, *389*, 457–484.
- [13] L. H. Thomas, *Math. Proc. Cambridge Philos. Soc.* **1927**, *23*, 542–548.
- [14] E. Fermi, *Rend. Accad. Naz. Lincei* **1927**, *6*, 602–607.
- [15] E. Fermi, *Zeitschrift für Phys.* **1928**, *48*, 73–79.
- [16] D. R. Hartree, *Math. Proc. Cambridge Philos. Soc.* **1928**, *24*, 89–110.
- [17] D. R. Hartree, *Math. Proc. Cambridge Philos. Soc.* **1928**, *24*, 111–132.
- [18] V. Fock, *Zeitschrift für Phys.* **1930**, *61*, 126–148.
- [19] J. C. Slater, *Phys. Rev.* **1930**, *35*, 210–211.
- [20] W. Pauli, *Zeitschrift für Phys.* **1925**, *31*, 765–783.
- [21] P. A. M. Dirac, *Math. Proc. Cambridge Philos. Soc.* **1930**, *26*, 376–385.
- [22] P. Hohenberg, W. Kohn, *Phys. Rev.* **1964**, *136*, B864–B871.
- [23] G. A. Bliss, *Lectures on the Calculus of Variations*, University Of Chicago Press, **1947**.
- [24] W. Kohn, L. J. Sham, *Phys. Rev.* **1965**, *140*, A1133–A1138.
- [25] R. Stowasser, R. Hoffmann, *J. Am. Chem. Soc.* **1999**, *121*, 3414–3420.
- [26] S. H. Vosko, L. Wilk, M. Nusair, *Can. J. Phys.* **1980**, *58*, 1200–1211.
- [27] A. D. Becke, *Phys. Rev. A* **1988**, *38*, 3098–3100.
- [28] J. P. Perdew, K. Burke, M. Ernzerhof, *Phys. Rev. Lett.* **1996**, *77*, 3865–3868.

- [29] J. P. Perdew, K. Burke, M. Ernzerhof, *Phys. Rev. Lett.* **1997**, *78*, 1396.
- [30] J. P. Perdew, *Phys. Rev. B* **1986**, *33*, 8822–8824.
- [31] J. P. Perdew, *Phys. Rev. B* **1986**, *34*, 7406.
- [32] J. P. Perdew, in *Electron. Struct. Solids '91* (Eds.: P. Ziesche, H. Eschig), Akademie Verlag, Berlin, Germany, **1991**, pp. 11–20.
- [33] C. Lee, W. Yang, R. G. Parr, *Phys. Rev. B* **1988**, *37*, 785–789.
- [34] E. I. Proynov, E. Ruiz, A. Vela, D. R. Salahub, *Int. J. Quantum Chem.* **1995**, *56*, 61–78.
- [35] J. P. Perdew, J. A. Chevary, S. H. Vosko, K. A. Jackson, M. R. Pederson, D. J. Singh, C. Fiolhais, *Phys. Rev. B* **1992**, *46*, 6671–6687.
- [36] J. P. Perdew, J. A. Chevary, S. H. Vosko, K. A. Jackson, M. R. Pederson, D. J. Singh, C. Fiolhais, *Phys. Rev. B* **1993**, *48*, 4978.
- [37] J. P. Perdew, K. Burke, M. Ernzerhof, *Phys. Rev. Lett.* **1996**, *77*, 3865–3868.
- [38] J. Tao, J. P. Perdew, *J. Chem. Phys.* **2005**, *122*, 114102.
- [39] J. Tao, J. P. Perdew, V. N. Staroverov, G. E. Scuseria, *Phys. Rev. Lett.* **2003**, *91*, 146401.
- [40] Y. Zhao, D. G. Truhlar, *J. Chem. Phys.* **2006**, *125*, 194101.
- [41] A. D. Becke, *J. Chem. Phys.* **1993**, *98*, 1372–1377.
- [42] A. D. Becke, *J. Chem. Phys.* **1996**, *104*, 1040–1046.
- [43] J. Tao, J. P. Perdew, V. N. Staroverov, G. E. Scuseria, *Phys. Rev. Lett.* **2003**, *91*, 146401.
- [44] Y. Zhao, D. G. Truhlar, *Acc. Chem. Res.* **2008**, *41*, 157–167.
- [45] Y. Zhao, D. G. Truhlar, *Theor. Chem. Acc.* **2008**, *120*, 215–241.
- [46] C. J. Cramer, D. G. Truhlar, *Phys. Chem. Chem. Phys.* **2009**, *11*, 10757–10816.
- [47] E. G. Hohenstein, S. T. Chill, C. D. Sherrill, *J. Chem. Theory Comput.* **2008**, *4*, 1996–2000.
- [48] N. Mardirossian, M. Head-Gordon, *J. Chem. Theory Comput.* **2016**, *12*, 4303–4325.
- [49] A. D. Becke, E. R. Johnson, *J. Chem. Phys.* **2005**, *123*, 154101.
- [50] S. Grimme, *J. Comput. Chem.* **2004**, *25*, 1463–1473.
- [51] S. Grimme, *J. Comput. Chem.* **2006**, *27*, 1787–1799.
- [52] S. Grimme, J. Antony, S. Ehrlich, H. Krieg, *J. Chem. Phys.* **2010**, *132*, 154104.
- [53] M. G. Medvedev, I. S. Bushmarinov, J. Sun, J. P. Perdew, K. A. Lyssenko, *Science* **2017**, *355*, 49–52.
- [54] S. Hammes-Schiffer, *Science* **2017**, *355*, 28–29.
- [55] N. Mardirossian, M. Head-Gordon, *J. Chem. Phys.* **2016**, *144*, 214110.
- [56] H. B. Schlegel, *J. Comput. Chem.* **2003**, *24*, 1514–1527.
- [57] F. F. Crim, *Faraday Discuss.* **2012**, *157*, 9.
- [58] H. B. Schlegel, *Wiley Interdiscip. Rev. Comput. Mol. Sci.* **2011**, *1*, 790–809.
- [59] R. B. Grossman, *The Art of Writing Reasonable Organic Reaction Mechanisms*, Springer, **2002**.
- [60] R. B. Jordan, *Reaction Mechanisms of Inorganic and Organometallic Systems*, Oxford University Press, **2007**.

- [61] O. Sackür, *Ann. Phys.* **1911**, 341, 958–980.
- [62] H. Tetrode, *Ann. Phys.* **1912**, 344, 255–256.
- [63] O. Sackür, in *Festschrift W. Nernst Zu Seinem 25jährigen Doktorjubiläum Gewidmet von Seinen Schülern*, Wilhelm Knapp, Halle an Der Salle, Germany, **1912**, pp. 405–423.
- [64] H. Tetrode, *Ann. Phys.* **1912**, 343, 434–442.
- [65] O. Sackür, *Ann. Phys.* **1913**, 345, 67–86.
- [66] D. H. Wertz, *J. Am. Chem. Soc.* **1980**, 102, 5316–5322.
- [67] M. H. Abraham, *J. Am. Chem. Soc.* **1981**, 103, 6742–6744.
- [68] M. Mammen, E. I. Shakhnovich, J. M. Deutch, G. M. Whitesides, *J. Org. Chem.* **1998**, 63, 3821–3830.
- [69] P. Kirkpatrick, C. Ellis, *Nature* **2004**, 432, 823.
- [70] K. L. M. Drew, H. Baiman, P. Khwaounjoo, B. Yu, J. Reynisson, *J. Pharm. Pharmacol.* **2012**, 64, 490–495.
- [71] B. Leimkuhler, C. Matthews, *Molecular Dynamics. With Deterministic and Stochastic Numerical Methods.*, Springer, **2015**.
- [72] J. A. Pople, D. L. Beveridge, *Approximate Molecular Orbital Theory*, McGraw-Hill, **1970**.
- [73] A. Warshel, M. Levitt, *J. Mol. Biol.* **1976**, 103, 227–249.
- [74] M. J. Field, P. A. Bash, M. Karplus, *J. Comput. Chem.* **1990**, 11, 700–733.
- [75] H. Lin, D. G. Truhlar, *Theor. Chem. Acc.* **2006**, 117, 185.
- [76] R. Car, M. Parrinello, *Phys. Rev. Lett.* **1985**, 55, 2471–2474.
- [77] N. Metropolis, A. W. Rosenbluth, M. N. Rosenbluth, A. H. Teller, E. Teller, *J. Chem. Phys.* **1953**, 21, 1087–1092.
- [78] C. Hansch, *Acc. Chem. Res.* **1969**, 2, 232–239.
- [79] C. Hansch, R. M. Muir, T. Fujita, P. P. Maloney, F. Geiger, M. Streich, *J. Am. Chem. Soc.* **1963**, 85, 2817–2824.
- [80] L. P. Hammett, *J. Am. Chem. Soc.* **1937**, 59, 96–103.
- [81] M. Karelson, V. S. Lobanov, A. R. Katritzky, *Chem. Rev.* **1996**, 96, 1027–1044.
- [82] R. Todeschini, V. Consonni, *Handbook of Molecular Descriptors*, Wiley-VCH, **2000**.
- [83] D. J. Livingstone, *J. Chem. Inf. Comput. Sci.* **2000**, 40, 195–209.
- [84] R. Poilblanc, M. Bigorgne, *Bull. Soc. Chim. Fr.* **1962**, 1301–1325.
- [85] W. Strohmei, F. J. Muller, *Chem. Berichte-Recueil* **1967**, 100, 2812.
- [86] G. Bouquet, A. Loutellier, M. Bigorgne, *J. Mol. Struct.* **1968**, 1, 211–237.
- [87] C. A. Tolman, *Chem. Rev.* **1977**, 77, 313–348.
- [88] R. W. Taft, *J. Am. Chem. Soc.* **1953**, 75, 4538–4539.
- [89] M. Charton, *J. Am. Chem. Soc.* **1969**, 91, 615–618.
- [90] M. Charton, *J. Am. Chem. Soc.* **1975**, 97, 1552–1556.
- [91] M. Charton, *J. Am. Chem. Soc.* **1975**, 97, 3691–3693.
- [92] M. Charton, *J. Am. Chem. Soc.* **1975**, 97, 3694–3697.
- [93] M. Charton, *J. Am. Chem. Soc.* **1975**, 97, 6159–6161.

- [94] M. Charton, B. Charton, *J. Am. Chem. Soc.* **1975**, *97*, 6472–6473.
- [95] H. J. V Barros, M. L. Ospina, E. Arguello, W. R. Rocha, E. V Gusevskaya, E. N. dos Santos, *J. Organomet. Chem.* **2003**, *671*, 150–157.
- [96] A. C. Hillier, W. J. Sommer, B. S. Yong, J. L. Petersen, L. Cavallo, S. P. Nolan, *Organometallics* **2003**, *22*, 4322–4326.
- [97] H. Clavier, S. P. Nolan, *Chem. Commun.* **2010**, *46*, 841–861.
- [98] K. Wu, A. G. Doyle, *Nat. Chem.* **2017**, *9*, 779.
- [99] M. Mantina, A. C. Chamberlin, R. Valero, C. J. Cramer, D. G. Truhlar, *J. Phys. Chem. A* **2009**, *113*, 5806–5812.
- [100] M. Dehmer, K. Varmuza, D. Bonchev, *Statistical Modelling of Molecular Descriptors in QSAR/QSPR*, Wiley-VCH, **2012**.
- [101] K. Roy, S. Kar, R. N. Das, *A Primer on QSAR/QSPR Modeling*, Springer, **2015**.
- [102] N. Fey, *Dalt. Trans.* **2010**, *39*, 296–310.
- [103] J. Jover, N. Fey, *Chem. – An Asian J.* **2014**, *9*, 1714–1723.
- [104] A. Milo, A. J. Neel, F. D. Toste, M. S. Sigman, *Science* **2015**, *347*, 737–743.
- [105] A. Nadin, C. Hattotuwigama, I. Churcher, *Angew. Chemie Int. Ed.* **2012**, *51*, 1114–1122.
- [106] K. D. Collins, A. Rühling, F. Glorius, *Nat. Protoc.* **2014**, *9*, 1348–1353.
- [107] K. D. Collins, T. Gensch, F. Glorius, *Nat. Chem.* **2014**, *6*, 859–871.
- [108] F. Weinhold, C. R. Landis, *Valency and Bonding. A Natural Bond Orbital Donor-Acceptor Perspective*, Cambridge University Press, **2005**.
- [109] G. N. Lewis, *J. Am. Chem. Soc.* **1916**, *38*, 762–785.
- [110] A. E. Reed, R. B. Weinstock, F. Weinhold, *J. Chem. Phys.* **1985**, *83*, 735–746.
- [111] H. A. Bent, *Chem. Rev.* **1961**, *61*, 275–311.
- [112] A. D. Walsh, *Discuss. Faraday Soc.* **1947**, *2*, 18–25.
- [113] R. F. W. Bader, *Atoms in Molecules: A Quantum Theory*, Clarendon Press, **1994**.
- [114] R. F. W. Bader, P. M. Beddall, P. E. Cade, *J. Am. Chem. Soc.* **1971**, *93*, 3095–3107.
- [115] R. F. W. Bader, M. E. Stephens, *J. Am. Chem. Soc.* **1975**, *97*, 7391–7399.
- [116] R. F. W. Bader, P. J. MacDougall, C. D. H. Lau, *J. Am. Chem. Soc.* **1984**, *106*, 1594–1605.
- [117] R. J. Gillespie, R. S. Nyholm, *Q. Rev. Chem. Soc.* **1957**, *11*, 339–380.
- [118] R. J. Gillespie, *Coord. Chem. Rev.* **2008**, *252*, 1315–1327.
- [119] A. D. Becke, K. E. Edgecombe, *J. Chem. Phys.* **1990**, *92*, 5397–5403.
- [120] R. J. Gillespie, E. A. Robinson, *J. Comput. Chem.* **2007**, *28*, 87–97.

Objectives



*Imagination will often carry us to worlds that never were.
But without it, we go nowhere*

— Carl Sagan —

UNIVERSITAT ROVIRA I VIRGILI
COMPUTATIONAL MODELING TO EXPLORE UNCONVENTIONAL REACTIVITY PATTERNS IN C-H ACTIVATION
AND BORON CHEMISTRY
Diego García López

3. Objectives

Probably no one would contradict the fact that computational modeling is an essential instrument in our era. Its importance is not only due to the deepest understandings we can achieve by now for specific processes, but also for the broadening in the data-based approaches allowing the generalization of phenomena for their use in other applications. These two guiding principles imply a commitment between scientific curiosity and practical goals for our own interest. The main aim of this thesis consists of combining these two philosophies to elucidate mechanistic paths and molecular interactions of certain systems as well as to build patterns for the widespread activity of some compounds.

The research carried out in this work has largely focused on collaborations with experimental groups in order to unveil the ultimate forces governing particular processes that include the activation of inert C–H bonds and unconventional boron chemistry. However, the dare is to employ modeling techniques to predict the outcome of untested chemical or physical phenomena in order to preserve time and resources. In this dissertation we have attempted to do both.

More specifically, the goals of this thesis are divided herein into its different chapters:

- **Chapter 4:** Mechanistic insights into C–H activation involving dimetallic titanium species

The experimental group of Dr. Santamaría, at the University of Alcalá, recently reported a series of dinuclear titanium complexes ($\{[Ti(\eta^5-C_5Me_5)R_2]_2(\mu-O)\}$, R = CH_2SiMe_3 , CH_2CMe_3 , and CH_2Ph) that can undergo sequential C–H bond activations on the adjacent titanium center to give a series of metallacycle complexes. By means of DFT calculations we intended to probe the existence of the transient alkylidene species that was proposed to enhance such transformations. Moreover, the different final outcome in the reactivity depends on the ligand (CH_2SiMe_3 , CH_2CMe_3 , and CH_2Ph) of the dimetallic system. Thus we pretended to elucidated a detailed mechanistic path capable of distinguish the different selectivity routes observed.

- **Chapter 5:** Unraveling the agostic interactions of arene $C(sp^2)$ –H at nickel pincer complexes

A reactive ligand (PCH_2NC_{Ph}) introduced by the experimental group of Prof. van der Vlugt, at the University of Amsterdam, was employed in reversible cyclometalation as strategy for cooperative catalysis, using a strongly chelating (P,N)-atoms. The aforementioned cyclometalation of this parent ligand and a related one with Ni^{II} and their posterior protonation generated two structurally characterized $Ni-(C_{Ph}-H)$

complexes. Intrigued by this rare example of interaction in solid state for a first row transition metal, we aimed to take a closer look and analyze whether there exists agostic Ni-(C-H) interactions using topological analysis of the electron density.

▪ **Chapter 6:** Tracing nucleophilic maps for trivalent boron compounds

Although traditional trivalent boron compounds are electrophiles, it has been widely reported that they can switch their reactivity from an electrophilic character to a nucleophilic behavior by changing the nature of the substituents attached to the boron atom. This novel achievement, even in a metal-free context, represents a milestone in the synthesis of organoboron compounds. For this reason, a qualitative tendency map was constructed previously in our group, establishing a gradient of nucleophilic character. In a step forward, we sought quantitative relationships between the structures of trivalent boron compounds and their nucleophilicity activity through ground state descriptors by employing multivariate regression techniques and a QSAR approach.

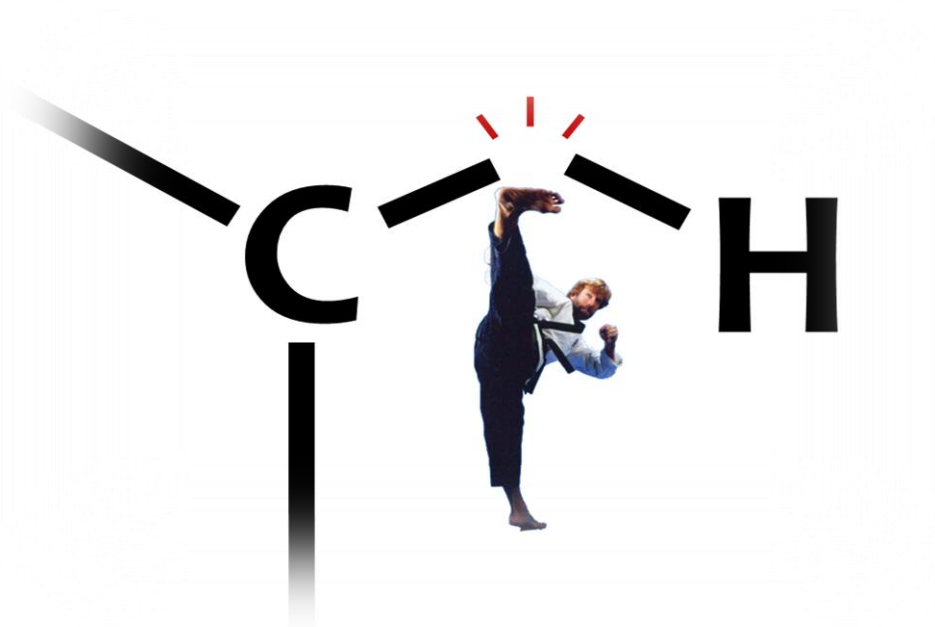
▪ **Chapter 7:** *Gem*-additions of unsymmetrical diboranes to ketones and aldehydes

Classic addition of diboron compounds to unsaturated bonds typically yields *syn* 1,2-difunctionalizations. However, the experimental group of Dr. Fernández, at the University of Tarragona, described the unsymmetrical 1,1-diboration of diazo compounds, formed *in situ* from aldehydes and cyclic and non-cyclic ketones in the absence of any metal. Interestingly, diastereoselectivity was observed for substituted cyclohexanones. Furthermore, a selective alkoxide-assisted protodeboration was performed. Our goal was to rationalize the origin of selectivity in geminal formation of the two C-B bonds by DFT calculations as well to establish whether the protodeboration process could involve a carbanion species.

▪ **Chapter 8:** Disclosing the mechanism of selenoborane *anti*-addition to alkynes

The reactivity of boron-interelement compounds offer a more diverse functionalization *via* push-pull effect, which enhances the nucleophilic character of the heteroatom attached to the boron by the previous activation of the latter by a Lewis base. In this context, the group of Dr. Fernández reported the regio- and stereoselectivity of the *anti*-3,4-selenoboration of α,β -acetylenic esters and ynamides using catalytic amounts of a basic phosphine. Oddly enough, in the absence of the phosphine the selenoboration switched from the formation of α -vinyl selenides to β -vinyl selenides. Based on some proposed mechanism available in the literature for *anti* additions, we aimed to elucidate the origin of this opposite reactivity trend by DFT calculations in order to establish a possible detailed path.

Activation of C—H bonds by early- and late-transition metals



*Some scientists claim that hydrogen, because it is so plentiful,
is the basic building block of the universe.
I dispute that. I say that stupidity is far more abundant than hydrogen,
and that is the basic building block of the universe.*

— Frank Zappa —

UNIVERSITAT ROVIRA I VIRGILI
COMPUTATIONAL MODELING TO EXPLORE UNCONVENTIONAL REACTIVITY PATTERNS IN C-H ACTIVATION
AND BORON CHEMISTRY
Diego García López

Outline

Selective C–H bond activation, and its subsequent functionalization involving transition-metal-based systems, has been one of the main research topics in organometallic chemistry for the last 30 years. This process typically comprises the interaction of a substrate with a metal, followed by C–H bond cleavage and formation of a M–C linkage. When early-transition metals are involved the activation usually occurs via σ -bond metathesis, whereas late-transition metals tend to employ oxidative additions. This dependence on the metal nature combined with the large abundance of starting materials and the oxidant-free reaction conditions to galvanize C–H bonds have not only broad potential in synthesis, but also pave the way for industrial large-scale applications. However, the inert nature of such unreactive bonds and the requirement for a site-selective functionalization make those process extremely challenging.

In this section, we analyse two different metal-depending aspects of C–H bond activation: (i) the reaction mechanism of cooperative intermetallic activation in dimetallic tetraalkyl μ -oxo titanium complexes, and (ii) the nature of the unusual intramolecular interaction of M–(C_{Ph}–H) bond in nickel complexes. In the first case (chapter 4), we determined computationally the mechanism of remote carbon–hydrogen activation on titanium dinuclear complexes ($\{Ti(\eta^5-C_5Me_5)R_2\}_2(\mu-O)$), R = CH₂SiMe₃, CH₂CMe₃, and CH₂Ph) that has been observed by the group of Dr. Santamaría at the University of Alcalá. DFT calculations show that the mechanism involves a first α -hydrogen abstraction to generate a transient titanium alkylidene, which enables it to activate β - and γ -C(sp³)–H bonds on the adjacent titanium center. The calculations also establish a reactivity order for the different type of γ -H abstractions, trimethylsilyl > neopentyl \cong benzyl, allowing us to explain the experimental selectivity. The mechanism illustrates how d⁰ early transition-metal complexes can promote the heterolytic C–H bond cleavage through metal-carbon multiple bonds that act as strong base. In the second case (chapter 5), we interpreted the rare Ni–(C_{Ph}–H) interaction in solid state structure of [NiBr(κ^3 -P,N,(C–H)-L^H)]BF₄ observed by the group of Prof. van der Vlugt at the University of Amsterdam. This structure can be directly related to a fast and facile C–H cyclometalation at the Ni^{II} center. The theoretical study includes the quantum theory of atoms in molecules (QTAIM) and electron localization function (ELF) analysis which characterize the nature of the Ni–(C_{Ph}–H) bond as a bona fide albeit weak (an)agostic coordinative interaction, with predominant Ni–(η^1 -C_{Ph}) character. This case represents an example of how late transition-metals can directly interact with C–H bonds to promote their cleavage.

UNIVERSITAT ROVIRA I VIRGILI
COMPUTATIONAL MODELING TO EXPLORE UNCONVENTIONAL REACTIVITY PATTERNS IN C-H ACTIVATION
AND BORON CHEMISTRY
Diego García López

4. Mechanistic insights into C–H activation involving dimetallic titanium species

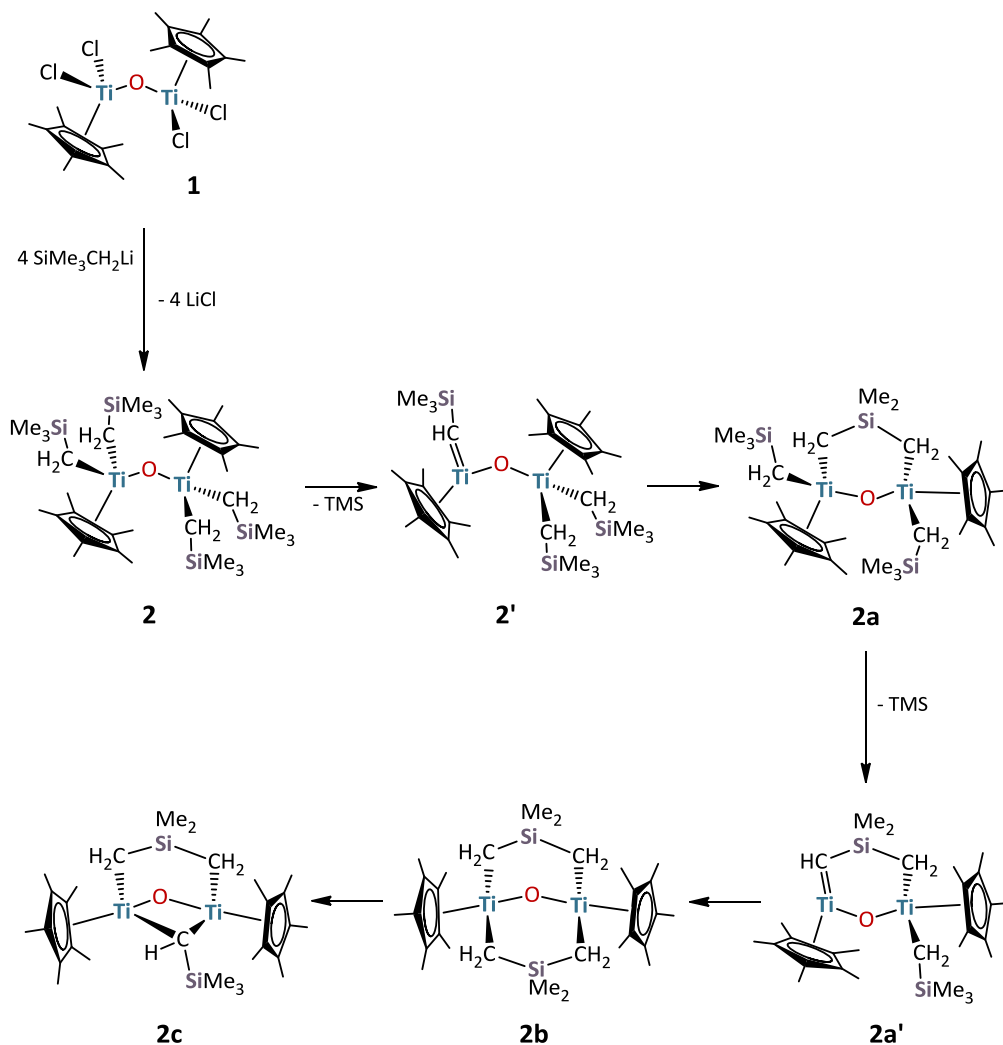
4.1. Introduction

One approach to transition-metal mediated C–H activation relies on the use of pre-existing functional groups (directing groups) in the substrate, in order to ensure the selectivity on the activation.^[1,2] Directed carbon-hydrogen activation processes classically proceed via five- or six-membered metallacycle intermediates, which are thermodynamically stable and therefore less reactive in the subsequent functionalization step. The emphasis in most synthetic and mechanistic studies about cyclometalation has been on mononuclear late transition metal systems; processes based on early transition metals are less known.^[3] Pioneering results in these latter showed that transient alkylidene species ($M=CHR$, $M = Ta$ and Ti) could assist in the aryloxy-mediated cyclometalation using high-valent tantalum and in the activation of the pentamethylcyclopentadienyl ligand in complex $[Ti(\eta^5-C_5Me_5)_2Me_2]$ to give the tuck-in compound $[Ti(\eta^5-C_5Me_5)(C_5Me_4CH_2)Me]$, respectively.^[4,5] Although there is now considerable precedent in the literature for cyclometalation processes via transient alkylidene intermediates in early transition metals,^[6–14] examples of such processes on dimetallic species have not yet been reported. A better knowledge of such compounds might provide valuable insights about cooperative effects between adjacent metal centers inaccessible in the mononuclear analogous.^[15]

In this context, the group of Dr. Santamaría recently reported that the dinuclear titanium complex $[\{Ti(\eta^5-C_5Me_5)(CH_2SiMe_3)_2\}_2(\mu-O)]$ (**2**), comprising sterically demanding (trimethylsilyl)methyl ligands, can undergo sequential $C(sp^3)$ -hydrogen bonds activation to give a series of metallacycle complexes (see Scheme 4.1).^[16] In addition, it was also proposed that transient alkylidene species might enable such transformations. In collaboration with this experimental group, our goal was to analyze theoretically the involvement of alkylidene intermediates in directing the selective activation of $C(sp^3)$ -H bonds on the adjacent titanium center. The study was also extended to other very common alkyl ligands in organometallic chemistry, namely, neopentyl (CH_2CMe_3) and benzyl (CH_2Ph) that have been obtained experimentally as well.

4.2. Experimental background

When a solution of $[\{\text{Ti}(\eta^5\text{-C}_5\text{Me}_5)\text{-(CH}_2\text{SiMe}_3)_2\}_2(\mu\text{-O})]$ (**2**) in benzene- d_6 was left overnight at room temperature and the solution was monitored by ^1H NMR spectroscopy, the formation of the metallacycle derivative $[\text{Ti}_2(\eta^5\text{-C}_5\text{Me}_5)_2(\mu\text{-CH}_2\text{SiMe}_2\text{CH}_2)(\text{CH}_2\text{SiMe}_3)_2(\mu\text{-O})]$ (**2a**) together with the loss of SiMe_4 (TMS) was observed, as illustrated in Scheme 4.1.

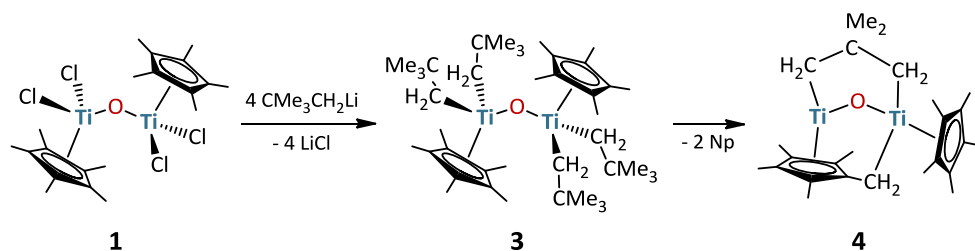


Scheme 4.1. Proposed mechanism for transformation of **2**, starting from its chloroderivative $[\{\text{Ti}(\eta^5\text{-C}_5\text{Me}_5)\text{Cl}_2\}_2(\mu\text{-O})]$ (**1**).

The solution kept at room temperature and monitored by ^1H NMR spectroscopy over a period of several days afforded the disappearance of **2a** and the additional formation of SiMe_4 as well as small amounts of a compound $[\text{Ti}_2(\eta^5\text{-C}_5\text{Me}_5)_2(\mu\text{-CH}_2\text{SiMe}_2\text{CH}_2)_2(\mu\text{-O})]$ (**2b**). Subsequent heating of this solution at temperatures over $45\text{ }^\circ\text{C}$ showed the presence of the μ -alkylidene compound $[\text{Ti}_2(\eta^5\text{-C}_5\text{Me}_5)_2(\mu\text{-CH}_2\text{SiMe}_2\text{CH}_2)(\mu\text{-CHSiMe}_3)(\mu\text{-O})]$ (**2c**), as outlined in Scheme 4.1. Finally, further heating over $120\text{ }^\circ\text{C}$ led to an intractable mixture.

All attempts to obtain complexes **2a** and **2c** in a pure form were unsuccessful; however, compound **2b** was isolated in pure crystalline form by crystallization of a hexane solution of **2a** and **2b** at $-20\text{ }^\circ\text{C}$. In this sense, while compound **2b** was fully characterized by NMR and IR spectroscopy, elemental analysis, and single-crystal X-ray diffraction, complexes **2a** and **2c** could only be characterized by NMR spectroscopy and by X-ray diffraction study in the case of **2c**.

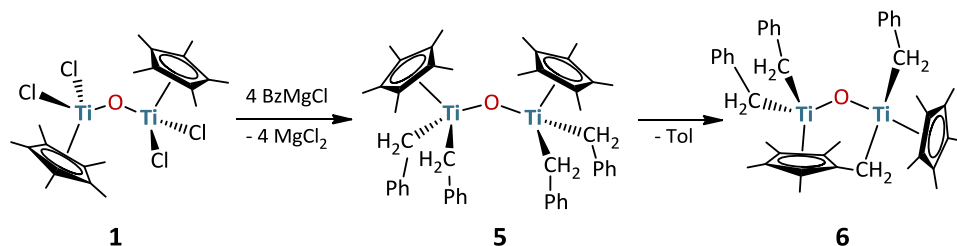
The synthesis and analysis of the analogous species comprising the neopentyl ligand (CH_2CMe_3) followed the same procedure described above (Scheme 4.2). Upon monitoring the reaction of chloroderivative $[\{\text{Ti}(\eta^5\text{-C}_5\text{Me}_5)\text{Cl}_2\}_2(\mu\text{-O})]$ (**1**) with 4 equivalents of $\text{LiCH}_2\text{CMe}_3$ in an NMR tube in benzene- d_6 at room temperature, the presence of neopentane and the formation of a mixture of tetralkyl compound $[\{\text{Ti}(\eta^5\text{-C}_5\text{Me}_5)(\text{CH}_2\text{CMe}_3)_2\}_2(\mu\text{-O})]$ (**3**) and tuck-over complex $[\text{Ti}_2(\eta^5\text{-C}_5\text{Me}_5)(\mu\text{-}\eta^5\text{-C}_5\text{Me}_4\text{CH}_2\text{-}\kappa\text{C})(\text{CH}_2\text{CMe}_3)(\mu\text{-CH}_2\text{CMe}_2\text{CH}_2)(\mu\text{-O})]$ (**4**) was revealed, as determined later by X-ray diffraction analysis. Although all attempts to prepare pure complex **3** have so far failed, it was possible to isolate and characterize compound **4** from a preparative-scale thermolysis reaction ($65\text{ }^\circ\text{C}$) in hexane in good yield (87%) (Scheme 4.2).



Scheme 4.2. Formation of complexes **3** and **4**.

In order to expand the study, the benzyl ligand was chosen as representative of different chemical and structural properties. The titanium tetrabenzyl oxoderivative, $[\{\text{Ti}(\eta^5\text{-C}_5\text{Me}_5)(\text{CH}_2\text{Ph})_2\}_2(\mu\text{-O})]$ (**5**), is cleanly accessible by a modification of the synthesis reported (Scheme 4.3). Thermolysis of **5** in benzene- d_6 solution for several days at $70\text{ }^\circ\text{C}$ and monitoring of the reaction by ^1H NMR spectroscopy disclosed gradual liberation of toluene and formation of the tucked over complex, $[\text{Ti}_2(\eta^5\text{-C}_5\text{Me}_5)(\mu\text{-}\eta^5\text{-C}_5\text{Me}_4\text{CH}_2\text{-}\kappa\text{C})(\text{CH}_2\text{Ph})_3(\mu\text{-O})]$ (**6**), according to Scheme 4.3. A dark red crystalline solid is obtained in 75% yield upon workup. After

crystallization from toluene, dark red crystals of **6** suitable for an X-ray diffraction study were isolated.



Scheme 4.3. Formation of complexes **5** and **6**.

4.3. Results and Discussion

Previous experimental work by the group of Dr. Santamaría have shown that the dinuclear oxocomplexes $[\{\text{Ti}(\eta^5\text{-C}_5\text{Me}_5)\text{R}_2\}_2(\mu\text{-O})]$ ($\text{R} = \text{CH}_2\text{SiMe}_3$ **2**, CH_2CMe_3 **3**, and CH_2Ph **5**) can promote the selective intramolecular cleavage of different unactivated β - and γ - $\text{C}(\text{sp}^3)\text{-H}$ bonds. Due to the importance of this transformation, it is important to elucidate the detailed reaction mechanism, including the origins of the C–H bond activation pathways for complexes **2**, **3**, and **5**, as well as the formation of “tuck-over” complexes **4** and **6**. Therefore, we decided to investigate the details of the reaction mechanism using DFT calculations.

Initially, we focused on the successive intramolecular C–H bond activation reactions of the complex $[\{\text{Ti}(\eta^5\text{-C}_5\text{Me}_5)(\text{CH}_2\text{SiMe}_3)_2\}_2(\mu\text{-O})]$ (**2**) and evaluated the mechanism step by step. The potential free energy profile has been splitted in two parts for convenience. Figure 4.1 displays the free energy profile for the first C–H activation and it is accompanied by the geometries of the key transition states (Figure 4.2) and the molecular orbitals of the intermediates (Figure 4.3); while Figure 4.4 shows the second C–H activation. In the first step, complex **2** may promote the direct formation of complex **2a** through γ -H abstraction by a trimethylsilylmethyl ligand bonded to the second metal center and loss of tetramethylsilane (TMS). However, the computed free energy barrier is too high ($46.4 \text{ kcal}\cdot\text{mol}^{-1}$) for a process occurring at room temperature. Alternatively, the formation of **2a** can occur in a two-step process via a Ti-alkylidene intermediate (**2'**), which results from an α -H abstraction by the alkyl ligand bonded to the same metal center.^[17] The calculated free energy barrier is moderate ($29.4 \text{ kcal}\cdot\text{mol}^{-1}$), and the reaction step is exergonic by $5 \text{ kcal}\cdot\text{mol}^{-1}$ (Figure 4.1).

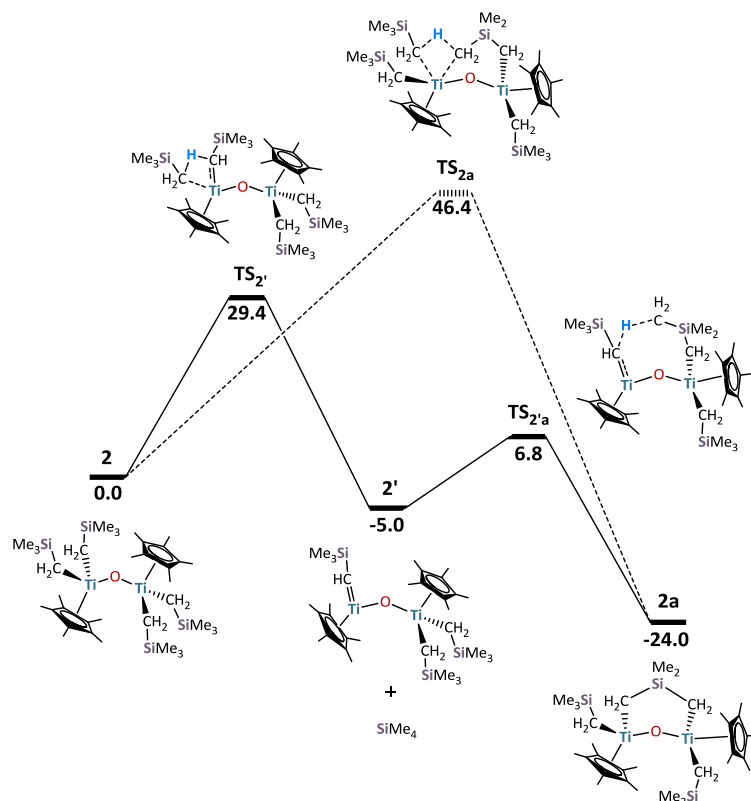


Figure 4.1. Gibbs free energy profile ($\text{kcal}\cdot\text{mol}^{-1}$) of intramolecular carbon-hydrogen bond activations for the α -H and γ -H abstraction in complex **2**.

The subsequent γ -H transfer from the methyl group of a $-\text{CH}_2\text{SiMe}_3$ ligand to the alkylidene moiety yields alkyl-metallacycle intermediate **2a** with a low free energy barrier ($11.8 \text{ kcal}\cdot\text{mol}^{-1}$). The corresponding transition state structure, **TS_{2'a}**, reveals that the H transfer is accompanied by simultaneous carbon-titanium bond formation (see Figure 4.2). In **2'**, the alkylidene carbon atom shows a strictly planar environment and a short Ti-C distance (1.86 \AA), suggesting that the group acts as a four-electron donor. In accordance, the HOMO molecular orbital corresponds mainly to a p-type orbital of the alkylidene carbon atom perpendicular to the Ti-C(H)-Si plane with some stabilizing π -type overlapping with the titanium d orbitals (see Figure 4.3). The HOMO of complex **2'** is significantly higher in energy (-5.18 eV) than that in Ti-alkyl complex **2** (-5.76 eV), indicating an enhanced nucleophilicity of the Ti-alkylidene moiety which is able to cleave unactivated $\text{C}(\text{sp}^3)\text{-H}$ bonds.

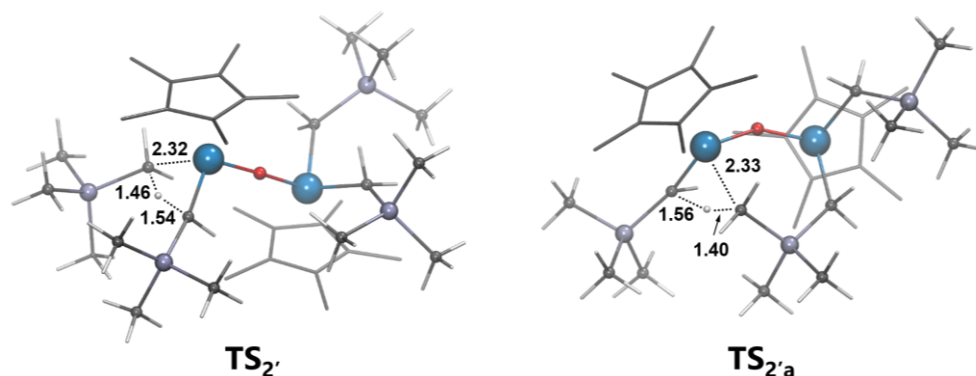


Figure 4.2. Computed molecular structures (distances in Å) of the transition states for α -H abstraction ($TS_{2'}$) and γ -H abstraction ($TS_{2'a}$) in complex **2**. The hydrogens of the pentamethylcyclopentadienyl ligands are omitted for clarity.

On the basis of these results, we proposed that the alkylidene functionality acts as directing group for the distal C-H activation on the adjacent metal center to yield an alkylmetallacycle compound. It is well-known that alkylidene complexes are active species in alkane/arene carbon-hydrogen bond activation in both intra- and intermolecular reactions.^[14,18–28] However, to the best of our knowledge on molecular species, studies have not been observed in which two metals are involved in distal C-H activations promoted by metal-ligand multiply bonded functionalities.

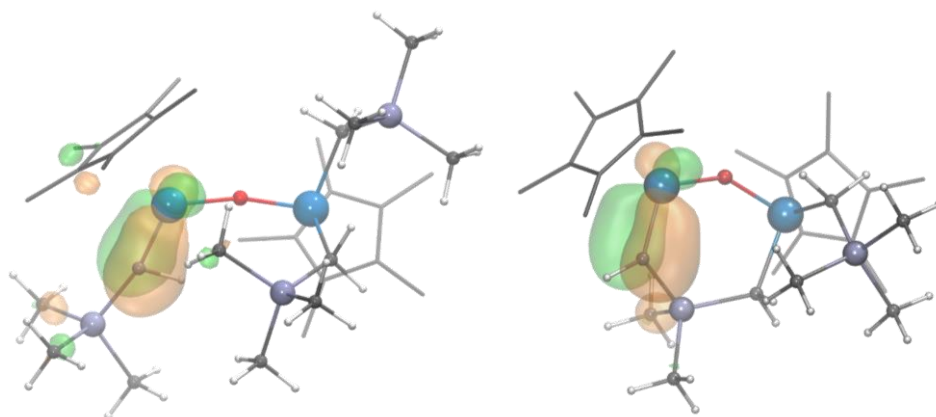


Figure 4.3. Representation of the π - δ -type HOMO orbitals for the two alkylidene intermediates, compound **2'** (left) and compound **2a'** (right). The hydrogens of the pentamethylcyclopentadienyl ligands are omitted for clarity

Compound **2a** can undergo the same sequence of two steps to form double alkyl-metallacycle species **2b** (see Figure 4.4). First, the α -H abstraction yields an alkylidene-metallacycle intermediate, **2a'**, and the loss of a second TMS molecule overcoming a moderate free energy

barrier of 28.3 kcal·mol⁻¹. Next, γ -H abstraction from a methyl group of the remaining –CH₂SiMe₃ ligand by the basic alkylidene moiety (see Figure 4.3) gives compound **2b** with a low free energy barrier of 9.4 kcal·mol⁻¹. The overall transformation from **2a** to **2b** is exergonic by 19.5 kcal·mol⁻¹, which is less favorable than the first metallacycle formation from **2** to **2a** (24.0 kcal·mol⁻¹) due to the larger strain of the double metallacyclic structure **2b**. Finally, the rearrangement of **2b** could lead to compound **2c**, but the direct process has a prohibitive free energy barrier of 60.1 kcal·mol⁻¹ (TS_{2c}). However, complex **2b** can react back to form **2a'** regenerating the alkylidene-metallacycle and the trimethylsilyl methyl ligand. From **2a'**, the α -H abstraction on the –CH₂SiMe₃ group via TS_{2a'c} transition state can yield final complex **2c**.

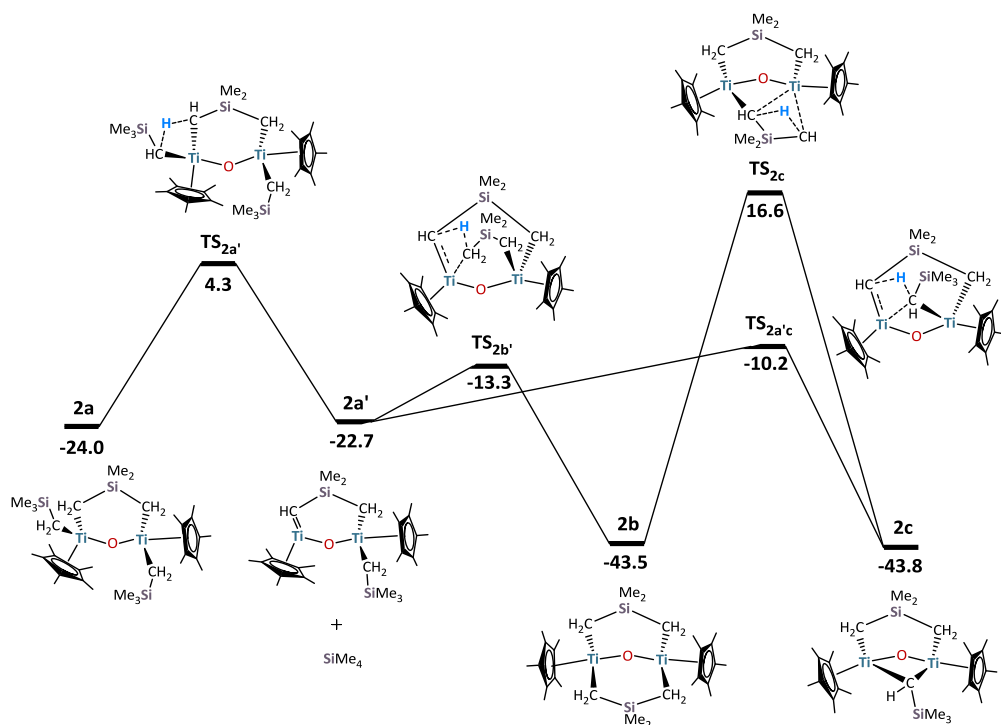


Figure 4.4. Gibbs free energy profile (kcal·mol⁻¹) for the successive intramolecular carbon–hydrogen bond activations in complex **2a**.

This process is kinetically disfavored by ~3 kcal·mol⁻¹ with respect to the formation of **2b** via γ -H abstraction on the –CH₂SiMe₃ group (TS_{2b'}). However, the formation of **2c** might be thermodynamically favored with respect to **2b** (by 0.3 kcal·mol⁻¹ at our computational level). Therefore, under conditions of thermodynamic control, at high temperature, compound **2c** is preferentially formed surpassing an overall free energy barrier of 33.3 kcal·mol⁻¹ (from **2b** to TS_{2a'c}). This high-energy value agrees well with the heating requirement to perform the experiment.^[8]

Replacing the trimethylsilylmethyl ligands in **2** by neopentyl (**3**) or benzyl (**5**) groups induced the unexpected intramolecular activation of a β -C(sp³)-H bond of a pentamethylcyclopentadienyl ligand to yield tuck-over complexes **4** and **6**, respectively. In order to illustrate the unusual formation of a d-block element tuck-over derivative, we discussed in more detail the reaction of these two complexes. Figure 4.5 represents the potential free energy profile for the transformation of **5**.

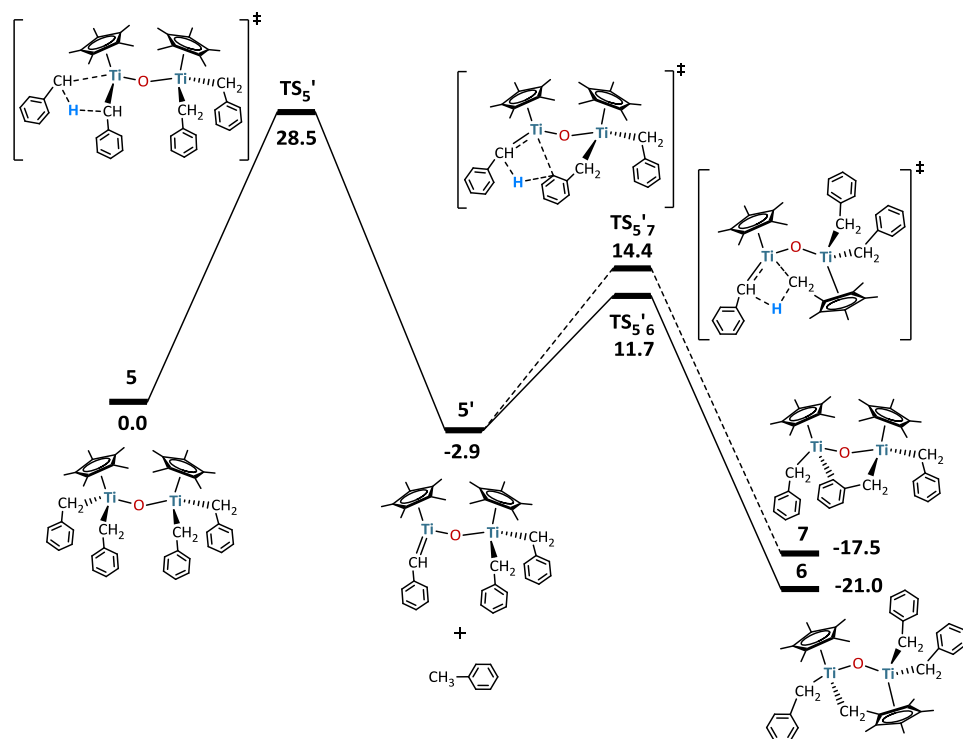


Figure 4.5. Gibbs free energy profile (kcal·mol⁻¹) for the intramolecular β -C(sp³)-H bond activations in compound **5**.

As in the previous case for compound **2**, the reaction starts by formation of Ti-alkylidene intermediate **5'** and the loss of toluene, with a similar computed free energy barrier (28.5 kcal·mol⁻¹). Then, a β -H abstraction from a η^5 -C₅Me₅ (14.6 kcal·mol⁻¹) is favored with respect to the γ -H abstraction from an sp²-carbon of a benzyl ligand (17.3 kcal·mol⁻¹), with the latter not being experimentally observed. Figure 4.6 shows the geometries of the transition states corresponding to the two competing pathways, **TS**_{5'6} and **TS**_{5'7}.

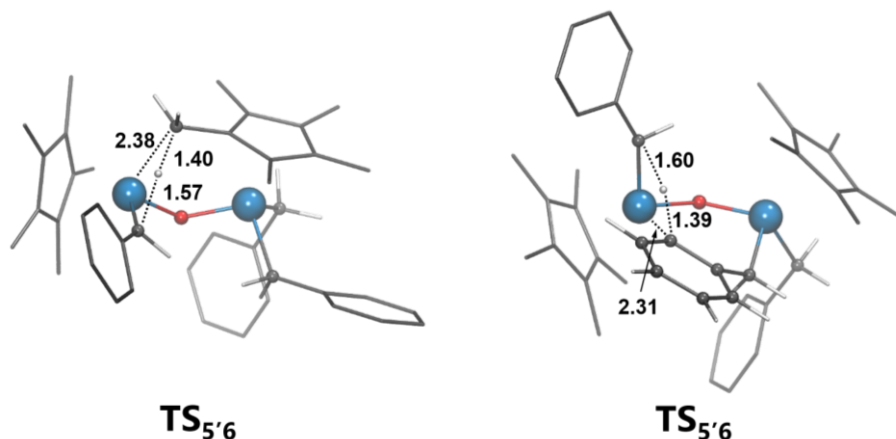


Figure 4.6. Computed molecular structures (distances in Å) of the transition states for β -H ($TS_{5'6}$) and the γ -H abstraction ($TS_{5'7}$) from complex **5'**. The hydrogens of the pentamethylcyclopentadienyl ligand and some phenyl groups are omitted for clarity.

Also, it is interesting to analyze the results obtained from complex $[\{Ti(\eta^5-C_5Me_5)(CH_2CMe_3)_2(\mu-O)\}]$ (**3**) where the activation of two different types of C-H bonds, the β - and the γ -C(sp^3)-H, are observed. The full potential free energy profile is shown in Figure 4.7 and Figure 4.8, and key structures are represented in Figure 4.9. Once the first titanium-alkylidene intermediate is formed (**3'**), the β -H abstraction from a pentamethylcyclopentadienyl group ($14.1 \text{ kcal}\cdot\text{mol}^{-1}$) is favored over the γ -H abstraction on an alkyl ligand ($16.2 \text{ kcal}\cdot\text{mol}^{-1}$), yielding a tuck-over complex with three alkyl ligands (**3a**). This complex can evolve further, forming a second titanium-alkylidene intermediate (**3a'**), from which double tuck-over complex **8** may be obtained. However, a β -H abstraction from the remaining pentamethylcyclopentadienyl is kinetically and thermodynamically disfavored with respect to a γ -H abstraction from the alkyl ligand ($\Delta G^\ddagger = 18.4$ and $8.8 \text{ kcal}\cdot\text{mol}^{-1}$ for $TS_{3a'8}$ and $TS_{3a'4}$ paths, respectively) to give compound **4**.

Mechanistic insights into C-H activation involving dimetallic titanium species

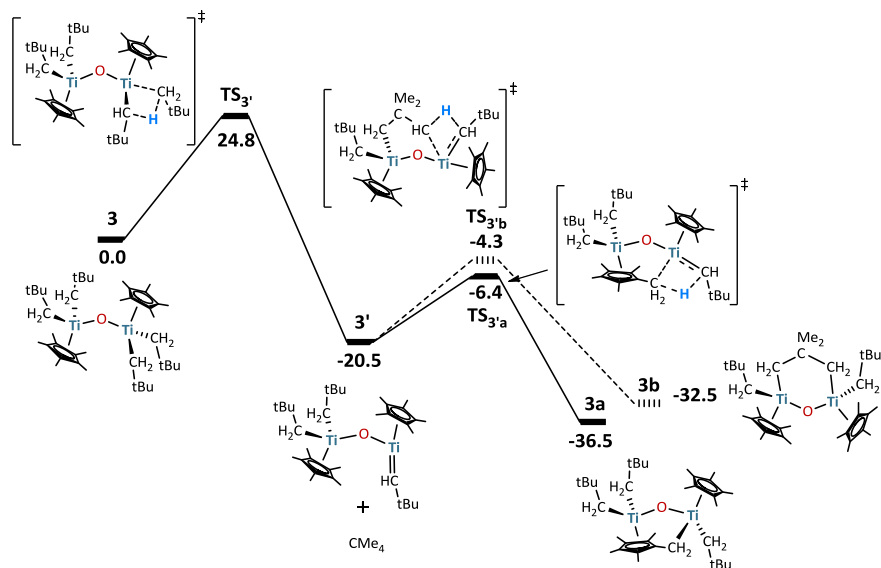


Figure 4.7. Gibbs free energy profile (kcal·mol⁻¹) for the first sequence of intramolecular C-H bond activations in compound **3**.

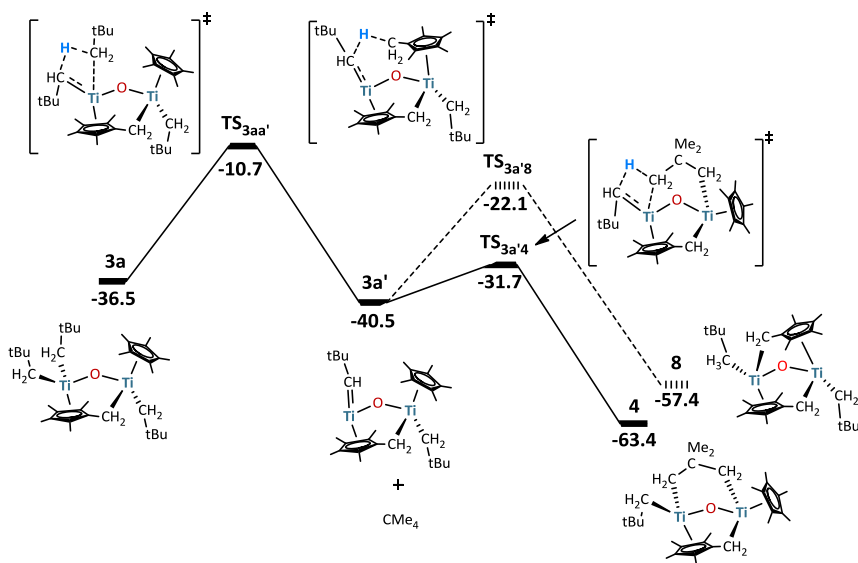


Figure 4.8. Gibbs free energy profile (kcal·mol⁻¹) for the second sequence of intramolecular C-H bond activations in compound **3**.

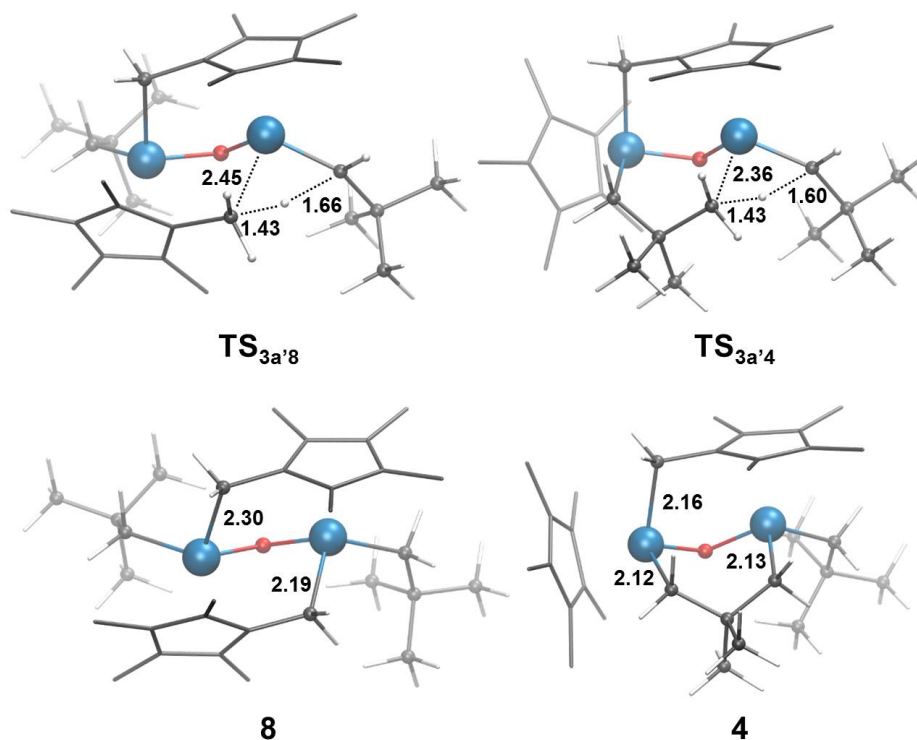


Figure 4.9. Computed molecular structures (distances in Å) of the key intermediates and transition states for the intramolecular C-H activations in compound $[\{\text{Ti}(\eta^5\text{-C}_5\text{Me}_5)(\text{CH}_2\text{CMe}_4)_2\}_2(\mu\text{-O})]$ (**3**). The hydrogens of the pentamethylcyclopentadienyl ligands are omitted for clarity.

The computational mechanistic path yielding the experimental products arising from complexes **2**, **3**, and **5** is summarized in Table 4.1. DFT calculations are in accordance with the determined chemoselectivity for the C-H bond abstraction, rendering both lower activation barriers and relative energies for those X-ray detected complexes. In addition, it was confirmed that the mechanism involves a more kinetically favoured first α -hydrogen abstraction to generate the transient titanium alkylidene intermediate, which is capable to activate remote C-H bonds in the titanium adjacent center. Table 4.2 collects the computed free-energy barriers ($\text{kcal}\cdot\text{mol}^{-1}$) for the first C-H activation process displayed by compounds **2**, **3**, and **5**, respectively.

Table 4.1. Summary of the C-H chemoselective activation process displayed by compounds **2**, **3**, and **5**, respectively.

Ligands	1 st C-H abstraction	2 nd C-H abstraction
-CH ₂ SiMe ₃	γ-H	γ-H
-CH ₂ CMe ₃	β-H	γ-H
-CH ₂ Ph	β-H	-

Table 4.2. Computed free-energy barriers (kcal·mol⁻¹) for the first C-H activation process displayed by compounds **2**, **3**, and **5**, respectively.

Ligands	α-H	β-H	γ-H
-CH ₂ SiMe ₃	29.4	-	46.4
-CH ₂ CMe ₃	24.8	50.1	51.7
-CH ₂ Ph	28.5	49.9	-

Table 4.3 summarizes the computational energy results collecting the key barriers for the transformation of the three complexes. From those values, we identified an order of reactivity for γ -H abstraction ($-\text{CH}_2\text{SiMe}_3 > -\text{CH}_2\text{CMe}_3 \cong -\text{CH}_2\text{Ph}$) with the computed ΔG^\ddagger values of 11.8, 16.2, and 17.3 kcal·mol⁻¹, respectively. In contrast, the free energy barriers for the β -H abstraction from the pentamethylcyclopentadienyl ligand vary in lesser extent and in the opposite direction. These two differentiated trends allow rationalizing the observed selectivity for C-H bond activation. Going from complex **2** to **3** and **5**, the γ -H abstraction becomes more disfavored; consequently, the β -H abstraction becomes competitive in full agreement with the experimental findings.

Table 4.3. Computed free-energy barriers (kcal·mol⁻¹) for α -H abstraction by Ti-alkyl moieties, γ -H abstraction by Ti-alkylidene groups, and $\eta^5\text{-C}_5\text{Me}_5$ β -H abstraction by Ti-alkylidene groups. Values at right and left correspond to the first and second H-abstraction, respectively. Free-energies in kcal·mol⁻¹.

Ligands	Ti-akyl		Ti-alkylidene	
	α -H	γ -H	β -H	β -H
$-\text{CH}_2\text{SiMe}_3$	29.4 / 28.3	11.8 / 9.4	16.1 / 13.8	
$-\text{CH}_2^t\text{Bu}$	24.8 / 25.8	16.2 / 8.8	14.1 / 18.4	
$-\text{CH}_2\text{Ph}$	28.5 / 32.6	17.3	14.6	

To further understand the differences in C-H activation barriers, we performed an analysis of the charge distribution in Ti-alkylidene intermediates **2'**, **3'**, and **5'**. In a combined experimental and computational work Baik *et al.* and Mindiola *et al.* have shown that the C-H bond cleavage by Ti-C multiple bonds is promoted in heterolytic fashion and that the reactivity can be correlated with bond polarization assessed using charges that are fit to the electrostatic potentials (ESP).^[27,28] The performance of such calculations in our complexes (see Figure 4.10) indicated that all the Ti=C(H)R bonds (R = $-\text{SiMe}_3$, $-\text{CMe}_3$, and $-\text{Ph}$) have similar polarizations ($\Delta q = 1.64$, 1.64 , and 1.63 au, respectively) with the carbon atom supporting the negative charges as it had been shown in MO orbitals of Figure 4.3. In contrast, the ESP-fit polarization of the γ -C-H bond in the $-\text{CH}_2\text{SiMe}_3$ moiety of complex **2'** ($\Delta q = 0.43$ au, averaged over all the bonds) was significantly larger than those computed for $-\text{CH}_2\text{CMe}_3$ and $-\text{CH}_2\text{Ph}$ moieties ($\Delta q = 0.27$ and 0.21 au in **3'** and **5'**, respectively). Those values correlate with the calculated energy barriers for the different types of γ -C-H bonds, establishing the same order: $-\text{CH}_2\text{SiMe}_3 < -\text{CH}_2\text{CMe}_3 \cong -\text{CH}_2\text{Ph}$ (Figure 4.10).

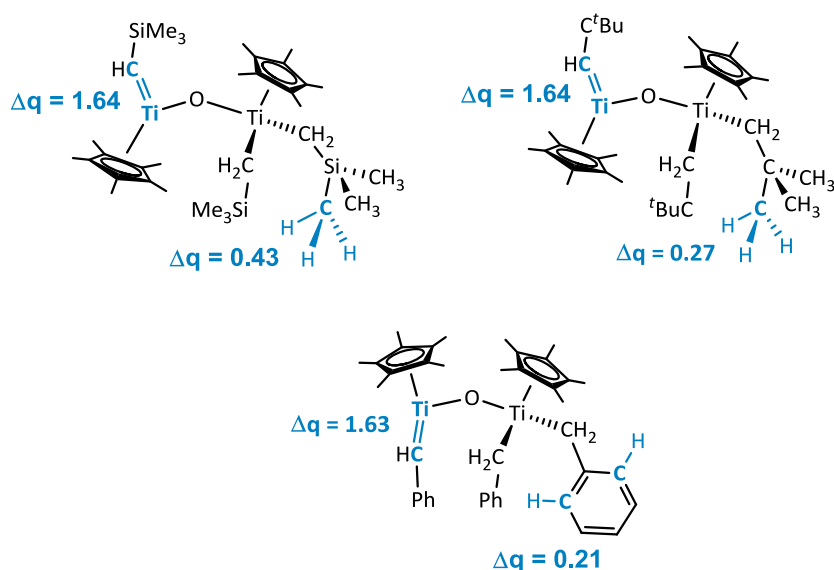


Figure 4.10. Computed ESP-fit polarization charges for complexes **2**, **3**, and **5** (from left to right).

4.4. Computational Details

Calculations were performed with the Gaussian09 series of programs^[29] within the framework of the density functional theory (DFT)^[30] using the B3LYP functional.^[31–33] The basis set for titanium and silicon atoms was associated with a pseudopotential,^[34] with a standard double- ξ LANL2DZ contraction, and the basis set was supplemented by f and d shells, respectively.^[35,36] The rest of atoms were described with a standard 6-31G(d,p) basis set.^[37–39] The stationary points were located without any restriction. Transition states were characterized by single imaginary frequency, whose normal mode corresponded to the expected motion. The use of larger basis set was also tested. The geometries were optimized with the method described above excluding the polarization functions of Ti and Si atoms, and the energy was calculated using an triple- ξ LANL2TZ basis set^[40] supplemented with an f shell^[35,36] for Ti and a 6-311+G(2d,p) basis set^[37–39] for the rest of atoms. The results show very small energy differences (<1 kcal·mol⁻¹) for the key initial steps (α - and γ -H abstraction), and qualitative, if not quantitative, fitting for the other reaction steps. Thus, the discussion is based on the more affordable, double- ξ quality basis set, what allows a straightforward comparison with previous studies on bond activation in related molecular titanium

oxides.^[41,42] The electronic structure of key species was analyzed using charges that are fit to the electrostatic potentials (ESPs).^[43]

4.5. Conclusions

The synthesis of a series of dinuclear titanium complexes $[\{\text{Ti}(\eta^5\text{-C}_5\text{Me}_5)\text{R}_2\}_2(\mu\text{-O})]$ made possible a study of their thermal behavior in solution. Sequential C–H activation undergone in these compounds formed metallacycle and/or “tuck-over” species. Our DFT study proved that the mechanistic pathway of such transformations involves a twostep process via alkylidene intermediates, which are basic enough to activate the quite inert C–H bonds. Generation of these intermediates occurred through α -H abstraction on the ligands attached to the same titanium atom, which is the determining step, whereas β - and γ -H abstractions took place between ligands of different metallic centers. This cooperative behavior allows the selective activation of the distal C–H bonds. The calculations also allowed establishment of a reactivity order for the different type of γ -C–H bonds: $-\text{CH}_2\text{SiMe}_3 > -\text{CH}_2\text{CMe}_3 \cong -\text{CH}_2\text{Ph}$. Since the energy barrier of the pentamethylcyclopentadienyl activation varies to a lesser extent along the series of compounds, the observed selectivity can be straightforwardly explained. The most reactive alkylsilyl fragments in compound **2** undergo only γ -H abstractions. In contrast, for the benzyl ligands in compound **5** the β -H abstraction on a pentamethylcyclopentadienyl fragment is preferred and is the only observed, whereas complex **3** has an intermediate behaviour and gives a mixture of β - and γ -H abstractions.

4.6. References

- [1] Y. Qin, L. Zhu, S. Luo, *Chem. Rev.* **2017**, *117*, 9433–9520.
- [2] Z. Chen, B. Wang, J. Zhang, W. Yu, Z. Liu, Y. Zhang, *Org. Chem. Front.* **2015**, *2*, 1107–1295.
- [3] M. Albrecht, *Chem. Rev.* **2010**, *110*, 576–623.
- [4] L. R. Chamberlain, A. P. Rothwell, I. P. Rothwell, *J. Am. Chem. Soc.* **1984**, *106*, 1847–1848.
- [5] C. McDade, J. C. Green, J. E. Bercaw, J. C. Green, *Organometallics* **1982**, *1*, 1629–1634.
- [6] L. R. Chamberlain, I. P. Rothwell, J. C. Huffman, *J. Am. Chem. Soc.* **1986**, *108*, 1502–

- 1509.
- [7] D. J. Duncalf, R. J. Harrison, A. McCamley, B. W. Royan, *J. Chem. Soc. Chem. Commun.* **1995**, 2421–2422.
- [8] J. S. Vilaro, M. A. Lockwood, L. G. Hanson, J. R. Clark, B. C. Parkin, P. E. Fanwick, I. P. Rothwell, *J. Chem. Soc. Dalton Trans.* **1997**, 3353–3362.
- [9] J. L. Polse, A. W. Kaplan, R. A. Andersen, R. G. Bergman, *J. Am. Chem. Soc.* **1998**, *120*, 6316–6328.
- [10] H. Lee, J. B. Bonanno, T. Hascall, J. Cordaro, J. M. Hahn, G. Parkin, *J. Chem. Soc. Dalton Trans.* **1999**, 1365–1368.
- [11] J. E. Kickham, F. Guérin, D. W. Stephan, *J. Am. Chem. Soc.* **2002**, *124*, 11486–11494.
- [12] H. Van Der Heijden, B. Hessen, *Inorganica Chim. Acta* **2003**, *345*, 27–36.
- [13] T. E. Hanna, I. Keresztes, E. Lobkovsky, W. H. Bernskoetter, P. J. Chirik, *Organometallics* **2004**, *23*, 3448–3458.
- [14] F. Basuli, B. C. Bailey, J. C. Huffman, D. J. Mindiola, *Organometallics* **2005**, *24*, 3321–3334.
- [15] Y. J. Park, J.-W. Park, C.-H. Jun, *Acc. Chem. Res.* **2008**, *41*, 222–234.
- [16] J. I. González-Pérez, A. Martín, M. Mena, C. Santamaría, *Organometallics* **2016**, *35*, 2488–2493.
- [17] R. R. Schrock, *Chem. Rev.* **2002**, *102*, 145–179.
- [18] C. S. Adams, P. Legzdins, E. Tran, *J. Am. Chem. Soc.* **2001**, *123*, 612–624.
- [19] C. S. Adams, P. Legzdins, E. Tran, *Organometallics* **2002**, *21*, 1474–1486.
- [20] K. Wada, C. B. Pamplin, P. Legzdins, *J. Am. Chem. Soc.* **2002**, *124*, 9680–9681.
- [21] K. Wada, C. B. Pamplin, P. Legzdins, B. O. Patrick, I. Tsyba, R. Bau, *J. Am. Chem. Soc.* **2003**, *125*, 7035–7048.
- [22] J. Y. K. Tsang, M. S. A. Buschhaus, P. Legzdins, B. O. Patrick, *Organometallics* **2006**, *25*, 4215–4225.
- [23] J. G. Andino, U. J. Kilgore, M. Pink, A. Ozarowski, J. Krzystek, J. Telsner, M.-H. Baik, D. J. Mindiola, *Chem. Sci.* **2010**, *1*, 351–356.
- [24] H. van der Heijden, B. Hessen, *J. Chem. Soc. Chem. Commun.* **1995**, 145–146.
- [25] J. Cheon, D. M. Rogers, G. S. Girolami, *J. Am. Chem. Soc.* **1997**, *119*, 6804–6813.
- [26] B. C. Bailey, H. Fan, E. W. Baum, J. C. Huffman, M.-H. Baik, D. J. Mindiola, *J. Am. Chem. Soc.* **2005**, *127*, 16016–16017.
- [27] B. C. Bailey, H. Fan, J. C. Huffman, M. H. Baik, D. J. Mindiola, *J. Am. Chem. Soc.* **2007**, *129*, 8781–8793.
- [28] J. A. Flores, V. N. Cavaliere, D. Buck, B. Pinter, G. Chen, M. G. Crestani, M.-H. Baik, D. J. Mindiola, *Chem. Sci.* **2011**, *2*, 1457–1462.

- [29] M. J. Frisch, G. W. Trucks, H. B. Schlegel, G. E. Scuseria, M. A. Robb, J. R. Cheeseman, G. Scalmani, V. Barone, B. Mennucci, G. A. Petersson, H. Nakatsuji, M. Caricato, X. Li, H. P. Hratchian, A. F. Izmaylov, J. Bloino, G. Zheng, J. L. Sonnenberg, M. Hada, M. Ehara, K. Toyota, R. Fukuda, J. Hasegawa, M. Ishida, T. Nakajima, Y. Honda, O. Kitao, H. Nakai, T. Vreven, J. A. Montgomery, Jr., J. E. Peralta, F. Ogliaro, M. Bearpark, J. J. Heyd, E. Brothers, K. N. Kudin, V. N. Staroverov, R. Kobayashi, J. Normand, K. Raghavachari, A. Rendell, J. C. Burant, S. S. Iyengar, J. Tomasi, M. Cossi, N. Rega, J. M. Millam, M. Klene, J. E. Knox, J. B. Cross, V. Bakken, C. Adamo, J. Jaramillo, R. Gomperts, R. E. Stratmann, O. Yazyev, A. J. Austin, R. Cammi, C. Pomelli, J. W. Ochterski, R. L. Martin, K. Morokuma, V. G. Zakrzewski, G. A. Voth, P. Salvador, J. J. Dannenberg, S. Dapprich, A. D. Daniels, O. Farkas, J. B. Foresman, J. V. Ortiz, J. Cioslowski, D. J. Fox, *Gaussian 09, Revis. A.02, Gaussian, Inc., Wallingford CT* **2009**.
- [30] R. G. Parr, Y. Weitao, *Density-Functional Theory of Atoms and Molecules*, Oxford University Press, **1994**.
- [31] C. Lee, W. Yang, R. G. Parr, *Phys. Rev. B* **1988**, *37*, 785–789.
- [32] A. D. Becke, *J. Chem. Phys.* **1993**, *98*, 5648–5652.
- [33] P. J. Stephens, F. J. Devlin, C. F. Chabalowski, M. J. Frisch, *J. Phys. Chem.* **1994**, *98*, 11623–11627.
- [34] P. J. Hay, W. R. Wadt, *J. Chem. Phys.* **1985**, *82*, 299–310.
- [35] A. Höllwarth, M. Böhme, S. Dapprich, A. W. Ehlers, A. Gobbi, V. Jonas, K. F. Köhler, R. Stegmann, A. Veldkamp, G. Frenking, *Chem. Phys. Lett.* **1993**, *208*, 237–240.
- [36] A. W. Ehlers, M. Böhme, S. Dapprich, A. Gobbi, A. Höllwarth, V. Jonas, K. F. Köhler, R. Stegmann, A. Veldkamp, G. Frenking, *Chem. Phys. Lett.* **1993**, *208*, 111–114.
- [37] M. M. Francl, W. J. Pietro, W. J. Hehre, J. S. Binkley, M. S. Gordon, D. J. DeFrees, J. A. Pople, *J. Chem. Phys.* **1982**, *77*, 3654–3665.
- [38] W. J. Hehre, R. Ditchfield, J. A. Pople, *J. Chem. Phys.* **1972**, *56*, 2257–2261.
- [39] P. C. Hariharan, J. A. Pople, *Theor. Chim. Acta* **1973**, *28*, 213–222.
- [40] L. E. Roy, P. J. Hay, R. L. Martin, *J. Chem. Theory Comput.* **2008**, *4*, 1029–1031.
- [41] S. Aguado-Ullate, J. J. Carbó, O. González-del Moral, A. Martín, M. Mena, J.-M. Poblet, C. Santamaría, *Inorg. Chem.* **2011**, *50*, 6269–6279.
- [42] J. J. Carbó, D. García-López, O. González-Del Moral, A. Martín, M. Mena, C. Santamaría, *Inorg. Chem.* **2015**, *54*, 9401–9412.
- [43] C. M. Breneman, K. B. Wiberg, *J. Comput. Chem.* **1990**, *11*, 361–373.

UNIVERSITAT ROVIRA I VIRGILI

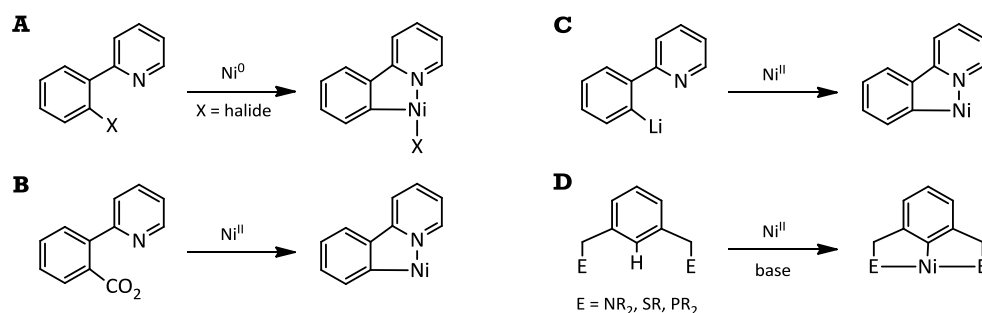
COMPUTATIONAL MODELING TO EXPLORE UNCONVENTIONAL REACTIVITY PATTERNS IN C-H ACTIVATION
AND BORON CHEMISTRY

Diego García López

5. Unraveling the agostic interactions of arene C(sp²)-H at nickel pincer complexes

5.1. Introduction

Cyclometalation typically precedes the functionalization of aryl C(sp²)-H bonds, often using the ligating effect of a neighboring group to orient the C-H bond within the metal coordination sphere.^[1] Pyridine has proven very efficient as a directing group, and a variety of second- and third-row metal-based systems facilitate the selective C-H metalation of pyridylarenes. In stark contrast to its second-row congener Pd, Ni-based systems were very underdeveloped for selective C(sp²)-H functionalization until recently.^[2–16] For stoichiometric cyclometalation at Ni, the Ni-C bond is generally induced via oxidative addition of a carbon-halogen fragment (to Ni⁰; Scheme 5.1.A),^[17–24] decarboxylation (Scheme 5.1.B),^[25] or transmetalation from a lithiated derivative (Scheme 5.1.C).^[26] Formation of a Ni-C bond from an unactivated C-H bond is common for encumbering ligand structures that enforce the C-H bond in close proximity of the metal, such as pincer-type ECE ligands and macrocyclic structures (Scheme 5.1.D).^[27–30] However, for less restricting (“nonpincer”) bidentate ligand structures, procedures involving direct C-H metalation pathways with nickel are rare,^[31–35] despite the fact that the first reported cyclometalated complex involves the reaction of nickelocene with azobenzene.^[36]



Scheme 5.1. Well-defined routes A-D toward cyclometalated Ni^{II} species

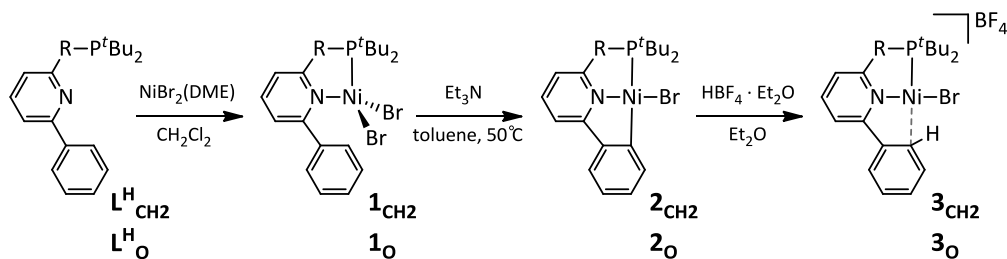
Although stoichiometric C-H metalation of ligands is uncommon for Ni^{II}, the formation of such a nickelacycle was recently postulated as a key step in the Ni-catalyzed aromatic C-H bond functionalization, using a bidentate directing-group approach.^[2–5,8–11,13,14,37–39] Despite their intermediacy in various catalytic processes, including ethylene oligo- and polymerization,^[40] only few systematic reactivity studies of the Ni-carbon bond in these entities are

reported.^[10,31–34] Furthermore, very little information is available on agostic interactions in Ni^{II} complexes, for which the C_{Ar}-H bond interacts with the Ni^{II} center.^[41] Although this type of bonding most likely precedes the actual C-H activation or metalation step and is therefore an interesting research topic for the comprehension of this linkage activation processes, isolated complexes with agostic interactions are scarcely documented for first-row transition metal pincer complexes.^[42,43]

Recently, a reactive ligand 2-di(*tert*-butylphosphanomethyl)-6-phenylpyridine (PCH₂NC_{Ph}, L_{CH₂^H) was introduced by the group of Prof. van der Vlugt in reversible cyclometalation as strategy for cooperative catalysis, using a strongly chelating P,N-ligand that featured a flanking phenyl arm.^[44] These results have been expanded in order to investigate the potential for cyclometalation and stabilization of an agostic M-(C-H) interaction using the versatile coordination chemistry displayed by ligands of this type.^[45–47] The cyclometalation of the previous ligand and the related 2-phosphinito-6-phenyl-pyridine ligand (PONC_{Ph}, L_{O^H) to Ni^{II} led to complexes bearing the cyclometalated phenyl group as a flanking entity. In contrast to the pivotal phenyl ring found in traditional pincer systems, these side arm positions were more accessible and susceptible to follow-up chemistry. Protonation of the Ni-C bond generated the example of two structurally characterized Ni-(C_{Ph}-H) complexes. In collaboration with this experimental group, we aimed to take a closer look and analyze whether there exists agostic Ni-(C-H) interactions using topological analysis of the electron density.}}

5.2. Experimental background

Reaction of ligands 2-di(*tert*-butylphosphanomethyl)-6-phenylpyridine, L_{CH₂^H, and 2-phosphinito-6-phenyl-pyridine, L_{O^H, with NiBr₂(DME) (DME = 1,2-dimethoxyethane) at room temperature yielded the purple paramagnetic complex NiBr₂(κ²-P,N-L_{CH₂^H) **1**_{CH₂ and the brown paramagnetic complex NiBr₂(κ²-P,N-L_{O^H) **1**_O respectively (Scheme 5.2), which were characterized by single-crystal X-ray crystallography (Figure 5.1, left up and left down). Addition of triethylamine to a toluene solution of either **1**_{CH₂ or **1**_O at 50 °C led to a gradual color change to yellow within 30 min, concomitant with appearance of a white precipitate corresponding to the NEt₃·HCl salt. Diamagnetic products **2**_{CH₂ and **2**_O were obtained that show well-defined NMR spectra.}}}}}}}



Scheme 5.2. Coordination of ligands **L**_{CH₂}^H (R = CH₂) and **L**_O^H (R = O) to Ni^{II}Br₂(DME) to form paramagnetic complexes **1**_{CH₂}/**1**_O, subsequent cyclometalation to complexes **2**_{CH₂}/**2**_O and selective protonation of the Ni-C bond to generate the cationic derivatives **3**_{CH₂}/**3**_O with a coordinative Ni-(C-H) interaction.

The molecular structures for **2**_{CH₂} and **2**_O (Figure 5.1, middle up and middle down) confirm the selective C-H metalation of the phenyl side arm of **L**_{CH₂}^H and **L**_O^H to give NiBr(κ³-P,N,C-**L**_{CH₂}^H) and NiBr(κ³-P,N,C-**L**_O^H) respectively. The Ni₁-C₁ bond lengths (1.928(4) Å for **2**_{CH₂} and 1.923(4) Å for **2**_O) are similar to that observed for other nickelacycles with a flanking phenyl ring, which all fall in the range of 1.91-1.95 Å.^[17-20,22-26,31-35] However, this linkage is long in comparison to related Ni-complexes, which have the phenyl ring in the pivotal position and have Ni-C bond lengths of 1.85-1.86 Å.^[48-51] The difference in Ni-C bond lengths indicates the impact of encumbering ligands. This can be seen in a slightly distorted square planar geometry around the nickel center, whose angles ∠P₁-Ni₁-C₁ are 169.82(1)° for **2**_{CH₂} and 166.28(12)° for **2**_O. This “forced” geometry combined with the mutual *trans* disposition of the σ-donating phenyl-fragment and the phosphane/phosphinite donor might potentially impose enhanced reactivity to the Ni-C fragment.

Addition of an equimolar amount of ethereal HBF₄ to a yellow toluene solution of either **2**_{CH₂} or **2**_O (Scheme 5.2) led to instantaneous precipitation of a blue and purple solid, respectively. Electrospray ionization mass spectrometry (ESI-MS) suggested the formation of mononuclear cationic species with a reprotonated ligand fragment. When **3**_{CH₂} was dissolved in dichloromethane, a band at λ = 577 nm was observed in the visible region of the UV-vis spectrum, while the corresponding band was observed at λ = 535 nm for **3**_O. NMR spectroscopy (³¹P, ¹H, or ¹³C) proved ineffective for both compounds since broad signals were observed.

Single-crystal X-ray diffraction corroborated the solid-state structure of complexes **3**_{CH₂} and **3**_O to be formulated as [NiBr(κ³-P,N,(C-H)-**L**_{CH₂}^H)]BF₄ and [NiBr(κ³-P,N,(C-H)-**L**_O^H)]BF₄, respectively (Figure 5.1, right up and right down). The molecular structures display a slightly distorted square planar Ni-center, due to a coordinative interaction in both cases with the aromatic C-H bond *ortho* to the pyridine ring. This interaction was evidenced by the Ni₁⋯H₁ distance of 2.12(4) Å for **3**_{CH₂} and 2.02(9) Å for **3**_O, and the Ni₁⋯C₁ distance of 2.407(4) Å for

3_{CH2} and 2.355(8) Å for **3**_o, which is much shorter than the van der Waals radii (3.3 Å for Ni⋯C) and indicates an interaction between Ni and the C-H bond.

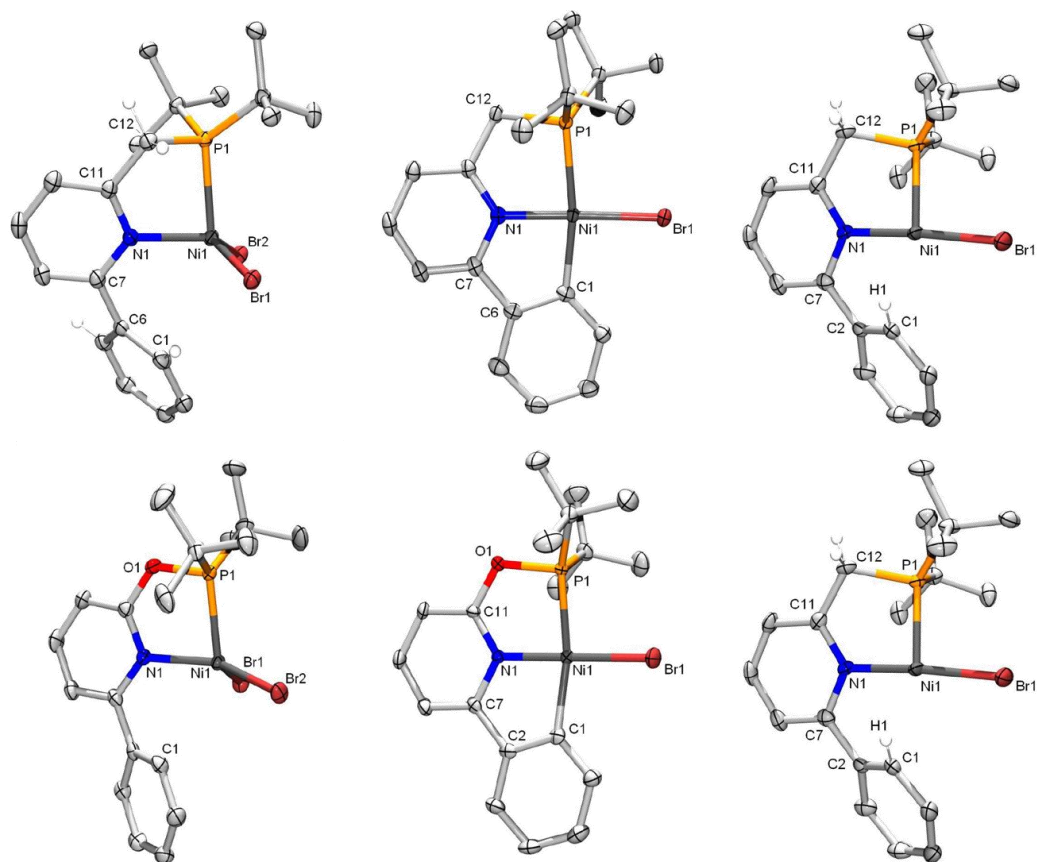


Figure 5.1. Displacement ellipsoid plots (50% probability level) for **1**_{CH2}/**1**_o (left up and left down), **2**_{CH2}/**2**_o (middle up and middle down), and **3**_{CH2}/**3**_o (right up and right down).

Furthermore, a $\pm 10^\circ$ tilting of H₁ from the aromatic plane is observed for both complexes, which is a feature that is present in related complexes with an M-(C-H) interaction. The closest related structure is from a nickel benzoporphyrin, which shows a Ni⋯(CH) distance of ~ 2.4 Å.^[42] Finally, addition of NEt₃ to a suspension of **3**_{CH2} and **3**_o in toluene at room temperature led to almost instantaneous regeneration of **2**_{CH2} and **2**_o respectively, suggestive of facile deprotonation of the C_{Ph}-H bond in these cationic complexes. The fact that such bond could be deprotonated within seconds suggests that its interaction with Ni might enhance the acidic behavior of the linkage C_{Ph}-H and thus facilitates cyclometalation. Intrigued by the observation of this unusual Ni-(C_{Ph}-H) interaction in the solid state, we were motivated to

understand the bonding in complex **3**_{CH₂} and **3**_o by means of DFT calculations and analysis of the electron density topology.

5.3. Results and Discussion

The solid-state structure of **3**_{CH₂} and **3**_o are well reproduced by DFT calculations in the gas-phase singlet state. The computed relevant metric parameters Ni₁...C₁ and Ni₁...H₁ distances (2.402 Å and 2.155 Å for **3**_{CH₂}, and 2.364 Å and 2.094 Å for **3**_o), and the tilting of H₁ from the planar phenyl ring (~10°), are nearly identical to the solid-state structure obtained from X-ray diffraction. In both complexes, the C₁-H₁ bond length is elongated with respect to that in the free ligand (from 1.085 to 1.097 Å for **3**_{CH₂} and to 1.099 Å for **3**_o), which indicates a weakening of the C-H bond. Furthermore, the C₁-H₁ stretching frequency decreases relatively to the free ligand (from 3233 to 3094 for **3**_{CH₂} and 3071 cm⁻¹ for **3**_o), which is another indication of the C-H bond weakening. These observations are indicative of an interaction between nickel and the C-H bond. Since it was detected an uncommon facile deprotonation of complexes **3**_{CH₂} and **3**_o, we want to determine the promoting degree of such process enhanced by the metal center. However, geometrical criteria might result ambiguous for unclear interactions. Hence, a computational treatment can shed some light into this presumably strengthless interaction. As previously stated in Chapter 1, agostic interactions weaken the involved C-H bond by simultaneous electro-donation from the C-H σ-bond to an unoccupied orbital of a hypovalent transition metal center and back-donation from the metal to the C-H π*-orbital. Methods based on the topology of electron density have proven to be an effective tool, not only to characterize, but also to classify the toughness of agostic interactions.^[52] These techniques were recently carried out to study the bonding scenario between Rh^I and the C_{Ph}-H fragment of a protonated PCP-pincer ligand, for which a marked agostic interaction was suggested.^[53] Therefore, inspired by this work, we performed analyses within the Quantum Theory of Atoms In Molecules (QTAIM)^[54] and the Electron Localization Function (ELF)^[55] for complexes **3**_{CH₂} and **3**_o (Table 5.1). Moreover, a direct comparison using the same computational level was made between these compounds and the aforementioned [Rh(CO)(PC^HP)]⁺ in order to benchmark our complexes with the reported agostic interaction.^[53,56]

The computed density map for a plane that contains Ni and the C_{Ph}-H fragment of complex **3**_o can be seen in Figure 5.2. The same density map was performed for complex **3**_{CH₂} giving indistinguishable picture results with respect to **3**_o. One bond critical point (BCP) linking the Ni and C₁ atoms was localized (indicated by a blue dot). According to QTAIM theory, a chemical bond exists if a line of locally maximum electron density links two neighboring atoms and also if along that line there is a BCP, evidencing in this case a Ni-(η¹-C₁) interaction. Noteworthy is

the curving of the bond path toward H₁, which indicates that two charge density maxima, corresponding to the Ni···H₁ and Ni···C₁ BCPs, and a minimum, corresponding to the ring critical point, were very closely situated and have collapsed into one maximum. At the BCP, the low value of the electronic charge density, ($\rho(\mathbf{r}) = 0.037$) and the low and positive values of the Laplacian of the charge density, ($\nabla^2\rho(\mathbf{r}) = 0.167$) are indicative of closed shell-type interaction (instead of a typical covalent electron sharing interaction).

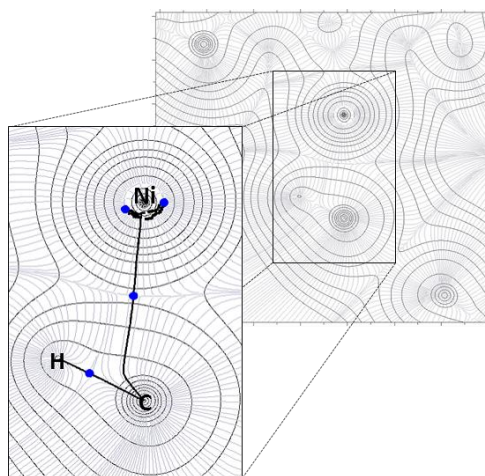


Figure 5.2. DFT-calculated contour map of electron charge density, $\rho(\mathbf{r})$, showing the BCP that links the Ni and C₁ atom in **3o**.

With ELF analysis a disynaptic $V(\text{M},\text{C})$ attractor was found between nickel and aromatic carbon C₁, indicating an electron sharing interaction between those atoms (Figure 5.3). This topology is analogous to that reported for $[\text{Rh}(\text{CO})(\text{PC}^{\text{H}}\text{P})]^+$, wherein a Rh-($\eta^1\text{-C}_{\text{Ph}}$) interaction with a concomitant agostic $\eta^2\text{-(C,H)}$ interaction was proposed.^[53,56] However, the population of the $V(\text{M},\text{C})$ basin in **3o** (0.16 e) is lower than in cationic $[\text{Rh}(\text{CO})(\text{PC}^{\text{H}}\text{P})]^+$ (0.31 e), suggesting that the bonding situation in **3o** is closer to the anagostic $\eta^1\text{-C}$ interaction (Table 5.1).

For complex **3CH₂** no valence attractor was found within ELF analysis, suggesting a weaker interaction compared to complex **3o**, that is, there is no significant electron sharing between the C_{Ar}-H and Ni. However, the other parameters comprised in Table 5.1 are almost identical between complex **3CH₂** and **3o**, although the values for **3CH₂** are lower in all cases. These results imply that the Ni···(C_{Ph}-H) interaction in **3o** is somewhat stronger compared to that found in **3CH₂**. This fact might be due to the more electron-withdrawing character of the phosphinite ligand, which would produce a more electron-deficient metal center that could in turn search for electron density through an enhanced agostic interaction with the C_{Ph}-H bond.

Table 5.1. Geometric, spectroscopic, QTAIM, and ELF parameters for the M-(C-H) interaction in complexes **3**_{CH2} and **3**_O [NiBr(κ³-P,N,(C-H)-L^H)]⁺ and the previously reported [Rh(CO)(P(C-H)P)]⁺ complex.^[56]

Distances (Å), angles (deg) and distance ratio			
$d(\text{C}\cdots\text{M})$	2.402	2.364	2.289
$d(\text{H}\cdots\text{M})$	2.155	2.094	2.006
$d(\text{C-H})$	1.097	1.099	1.122
$\angle(\text{C-H})_{\text{out of plane}}$	10.8	12.6	14.7
$\frac{d(\text{C-H})}{d(\text{H}\cdots\text{Ni})}$	0.51	0.52	0.56
Vibrational frequencies (cm ⁻¹) and frequency ratio			
$\nu(\text{C-H})$	3094	3071	2807
$\frac{\nu(\text{C-H})}{\nu(\text{C-H})_{\text{free lig.}}}$	0.96	0.95	0.88
Electron density, ρ , and Laplacian, $\nabla^2\rho$, at the BCP's (a.u.), and ρ_{BCP} ratio			
BCP(C \cdots M)	0.033 / 0.146	0.037 / 0.167	0.062 / 0.215
BCP(C-H)	0.274 / -0.937	0.272 / -0.919	0.254 / 0.779
$\frac{\rho_{\text{BCP}}(\text{C-H})}{\rho_{\text{BCP}}(\text{C-H})_{\text{free lig.}}}$	0.95	0.95	0.90
ELF population of valance basins (a.u.)			
$V(\text{M,C})$	-	0.16	0.31
$V(\text{C,H})$	2.19	2.20	2.18

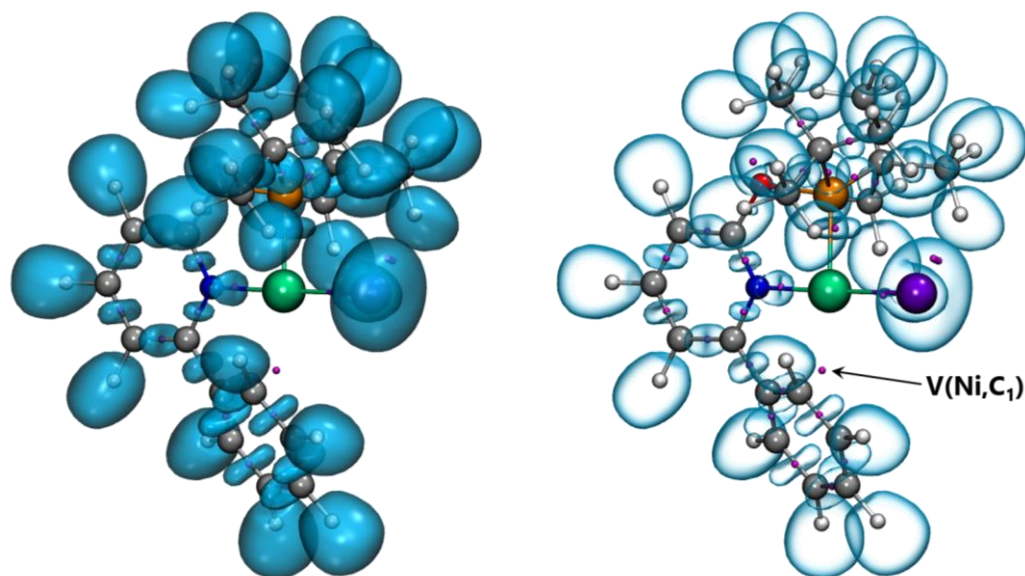
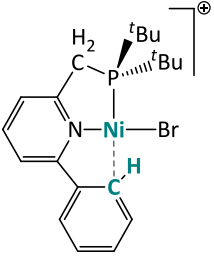
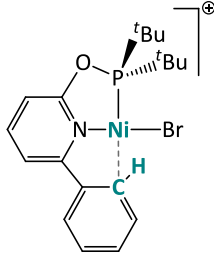


Figure 5.3. ELF localization domains (ELF = 0.83) for **3_o** and the disynaptic V(M,C) attractor with a populated basin of 0.16 e.

The procedures to evaluate this type of intramolecular bond strengths are not straightforward. Another strategy to estimate them is by calculating the energy difference of the structure displaying a Ni-(C-H) interaction and a conformation lacking this binding motif. Hence, we determined the transition state for aryl rotation, wherein the aryl ring is perpendicular to the pyridine ring and the C-H bonds are remote from the Ni. The computed free energy transition state barrier are very low, 3.9 and 4.2 kcal·mol⁻¹ for complexes **3_{CH2}** and **3_o** respectively, indicating that the interaction between the nickel center and the phenyl C-H fragment is certainly weak. This is in agreement with previous observation for a very similar [Rh(CO)(PNC^H)]⁺ complex, showing fast rotation around C_{Ph}-C_{Py} even at -90 °C.^[45] Recently, several criteria based on geometric, spectroscopic, and QTAIM parameters were proposed to classify the strength of agostic bonding as anagostic, weak-to-medium agostic, medium-to-strong agostic, or prehydride.^[52] Some of these criteria include the three normalized parameters that consist of the ratio between the C-H_{agostic} distance and the H_{agostic}···M distance, the ratio between the stretching frequency of C-H_{agostic} bond in the complex and in the free ligand, and the ratio between the electron density at the BCP, ρ_{BCP} , in the complex and in the free ligand (Table 5.1 and Table 5.2). The computed values for complexes **3_{CH2}** and **3_o** provide a mixed situation. The geometric parameters fulfill the criteria set for a weak-to-medium agostic C-H interaction (ratio range: 0.5-0.7), but the spectroscopic and topological parameters do not, showing values typical of anagostic bonding (ratio range ≥ 0.90 for both). We therefore tend to favor the description of a Ni-(C_{Ph}-H) interaction in the solid state with predominant Ni-(η^1 -C_{Ph}) character.

Table 5.2. Geometric, spectroscopic, and QTAIM criteria for the strength classification of an M-(C-H) interaction in complexes **3**_{CH₂} and **3**_O [NiBr(κ³-P,N,(C-H)-L^H)]⁺

AGOSTIC BOND INTERVAL			
Geometric:	$0.5 < \frac{d(\text{C-H})}{d(\text{H}\cdots\text{Ni})} < 1$	0.51	0.52
Spectroscopic:	$0.65 < \frac{\nu(\text{C-H})}{\nu(\text{C-H})_{\text{free lig.}}} \leq 0.90$	0.96	0.95
Topological:	$0.65 < \frac{\rho_{\text{BCP}}(\text{C-H})}{\rho_{\text{BCP}}(\text{C-H})_{\text{free lig.}}} \leq 0.90$	0.95	0.95

5.4. Computational Details

Complex [NiBr(κ³-P,N,(C-H)-L^H)]⁺ (**3**) and the previously reported [Rh(CO)(P(C-H)P)]⁺ pincer complex^[56] exhibiting a Rh-η¹-C bonding with concomitant α-agostic η²-(C,H) were computed at the same level in order to compare them (Table 5.1). Geometry optimizations and wave function generation for analysis were performed with Gaussian09 series of programs.^[57] The nature of the minima stationary points encountered was characterized by means of harmonic vibrational frequencies analysis. Full quantum mechanical calculations were performed within the framework of DFT^[58] by using the B3PW91 functional.^[59–61] The basis set for Ni, Rh, Br, and P atoms was that associated with a pseudopotential,^[62] with a standard double-ξ LANL2DZ contraction, and the basis set was supplemented by f and d shells, respectively.^[63,64] The rest of the atoms were described with a standard 6-31G(d,p) basis set.^[65–67] The MULTIWFN software^[68] was used for the topological analysis of electron density within the QTAIM,^[54] and for the topological analysis of the ELF.^[55]

5.5. Conclusions

We have examined computationally the nature of the Ni-(C_{Ph}-H) bond in the solid state of [NiBr(κ³-P,N,(C-H)-L^H)]BF₄ (**3**_{CH₂} and **3**_O) complexes, which derive from the facile base-induced cyclometalation of a pendant phenyl ring within the novel ligands L_{CH₂^H} and L_{O^H} in NiBr₂(κ²-P,N-L^H) (**1**_{CH₂} and **1**_O) and subsequent protonation. To establish a description of such interaction and the consequences on C(sp²)-H bond activation, we employed geometric, spectroscopic, and topologic criteria.^[52] This bond interplay has been proven to be a bona fide albeit weak (an)agostic coordinative interaction, with predominant Ni-(η¹-C_{Ph}) character. Compounds **2** and **3** can undergo their mutual interconversion through facile protonation/deprotonation processes due to the labile binding of the Ni-C_{Ph}. This fact may induce these complexes to be viewed as models for key intermediates in cooperative catalysis.

5.6. References

- [1] M. Albrecht, *Chem. Rev.* **2010**, *110*, 576–623.
- [2] H. Shiota, Y. Ano, Y. Aihara, Y. Fukumoto, N. Chatani, *J. Am. Chem. Soc.* **2011**, *133*, 14952–14955.
- [3] Y. Aihara, N. Chatani, *J. Am. Chem. Soc.* **2013**, *135*, 5308–5311.
- [4] Y. Aihara, M. Tobisu, Y. Fukumoto, N. Chatani, *J. Am. Chem. Soc.* **2014**, *136*, 15509–15512.
- [5] Z. Ruan, S. Lackner, L. Ackermann, *Angew. Chemie Int. Ed.* **2016**, *55*, 3153–3157.
- [6] W. Song, S. Lackner, L. Ackermann, *Angew. Chemie Int. Ed.* **2014**, *53*, 2477–2480.
- [7] X. Cong, Y. Li, Y. Wei, X. Zeng, *Org. Lett.* **2014**, *16*, 3926–3929.
- [8] X. Ye, J. L. Petersen, X. Shi, *Chem. Commun.* **2015**, *51*, 7863–7866.
- [9] S.-Y. Yan, Y.-J. Liu, B. Liu, Y.-H. Liu, B.-F. Shi, *Chem. Commun.* **2015**, *51*, 4069–4072.
- [10] K. Yang, Y. Wang, X. Chen, A. A. Kadi, H.-K. Fun, H. Sun, Y. Zhang, H. Lu, *Chem. Commun.* **2015**, *51*, 3582–3585.
- [11] N. Barsu, D. Kalsi, B. Sundararaju, *Chem. - A Eur. J.* **2015**, *21*, 9364–9368.
- [12] J. Yi, L. Yang, C. Xia, F. Li, *J. Org. Chem.* **2015**, *80*, 6213–6221.
- [13] Q. Yan, Z. Chen, W. Yu, H. Yin, Z. Liu, Y. Zhang, *Org. Lett.* **2015**, *17*, 2482–2485.
- [14] K. Ogata, Y. Atsuumi, D. Shimada, S. Fukuzawa, *Angew. Chemie Int. Ed.* **2011**, *50*, 5896–5899.

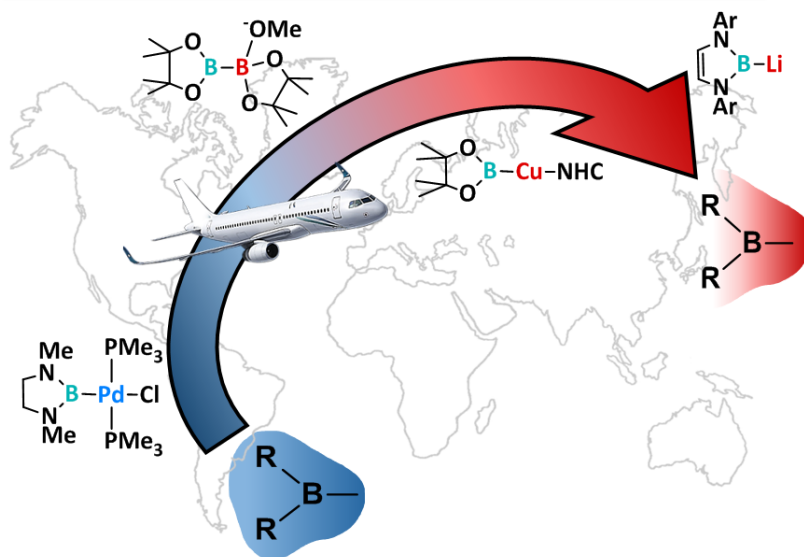
- [15] N. M. Camasso, M. S. Sanford, *Science* **2015**, *347*, 1218–1220.
- [16] J. R. Bour, N. M. Camasso, M. S. Sanford, *J. Am. Chem. Soc.* **2015**, *137*, 8034–8037.
- [17] A. Klein, B. Rausch, A. Kaiser, N. Vogt, A. Krest, *J. Organomet. Chem.* **2014**, *774*, 86–93.
- [18] A. T. Higgs, P. J. Zinn, M. S. Sanford, *Organometallics* **2010**, *29*, 5446–5449.
- [19] A. T. Higgs, P. J. Zinn, S. J. Simmons, M. S. Sanford, *Organometallics* **2009**, *28*, 6142–6144.
- [20] K. Ruhland, A. Obenhuber, S. D. Hoffmann, *Organometallics* **2008**, *27*, 3482–3495.
- [21] R. M. Ceder, J. Granell, G. Muller, *J. Chem. Soc. Dalt. Trans.* **1998**, 1047–1052.
- [22] R. M. Ceder, J. Granell, G. Muller, M. Font-Bardía, X. Solans, *Organometallics* **1996**, *15*, 4618–4624.
- [23] R. M. Ceder, J. Granell, G. Muller, M. Font-Bardía, X. Solans, *Organometallics* **1995**, *14*, 5544–5551.
- [24] G. Muller, D. Panyella, M. Rocamora, J. Sales, M. Font-Bardía, X. Solans, *J. Chem. Soc. Dalt. Trans.* **1993**, 2959–2967.
- [25] P. G. Cookson, G. B. Deacon, *J. Organomet. Chem.* **1971**, *33*, C38–C40.
- [26] Q. Zhang, X.-Q. Zhang, Z.-X. Wang, *Dalt. Trans.* **2012**, *41*, 10453–10464.
- [27] D. Zargarian, A. Castonguay, D. M. Spasyuk, in (Eds.: G. van Koten, D. Milstein), Springer Berlin Heidelberg, Berlin, Heidelberg, **2013**, pp. 131–173.
- [28] M. Stępień, L. Latos-Grażyński, L. Szterenberga, *Inorg. Chem.* **2004**, *43*, 6654–6662.
- [29] S. Sripathongnak, N. Barone, C. J. Ziegler, *Chem. Commun.* **2009**, 4584–4586.
- [30] C. Yang, W.-D. Wu, L. Zhao, M.-X. Wang, *Organometallics* **2015**, *34*, 5167–5174.
- [31] D. G. Morrell, J. K. Kochi, *J. Am. Chem. Soc.* **1975**, *97*, 7262–7270.
- [32] E. C. Volpe, A. R. Chadeayne, P. T. Wolczanski, E. B. Lobkovsky, *J. Organomet. Chem.* **2007**, *692*, 4774–4783.
- [33] A. Tsybizova, L. Rulíšek, D. Schröder, T. A. Rokob, *J. Phys. Chem. A* **2013**, *117*, 1171–1180.
- [34] B. Vabre, F. Deschamps, D. Zargarian, *Organometallics* **2014**, *33*, 6623–6632.
- [35] Y. Wei, A. Petronilho, H. Mueller-Bunz, M. Albrecht, *Organometallics* **2014**, *33*, 5834–5844.
- [36] J. P. Kleiman, M. Dubeck, *J. Am. Chem. Soc.* **1963**, *85*, 1544–1545.
- [37] Z.-Y. Xu, Y.-Y. Jiang, H.-Z. Yu, Y. Fu, *Chem. - An Asian J.* **2015**, *10*, 2479–2483.
- [38] H. Tang, X.-R. Huang, J. Yao, H. Chen, *J. Org. Chem.* **2015**, *80*, 4672–4682.
- [39] L. C. M. Castro, N. Chatani, *Chem. Lett.* **2015**, *44*, 410–421.
- [40] P. Boulens, E. Pellier, E. Jeanneau, J. N. H. Reek, H. Olivier-Bourbigou, P.-A. R. Breuil, *Organometallics* **2015**, *34*, 1139–1142.
-

- [41] M. Brookhart, M. L. H. Green, G. Parkin, *Proc. Natl. Acad. Sci.* **2007**, *104*, 6908–6914.
- [42] M. Stępień, L. Latos-Grażyński, L. Sztterenber, J. Panek, Z. Latajka, *J. Am. Chem. Soc.* **2004**, *126*, 4566–4580.
- [43] S. Murugesan, B. Stöger, E. Pittenauer, G. Allmaier, L. F. Veiros, K. Kirchner, *Angew. Chemie Int. Ed.* **2016**, *55*, 3045–3048.
- [44] L. S. Jongbloed, B. de Bruin, J. N. H. Reek, M. Lutz, J. I. van der Vlugt, *Catal. Sci. Technol.* **2016**, *6*, 1320–1327.
- [45] L. S. Jongbloed, B. de Bruin, J. N. H. Reek, M. Lutz, J. I. van der Vlugt, *Chem. - A Eur. J.* **2015**, *21*, 7297–7305.
- [46] Y. Gloaguen, L. M. Jongens, J. N. H. Reek, M. Lutz, B. de Bruin, J. I. van der Vlugt, *Organometallics* **2013**, *32*, 4284–4291.
- [47] S. Oldenhof, F. G. Terrade, M. Lutz, J. I. van der Vlugt, J. N. H. Reek, *Organometallics* **2015**, *34*, 3209–3215.
- [48] D. M. Spasyuk, D. Zargarian, A. van der Est, *Organometallics* **2009**, *28*, 6531–6540.
- [49] D. M. Spasyuk, D. Zargarian, *Inorg. Chem.* **2010**, *49*, 6203–6213.
- [50] B.-S. Zhang, W. Wang, D.-D. Shao, X.-Q. Hao, J.-F. Gong, M.-P. Song, *Organometallics* **2010**, *29*, 2579–2587.
- [51] B. Mougang-Soumé, F. Belanger-Gariépy, D. Zargarian, *Organometallics* **2014**, *33*, 5990–6002.
- [52] E.-L. Zins, B. Silvi, M. E. Alikhani, *Phys. Chem. Chem. Phys.* **2015**, *17*, 9258–9281.
- [53] A. Vigalok, O. Uzan, L. J. W. Shimon, Y. Ben-David, J. M. L. Martin, D. Milstein, *J. Am. Chem. Soc.* **1998**, *120*, 12539–12544.
- [54] R. F. W. Bader, *Chem. Rev.* **1991**, *91*, 893–928.
- [55] A. D. Becke, K. E. Edgecombe, *J. Chem. Phys.* **1990**, *92*, 5397–5403.
- [56] C. Lepetit, J. Poater, M. E. Alikhani, B. Silvi, Y. Canac, J. Contreras-García, M. Solà, R. Chauvin, *Inorg. Chem.* **2015**, *54*, 2960–2969.
- [57] M. J. Frisch, G. W. Trucks, H. B. Schlegel, G. E. Scuseria, M. A. Robb, J. R. Cheeseman, G. Scalmani, V. Barone, B. Mennucci, G. A. Petersson, H. Nakatsuji, M. Caricato, X. Li, H. P. Hratchian, A. F. Izmaylov, J. Bloino, G. Zheng, J. L. Sonnenberg, M. Hada, M. Ehara, K. Toyota, R. Fukuda, J. Hasegawa, M. Ishida, T. Nakajima, Y. Honda, O. Kitao, H. Nakai, T. Vreven, J. A. Montgomery, Jr., J. E. Peralta, F. Ogliaro, M. Bearpark, J. J. Heyd, E. Brothers, K. N. Kudin, V. N. Staroverov, R. Kobayashi, J. Normand, K. Raghavachari, A. Rendell, J. C. Burant, S. S. Iyengar, J. Tomasi, M. Cossi, N. Rega, J. M. Millam, M. Klene, J. E. Knox, J. B. Cross, V. Bakken, C. Adamo, J. Jaramillo, R. Gomperts, R. E. Stratmann, O. Yazyev, A. J. Austin, R. Cammi, C. Pomelli, J. W. Ochterski, R. L. Martin, K. Morokuma, V. G. Zakrzewski, G. A. Voth, P. Salvador, J. J. Dannenberg, S. Dapprich, A. D. Daniels, O. Farkas, J. B. Foresman, J. V. Ortiz, J. Cioslowski, D. J. Fox,

- Gaussian 09, Revis. A.02, Gaussian, Inc., Wallingford CT 2009.*
- [58] R. G. Parr, *Library (Lond)*. **1994**, 352.
- [59] A. D. Becke, *Phys. Rev. A* **1988**, *38*, 3098–3100.
- [60] A. D. Becke, *J. Chem. Phys.* **1996**, *104*, 1040–1046.
- [61] J. P. Perdew, in *Electron. Struct. Solids '91 Proc. 75th WE-Heraeus-Seminar* (Eds.: P. Ziesche, H. Eschig), Akademie Verlag, Berlin, **1991**, pp. 11–20.
- [62] P. J. Hay, W. R. Wadt, *J. Chem. Phys.* **1985**, *82*, 299–310.
- [63] A. W. Ehlers, M. Böhme, S. Dapprich, A. Gobbi, A. Höllwarth, V. Jonas, K. F. Köhler, R. Stegmann, A. Veldkamp, G. Frenking, *Chem. Phys. Lett.* **1993**, *208*, 111–114.
- [64] A. Höllwarth, M. Böhme, S. Dapprich, A. W. Ehlers, A. Gobbi, V. Jonas, K. F. Köhler, R. Stegmann, A. Veldkamp, G. Frenking, *Chem. Phys. Lett.* **1993**, *208*, 237–240.
- [65] M. M. Francl, W. J. Pietro, W. J. Hehre, J. S. Binkley, M. S. Gordon, D. J. DeFrees, J. A. Pople, *J. Chem. Phys.* **1982**, *77*, 3654–3665.
- [66] W. J. Hehre, R. Ditchfield, J. A. Pople, *J. Chem. Phys.* **1972**, *56*, 2257–2261.
- [67] P. C. Hariharan, J. A. Pople, *Theor. Chim. Acta* **1973**, *28*, 213–222.
- [68] T. Lu, F. Chen, *J. Comput. Chem.* **2012**, *33*, 580–592.

Tracing a nucleophilic map for trivalent boron compounds

$$\text{"nucleophilicity"} = a_0 + a_1 p/s + a_2 q[B] + a_3 V_w$$



*The real voyage of discovery consists not in seeking new landscapes,
but in having new eyes.*

— Marcel Proust —

UNIVERSITAT ROVIRA I VIRGILI
COMPUTATIONAL MODELING TO EXPLORE UNCONVENTIONAL REACTIVITY PATTERNS IN C-H ACTIVATION
AND BORON CHEMISTRY
Diego García López

Outline

Boryl-transition-metal complexes have largely been regarded as reagents that contain an electrophilic $-BRR'$ moiety to react with nucleophiles in a stoichiometric and catalytic way. However, the nature of the d-block metals might switch the reactivity of the boryl moiety from an electrophilic behaviour to a nucleophilic character. Moreover, the nature of the boron substituents may also affect the σ interaction between the boron and the metal and therefore the potential nucleophilicity of boron. It is a question of a balance between the intrinsic Lewis acidity of the boron, due to its empty p orbital perpendicular to the molecular plane, and the accumulated electron density in the polarized σ bonds. Furthermore, this nucleophilic performance has recently been extended to a metal-free context for diboron reagents providing a wide variety of examples wherein activated boryl synthons are capable of generating organoboron compounds.

In this section, we describe the development of quantitative structure-activity relationships (QSAR) for the nucleophilicity of trivalent boron compounds covering boryl fragments bonded to alkali and alkaline-earth metals, to transition metals, and to sp^3 boron units in diboron reagents. A detailed analysis of the potential energy surfaces of different types of boron substituents provided insight into the mechanism and established an order of nucleophilicity for boron in $B-X$: $X = Li > Cu > B(sp^3) > Pd$. For determining a relationship between ground-state properties and nucleophilic activity we used the charge of the boryl fragment ($q[B]$) and the boron p/s orbital population ratio (p/s) to describe the electronic structures of boryl moieties, whereas the distance-weighted volume (V_w) descriptor was used to evaluate the steric effects. The resulting three-term easy-to-interpret QSAR model showed statistical significance and predictive ability ($r^2 = 0.88$, $q^2 = 0.83$). The use of chemically meaningful descriptors has allowed identification of the factors governing the boron nucleophilicity and indicates that the most efficient nucleophiles are those with enhanced polarization of the $B-X$ bond towards the boron atom and reduced steric bulk. Finally, we used the QSAR model to make a priori predictions of experimentally untested compounds.

For the metal-free scenario, we divided the selected compounds into three subsets regarding the nature of the boryl synthons: *i*) symmetric diborane units, *ii*) unsymmetric diboranes, and *iii*) interelement borane complexes. The first group evaluated the effect of the activating Lewis base in the nucleophilicity, finding a strong dependence on the electronic transference degree of such base into the diboron compound. In the second subset the impact of changing the

nature of the non-quaternized boryl unit was analyzed and deviations of linearity of the descriptors employed previously were noticed. The last bloc comprising boryl-interelement adducts afforded remarkable adjustment to the three-parameter equation stemmed in first ensemble containing boron-metal bonds. Additionally, a final ensemble comprising the most representative compounds of each subset was constructed aiming to establish quantitative relationships as well. The best predictive statistical model ($r^2 = 0.84$, $q^2 = 0.79$) highlights the importance of incorporating the distance-weighted volume (V_w) descriptor into the estimation capability of the electronic parameters (p/s , $q[B]$).

6. Tracing a nucleophilic map for the use of trivalent boron compounds

6.1. Introduction

The electrophilic synthesis of organoboron compounds was highly enlarged with the discovery of boryl-transition-metal complexes.^[1-3] In most of these species the metal atom is not able to donate enough electron density to fill the outer orbital of the boron atom, so it keeps prone to electrophilic processes. However, these compounds can modify their reactivity from an electrophilic character to a nucleophilic behavior by tuning the nature of the substituents attached to boron.^[4-6] Indeed, such changes may affect the σ -interaction between the boron and the metal and therefore the potential nucleophilicity of the former. In addition, the intrinsic characteristics of the transition metal might also switch the reactivity of the boryl moiety.^[4-6] Thus, the existence of a powerful method to predict the electronic behavior of boryl-transition-metal complexes would be fundamental for experimentalists to consider a design *a la carte* of the best M-BRR' reagent to guarantee a precise reactivity.

Quantum chemistry methods, such as DFT, have proven to be powerful tools for characterizing the nucleophilicity of specific boryl species through the location and analysis of the corresponding transition state (TS) on the potential energy surface (PES). These kinds of calculations have shown that trivalent boron compounds can react with suitable electrophilic reagents when boron is bonded to a main-group metal such as lithium,^[7] to a transition metal such as copper,^[8] and to an sp^3 -hybridized boryl unit.^[9,10] Alternatively, one could use other computational methods based on quantitative structure-activity relationship (QSAR) or structure-property relationship (QSPR) approaches, which are analogous to those used in drug design.^[11-14] One of the most attractive aspects of these methods is that they generate simple equations, which allow *a priori* prediction of catalytic activity or selectivity. Although QSAR techniques are not of common use in chemical inorganic reactivity, there are some outstanding examples that correlate catalytic activity and selectivity.^[15-29] It is worth noting that predicting the reactivity or designing *de novo* compounds through these approaches is quite challenging and present some limitations.^[30,31] In particular, it has been pointed out that predictive computational chemistry can lead to promising suggestions but it is limited to related compounds due to the difficulties of sampling the chemical space widely.^[31]

Recently, our group analyzed systematically the electronic features of several types of boryl moieties by evaluating the charge of the boryl fragment and the boron p/s population ratio.^[6] By using these easily accessible parameters of the ground-state structures, they were able to construct a qualitative tendency map, which established a gradient of nucleophilic character. As a

step forward, we sought herein for quantitative relationships between the structures of trivalent boron compounds and their nucleophilicity. To this end, in addition to previous electronic descriptors, we employed a steric descriptor, the distance-weighted volume (V_w),^[32–34] and defined a dataset of boryl units bonded to alkali and alkaline-earth metals, transition metals, and also sp^3 -hybridized boron units in diboron reagents activated by Lewis bases. We also performed a priori predictions of experimentally untested compounds, thereby evaluating externally the QSAR model.

However, nucleophilic reactivity of trivalent boron compounds has experienced recently an exceptional development within a metal-free context.^[35] This attainment comprises a landmark towards the synthesis of organoboranes and might expand its applicability in organic chemistry. The nucleophilic activity can be reached by the interaction of a suitable Lewis base to form a $B(sp^2)-B(sp^3)$ adduct that polarizes the σ_{B-B} bond in the direction of the non-quaternized boron. We took awareness of such finding and included a more specific study on the structure-nucleophilicity relationships for metal-free diboron reagents, by varying both the ligands attached to boron atom and the activating Lewis base.

6.2. Results and discussion

6.2.1. QSAR model for the nucleophilicity of trivalent boron compounds

- **Data set and structure generation**

The trivalent boron compounds used for the QSAR modeling of boron nucleophilic activity are presented in *Figure 6.1*. The 17 species were selected from previous bibliographic reviews^[4,5] and a previously constructed tendency map.^[6] We chose three or four representative structures of each boryl class, and incorporated additional rhodium and iridium complexes to avoid a nonbalanced or biased dataset (see below). Thus, the dataset covers the full range of chemical space, including different prototypes of nucleophilic and electrophilic boron reagents in a balanced manner. These prototypes can be divided into four categories: *i*) Nucleophilic reagents with boryl fragments bonded to alkali and alkaline-earth metals (**1-4**), *ii*) nucleophilic diboron compounds activated by Lewis bases (**5-7**), *iii*) nucleophilic reagents with boryl fragments bonded to transition metals such as copper and scandium (**8-10**), and *iv*) electrophilic boron reagents with the boron bonded to transition metals such as palladium, iridium, and rhodium (**11-17**).

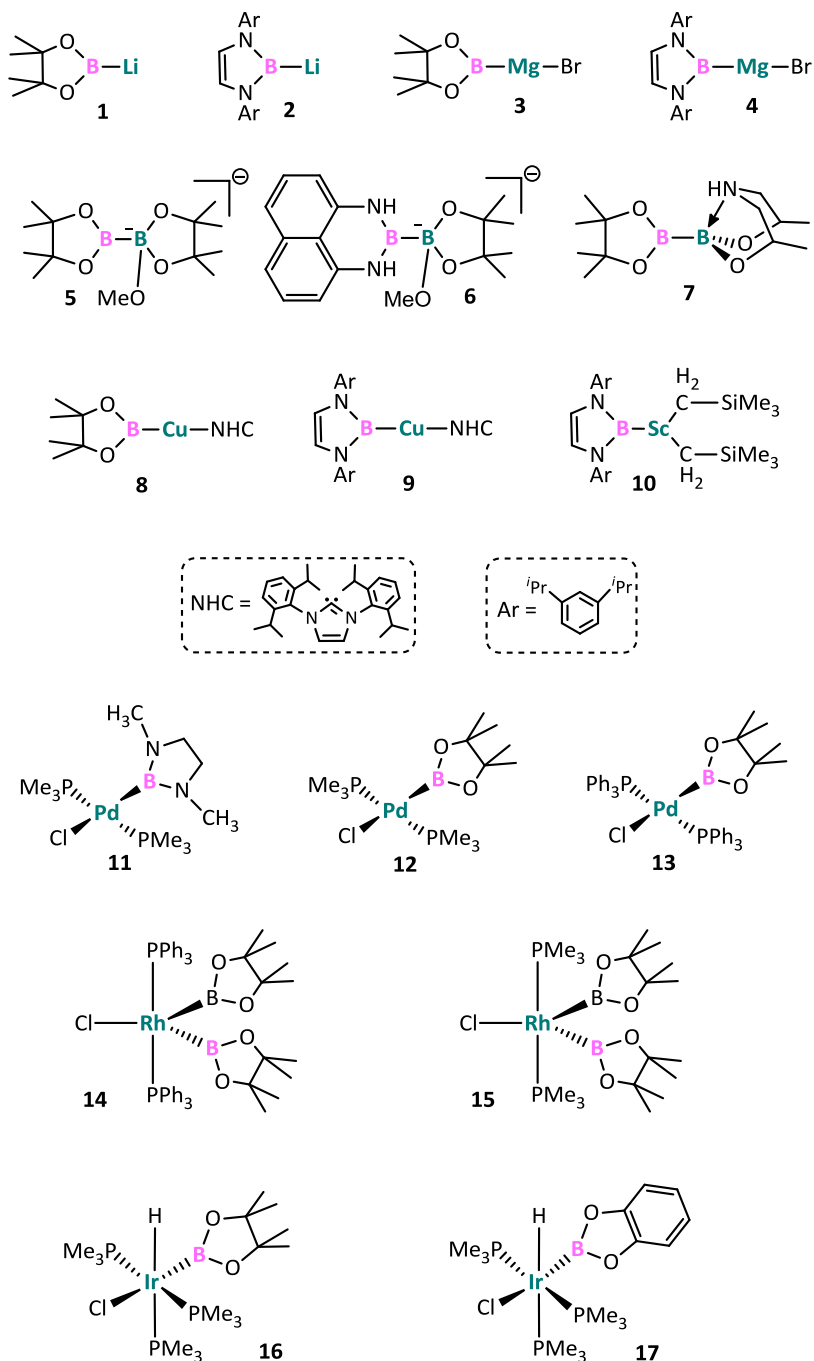


Figure 6.1. Selected dataset of trivalent boron-containing compounds.

Regarding the lithioboranes, their potential nucleophilic character was predicted computationally.^[7] Later, a diamino-substituted boryllithium compound (**2**) was isolated and reported to react with several organic electrophiles.^[36–40] The analogous borylmagnesium

compound (**4**) also reacts as a nucleophile but its reaction outcome is different.^[41] In the case of benzaldehyde as substrate, the boryllithium gave the α -borylbenzyl alcohol,^[36–40] whereas the borylmagnesium afforded a mixture of products in which benzoylborane was the main product.^[41] The activation of diboron compounds by Lewis bases can also generate nucleophilic boryl moieties.^[4,5,35,42–44] The quaternization of one boron by the base polarizes the B–B bond inducing nucleophilic character on the sp^2 boron.^[9,10] Here, we considered adducts derived from intermolecular alkoxide activation of symmetric bis(pinacolato) diboron (B_2pin_2 , **5**)^[9,10,45–47] and unsymmetrical diboron Bpin-Bdan (dan = 1,8-diaminonaphthalene, **6**),^[48,49] as well as the intramolecular activation by the nitrogen atom in the pinacolato diisopropanolaminato diboron **7**.^[50–52]

Moving to boryl-transition-metal complexes, we noted that their reactivity switches depending on the nature of the transition metal. One striking example is the reactivity of boryl-copper and -palladium complexes with the same substrate. The boryl-copper complexes behave as nucleophiles^[53] and β -borate α,β -unsaturated carbonyl ketones.^[54–56] On the other hand, the boryl-palladium complex *trans*-[Pd{B(MeN-CH₂-CH₂-NMe)}(Cl)(PMe₃)₂] (**11**) reacts as an electrophile providing the 1,4-addition product in which the boryl unit is bonded to the oxygen atom.^[57] Thus, we selected complex **11** and gauged the electrophilic character of palladium complexes by replacing the boryl unit (**12**) and then the ligands (**13**; see Figure 6.1). To represent boryl-copper species, we analyzed the isolated complex [Cu(Bpin)(NHC)] (NHC=1,3-bis(2,6-diisopropylphenyl)imidazol-2-ylidene; **8**),^[58] which also behaves as a nucleophile reducing CO₂, and the analogous virtual non-synthesized complex [Cu(ArN-CH₂-CH₂-NAr)(NHC)] (**9**), which differs in the nature of the boryl ligand. Another example of a transition metal supporting a nucleophilic boryl moiety is the boryl-scandium complex [Sc(CH₂SiMe₃)₂(THF)_n{B(NDippCH)₂}] (Dipp=2,6-diisopropylphenyl; **10**), which can undergo insertion reactions with CO to yield a product with the boron atom bonded to the carbon atom.^[59] Finally, to balance the training dataset, we included the boryl-rhodium and -iridium complexes, which were expected to behave as electrophiles. The rhodium structures **14** and **15** are analogous to the complex used in the first confirmed example of the insertion of an alkene into a Rh–B bond.^[60] Similarly, the boryl-iridium complex [Ir(Me₃P)₃(Cl)(H)(Bcat)] (**16**) was synthesized and employed as catalyst in the hydroboration of alkynes.^[61] Then, by replacing the Bcat ligand by Bpin, we obtained the complex **17**.

▪ Descriptors correlating nucleophilicity

In the multidimensional modeling, several molecular descriptors were related to the boron nucleophilicity through multivariate regression techniques. They were obtained from the ground-state structures depicted in Figure 6.1. Note that relying on ground-state properties to predict the activity of novel compounds avoids the difficult, and sometimes elusive, determination of transition states and characterization of the full mechanism. In a previous contribution two electronic descriptors were identified that could be used to classify qualitatively the nucleophilic character of boryl moieties:^[6] the overall charge of the boryl fragment ($q[B]$) and the boron p/s population ratio (ρ/s). The projection of 23 compounds onto the plot mapping the two electronic

descriptors showed a clear clustering of the species.^[6] The clusters identified by visual analysis were closely related to the chemical nature of the atom bonded to boron and to the observed nucleophilic character.

The $q[B]$ descriptor measures the charge that is supported by the overall boryl fragment computed as the sum of all the natural bond order (NBO) atomic charges. Replacing the metal fragment in the M–Bpin complexes $[\text{Rh}(\text{Bpin})_2\text{Cl}(\text{PMe}_3)_2]$, $[\text{Cu}(\text{Bpin})(\text{NHC})]$, and $[\text{Li}(\text{Bpin})]$, the computed activation barriers for the nucleophilic addition of Bpin to formaldehyde (50.6, 16.4, and 2.0 kcal·mol⁻¹, respectively) correlate with the overall charge of the Bpin moiety (+0.13, –0.43, and –0.59 a.u., respectively). Thus, the more negatively charged the boryl fragment, the lower is the energy barrier. The p/s descriptor is the boron population ratio of atomic p and s orbitals in the B–X σ bond within the NBO partition scheme. It was first introduced by Lin and Marder to gauge the polarity of boron-transition-metal bonds, who concluded that the greater the s character, the more polarized the bond becomes towards the boron atom.^[62] Our group also observed that in strongly polar B–X bonds, the less s character the more reactive the boryl fragment is as a nucleophile.^[6] In the lithioboranes $(\text{CH}_3)_2\text{BLi}$, H_2BLi , and F_2BLi , computational studies by v. R. Schleyer and co-workers established the following nucleophilicity trend for boryl fragments: $\text{F}_2\text{B} < \text{H}_2\text{B} < (\text{CH}_3)_2\text{B}$.^[7] In this work we found that within this series, the nucleophilicity correlates with the increase in the p/s ratio (1.4, 2.1, and 2.7, respectively), but not with the increase in the negative charge at the boryl moiety (–0.54, –0.54, and –0.47, respectively). Therefore it is reasonable to assert that $q[B]$ provides an indication of the nucleophilic character that is induced by its counterpart, whereas the boron p/s ratio gives a measure of the intrinsic nucleophilicity of the boryl fragment.

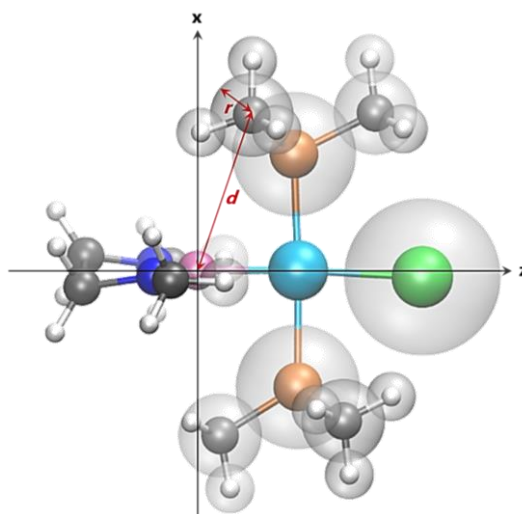


Figure 6.2. Illustration of the determination of the distance-weighted volume (V_w) descriptor for *trans*- $[\text{Pd}\{\text{B}(\text{MeN-CH}_2\text{-CH}_2\text{-NMe})\}\{\text{Cl}\}(\text{PMe}_3)_2]$ (**11**).

In a step forward, we introduced an additional descriptor to evaluate the steric effects of the boron environment on the reactivity. We selected the distance-weighted volume (V_w) parameter,^[32–34] which measures the steric bulkiness of the molecular environment and its impact on the boron center. The calculation of V_w entails the alignment of boron compounds as follows: the boron atom is placed at the origin with the bonded metal (X atom) along the positive z axis (see Figure 6.2). Then we quantify the bulk produced by the atoms to the front of the boron ($z > 0$) by considering three parameters: *i*) The number of atoms, excluding X, in the region defined by the alignment hypothesis, *ii*) the size of the atom (r = van der Waals radii in Å),^[63] and *iii*) the distance (d) from the atom to the boron center (in Å). The factor r^3 is divided by d for each atom and the sum is extended to all of the atoms in the given region (see eq 6.1).

$$V_w = \sum_{i=1}^N \frac{r_i^3}{d_i} \quad (6.1)$$

▪ Response variable and mechanistic insight

In this case there are no experimentally recorded activities that encompass a broad range of trivalent boron compounds under comparable experimental conditions, which precludes their simultaneous use in multivariate modeling. Therefore, the response variables measuring nucleophilicity were derived from DFT calculations. These were determined as the free energy barriers required to transfer the boryl moiety to the electrophilic carbon atom of the model substrate formaldehyde (ΔG_{Nu}^\ddagger). As illustrated in Figure 6.3, formaldehyde is a simple species with electrophilic and nucleophilic counterparts, thereby allowing identification and quantification of the nature of the reactivity of boron compounds.

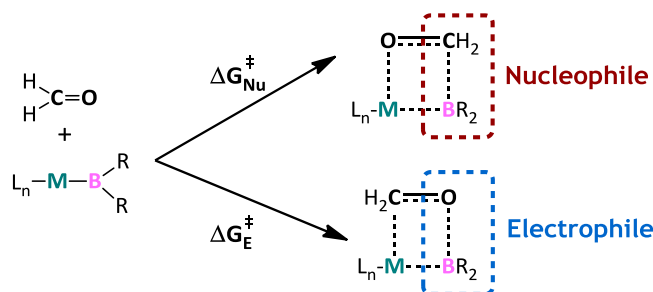


Figure 6.3. Evaluation of the nucleophilic and electrophilic reactivity of trivalent boron compounds using formaldehyde as a model substrate.

To check the reliability of our approach and to gain additional mechanistic insight, we analyzed in more detail the potential energy profiles of four prototypical boryl fragments bonded to copper, palladium, lithium, and sp^3 -hybridized boron using formaldehyde as a model substrate. Figure 6.4 and Figure 6.7 depict the computed free-energy profiles and Figures 6.5, 6.6, 6.8 and 6.9 show representative molecular structures and selected geometrical parameters. Marder and Lin have

already used this model substrate to demonstrate that the boryl ligand in the complex $[(\text{NHC})\text{Cu}(\text{Bpin})]$ (**8**) has nucleophilic character.^[8] Figure 6.4A shows the essential stationary points of the electrophilic and nucleophilic paths. For the sake of simplicity, we omitted the two shallow η^2 -aldehyde intermediates that can be formed when the substrate approaches the copper center.^[8] The boryl ligand preferentially migrates to the carbon atom leading to the $[(\text{NHC})\text{Cu}-\text{OCH}_2\text{Bpin}]$ complex as the kinetic product. At our computational level, the free-energy barrier (16.4 kcal·mol⁻¹) is significantly lower than that for the electrophilic boryl migration to the oxygen atom of the aldehyde (40.8 kcal·mol⁻¹).

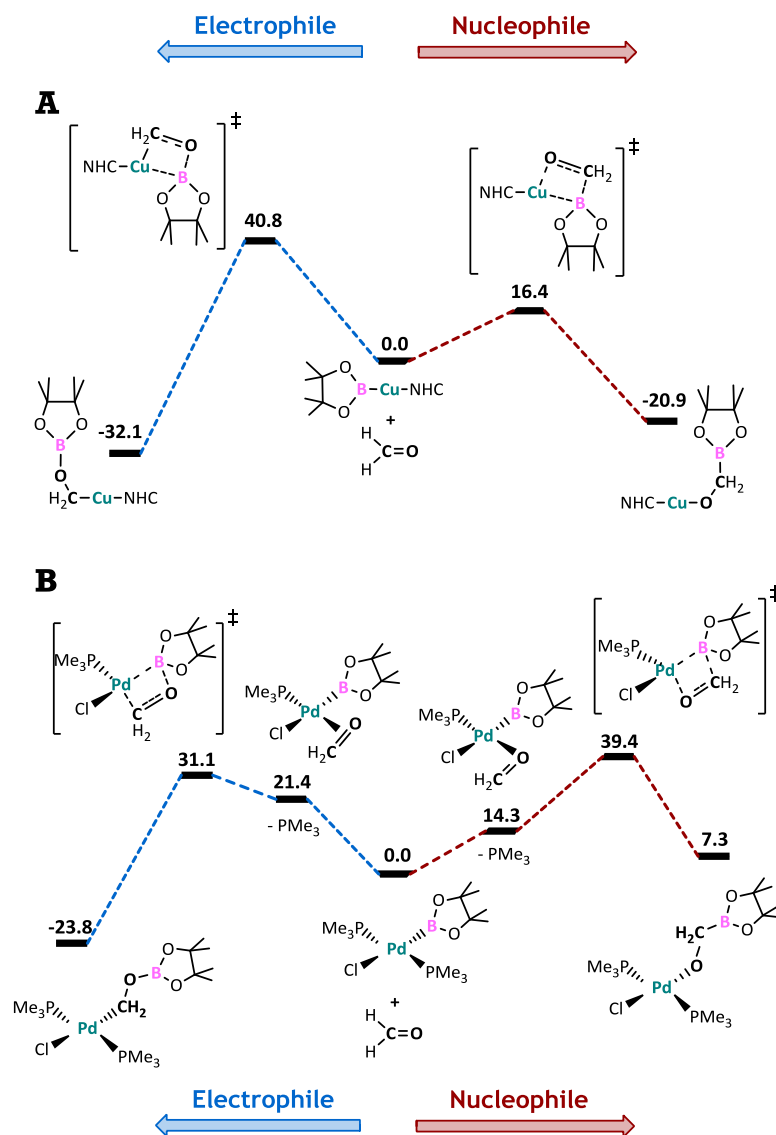


Figure 6.4. Free-energy profiles [kcal·mol⁻¹] for the electrophilic and nucleophilic paths of aldehyde boration by the B-Cu complex $[\text{Cu}(\text{Bpin})(\text{NHC})]$ (**8**) and the B-Pd complex $trans\text{-}[\text{Pd}(\text{Bpin})(\text{Cl})(\text{PMe}_3)_2]$ (**12**).

For the electrophilic boryl-palladium complex $[\text{Pd}(\text{Bpin})\text{Cl}(\text{PMe}_3)_2]$ (**12**), the trend is inverted and the electrophilic path is kinetically favored over the nucleophilic path (Figure 6.4B). Previously, Wu and co-workers had characterized computationally the mechanism for palladium-catalyzed alkyne cyanoboration, the rate-determining step of which was found to be the insertion of the $\text{C}\equiv\text{C}$ triple bond into the $\text{Pd}-\text{B}$ bond.^[64] In this case the formation of the key intermediate, $[\text{Pd}(\text{BX}_2)\text{Cl}(\text{HCCH})(\text{PH}_3)]$, involves one phosphine dissociation and the coordination of the π substrate. Based on these findings we propose a dissociative mechanism involving the innersphere insertion of the substrate into the $\text{Pd}-\text{B}$ bond (Figure 6.4B). Hence, one of the PMe_3 ligands dissociates from complex **12** with a moderate energy cost (ca. $20 \text{ kcal}\cdot\text{mol}^{-1}$) and then the aldehyde coordinates either through the oxygen ($\eta^1\text{-O}$) or through the carbon-oxygen π bond ($\eta^2\text{-(C,O)}$). The relative free energies of the corresponding intermediates are $+14.3$ and $+21.4 \text{ kcal}\cdot\text{mol}^{-1}$, respectively, above the reactants. Because the reaction by the electrophilic pathway leads to an alkyl-palladium complex, the transition state for the insertion into the $\text{Pd}-\text{B}$ bond should involve the $\eta^2\text{-(C,O)}$ π complex, whereas for the nucleophilic path, the formation of the palladium-alkoxide product could occur directly from the $\eta^1\text{-O}$ σ complex. Overall, however, the ligand/substrate exchange process occurs with a lower energy than the aldehyde insertion, which is the step governing the boryl-palladium activity. Thus, the calculations predict a global free-energy barrier of $31.1 \text{ kcal}\cdot\text{mol}^{-1}$ for electrophilic boryl migration and of $39.4 \text{ kcal}\cdot\text{mol}^{-1}$ for the nucleophilic migration. This result is consistent with what was observed in the boration of α,β -unsaturated carbonyl ketones in the presence of palladium complexes.^[57]

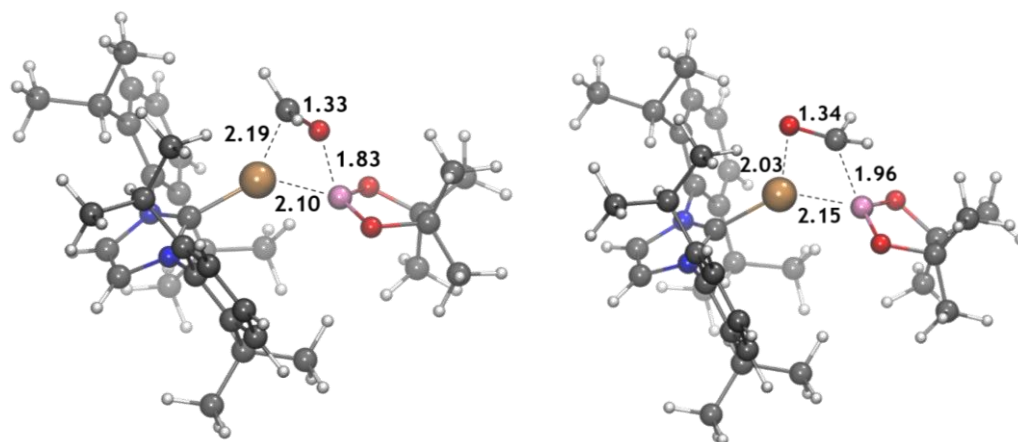


Figure 6.5. Computed molecular structures for selected species in the reaction of formaldehyde with (NHC)CuBpin complex (**8**), (NHC = 1,3-bis-(2,6-diisopropyl)phenylimidazole-2-ylidene, Bpin = pinacolboryl): electrophilic transition state (left) and nucleophilic transition state (right). Distances in Å.

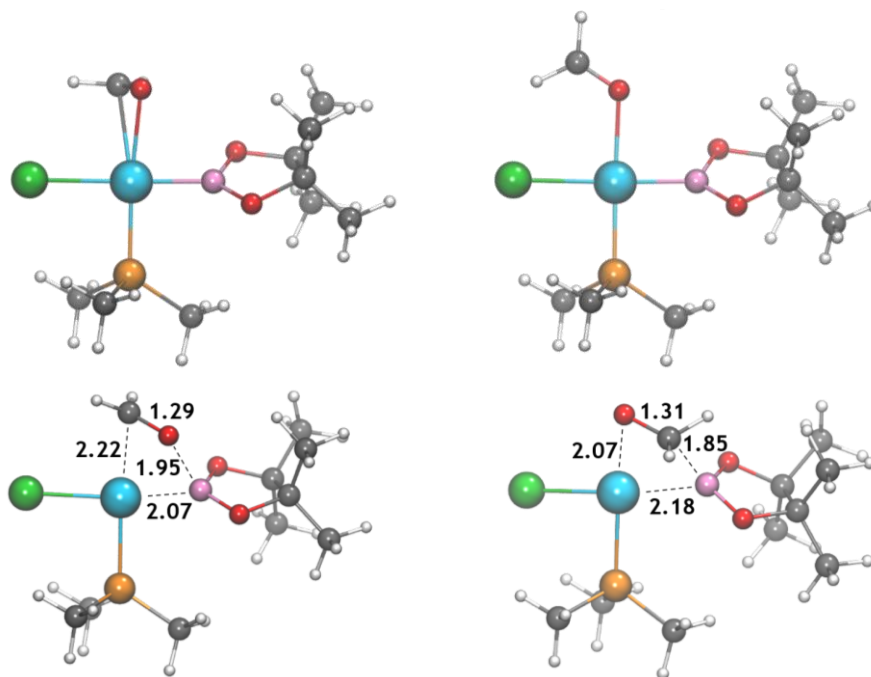


Figure 6.6. Computed molecular structures for selected species in the reaction of formaldehyde with [Pd(Bpin)(Cl)(PMe₃)] complex (**12**), (Bpin = pinacolboronyl): electrophilic intermediate (left, up), nucleophilic intermediate (right, up), electrophilic transition state (left, down), and nucleophilic transition state (right, down). Distances in Å.

The nucleophilic addition of lithioboranes to formaldehyde^[7] and to organohalides^[65] has already been studied computationally. In this previous study, the model lithioboranes LiB(CH₃)₂, H₂BLi, and F₂BLi were analyzed;^[7] these species initially interact with the substrate to form precursor complexes with the carbonyl oxygen coordinated side-on to lithium. After overcoming low activation barriers, these precursors yield three-membered B–C–O ring structures with a dative boron-oxygen bond.^[7] In the case of the more realistic LiBpin (**1**), we obtained a similar energy profile (see Figure 6.7A). The free energy of the precursor complex is $-10.4 \text{ kcal}\cdot\text{mol}^{-1}$, the subsequent activation barrier is low, $2.0 \text{ kcal}\cdot\text{mol}^{-1}$, and the overall process is exergonic by $-57.6 \text{ kcal}\cdot\text{mol}^{-1}$. Interestingly, we found another isomeric product slightly lower in energy ($-59.3 \text{ kcal}\cdot\text{mol}^{-1}$ with respect to the reactants) containing a five-membered O–B–C–O–Li ring structure (Figure 6.8). For the novel electrophilic path, we were unable to locate a minimum with the carbonyl oxygen coordinated to boron. The approach of the aldehyde leads directly to the transition state in which a new B–O bond is formed and the lithium migrates to occupy a bridging position over the oxygen-carbon bond of the substrate. The computed free-energy barrier ($18.5 \text{ kcal}\cdot\text{mol}^{-1}$) is significantly higher than that for the nucleophilic reaction, thereby proving the nucleophilic character of lithioboranes.

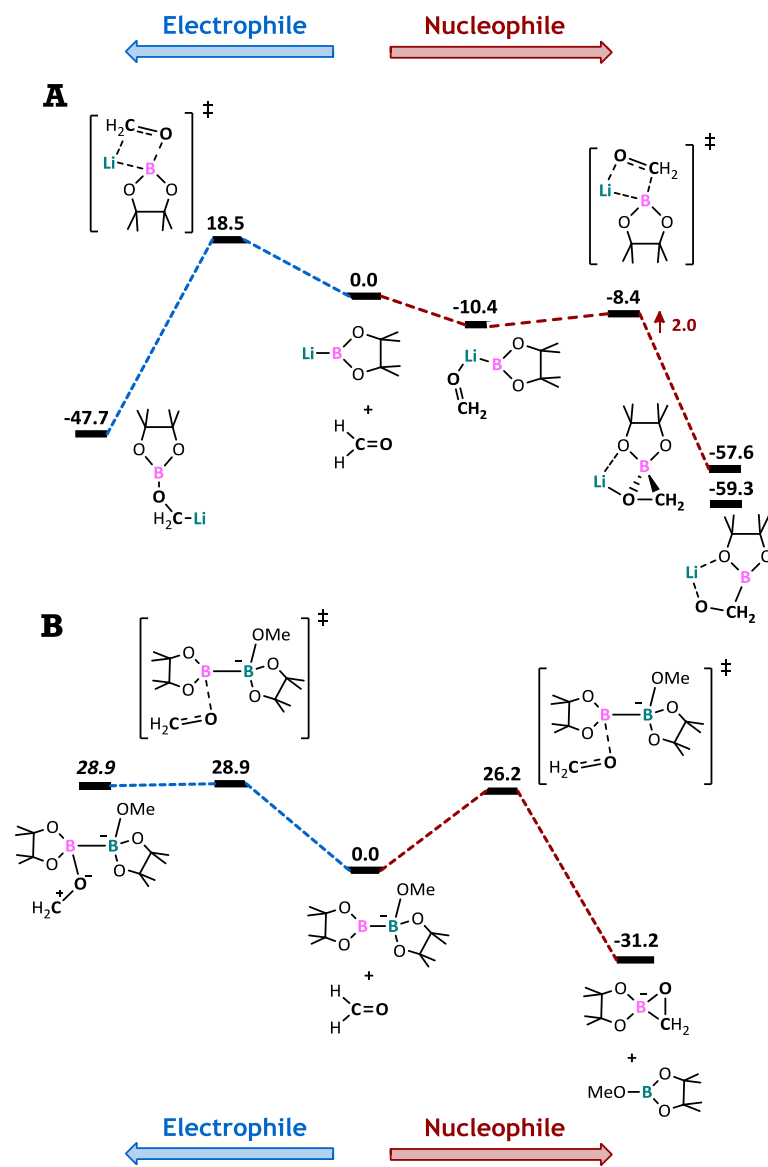


Figure 6.7. Free energy profiles (kcal·mol⁻¹) for the electrophilic and nucleophilic paths of aldehyde boration by the lithioborane compound [Li(Bpin)] (**1**) and the diboron compound MeO⁻→Bpin-Bpin (**5**).

Finally, we analyzed the reactivity of a diboron compound activated by a Lewis base, MeO⁻→Bpin-Bpin (**5**; Figure 6.7B). Previous DFT studies have already demonstrated the nucleophilic character of the sp² boron moiety towards suitable electrophilic reagents,^[9,10,48,49] but its reactivity towards nucleophilic counterparts has not yet been explored. As shown in Figure 6.7B, nucleophilic attack at the carbonyl carbon by the sp² boron moiety has a free-energy barrier of 26.2 kcal·mol⁻¹, qualitatively close to that previously computed for styrene.^[9,10] As shown previously for

alkenes,^[9,10] the transition state can rearrange to a “monoborated” anionic product with a three-membered B–C–O ring structure and a (pin)B–OMe compound. The process develops a negative charge at the carbonyl oxygen that is better delocalized through the pinacolboryl unit, thereby inducing the formation of the cycle. The attack at the carbonyl oxygen by the sp^2 boron moiety is different in nature. The electrophilic boron approaches in-plane the aldehyde in order to interact with the oxygen lone pairs, whereas the nucleophilic attack of the diboron occurs perpendicular to the molecular plane to interact with the π -antibonding C=O orbital. We computed a free-energy barrier of 28.9 kcal·mol⁻¹ for the addition of the carbonyl oxygen to the sp^2 boron, which results in a high-energy shallow intermediate from which the reaction can easily proceed backwards (Figure 6.7B). The stationary point corresponding to the intermediate was located in the potential electronic energy surface, and has an energy 0.02 kcal·mol⁻¹ lower than that of the preceding transition state. However, upon the addition of thermal and entropic corrections to obtain the Gibbs free energies, the energy of the intermediate becomes slightly higher than the transition state (0.4 kcal·mol⁻¹) due to the approximations performed in the statistical mechanics treatment. We could also characterize another transition state connecting the intermediate with the monoborated anionic product that is isoenergetic to the TS for the backward reaction. In this TS, the newly quaternized boron atom becomes more negative and is capable of interacting with the positively charged carbonyl carbon releasing the (pin)B–OMe fragment through B–B bond cleavage (Figure 6.9).

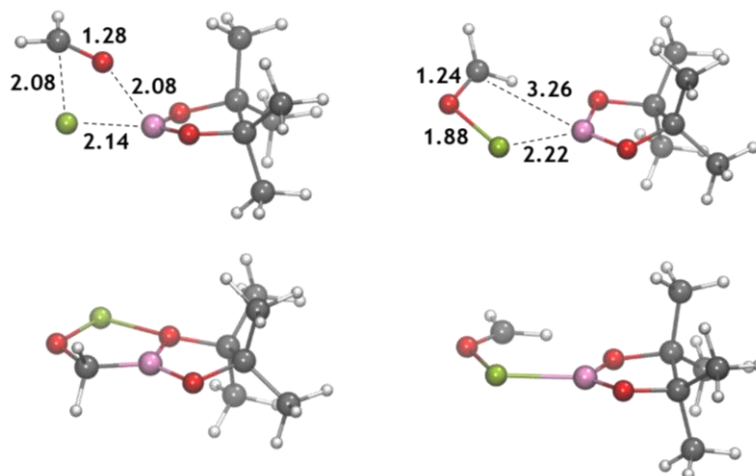


Figure 6.8. Computed molecular structures for selected species in the reaction of formaldehyde with Li–Bpin complex (Bpin = pinacolboryl): electrophilic transition state (left, up), nucleophilic transition state (right, up), nucleophilic product (left, down) and nucleophilic intermediate (right, down). Distances in Å.

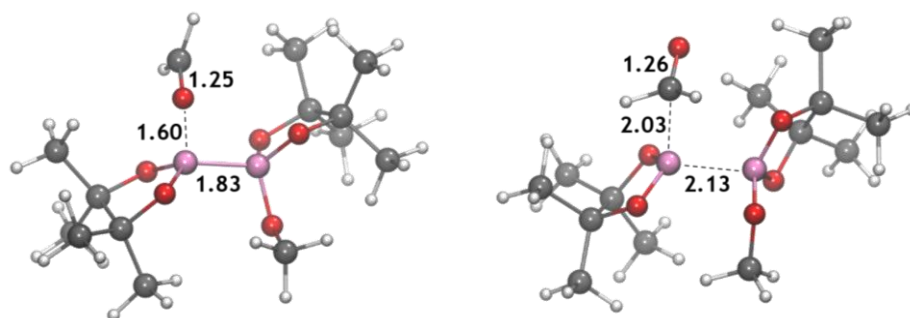


Figure 6.9. Computed molecular structures for selected species in the reaction of formaldehyde with $\text{MeO}^- \rightarrow \text{Bpin}-\text{Bpin}$ complex (Bpin = pinacolboronyl): electrophilic transition state (left) and nucleophilic transition state (right). Distances in Å.

The overall analysis of the four potential energy profiles demonstrates that the aldehyde substrate can serve as a model for predicting the nucleophilic/electrophilic activity of the full range of trivalent boron compounds. Within the body of examples, the values of the computed energy barriers predict the right reactivity character observed experimentally, that is, nucleophilic character for boryl fragments bonded to lithium, copper, and sp^3 boron and electrophilic character for boryl-palladium species (see Figures 6.4 and 6.7). Moreover, we identified an order of nucleophilic reactivity ($\text{Li} > \text{Cu} > \text{B}(\text{sp}^2)-\text{B}(\text{sp}^3) > \text{Pd}$) from the computed $\Delta G^\ddagger_{\text{Nu}}$ values (2, 16.4, 26.2, and 39.4 $\text{kcal}\cdot\text{mol}^{-1}$, respectively) that is fully consistent with experimental experience. In addition, this supports the use of nucleophilic free-energy barriers as a response variable in QSAR modeling.

The $\Delta G^\ddagger_{\text{Nu}}$ values for all the selected trivalent boron compounds are presented in Table 6.1. The values span more than 50 $\text{kcal}\cdot\text{mol}^{-1}$, which indicates that the nature of the substituent has a profound influence on the reactivity character of trivalent boron. They can be roughly divided into three classes: *i*) Nucleophilic boryl fragments bonded to alkali and alkaline earth metals, scandium, and copper exhibiting free-energy barriers ranging from 2 to 27 $\text{kcal}\cdot\text{mol}^{-1}$ (**1-4**, **8-10**), *ii*) electrophilic boryl fragments bonded to late-transition metals with barriers ranging from 29 to 59 $\text{kcal}\cdot\text{mol}^{-1}$ (**11-17**), and *iii*) boryl fragments with moderate nucleophilicity, which correspond to activated diboron compounds with free-energy barriers ranging from 26 to 38 $\text{kcal}\cdot\text{mol}^{-1}$ (**5-7**). Note that within the first group the diamino-substituted boryl-copper complex (**9**) has the highest barrier, which is significantly higher than the previous one in the series. As we discuss below, this is because its crowded reaction center might lower its nucleophilicity. The ancillary ligands of transition metals can influence the reactivity in different directions. In the dissociation mechanism of boryl-palladium complexes, replacing the PMe_3 ligands in **12** by the less basic phosphine PPh_3 in **13** reduces the nucleophilic free-energy barrier by around 10 $\text{kcal}\cdot\text{mol}^{-1}$, because the coordinated aldehyde becomes more electrophilic towards the boryl moiety. Conversely, for the associative mechanism of boryl-rhodium complexes, the same phosphine replacement (from PMe_3 in **15** to PPh_3 in **14**) increases the $\Delta G^\ddagger_{\text{Nu}}$ by around 8 $\text{kcal}\cdot\text{mol}^{-1}$ due to the greater bulkiness of PPh_3 in **14**.

Table 6.1. Computed nucleophilic free-energy barriers (ΔG^\ddagger_{Nu}) and values of the molecular descriptors: p/s atomic orbital ratio in the B–X σ -bond, charge of the boryl fragment ($q[B]$), and distance-weighted volume (V_w) employed for the trivalent boron compounds **1–17**.^[a]

Compound	ΔG^\ddagger_{Nu} ^[a]	p/s	$q[B]$ ^[a]	V_w
1	2.0	1.48	-0.59	0.0
2	3.6	1.51	-0.63	8.7
3	4.5	1.58	-0.42	1.3
4	8.5	1.49	-0.43	12.6
5	26.2	1.05	-0.13	17.0
6	29.1	1.15	-0.15	16.9
7	38.3	1.19	-0.02	15.1
8	16.4	0.94	-0.43	33.0
9	26.9	1.25	-0.45	46.6
10	5.5	1.03	-0.30	25.4
11	36.1	1.47	0.02	18.1
12	39.4	1.47	0.02	16.7
13	29.2	1.14	-0.02	38.4
14	58.7	1.21	0.09	47.9
15	50.6	1.39	0.13	28.2
16	44.1	1.22	0.12	25.2
17	47.2	1.52	0.17	25.8

^[a]Free-energy barriers in kcal·mol⁻¹ and charges of boryl fragment in a.u.

▪ QSAR modeling and interpretation

The calculated nucleophilicities (ΔG^\ddagger_{Nu}) for the representative set of complexes were correlated to the molecular descriptors p/s , $q[B]$, and V_w by using partial least-squares regression (PLSR). The computed values of the nucleophilicities and the descriptors for the different compounds are presented in Table 6.1. To evaluate the predicting ability of the QSAR models we employed the Pearson correlation coefficient (r^2) of the fitting stage and the predictive ability (q^2) calculated by using the leave-one-out (LOO) cross-validation method (see Computational Details for a complete description of the methodology). The statistical parameters for the validation of multivariate models using different combinations of descriptors are presented in Table 6.2.

Initially, we built a QSAR model for predicting nucleophilicity values by selecting the two electronic descriptors used for the construction of the previous tendency map,^[6] the $q[B]$ and p/s parameters. Full cross-validation of the 17 compounds led to a value of r^2 for the fitting of 0.82 and a predictive ability q^2 of 0.78 with one PLS (entry 1, Table 6.2). In drug design, a model is considered to be predictive when the value of q^2 is higher than 0.5 (halfway between perfect prediction, 1.0, and no model at all, 0.0). Thus, the value of 0.78 for q^2 indicates that the model can be considered predictive and that the previous tendency map had a hidden quantitative relationship. Introducing the steric descriptor V_w , the statistical parameters improve significantly ($r^2 = 0.88$ and $q^2 = 0.83$, entry 2, Table 6.2), which reveals that not only the electronic effects but also the steric effects have a marked influence in determining the reactivity of these compounds. For example, the computed ΔG^\ddagger_{Nu} for **8** (16.4 kcal·mol⁻¹) is significantly lower than that of the analogous boryl-copper complex **9** with a much bulkier boryl fragment (26.9 kcal·mol⁻¹). In fact, the QSAR model with the two electronic parameters predicts the wrong nucleophilicity order for these complexes (12.3 and 10.9 kcal·mol⁻¹ for **8** and **9** in the fitting stage), whereas the QSAR model with the steric parameter predicts the right order and values that are closer to the response variables (17.1 and 19.9 kcal·mol⁻¹ for **8** and **9** in the fitting stage).

Table 6.2. Statistical parameters of the leave-one-out cross-validation for ΔG^\ddagger_{Nu} by using different descriptors.^[a]

Descriptor	r^2	q^2
$p/s, q[B]$	0.82	0.78
$p/s, q[B], V_w$	0.88	0.83
$p/s, q[B], V_w, (p/s)^2, (q[B])^2, (V_w)^2$	0.87	0.83
$p/s, q[B], V_w, (p/s \cdot q[B]), (p/s \cdot V_w), (q[B] \cdot V_w)$	0.90	0.83
<i>all</i>	0.90	0.82

^[a]Slope (fitting/prediction), intercept (fitting/prediction) in kcal·mol⁻¹ and error (fitting/prediction) in kcal·mol⁻¹: 0.83/0.80, 4.8/5.4 and 7.1/8.3 for model in entry 1; 0.88/0.85, 3.4/4.1 and 6.2/7.1 for model in entry 2; 0.87/0.84, 3.6/4.3 and 6.3/7.2 for model in entry 3; 0.90/0.87, 2.9/3.3 and 5.7/7.3 for model in entry 4; 0.90/0.86, 2.8/3.3 and 5.6/7.6 for model in entry 5.

To try to improve data description, we fitted the nucleophilicities to polynomial functions including higher-order and crossing terms. As represented by Equation 6.2, we built polynomials that include the descriptors raised to the second power (D_i^2) to account for the possible deviations from linearity in the correlation and the $D_i D_j$ crossing terms to evaluate the possible interplay between descriptors. Note that in Equation 6.2 the D_i terms correspond to the molecular descriptors, and the a_i , b_i , and c_i terms are the coefficients of QSAR equation. When the higher-order, the crossing, or all the possible terms of the equation were considered, the new models did not improve appreciably the correlation of the data nor the predicting ability ($r^2 = 0.87, 0.90$, and 0.90 and $q^2 = 0.83, 0.83$, and 0.82 , respectively, Table 6.2). This indicates that there is a linear

relationship between ΔG_{Nu}^\ddagger and the defined descriptors, and that these descriptors are independent of each other and describe different chemical features. Thus, for further analyses, we selected the simpler QSAR model fitted to first-order polynomials with three variables.

$$\Delta G_{Nu}^\ddagger = a_0 + \sum_{i=1}^3 a_i D_i + \sum_{i=1}^3 b_i D_i^2 + \sum_{i=1}^3 \sum_{j>i}^3 c_{ij} D_i D_j \quad (6.2)$$

Figure 6.10 shows the computed ΔG_{Nu}^\ddagger values plotted against the fitted ΔG_{Nu}^\ddagger values and the normalized coefficients of the QSAR equation for the first-order polynomial with three variables. The graph uses a color code to distinguish between the different classes of compounds defined above, namely the strong nucleophiles, the moderate nucleophiles, and the electrophiles. The correlation is fairly good for all compounds. A more accurate inspection shows that boryl-scandium (**10**) is the only early-transition metal complex in the dataset, which explains the difficulties in predicting it. QSAR methods require a wide sampling of the chemical space, which is not available here for early transition metals, to produce accurate predictions.^[30,31] A QSAR equation with non-normalized coefficients was also derived ($r^2 = 0.90$, $q^2 = 0.85$) in order to employ it directly with no need to normalize previously the obtained descriptors (Figure 6.11).

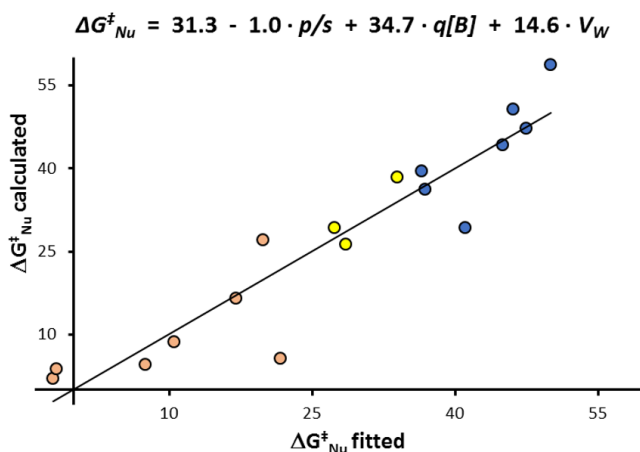


Figure 6.10. Calculated versus fitted free-energy barriers in kcal·mol⁻¹ for the dataset of 17 compounds using the first-order polynomial with p/s , $q[B]$ and V_w descriptors; and the resulting QSAR equation. Circles in red (●) correspond to strong nucleophiles, in yellow (●) to moderate nucleophiles, and in blue (●) to electrophiles.

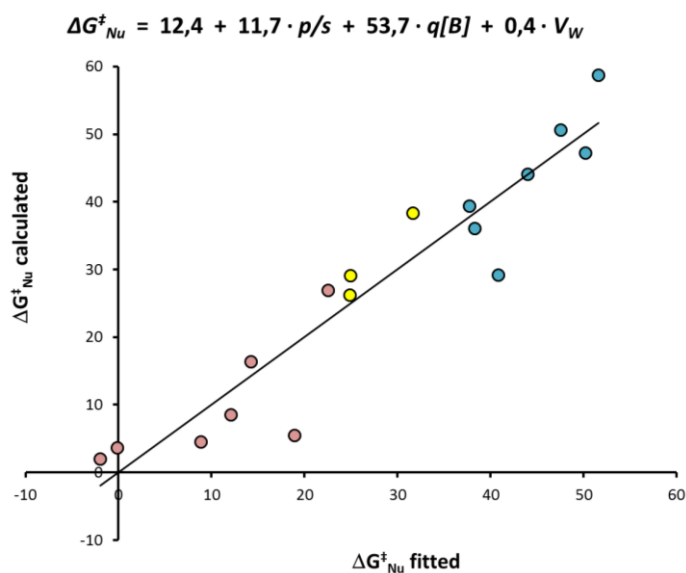


Figure 6.11. Resulting QSAR equation with non-normalized descriptor values for the dataset of 17 compounds using the first-order polynomial with p/s , $q[B]$ and V_w descriptors; and calculated vs fitted free-energy barriers in kcal·mol⁻¹. Circles in red (●) correspond to strong nucleophiles, in yellow (●) to moderate nucleophiles, and in blue (●) to electrophiles.

In addition to the predictive ability of the mathematical model, it is also possible to obtain further chemical information from the analysis of the QSAR equation with normalized coefficients since those account for the statistical weight within the equation. Thus, the positive coefficient for the steric descriptor (V_w) indicates that reducing the steric bulk would lower the free energy barrier and, consequently, increase the nucleophilicity of the boryl fragment. For example, the borylmagnesium compound **3** ($V_w = 1.3$) and the boryl-rhodium complex **15** ($V_w = 28.2$) have lower ΔG^\ddagger_{Nu} values (4.5 and 50.6 kcal·mol⁻¹, respectively) than the analogous compounds **4** and **14** (8.5 and 58.7 kcal·mol⁻¹, respectively) with a bulkier boryl fragment ($V_w = 12.6$) and auxiliary ligands ($V_w = 47.9$), respectively (Table 6.1 and Figure 6.1). The QSAR coefficient for the electrostatic $q[B]$ descriptor is also positive, thereby confirming the initial intuitive interpretation: the more negatively charged the boryl fragment, the lower is the energy barrier and the higher the nucleophilicity. Extending the example of the previous section, the computed ΔG^\ddagger_{Nu} values for compounds **15**, **12**, **5**, **8**, and **1** are 50.6, 39.4, 26.2, 16.4, and 2.0 kcal·mol⁻¹, respectively, and the overall charges of the Bpin moieties are +0.13, +0.02, -0.13, -0.43, and -0.59 a.u., respectively.

Finally, we noted that the value of the coefficient for the p/s descriptor has significantly lower weight (lower absolute value) than the other two descriptors, which indicates that the p/s ratio does not have a big influence on the nucleophilicity, but it could tune it. In fact, as mentioned before, the energy barrier on going from lithioborane (CH₃)₂BLi to F₂BLi varies by only 1.3 kcal·mol⁻¹ despite the significant chemical differences.^[7] This indicates that the nature of the boryl

fragment is significantly less important than the nature of the bonded metal in determining the reactivity character, and consequently it is possible to build a simpler two-term equation with $q[B]$ and V_w descriptors showing very similar statistical parameters ($r^2 = 0.88$, $q^2 = 0.84$) and coefficients (Figure 6.13). Nevertheless, we think that it is conceptually more interesting to use the p/s descriptor to fine-tune the QSAR model as a function of boryl nature.

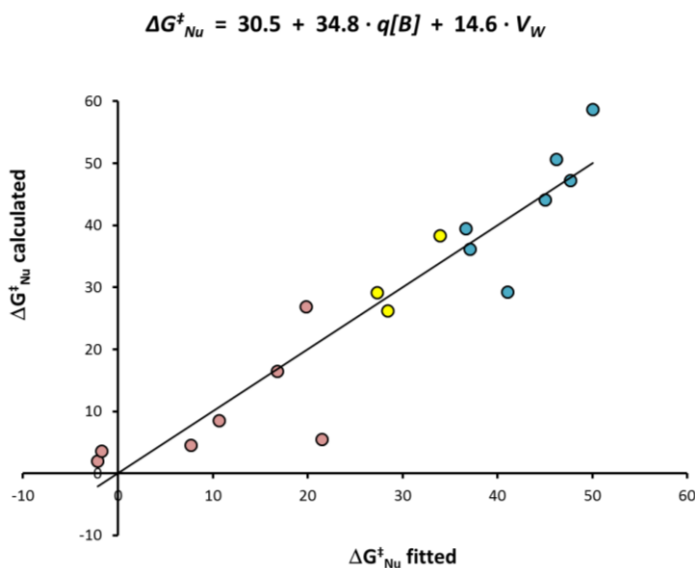


Figure 6.13. Resulting QSAR equation with normalized descriptor values for the dataset of 17 compounds using the first-order polynomial with $q[B]$ and V_w descriptors; and calculated vs fitted free-energy barriers in kcal·mol⁻¹. Circles in red (●) correspond to strong nucleophiles, in yellow (●) to moderate nucleophiles, and in blue (●) to electrophiles.

To externally validate the QSAR model within a blind test, we attempted to a priori predict the performance of the first four compounds depicted in Figure 6.14. Additionally, this will serve to evaluate the robustness of the model, because none of the compounds were used to build or to decide the parameters of the QSAR equation. We selected one ligand-modified boryl-copper complex (**T1**), one base-modified diboron compound (**T2**), and two complexes with new metal fragments, the boryl-silver **T3** and boryl-titanium **T4**. The calculated and predicted ΔG_{Nu}^\ddagger values were derived from the coefficient-normalized equation (Figure 6.10) and are presented in Table 6.3. The predictions are excellent for the complexes **T1** and **T2**, whereas for the complexes **T3** and **T4**, the metal fragments of which are not in the training set, the predictions are poorer.

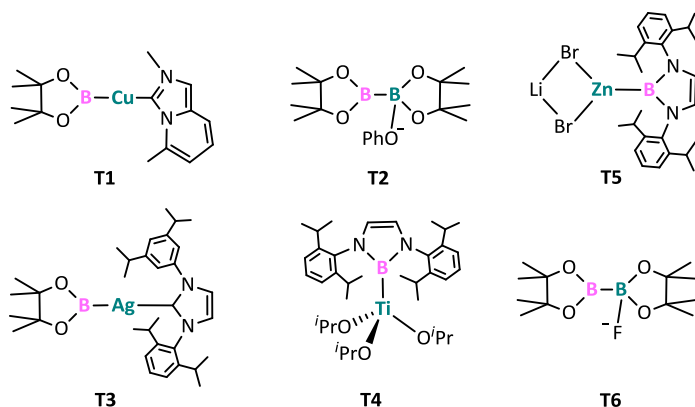


Figure 6.14. Selected trivalent boron compounds for the external blind test (**T1-T4**) and for the experimentally tested set (**T5** and **T6**).

In **T1**, we replaced the imidazol-2-ylidene (NHC) ligand of **8** by the imidazopyridin-2-ylidene derivative (NHC1).^[66] This type of carbene substitution has had a marked influence on the reactivity of gold chemistry.^[67] Here, the predicted nucleophilicity for the virtual boryl-copper complex **T1** is higher than that for complex **8** (Table 1 and Table 3), because the steric parameter estimates a less crowded reaction center for **T1** ($V_w = 33.0$ and 11.8 for **8** and **T1**, respectively). Marder and co-workers isolated an sp^2 - sp^3 diborane prepared by the addition of aryl oxide, but they did not report its reactivity.^[42,43] Therefore, we evaluated the ability of $\text{PhO}^- \rightarrow \text{Bpin-Bpin}$ (**T2**) to act as a source of nucleophilic boryl anions, and it turned out to be less efficient than the methoxy adduct **5** ($\Delta G^\ddagger_{Nu} = 32.2$ vs. 26.2 kcal·mol⁻¹). However, compound **T2** can still be classified as a moderate nucleophile.

Table 6.3. Calculated versus predicted free-energy barriers (ΔG^\ddagger_{Nu} in kcal·mol⁻¹) for a blind test subset ($N = 4$) employing the three-parameter QSAR model generated from the initial set ($N = 17$).

Label	Compound	ΔG^\ddagger_{Nu} calculated	ΔG^\ddagger_{Nu} predicted
T1	[Cu(Bpin)(NHC1)] ^[a]	14.6	13.3
T2	$\text{PhO}^- \rightarrow \text{Bpin-Bpin}$	32.2	32.7
T3	[Ag(Bpin)(NHC)]	29.2	21.3
T4	[Ti(B(NAr)(CH ₂) ₂ NAr)(O ⁱ Pr) ₃]	29.2	37.9

^[a]NHC1 = imidazopyridine-2-ylidene derivative

The boryl-silver complex **T3** is another virtual structure, which results from the replacement of the metal in the boryl-copper **8**. Previous theoretical calculations on [M(Bpin)(NHC)] (M = Cu and Ag) showed that the polarity of the M–B bond increases in the order AgI < CuI, and hence it can be assumed that boryl-silver species have lower nucleophilic character than boryl-copper.^[6] Indeed,

here we show that the ΔG^{\ddagger}_{Nu} values for **T3** (21.3 by prediction and 29.2 kcal·mol⁻¹ by DFT calculation) are larger than that computed for **8** (16.4 kcal·mol⁻¹). Even so, the value of the barrier is within the energy range defined for moderate nucleophiles, which indicates that this boryl-silver complex could behave as a nucleophile under certain conditions. The boryl-titanium triisopropoxide **T4** has been synthesized^[68] and its boron nucleophilic reactivity suggested.^[69] Since then, however, the use of **T4** in the borylation of organic substrates has not been reported, presumably because its boryl moiety has a low reactivity. Here, the predicted ΔG^{\ddagger}_{Nu} value differs quantitatively from the computed value (37.9 vs. 29.2 kcal·mol⁻¹), but both values are within the energy range defined for moderate nucleophiles.

Summarizing the external validation results, our QSAR model can predict with good precision the nucleophilic character of boryl fragments bonded to the atoms used to build the QSAR equation, whereas for other metals the model seems to be limited to screening purposes. This trend is not surprising because the predicting ability of QSAR models relies on the availability of a large dataset that samples chemical space widely.^[30,31] With these features in hand, we propose a novel boryl-copper complex as a source of a strong nucleophilic boryl moiety, and that diboranes activated with aryl oxides and the boryl-silver and boryl-titanium complexes can show moderate-to-low nucleophilicity.

We also tested whether it was possible to anticipate the nucleophilic behavior of two experimentally tested boryl compounds coming from two independent laboratories. We selected the boryl-zinc complex [ZnBr₂(THF)_n{B(NdippCH)₂}]Li (dipp = 2,6-diisopropylphenyl;^[70] **T5**) and the activated diboron F⁻→Bpin–Bpin (**T6**)^[43] (see Figure 7). The QSAR model predicts free-energy barriers of 15.0 and 27.7 kcal·mol⁻¹, respectively, which are in full agreement with experimental observations. Thus, the boryl-zinc complex **T5** can be correctly classified as a nucleophile, because its predicted ΔG^{\ddagger}_{Nu} (15 kcal·mol⁻¹) is in the range of values calculated for nucleophilic boryl fragments (2-27 kcal·mol⁻¹, see above). Similarly, **T6** can be correctly classified as a moderate nucleophile, its predicted ΔG^{\ddagger}_{Nu} value (27.7 kcal·mol⁻¹) being in the range of other activated diboron compounds acting as nucleophiles (26-38 kcal·mol⁻¹, see above). Therefore, this external blind test demonstrates that the QSAR model allows a priori predictions for both **T5** and **T6**, further proving its predictive ability.

6.2.2. Specific structure-nucleophilicity relationships in transition-metal-free B–B and B–interelement

Following the same procedure of the M–BRR' reagents, we sought to expand the study into the nucleophilic activity of diborane compounds R₂B–BR₂' in a metal-free context. Conversely to the first row of homoatomic junctions (C–C, N–N, O–O, and F–F), boron is distinctly reluctant to form such electron-precise, saturated bonds. For this reason, the study of diborane complexes is witnessing strong growth spurred on by the discovery of new capabilities of these compounds to perform metal-free borylation reactions.^[35,42–44] Indeed, the switchable nature of B make diborane

units a special synthon for its use in organic chemistry since it is now possible to access to organoborane molecules without the presence of a metal capable of tuning boron's electronic properties. Furthermore, the presence of an interelement Y in Lewis-activated boron moieties $X \rightarrow B(R_2) - Y$ may enhance its nucleophilic activity promoted by the polarization of the B–Y linkage towards the heteroatom, which is in turn an appealing strategy for the formation of C–Y bonds.^[35]

The borane compounds chosen for modeling its nucleophilic activity in a metal-free context by the QSAR methodology were selected from the literature^[35,42–44] and can be classified into three subsets: *i*) symmetric diborane units, $X \rightarrow (\text{pin})B - B(\text{pin})$ (**F1-F24**, Figure 6.15); *ii*) unsymmetric diboranes, $[\text{MeO} \rightarrow (\text{pin})B - B(R_2)]^-$ (**F25-F30**, Figure 6.16); and *iii*) interelement borane complexes, $[\text{MeO} \rightarrow (\text{pin})B - Y]^-$ (**F31-F39**, Figure 6.17). Compounds of each subset will be ordered following their computed nucleophilic energy barrier, from lowest to highest.

▪ Correlation for $X \rightarrow (\text{pin})B - B(\text{pin})$ subset

As it has been commented above, Lewis bases can activate diboron compounds to generate nucleophilic boryl moieties *via* quaternization of one boron and polarization of the B–B bond. Here, we analyzed the effect of those Lewis bases on the nucleophilicity using as reference the symmetric diborane complex bis(pinacolato)diboron (pinB–Bpin). Thus, the only variable of the entire subset is the activating Lewis-base, ranging from negatively charged to neutral molecules and including C-, N-, O-, F- and S-donor atoms. Besides the commonly employed alkoxide bases, it has been recently reported the first diborane unit activated with a carbanion species for its use in the synthesis of organoborane compounds. This species corresponds to Ph^- , although its structure was not confirmed by means of an X-ray analysis.^[71] The scarce use of this type of bases is probably due to their preference for deprotonating instead of coordinating, however their inclusion in the model (**F1** and **F2**) might help to elucidate the main effects governing the nucleophilic activation of diboron compounds by those bases. Conversely, alkoxides have been largely employed as activating agents, being MeO^- (**F3**) the most exploited by far since its discovery.^[9,10] Other analogous bases such as ${}^i\text{PrO}^-$ (**F8**), ${}^t\text{BuO}^-$ (**F9**), PhO^- (**F11**), or BuO^- have also been applied in a metal-free context and inspired the construction of untested diboranes (**F4-F6**, **F10**, **F13**, **F15**, **F16**).^[10,42,43] Regarding negatively charged halogens, our DFT calculations show that fluoride is the only one forming a monocoordinated $\text{sp}^3\text{-sp}^2$ adduct. The rest of halogens yielded species where each anion was acting as bridge between the two borons with almost identical distances. This bonding situation might prevent the formation of a nucleophilic sp^2 boryl fragment. The $\text{F}^- \rightarrow (\text{pin})B - B(\text{pin})$ compound (**F7**) has been experimentally isolated but its reactivity towards electrophilic reagents has not been reported yet.^[43] For chalcogenides such as sulphur and selenium, calculations also showed the formation of bridging structures except for MeS^- , which was indeed capable of quaternizing a single boron atom (**F12**). Nevertheless, no experimental evidences are available for this species. The two traditionally good leaving groups bis(*p*-toluenesulfonate)amide (Ts_2N^- , **F14**) and *p*-toluenesulfonate (TsO^- , **F17**) have also been evaluated as a Lewis activating base with no experimental proofs about its behavior.

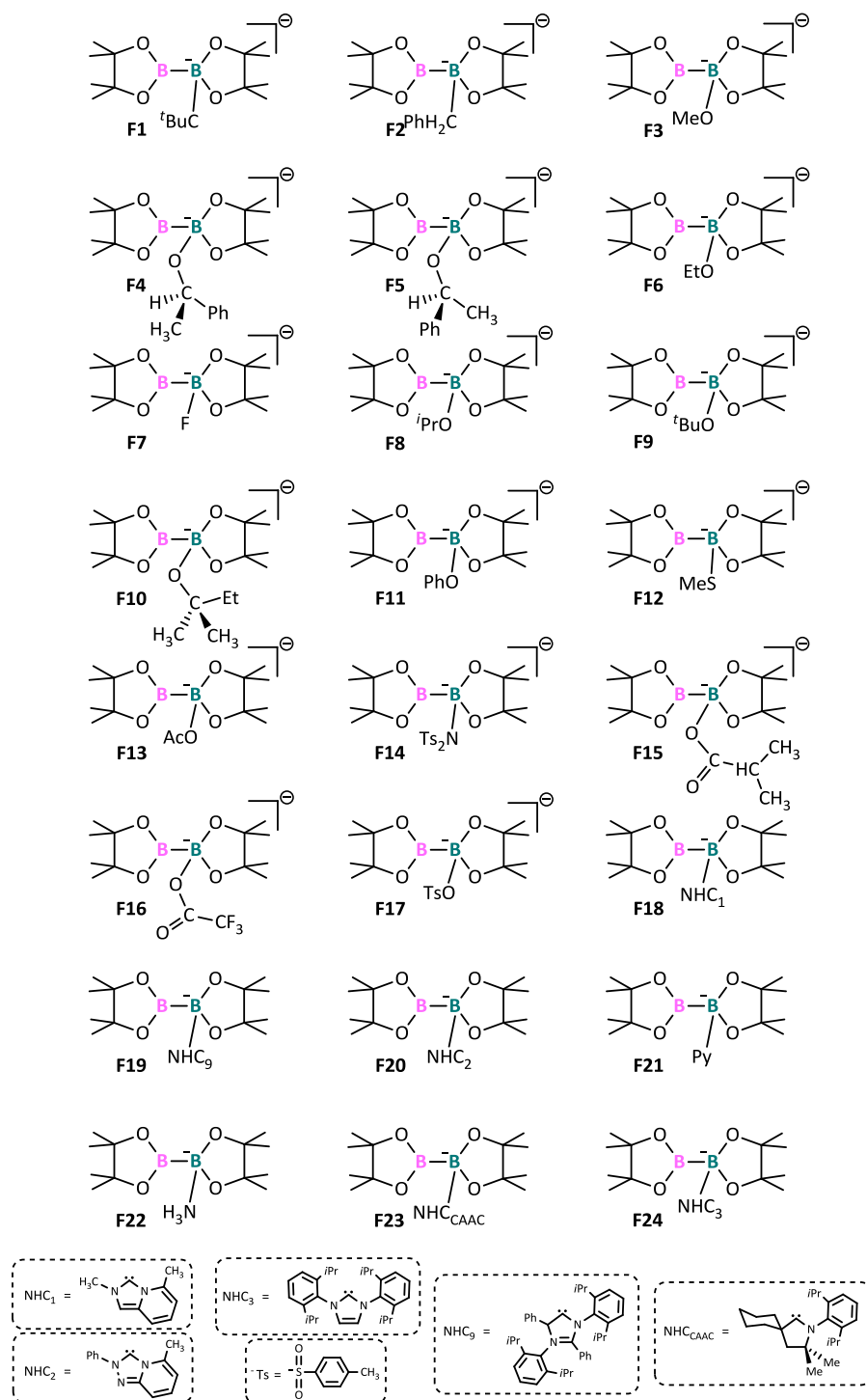


Figure 6.15. Selected data set of symmetric diborane compounds activated with Lewis bases, $\text{X} \rightarrow (\text{pin})\text{B}-\text{B}(\text{pin})$.

Moving into neutral electron-donors, carbenes are widely used in transition-metal chemistry as ancillary ligands displaying strong σ -donating properties. This characteristic was put into action by applying carbenes as activating agent in one of the first examples of nucleophilic reactivity of diboron compounds in a metal-free context.^[72] Inspired by this fact, we have considered the inclusion of 1,3-bis(2,6-diisopropyl)phenyl imidazol-2-ylidene (**F24**) and two imidazopyridine-2-ylidene analogues (**F18** and **F20**).^[66,67] In addition, a more basic carbene was managed to be isolated in solid state and in solution, exhibiting strong electron delocalization (**F19**).^[73] Even so, beyond *N*-heterocyclic carbenes, related cyclic alkylaminocarbenes (CAAC, **F23**) have computationally suggested to be more σ -donating than their NHC counterparts through a higher HOMO.^[74] Finally, the reaction of pinB–Bpin with neutral Lewis bases, such as PMe_3 , pyridine, 4-dimethylaminopyridine (DMAP), or pyrrolidine, gave no adduct formation (analyzed by ^1H and $^{11}\text{B}\{^1\text{H}\}$ NMR spectroscopy), even in the presence of excess base.^[43] However, it has been very recently reported that xylenolisocyanide and pyridine afford pyridine-coordinated boraalkenes *via* insertion into the B–B bond of an unsymmetric diboron compound.^[75] This reactivity made us think in the inclusion of neutral nitrogen bases to cover a wider data set (**F21** and **F22**).

Table 6.3. Statistical parameters of the leave-one-out cross-validation for ΔG^\ddagger_{Nu} of the symmetric diboron species by using different descriptors.^[a]

Descriptor	r^2	q^2
$q[B]$	0.72	0.68
$p/s, q[B]$	0.72	0.68
$p/s, q[B], V_w$	0.73	0.67
$p/s, q[B], V_w, (p/s)^2, (q[B])^2, (V_w)^2$	0.78	0.68
$p/s, q[B], V_w, (p/s \cdot q[B]), (p/s \cdot V_w), (q[B] \cdot V_w)$	0.70	0.65
<i>all</i>	0.71	0.67

^[a]Slope (fitting/prediction), intercept (fitting/prediction) in kcal-mol⁻¹ and error (fitting/prediction) in kcal-mol⁻¹: 0.72/0.71, 10.4/10.8 and 5.3/5.6 for model in entry 1; 0.72/0.71, 10.3/10.7 and 5.2/5.6 for model in entry 2; 0.73/0.71, 9.8/10.6 and 5.1/5.7 for model in entry 3; 0.78/0.74, 8.2/9.9 and 4.6/5.7 for model in entry 4; 0.70/0.69, 11.0/11.6 and 5.4/5.9 for model in entry 5; 0.71/0.69, 10.6/11.3 and 5.3/5.7 for model in entry 6.

Likewise the previous case, we carried out DFT calculations for the boryl fragment transfer to the electrophilic carbon of formaldehyde model substrate and evaluated the correlation between computed and predicted nucleophilicities with the selected descriptors p/s , $q[B]$ and V_w . Table 6.3 collects the statistical parameters for the validation of multivariate models using different combinations of descriptors. Our hypothesis is that for a given diboron compound its nucleophilicity is mainly dependent on the electronic transference degree of the activating base and the concomitant polarization of the B–B bond. This is reflected in the correlation between the

sole $q[B]$ descriptor with the response variable ΔG^{\ddagger}_{Nu} (first entry of Table 6.3). Confirmation of our presumption is shown in subsequent entries, where the addition of further descriptors does not improve significantly the model. Hence, the higher nucleophilic activity of the boryl moiety (lower values of ΔG^{\ddagger}_{Nu}) is directly related with its increasing negative charge, which is induced by the activating base employed.

▪ Correlation for [OMe→(pin)B–B(R₂)][–] subset

In order to look for the impact that nature of the activated (non-quaternized) boron unit has on the nucleophilicity, we have selected a new subset in which the activating base, MeO[–], and the sp³-boryl fragment, –Bpin, are kept fixed while varying the sp²-boryl unit (Figure 6.16). Interestingly, unsymmetrical diboron compounds are beginning to forge its way in organic synthesis as different reactivities and regioselectivities can be achieved in reactions using these unusual species. The common characteristic of B(sp²)–B(sp²) diboron compounds to stabilize their electro-poor linkage usually is substituents with lone pair electrons, so those can transfer electron density to the unoccupied orbital of boron. However, there some unusual examples, such as aryl-substituted boryl synthons, which have been synthesized containing mesityl groups showing dramatically enhanced stability over their tert-butyl analogues.^[76,77] Although their applications are still limited, it has been recently reported a direct and base-catalyzed diboration of alkynes and a facile scission of isonitrile carbon-nitrogen triple bond by using the unsymmetrical pinB–BMes (**F29**) as a reagent in both cases.^[78,79] In addition, we have built a virtual and saturated alkynylboron moiety (**F25**), from which a great nucleophilic potential is expected due its incapability for loading the empty boron orbital.

The development of new tetraalkoxydiboron and related derivatives is an area that is receiving increasing attention for their use in in catalytic borylation reactions. Among them, the most widely employed probably are bis(catecholato)-, bis(neopentylglycolato)-, and bis(pinacolato)diboron (**F3**) (B₂cat₂, B₂neo₂, and B₂pin₂, respectively),^[80–82] but unsymmetric derivatives are not exploited owing to their similarities (**F26** and **F27**). Turning diboron substituents from oxygen- to nitrogen-based, one of the most commonly known is Bdan (dan = 1,8-diaminonaphthalene, **F28**), whose mixture with Bpin offers an excellent chemoselective reactivity scope.^[48,49,83] Finally, the steric bulkiness of the *N,N*-bis(2,6-diisopropylphenyl)-2-bromo-2,3-dihydro-1*H*-1,3,2-diazaborole fragment^[36] (**F30**) paired to an unobstructed BH₃[–],^[84] makes this species interesting for being isoelectronic with *N*-heterocyclic carbenes. Thus, its inclusion in the data set is an appealing issue.

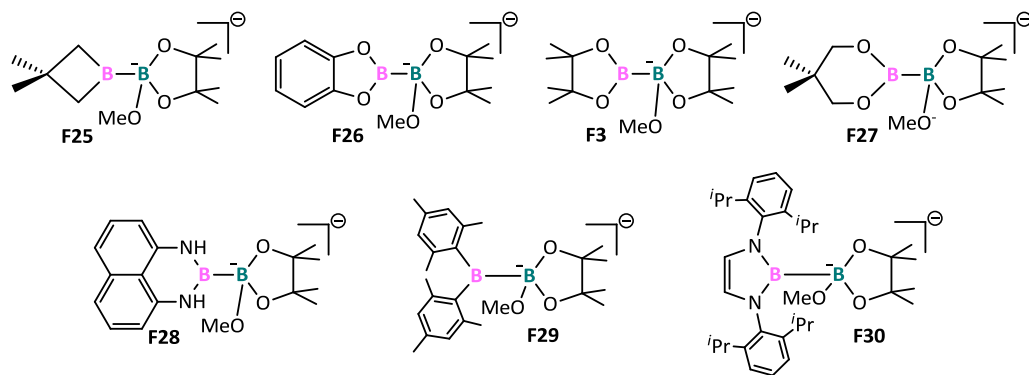


Figure 6.16. Selected dataset of unsymmetric diborane compounds activated by a methoxy base, $[\text{MeO} \rightarrow (\text{pin})\text{B}-\text{B}(\text{R}_2)]^-$.

Table 6.4. Statistical parameters of the leave-one-out cross-validation for $\Delta G_{\text{Nu}}^\ddagger$ of the unsymmetric diboron species $[\text{MeO} \rightarrow (\text{pin})\text{B}-\text{B}(\text{R}_2)]^-$ by using different descriptors.^[a]

Descriptor	r^2	q^2
$p/s, q[B]$	0.49	0.04
$p/s, q[B], V_w$	0.82	0.54
$p/s, q[B], V_w, (p/s)^2, (q[B])^2, (V_w)^2$	0.93	0.72
$p/s, q[B], V_w, (p/s \cdot q[B]), (p/s \cdot V_w), (q[B] \cdot V_w)$	0.86	0.52
<i>all</i>	0.92	0.66

^[a]Slope (fitting/prediction), intercept (fitting/prediction) in $\text{kcal}\cdot\text{mol}^{-1}$ and error (fitting/prediction) in $\text{kcal}\cdot\text{mol}^{-1}$: 0.49/0.14, 14.4/23.7 and 4.7/7.3 for model in entry 1; 0.82/0.68, 5.0/9.5 and 2.8/4.7 for model in entry 2; 0.93/0.78, 2.1/6.1 and 1.8/3.5 for model in entry 3; 0.86/0.78, 3.9/5.6 and 2.5/5.2 for model in entry 4; 0.92/0.78, 2.2/5.9 and 1.8/4.0 for model in entry 5.

Statistical parameters for the validation of multivariate models using different combinations of the descriptors detailed above are collected in Table 6.4. It can be noticed in the first entry of this subset that electronic descriptors (p/s and $q[B]$) do not play the same important role as the previously analyzed ensembles, showing a model without predictive ability ($q^2 = 0.04$). The addition of the steric factor does improve significantly the statistics ($q^2 = 0.54$), leading to a model that is in the limit of predictive ability. This fact can be understood if it is taken into consideration that the molecular unit responsible of insulating electron density to the reactive boryl synthon ($\text{MeO}^- \rightarrow \text{Bpin}$) remain unaltered along all diboron compounds of this subset. Therefore, the intrinsic features of the sp^2 boryl moiety, including the steric hindrance, is what determines its nucleophilicity activity. Nevertheless, the predicting ability keeps improving by the inclusion of

high order descriptors, which can be translated into a deviation of linearity dependence of the response variable, ΔG^\ddagger_{Nu} . This QSAR model reaches a good predictive ability at $q^2 = 0.72$. Finally, the use of crossed terms instead of higher order terms in the model does not offer a better prediction due to the lack of correlation between descriptors. All in all, this subset seems to involve more complicated relationships than previous groups.

▪ Correlation for $[\text{MeO} \rightarrow (\text{pin})\text{B}-\text{Y}]^-$ subset

The last subset comprises interelement borane complexes $[\text{MeO} \rightarrow (\text{pin})\text{B}-\text{Y}]^-$ forming a direct B–Y bond, being Y an atom of the p-block of the periodic table (Figure 6.17). Regarding selenium, it has been demonstrated the efficient and direct addition (without any metal nor organocatalytic assistance) of phenylselenium borane to activated α,β -unsaturated olefins, such as ketones and aldehydes.^[85] Previous DFT calculations showed that the carbonyl formed an adduct with the selenoborane during the course of the reaction.^[85] However, in the case of our model compound $[\text{MeO} \rightarrow (\text{pin})\text{B}-\text{SePh}]^-$, we found that coordination of the strong methoxy base triggers the cleavage of the B–Se junction spontaneously. Instead, the $[\text{MeO} \rightarrow (\text{pin})\text{B}-\text{SeMe}]^-$ (**31**) was the only selenium-based compound considered in our dataset. Thioboranes behave in a similar way as selenoboranes towards alkenyl substrates.^[86] The mechanism of 1,4- versus 1,2-addition of $\text{RS}-\text{Bpin}$ ($\text{R} = -\text{Tol}, -\text{Ph}, -\text{Bn}$) to an α,β -unsaturated ketone was investigated by means of DFT calculations. Hence, we included $-\text{SPh}$ (**32**) and the less electro-withdrawing $-\text{SMe}$ (**34**) substituents in the dataset.

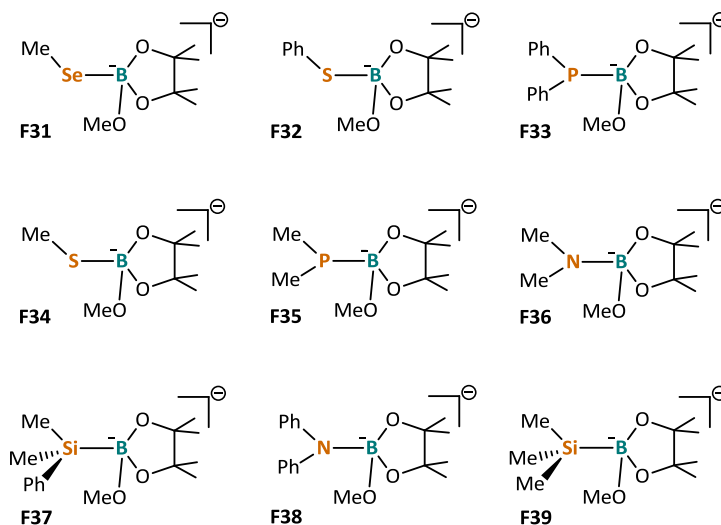


Figure 6.17. Interelement borane compounds $[\text{MeO} \rightarrow (\text{pin})\text{B}-\text{Y}]^-$.

Looking into P–B linkages, it has been found that the π -donation of the phosphorus' lone pair to the vacant boron's orbital can be relieved by the selection of proper substituents in those atoms.^[87] Likewise the sulphur case, we considered as well $-\text{PPh}_2$ (**33**) and $-\text{PMe}_2$ (**35**). Unactivated

addition of N–B bonds was carried out several years ago with a limited substrate scope.^[88–91] More recently, the presence of an activating Lewis-base coordinated to boron enhances nitrogen nucleophilicity and broadens the applicability of this adduct.^[92] Once again, –NPh₂ (**38**) and –NMe₂ (**36**) are chosen as representative substituents. At last, reactivity of Si–B junctions allows for a wide variety of outcomes,^[35] so we included two of the most used silicon substituents (**37** and **39**).

Table 6.5. Statistical parameters of the leave-one-out cross-validation for ΔG^{\ddagger}_{Nu} of the interelement-boron species [MeO→(pin)B–Y][–] by using different descriptors.^[a]

Descriptor	r^2	q^2
$p/s, q[B]$	0.89	0.57
$p/s, q[B], V_w$	0.94	0.85
$p/s, q[B], V_w, (p/s)^2, (q[B])^2, (V_w)^2$	0.97	0.85
$p/s, q[B], V_w, (p/s \cdot q[B]), (p/s \cdot V_w), (q[B] \cdot V_w)$	0.96	0.88
<i>all</i>	0.99	0.96

^[a]Slope (fitting/prediction), intercept (fitting/prediction) in kcal·mol^{–1} and error (fitting/prediction) in kcal·mol^{–1}: 0.89/0.51, 1.3/3.8 and 2.1/4.5 for model in entry 1; 0.94/0.90, 0.6/1.0 and 1.5/2.4 for model in entry 2; 0.97/0.85, 0.3/1.9 and 1.1/2.4 for model in entry 3; 0.96/0.91, 0.5/0.8 and 1.3/2.2 for model in entry 4; 0.99/0.95, 0.1/0.5 and 0.45/1.2 for model in entry 5.

Building a QSAR model based just on the simple form of electronic descriptors (p/s and $q[B]$) would have screening ability (Table 6.5). However, inclusion of the steric factor improves drastically the predicting ability, giving the highest value of q^2 for all subsets studied. Subsequent inclusion of descriptors into the treatment slightly refines the model, and consideration of all variables leads to a notable improvement. Despite that, such level of parametrization can cause erroneous predictions in compounds whose nature is far apart from the ones enrolled in model construction.

▪ QSAR model for transition-metal-free nucleophilic reagents

Finally, a blended ensemble of the three subsets previously reported is displayed in Figure 6.18, preserving the nomenclature of the preceding subgroups. Some of the compounds forming the first subset of symmetric diboranes have been discarded in order to avoid an unbalanced combined ensemble due to greater amount of molecules comprising that symmetrical group. Those selected compounds follow the criteria to be as chemically distinct as possible to cover a wider range of the response variable ΔG^{\ddagger}_{Nu} .

Table 6.6. Statistical parameters of the leave-one-out cross-validation for ΔG^{\ddagger}_{Nu} of the combined ensemble of boryl species by using different descriptors.^[a]

Descriptor	r^2	q^2
$p/s, q[B]$	0.69	0.65
$p/s, q[B], V_w$	0.84	0.79
$p/s, q[B], V_w, (p/s)^2, (q[B])^2, (V_w)^2$	0.82	0.76
$p/s, q[B], V_w, (p/s \cdot q[B]), (p/s \cdot V_w), (q[B] \cdot V_w)$	0.84	0.78
<i>all</i>	0.80	0.71

^[a]Slope (fitting/prediction), intercept (fitting/prediction) in kcal·mol⁻¹ and error (fitting/prediction) in kcal·mol⁻¹: 0.69/0.66, 7.6/8.6 and 7.1/7.7 for model in entry 1; 0.84/0.79, 4.1/5.0 and 5.2/6.0 for model in entry 2; 0.82/0.76, 4.5/5.4 and 5.5/6.3 for model in entry 3; 0.84/0.85, 4.1/3.9 and 5.2/6.0 for model in entry 4; 0.80/0.73, 5.0/6.1 and 5.8/7.0 for model in entry 5.

A summary of the modeling descriptors and the results of the multivariate analysis employed within this last combined set can be found in Table 6.6. The combination of both electronic descriptors (p/s and $q[B]$) yielded a QSAR model with predictive ability that improved notably upon incorporation of the steric distance-weighted volume, V_w . Further addition of descriptors involving their correlation and deviation of linearity do not offer better results. Therefore, the three-term equation derived in the first set containing metal-boryl compounds is still valid and meaningful for the nonmetallic scenario, albeit the coefficient preceding each descriptor have different statistical weight accounting for the distinct nature of the members of the corresponding ensembles.

6.4. Computational details

Full quantum mechanical calculations were carried out by using the Gaussian 09 suite of programs.^[93] Calculations were performed within the framework of DFT^[94] using the B3LYP functional.^[95–97] The basis set used for the transition metals and the silicon, phosphorus, chlorine, and bromine atoms was that associated with a pseudopotential with a standard double- ξ LANL2DZ contraction,^[98] and was supplemented by f and d shells, respectively.^[99,100] The rest of the atoms were described by using a standard 6-31G(d,p) basis set.^[101–103] All geometry optimizations were executed with no restrictions. The nature of the stationary points encountered was characterized by means of harmonic vibrational frequencies analysis. The bonding of the molecules as well as the fragment charges were analyzed by using the NBO method,^[104] from which we derived the p/s and $q[B]$ descriptors.

We used partial least-squares (PLS) regression^[105,106] as the multivariate regression technique. External and full cross-validations were considered for model building and evaluation. Different statistical parameters were employed to evaluate the predictive ability of the models during the fitting and test stages, namely, the Pearson correlation coefficient (r^2), the determination coefficient (q^2), the sample standard error, and the slope and intercept of the fitted/predicted versus observed values.^[107] Because the numerical values of the descriptors can vary significantly, each set of descriptors was normalized with respect to the maximum absolute value of the set to ensure they have equal weight in multivariate analysis.

6.5. Conclusions

A QSAR model has been generated for predicting the nucleophilicity of trivalent boron compounds using a varied dataset that includes boryl moieties bonded to alkali and alkaline-earth metals, to transition metals, and to sp^3 -hybridized boryl units. The optimal predictive model ($r^2 = 0.88$, $q^2 = 0.83$) was obtained by using the computed free-energy barrier (ΔG^\ddagger_{Nu}) as a response variable and three molecular descriptors, namely the p/s orbital population ratio (p/s), the charge of the boryl fragment ($q[B]$), and the steric bulk evaluated with the distance-weighted volume (V_w) parameter. This yields a three-term easy-to-interpret QSAR equation that shows good predictive abilities establishing a direct connection between the nucleophilicity and the properties of bonded metal fragments.

The use of chemically meaningful descriptors provides insight into the factors governing the nucleophilicity. Thus, the metal fragments that most effectively promote nucleophilic activity are those that polarize the B–M bond to yield negatively charged boryl moieties. The predictive ability of the QSAR model was improved by introducing the distance-weighted volume to account for the steric effects induced by the metal fragments and bulky substituents in the boron moiety. Reducing the steric bulk on the reaction center would favor substrate coordination and reactivity. In addition, the analysis of the potential energy profiles of four prototypical boryl fragments bonded to lithium, sp^3 boron, copper, and palladium has given detailed molecular insight into the reaction mechanisms and established the following order of nucleophilicity: $Li > Cu > B(sp^2)-B(sp^3) > Pd$.

This computational methodology has also been used to make a priori predictions of experimentally untested compounds, evaluating externally the QSAR model. The predictions show good precision for boryl fragments bonded to any of the metals used to build the QSAR equation, whereas the model has screening ability when the nature of the metal bonded to the boryl is outside the training dataset. We propose that boryl-copper complexes with less sterically hindered *N*-heterocyclic carbenes could enhance their nucleophilicity. Moreover, diboranes

activated with aryl oxides and boryl-silver and boryl-titanium complexes could behave as moderate nucleophiles under certain conditions.

Establishing tendencies for the nucleophilicity of boryl fragments activated by a Lewis base and in a metal-free context was also possible. We divided the study in three subsets regarding on the different nature of the adducts considered. In the first group, the effect of the base was evaluated and a strong reliance on the charge of the boryl synthon was identified. In the second subset the impact of changing the nature of the non-quaternized boryl unit was analyzed and found out to have deviations of linearity since higher order descriptors are needed for a good predictive ability. The last bloc comprised boryl-interelement adducts, which afforded remarkable adjustment to the three-parameter equation stemmed in first ensemble containing boron-metal bonds. Additionally, a combined ensemble mixing some of the previous compounds from different subset was built in order to establish unified tendencies for the nonmetallic scenario. The model based on the three descriptors employed for the metal-boryl compounds is also valid and meaningful for this case, rendering good predictive ability ($r^2 = 0.84$, $q^2 = 0.79$).

From the studies performed in all boryl ensembles and the trends extracted from each of them, we hope these tendencies can be straightforwardly used for *a priori* evaluation of the nucleophilic character of other trivalent boron compounds, and for deriving guidelines for novel agent design.

6.6. References

- [1] H. Nöth, G. Schmid, *Angew. Chemie Int. Ed. English* **1963**, *2*, 623.
- [2] H. Braunschweig, *Angew. Chemie Int. Ed.* **1998**, *37*, 1786–1801.
- [3] G. J. Irvine, M. J. G. Lesley, T. B. Marder, N. C. Norman, C. R. Rice, E. G. Robins, W. R. Roper, G. R. Whittell, L. J. Wright, *Chem. Rev.* **1998**, *98*, 2685–2722.
- [4] L. Dang, Z. Lin, T. B. Marder, *Chem. Commun. (Camb)*. **2009**, 3987–3995.
- [5] J. Cid, H. Gulyás, J. J. Carbó, E. Fernández, *Chem. Soc. Rev.* **2012**, *41*, 3558.
- [6] J. Cid, J. J. Carbó, E. Fernández, *Chem. - A Eur. J.* **2012**, *18*, 12794–12802.
- [7] M. Wagner, N. J. R. van Eikema Hommes, H. Noeth, P. v. R. Schleyer, *Inorg. Chem.* **1995**, *34*, 607–614.
- [8] H. Zhao, L. Dang, T. B. Marder, Z. Lin, *J. Am. Chem. Soc.* **2008**, *130*, 5586–5594.
- [9] A. Bonet, C. Pubill-Ulldemolins, C. Bo, H. Gulyás, E. Fernández, *Angew. Chemie Int. Ed.* **2011**, *50*, 7158–7161.
- [10] C. Pubill-Ulldemolins, A. Bonet, C. Bo, H. Gulyás, E. Fernández, *Chem. - A Eur. J.* **2012**, *18*, 1121–1126.
- [11] A. G. Maldonado, J. A. Hageman, S. Mastroianni, G. Rothenberg, *Adv. Synth. Catal.* **2009**, *351*, 387–396.
- [12] N. Fey, A. G. Orpen, J. N. Harvey, *Coord. Chem. Rev.* **2009**, *253*, 704–722.

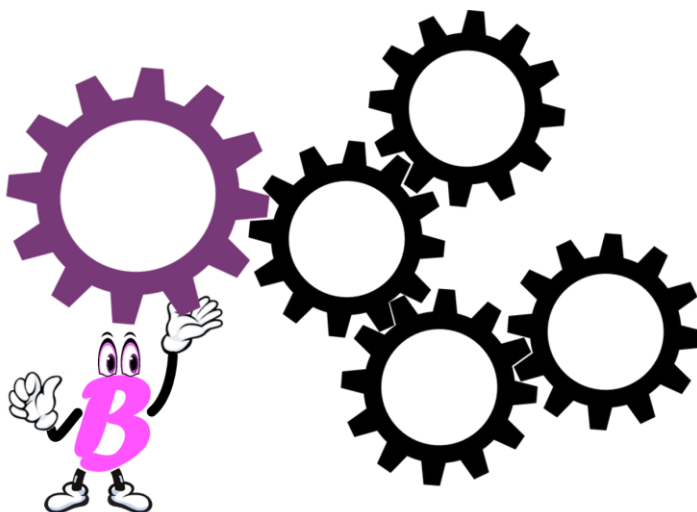
- [13] N. Fey, *Dalt. Trans.* **2010**, *39*, 296–310.
- [14] C. R. Corbeil, N. Moitessier, *J. Mol. Catal. A Chem.* **2010**, *324*, 146–155.
- [15] M. C. Kozlowski, S. L. Dixon, M. Panda, G. Lauri, *J. Am. Chem. Soc.* **2003**, *125*, 6614–6615.
- [16] K. B. Lipkowitz, M. Pradhan, *J. Org. Chem.* **2003**, *68*, 4648–4656.
- [17] S. Sciabola, A. Alex, P. D. Higginson, J. C. Mitchell, M. J. Snowden, I. Morao, *J. Org. Chem.* **2005**, *70*, 9025–9027.
- [18] V. L. Cruz, J. Ramos, S. Martinez, A. Muñoz-Escalona, J. Martinez-Salazar, *Organometallics* **2005**, *24*, 5095–5102.
- [19] J. A. Hageman, J. A. Westerhuis, H. Frühauf, G. Rothenberg, *Adv. Synth. Catal.* **2006**, *348*, 361–369.
- [20] G. Occhipinti, H.-R. Bjørsvik, V. R. Jensen, *J. Am. Chem. Soc.* **2006**, *128*, 6952–6964.
- [21] J. C. Ianni, V. Annamalai, P. Phuan, M. Panda, M. C. Kozlowski, *Angew. Chemie Int. Ed.* **2006**, *45*, 5502–5505.
- [22] M. Urbano-Cuadrado, J. J. Carbó, A. G. Maldonado, C. Bo, *J. Chem. Inf. Model.* **2007**, *47*, 2228–2234.
- [23] V. L. Cruz, J. Martinez, J. Martinez-Salazar, J. Ramos, M. L. Reyes, A. Toro-Labbe, S. Gutierrez-Oliva, *Polymer (Guildf)*. **2007**, *48*, 7672–7678.
- [24] Z. Strassberger, M. Mooijman, E. Ruijter, A. H. Alberts, A. G. Maldonado, R. V. A. Orru, G. Rothenberg, *Adv. Synth. Catal.* **2010**, *352*, 2201–2210.
- [25] S. Aguado-Ullate, L. Guasch, M. Urbano-Cuadrado, C. Bo, J. J. Carbo, *Catal. Sci. Technol.* **2012**, *2*, 1694–1704.
- [26] T. A. Manz, J. M. Caruthers, S. Sharma, K. Phomphrai, K. T. Thomson, W. N. Delgass, M. M. Abu-Omar, *Organometallics* **2012**, *31*, 602–618.
- [27] S. Aguado-Ullate, J. A. Baker, V. Gonzalez-Gonzalez, C. Muller, J. D. Hirst, J. J. Carbo, *Catal. Sci. Technol.* **2014**, *4*, 979–987.
- [28] H. Huang, H. Zong, B. Shen, H. Yue, G. Bian, L. Song, *Tetrahedron* **2014**, *70*, 1289–1297.
- [29] T. A. Manz, *RSC Adv.* **2015**, *5*, 48246–48254.
- [30] J. Jover, N. Fey, *Chem. – An Asian J.* **2014**, *9*, 1714–1723.
- [31] N. Fey, *Chem. Cent. J.* **2015**, *9*, 38.
- [32] S. Aguado-Ullate, S. Saureu, L. Guasch, J. J. Carbó, *Chem. - A Eur. J.* **2012**, *18*, 995–1005.
- [33] S. Aguado-Ullate, M. Urbano-Cuadrado, I. Villalba, E. Pires, J. I. García, C. Bo, J. J. Carbó, *Chem. - A Eur. J.* **2012**, *18*, 14026–14036.
- [34] M. Álvarez, D. García-López, J. J. Carbó, <http://rodi.urv.es/~carbo/quadrants/index.html>.
- [35] A. B. Cuenca, R. Shishido, H. Ito, E. Fernandez, *Chem. Soc. Rev.* **2017**, *46*, 415–430.
- [36] Y. Segawa, M. Yamashita, K. Nozaki, *Science (80-)*. **2006**, *314*, 113 LP-115.
- [37] T. B. Marder, *Science (80-)*. **2006**, *314*, 69 LP-70.
- [38] Y. Segawa, M. Yamashita, K. Nozaki, *Angew. Chemie Int. Ed.* **2007**, *46*, 6710–6713.
- [39] Y. Segawa, Y. Suzuki, M. Yamashita, K. Nozaki, *J. Am. Chem. Soc.* **2008**, *130*, 16069–16079.
- [40] M. Yamashita, K. Nozaki, *Pure Appl. Chem.* **2008**, *80*, 1187–1194.
- [41] M. Yamashita, Y. Suzuki, Y. Segawa, K. Nozaki, *J. Am. Chem. Soc.* **2007**, *129*, 9570–9571.
- [42] R. D. Dewhurst, E. C. Neeve, H. Braunschweig, T. B. Marder, *Chem. Commun.* **2015**, *51*,

- 9594–9607.
- [43] S. Pietsch, E. C. Neeve, D. C. Apperley, R. Bertermann, F. Mo, D. Qiu, M. S. Cheung, L. Dang, J. Wang, U. Radius, et al., *Chem. - A Eur. J.* **2015**, *21*, 7082–7098.
- [44] E. C. Neeve, S. J. Geier, I. A. I. Mkhalid, S. A. Westcott, T. B. Marder, *Chem. Rev.* **2016**, *116*, 9091–9161.
- [45] C. Sole, H. Gulyas, E. Fernandez, *Chem. Commun.* **2012**, *48*, 3769–3771.
- [46] C. Pubill-Ulldemolins, A. Bonet, H. Gulyas, C. Bo, E. Fernandez, *Org. Biomol. Chem.* **2012**, *10*, 9677–9682.
- [47] X. Sanz, G. M. Lee, C. Pubill-Ulldemolins, A. Bonet, H. Gulyas, S. A. Westcott, C. Bo, E. Fernandez, *Org. Biomol. Chem.* **2013**, *11*, 7004–7010.
- [48] J. Cid, J. J. Carbó, E. Fernández, *Chem. - A Eur. J.* **2014**, *20*, 3616–3620.
- [49] N. Miralles, J. Cid, A. B. Cuenca, J. J. Carbó, E. Fernández, *Chem. Commun.* **2015**, *51*, 1693–1696.
- [50] M. Gao, S. B. Thorpe, W. L. Santos, *Org. Lett.* **2009**, *11*, 3478–3481.
- [51] S. B. Thorpe, X. Guo, W. L. Santos, *Chem. Commun.* **2011**, *47*, 424–426.
- [52] M. Gao, S. B. Thorpe, C. Kleeberg, C. Sleboznick, T. B. Marder, W. L. Santos, *J. Org. Chem.* **2011**, *76*, 3997–4007.
- [53] L. Dang, Z. Lin, T. B. Marder, *Organometallics* **2008**, *27*, 4443–4454.
- [54] H. Ito, H. Yamanaka, J. Tateiwa, A. Hosomi, *Tetrahedron Lett.* **2000**, *41*, 6821–6825.
- [55] K. Takahashi, T. Ishiyama, N. Miyaura, *Chem. Lett.* **2000**, *29*, 982–983.
- [56] K. Takahashi, T. Ishiyama, N. Miyaura, *J. Organomet. Chem.* **2001**, *625*, 47–53.
- [57] S. Onozawa, M. Tanaka, *Organometallics* **2001**, *20*, 2956–2958.
- [58] D. S. Laitar, P. Müller, J. P. Sadighi, *J. Am. Chem. Soc.* **2005**, *127*, 17196–17197.
- [59] S. Li, J. Cheng, Y. Chen, M. Nishiura, Z. Hou, *Angew. Chemie Int. Ed.* **2011**, *50*, 6360–6363.
- [60] R. T. Baker, J. C. Calabrese, S. A. Westcott, P. Nguyen, T. B. Marder, *J. Am. Chem. Soc.* **1993**, *115*, 4367–4368.
- [61] J. S. Merola, J. R. Knorr, *J. Organomet. Chem.* **2014**, *750*, 86–97.
- [62] J. Zhu, Z. Lin, T. B. Marder, *Inorg. Chem.* **2005**, *44*, 9384–9390.
- [63] M. Mantina, A. C. Chamberlin, R. Valero, C. J. Cramer, D. G. Truhlar, *J. Phys. Chem. A* **2009**, *113*, 5806–5812.
- [64] M. Y. Wang, L. Cheng, Z. J. Wu, *J. Comput. Chem.* **2008**, *29*, 1825–1839.
- [65] M. S. Cheung, T. B. Marder, Z. Lin, *Organometallics* **2011**, *30*, 3018–3028.
- [66] M. Alcarazo, S. J. Roseblade, A. R. Cowley, R. Fernández, J. M. Brown, J. M. Lassaletta, *J. Am. Chem. Soc.* **2005**, *127*, 3290–3291.
- [67] M. Alcarazo, T. Stork, A. Anoop, W. Thiel, A. Fürstner, *Angew. Chemie Int. Ed.* **2010**, *49*, 2542–2546.
- [68] T. Terabayashi, T. Kajiwara, M. Yamashita, K. Nozaki, *J. Am. Chem. Soc.* **2009**, *131*, 14162–14163.
- [69] A. V Protchenko, L. M. A. Saleh, D. Vidovic, D. Dange, C. Jones, P. Mountford, S. Aldridge, *Chem. Commun.* **2010**, *46*, 8546–8548.
- [70] T. Kajiwara, T. Terabayashi, M. Yamashita, K. Nozaki, *Angew. Chemie Int. Ed.* **2008**, *47*, 6606–6610.

- [71] J. Zheng, Y. Wang, Z. H. Li, H. Wang, *Chem. Commun.* **2015**, *51*, 5505–5508.
- [72] K. Lee, A. R. Zhugralin, A. H. Hoveyda, *J. Am. Chem. Soc.* **2010**, *132*, 12766.
- [73] Eugenia Aldeco-Perez, A. J. Rosenthal, B. Donnadiou, P. Pattiyil, G. Frenking, G. Bertrand, *Science (80-)*. **2009**, *326*, 556–559.
- [74] M. Melaimi, M. Soleilhavoup, G. Bertrand, *Angew. Chemie - Int. Ed.* **2010**, *49*, 8810–8849.
- [75] Y. Katsuma, H. Asakawa, M. Yamashita, *Chem. Sci.* **2018**, *9*, 1301–1310.
- [76] A. Moezzi, M. M. Olmstead, R. A. Bartlett, P. P. Power, *Organometallics* **1992**, *11*, 2383–2388.
- [77] H. Hommer, H. Noth, J. Knizek, W. Ponikwar, H. Schwenk-Kircher, *Eur. J. Inorg. Chem.* **1998**, 1519–1527.
- [78] H. Asakawa, K.-H. Lee, Z. Lin, M. Yamashita, *Nat. Commun.* **2014**, *5*, 4245.
- [79] C. Kojima, K.-H. Lee, Z. Lin, M. Yamashita, *J. Am. Chem. Soc.* **2016**, *138*, 6662–6669.
- [80] P. Nguyen, G. Lesley, N. J. Taylor, T. B. Marder, N. L. Pickett, W. Clegg, M. R. J. Elsegood, N. C. Norman, *Inorg. Chem.* **1994**, *33*, 4623–4624.
- [81] F. J. Lawlor, N. C. Norman, N. L. Pickett, E. G. Robins, P. Nguyen, G. Lesley, T. B. Marder, J. A. Ashmore, J. C. Green, *Inorg. Chem.* **1998**, *37*, 5282–5288.
- [82] W. Clegg, M. R. J. Elsegood, F. J. Lawlor, N. C. Norman, N. L. Pickett, E. G. Robins, A. J. Scott, P. Nguyen, N. J. Taylor, T. B. Marder, *Inorg. Chem.* **1998**, *37*, 5289–5293.
- [83] A. Verma, R. F. Snead, Y. Dai, C. Slebodnick, Y. Yang, H. Yu, F. Yao, W. L. Santos, *Angew. Chemie Int. Ed.* **2017**, *56*, 5111–5115.
- [84] K. Nozaki, Y. Aramaki, M. Yamashita, S.-H. Ueng, M. Malacria, E. Lacôte, D. P. Curran, *J. Am. Chem. Soc.* **2010**, *132*, 11449–11451.
- [85] X. Sanz, C. M. Vogels, A. Decken, C. Bo, S. A. Westcott, E. Fernandez, *Chem. Commun.* **2014**, *50*, 8420–8423.
- [86] M. G. Civit, X. Sanz, C. M. Vogels, J. D. Webb, S. J. Geier, A. Decken, C. Bo, S. A. Westcott, E. Fernández, *J. Org. Chem.* **2015**, *80*, 2148–2154.
- [87] M. Kaaz, J. Bender, D. Forster, W. Frey, M. Nieger, D. Gudat, *Dalt. Trans.* **2014**, *43*, 680–689.
- [88] R. H. Cragg, M. F. Lappert, B. P. Tilley, *J. Chem. Soc.* **1964**, 2108–2115.
- [89] R. Jefferson, M. F. Lappert, B. Prokai, B. P. Tilley, *J. Chem. Soc. A Inorganic, Phys. Theor.* **1966**, 1584–1590.
- [90] P. Schreyer, P. Paetzold, R. Boese, *Chem. Berichte-Recueil* **1988**, *121*, 195–205.
- [91] B. Singaram, *Heteroat. Chem.* **1992**, *3*, 245–249.
- [92] C. Solé, E. Fernández, *Angew. Chemie Int. Ed.* **2013**, *52*, 11351–11355.
- [93] M. J. Frisch, G. W. Trucks, H. B. Schlegel, G. E. Scuseria, M. A. Robb, J. R. Cheeseman, G. Scalmani, V. Barone, B. Mennucci, G. A. Petersson, H. Nakatsuji, M. Caricato, X. Li, H. P. Hratchian, A. F. Izmaylov, J. Bloino, G. Zheng, J. L. Sonnenberg, M. Hada, M. Ehara, K. Toyota, R. Fukuda, J. Hasegawa, M. Ishida, T. Nakajima, Y. Honda, O. Kitao, H. Nakai, T. Vreven, J. A. Montgomery, Jr., J. E. Peralta, F. Ogliaro, M. Bearpark, J. J. Heyd, E. Brothers, K. N. Kudin, V. N. Staroverov, R. Kobayashi, J. Normand, K. Raghavachari, A. Rendell, J. C. Burant, S. S. Iyengar, J. Tomasi, M. Cossi, N. Rega, J. M. Millam, M. Klene, J. E. Knox, J. B. Cross, V. Bakken, C. Adamo, J. Jaramillo, R. Gomperts, R. E. Stratmann, O. Yazyev, A. J.

- Austin, R. Cammi, C. Pomelli, J. W. Ochterski, R. L. Martin, K. Morokuma, V. G. Zakrzewski, G. A. Voth, P. Salvador, J. J. Dannenberg, S. Dapprich, A. D. Daniels, O. Farkas, J. B. Foresman, J. V. Ortiz, J. Cioslowski, D. J. Fox, *Gaussian 09, Revis. A.02*, Gaussian, Inc., Wallingford CT **2009**.
- [94] R. G. Parr, W. Yang, *Density-Functional Theory of Atoms and Molecules*, Oxford University Press, **1994**.
- [95] C. Lee, W. Yang, R. G. Parr, *Phys. Rev. B* **1988**, *37*, 785–789.
- [96] A. D. Becke, *J. Chem. Phys.* **1993**, *98*, 5648–5652.
- [97] P. J. Stephens, F. J. Devlin, C. F. Chabalowski, M. J. Frisch, *J. Phys. Chem.* **1994**, *98*, 11623–11627.
- [98] P. J. Hay, W. R. Wadt, *J. Chem. Phys.* **1985**, *82*, 299–310.
- [99] A. Höllwarth, M. Böhme, S. Dapprich, A. W. Ehlers, A. Gobbi, V. Jonas, K. F. Köhler, R. Stegmann, A. Veldkamp, G. Frenking, *Chem. Phys. Lett.* **1993**, *208*, 237–240.
- [100] A. W. Ehlers, M. Böhme, S. Dapprich, A. Gobbi, A. Höllwarth, V. Jonas, K. F. Köhler, R. Stegmann, A. Veldkamp, G. Frenking, *Chem. Phys. Lett.* **1993**, *208*, 111–114.
- [101] M. M. Francl, W. J. Pietro, W. J. Hehre, J. S. Binkley, M. S. Gordon, D. J. DeFrees, J. A. Pople, *J. Chem. Phys.* **1982**, *77*, 3654–3665.
- [102] W. J. Hehre, R. Ditchfield, J. A. Pople, *J. Chem. Phys.* **1972**, *56*, 2257–2261.
- [103] P. C. Hariharan, J. A. Pople, *Theor. Chim. Acta* **1973**, *28*, 213–222.
- [104] A. E. Reed, L. A. Curtiss, F. Weinhold, *Chem. Rev.* **1988**, *88*, 899–926.
- [105] P. Geladi, B. R. Kowalski, *Anal. Chim. Acta* **1986**, *185*, 1–17.
- [106] S. Wold, M. Sjöström, L. Eriksson, *Chemom. Intell. Lab. Syst.* **2001**, *58*, 109–130.
- [107] D. M. Hawkins, S. C. Basak, D. Mills, *J. Chem. Inf. Comput. Sci.* **2003**, *43*, 579–586.

Unconventional reaction mechanisms of trivalent boron compounds: *gem* and *anti* additions



Human progress has always been driven by a sense of adventure and unconventional thinking.

— Andréi Geim —

It is better to fail in originality than to succeed in imitation.

— Herman Melville —

UNIVERSITAT ROVIRA I VIRGILI
COMPUTATIONAL MODELING TO EXPLORE UNCONVENTIONAL REACTIVITY PATTERNS IN C-H ACTIVATION
AND BORON CHEMISTRY
Diego García López

Outline

Organoboron compounds are among the most versatile compounds in organic synthesis owing to their utility for the construction of carbon-carbon and carbon-heteroatom bonds. Regarding the addition of diboron compounds to unsaturated bonds of organic molecules in a metal-free context the outcome mostly results in a *syn* 1,2-difunctionalization, although routes to perform 1,1-additions or *anti* 1,2-additions selectively are beginning to appear. Concerning boron-interelement reagents, the reactivity might offer a wider scope *via* push-pull effect. This phenomena enhances the nucleophilic character to the heteroatom attached to the boryl moiety, previously activated by a Lewis base, to render the attack to an electrophilic carbon.

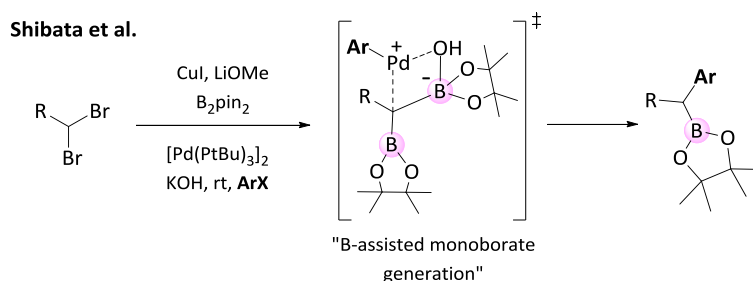
In collaboration with the experimental group of Dr. Elena Fernández, this part is focussed on mechanistic studies of two unconventional, transition-metal free reactions involving trivalent boryl species as reagents: (i) the unsymmetrical 1,1-diboration of diazo compounds, formed *in situ* from aldehydes and cyclic and non-cyclic ketones, and (ii) the stereoselective *anti*-addition of selenoboranes to α,β -acetylenic esters and ynamides. In the first case (Chapter 7), the heterolytic cleavage of the mixed diboron reagent, Bpin–Bdan, and the formation of two geminal C–Bpin and C–Bdan bonds was rationalised based on DFT calculations to occur *via* a concerted yet asynchronous mechanism. Diastereoselection is attained on substituted cyclohexanones and such computational studies provide understanding on the origin of the selectivity. We also studied the observed alkoxide-assisted, selective deborylation of Bpin from multisubstituted sp^3 -carbon *via* generation of a Bdan stabilized carbanion that easily conducts to a selective protodeboration sequence. In the second case (Chapter 8), theoretical calculations rationalized the observed regio- and stereoselectivity of the *anti*-3,4-selenoboration of α,β -acetylenic esters and ynamides using catalytic amounts of PCy₃. Interestingly, in the absence of phosphine the selenoboration switched from the formation of α -vinyl selenides to β -vinyl selenides. The computational study discovered a novel mechanism which differs from previous mechanistic proposals for analogous *anti*-selective carboration, silaboration and diboration. The phosphine adds to the β position of the alkynoate switching the polarity of the triple bond and favoring the 1,3-selenoboration which produces the α -addition of selenyl group. Then, the autocatalytic action of a second selenoborane reagent, which coordinates to the phosphorus ylide intermediate, determines the stereoselectivity and completes the catalytic process.

UNIVERSITAT ROVIRA I VIRGILI
COMPUTATIONAL MODELING TO EXPLORE UNCONVENTIONAL REACTIVITY PATTERNS IN C-H ACTIVATION
AND BORON CHEMISTRY
Diego García López

7. Geminal-additions of unsymmetrical diboranes to ketones and aldehydes

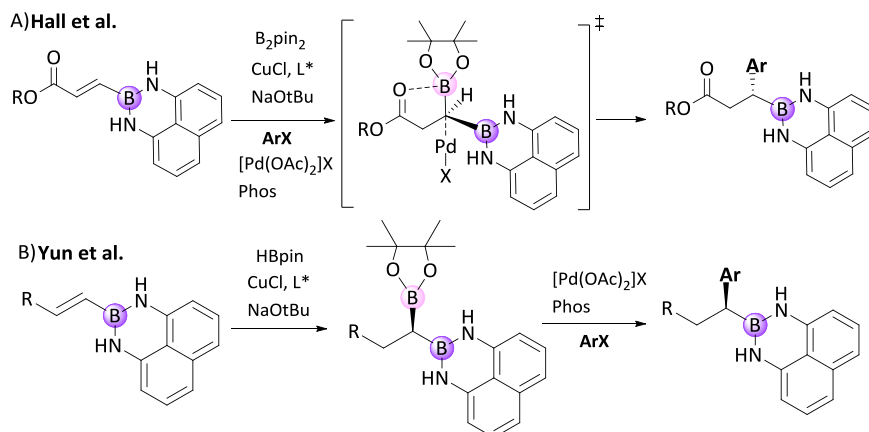
7.1. Introduction

1,1-Diborylalkanes are attracting the attention of synthetic researchers since Shibata and co-workers demonstrated in 2010 that two consecutive Suzuki–Miyaura cross-coupling (SMC) reactions can be performed in a chemo and regioselective manner, even at room temperature.^[1–3] This new concept, based on the protection-free selective cross-coupling on a multisubstituted sp^3 -carbon, succeeded by virtue of the adjacent B atom in 1,1-diborylalkanes (Scheme 7.1). When chiral ligands modify the Pd complex, the reaction can take place through a stereochemical-determining transmetalation with inversion of configuration at carbon.^[4,5] The accomplishment of a second cross-coupling reaction guarantees the formation of unsymmetrical diarylated compounds from simple 1,1-dibromoalkanes.^[6,7]



Scheme 7.1. Protection-free cross-coupling on a multisubstituted sp^3 -carbon.

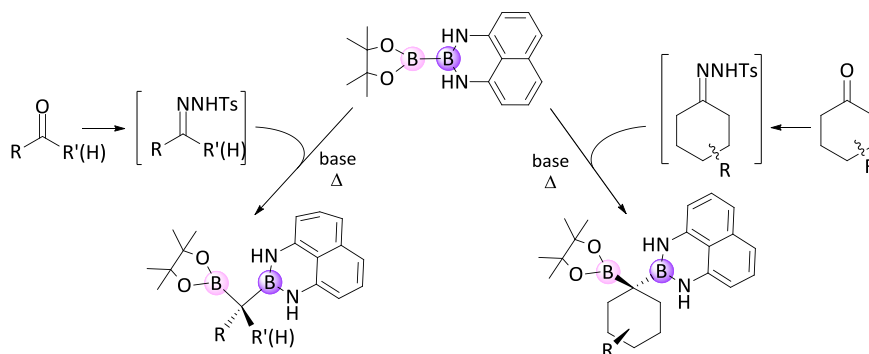
The unsymmetrical formation of 1,1-diborylalkane compounds has been elegantly performed by the groups of Hall^[8] and Yun,^[9] through copper mediated asymmetric borylation of β -boronylacrylates (Scheme 7.2A) and asymmetric hydroboration of borylalkenes (Scheme 7.2B), respectively. Both strategies share the fact that the substrate already contains the C–B_{dan} functionality (B_{dan} = 1,8-naphthalenediaminoboryl) and the B_{pin} moiety (B_{pin} = pinacolboryl) is stereoselectively introduced using a copper catalyst modified with a chiral ligand. Interestingly, although in both cases the enantioselection is transferred along the Suzuki–Miyaura cross-coupling^[10] (via the trifluoroborate salt), the configuration is inverted for β , β' -diborylacrylates and retained for 1,1'-diborylalkanes.



Scheme 7.2. Copper mediated unsymmetrical step wise formation of 1,1-diborylalkane compounds and further functionalization.

To complete the picture of the synthesis and application of 1,1-diborylalkane compounds,^[11–22] two parallel strategies have proved their efficiency in formal 1,1-diboration with a symmetrical B–B bond: (a) Pt-catalysed diborylation of diazoalkanes with Bpin–Bpin^[23–25] and (b) metal-free carbon insertion of *N*-tosylhydrazones into Bpin–Bpin.^[26,27]

Inspired by the last strategy, the experimental group of Dr. Elena Fernández studied the heterolytic B–B bond cleavage, from the Bpin–Bdan diboron reagent, employing *N*-tosylhydrazones derived from aldehydes and ketones. In particular, for *N*-tosylhydrazones derived from cyclic ketones, they looked at the potential of diastereoselection when employing diazo precursors possessing diastereotopic π faces (Scheme 7.3). Our goal is then elucidating, by means of DFT calculations, a plausible mechanism for the 1,1-diboration of Bpin–Bdan as well as the diastereoselective preferences, together with a prediction of the functionalization of the Bpin unit.



Scheme 7.3. Metal-free carbon insertion of *N*-tosylhydrazones into Bpin–Bdan.

7.2. Experimental background

Initially, hydrocinnamaldehyde (**1**) was reacted with *N*-tosylhydrazine. After isolation and recrystallization of the corresponding tosylhydrazone (**2**), the sodium salt of the tosylhydrazone was generated in situ by treatment with NaH (1.2 eq.) at room temperature (rt). After 1 h, at this temperature, 1.2 eq. of Bpin–Bdan was added and the reaction was heated to promote the formation of the diazo intermediate and the subsequent formal carbon insertion in the unsymmetrical B–B bond. Upon workup, the target 1,1-diborylalkane compound (**3**) was isolated in 71% yield (Table 7.1, entry 1). Interestingly, when *N*-tosylhydrazone **2** was used without purification, the final 1,1-diborylalkane product **3** was isolated in a comparable isolated yield, 75% (Table 7.1, entry 2). Encouraged by this promising streamlined 1,1-diboration with an unsymmetrical diboron reagent, then a series of aldehydes were transformed into 1,1-diborylalkane compounds following this one-pot insertion strategy. The aliphatic aldehydes were converted into the desired products in comparable good yields (Table 7.1, entries 3-6). Particularly noteworthy was the conversion of substrates **4** and **6** featuring an increased steric bulkiness around the C α . Extension of the 1,1-diboration protocol to ketones, such as benzylacetone (**12**) and 2-hexanone (**14**) resulted in a diminished reactivity towards the corresponding 1,1-diborylalkanes **13** and **15**, respectively, most probably due to the steric hindrance.

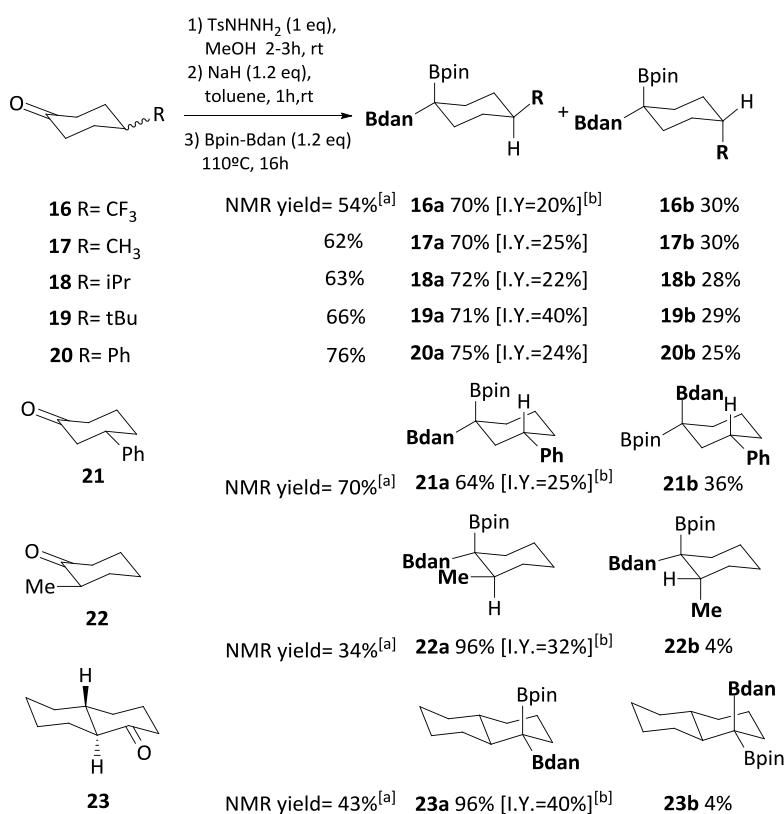
With the aim of exploring the diastereoselection in the multisubstituted sp³-carbon formed, a series of cyclic ketones were selected to in situ generate the diazo compound and promote the insertion into the Bpin–Bdan molecule. Interestingly, when 4-(trifluoromethyl)cyclohexanone (**16**) was subjected to the diboration protocol, the corresponding insertion took place in a diastereoselective manner and compound **16a** was obtained as a major diastereoisomer in a (70/30) proportion (Scheme 7.4). A similar diastereoselection has been observed for the 1,1-diboration of 4-methyl-, 4-tert-butyl-, 4-isopropyl-, and 4-phenylcyclohexanones with a major diastereomeric ratio observed for **20a/20b** (75/25) (Scheme 7.4). Diastereoisomers **16a-20a** could be isolated in a pure form. Through the X-ray analysis of suitable single crystals of **16a** (Figure 7.1, left) the diequatorial (*trans*) position of the Bdan fragment and the CF₃ group was unequivocally established. There is only one precedent in the literature that reports the 1,1-diboration of 4-Phcyclohexanone (**20**) with B₂pin₂, with comparable yields but, logically, without diastereoselection due to the symmetry of the diboron reagent.^[27]

Table 1. 1,1-Diboration of aldehydes and ketones with Bpin-Bdan, via *N*-tosylhydrazones/diazo intermediates formation.^[a]

Entry	Substrate	Product	NMR Yield (%) ^[b]	Isolated Yield (%) ^[c]
1			75	71
2		“ “	81	75
3			68	49
4			83	71
5			82	73
6			95	77
7			55	43
8			44	27

^[a]Reaction conditions for *N*-tosylhydrazone formation: substrate (0.25 mmol), TsNHNH₂ (0.25 mmol), MeOH, 2-3 h, rt; for hydrazine sodium salt formation: NaH (1.2 eq.), 1 h, rt; for diazoalkane generation and insertion: BpinBdan (1.2 eq.), 110 °C, 16 h. ^[b]Yield calculated by NMR spectroscopy with ferrocene as the internal standard. ^[c]Isolated yield calculated based on the aldehyde or ketone substrate.

When the 1,1-diboration of 3-Ph-cyclohexanone (**21**) with Bpin–Bdan was conducted, the diastereomeric ratio 64/36 was in favor of the stereoisomer **21a** with Bdan and Ph in *cis* relative configuration (Scheme 7.4). The 2-Ph-cyclohexanone did not undergo any insertion reaction, likely due to steric hindrance. Interestingly, the analogue 2-Me-cyclohexanone (**22**) did react with Bpin–Bdan providing the highest stereoselection of 96/4 in favor of the diastereomer with Bdan and Ph in a *trans* configuration (Scheme 7.4). As a proof of concept, trans-1-decalone (**23**) was selected to be transformed into the corresponding diazo compound and explore its insertion into the Bpin–Bdan molecule. The new multisubstituted sp³-carbon was formed with moderate yield but outstanding diastereoselectivity, towards the isomer with the Bdan moiety in the equatorial position **23a** (Figure 7.1, right).



Scheme 7.4. 1,1-Diboration of substituted cyclohexanones and trans-decalone. ^[a]Yield determined by NMR spectroscopy with ferrocene as the internal standard. ^[b]Isolated yield based on the ketone.

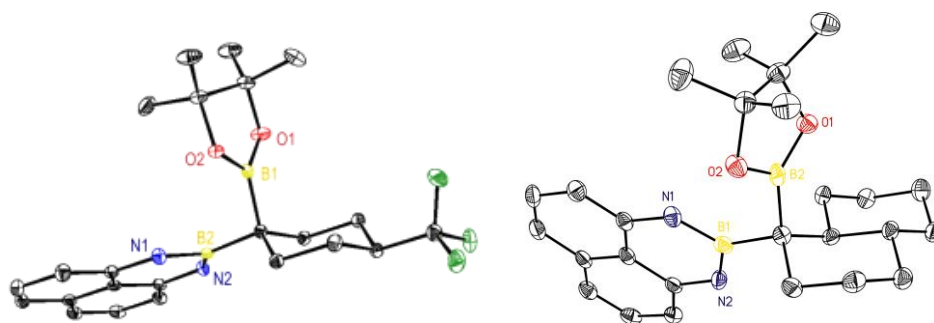
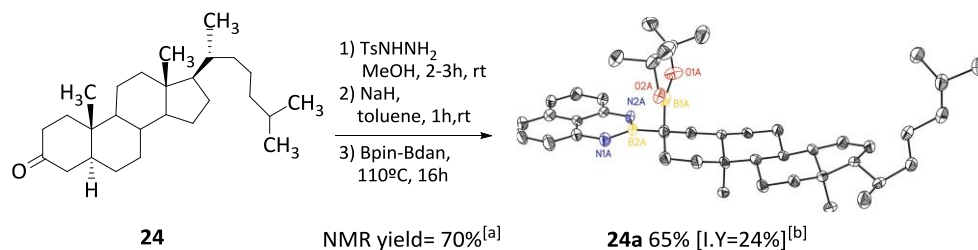


Figure 7.1. X-ray structure determination of major isomers **16a** (left) and **23a** (right).

Taking advantage of the potential diastereoselection on this new metal-free 1,1-diboration of cyclic ketones, the bioactive compound 5- α -cholestan-3-one (**24**) was selected to transform its carbonyl functional group into a chiral multisubstituted sp^3 -carbon in a one-pot protocol. Scheme 7.5 illustrates the formation of the chiral *gem*-diborated product in 70% yield with a diastereomeric ratio 65/35, with the Bdan unit located in the equatorial position and Bpin in the axial position, as the preferred isomer.



Scheme 7.5. 1,1-Diboration of 5- α -cholestan-3-one (**24**) and X-Ray structural determination for major isomer **24a**.

Furthermore, the next goal was to establish a selective C–Bpin functionalization from the enriched diastereoselective *gem*-diborated products. It has been recently described that the alkoxide-assisted deborylation and generation of a boron-stabilized carbanion, from 1,1-bis(pinacolboronate)esters, allow the reactivity with alkyl halides.^[28] Thus, the exclusive diastereoisomer **22a** was efficiently protodeboronated into the corresponding *trans*-**25(H)** (Figure 7.2) in the presence of 5 eq. KO^tBu at room temperature. Similarly, the protodeboronation on the diastereomeric mixture of **17a/17b** (carried out at 0 °C in the presence of 3 eq. of KO^tBu) and **21a/21b** was conducted to afford principally the *trans*-**26(H)** and *cis*-**27(H)**, respectively (Figure 7.2). This is a new approach towards the diastereoselective C–H bond formation, which complements other efficient protodeboronations on tertiary

diarylalkyl boronic esters or tertiary aryldialkyl boronic esters, with CsF·H₂O or TBAF·3H₂O, respectively.^[29]

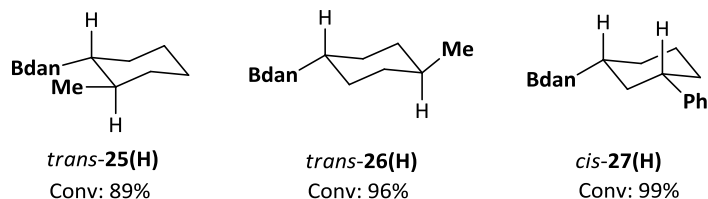
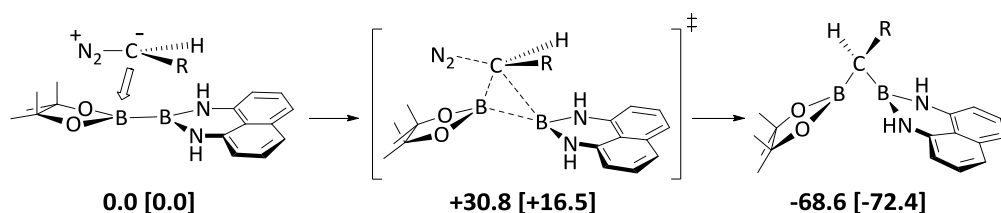


Figure 7.2. Alkoxide-assisted protodeboronation process

7.3. Results and discussion

A plausible mechanistic pathway was elucidated by DFT calculations using Bpin–Bdan and CH₃(H)CN₂ as model diazoalkane. The outcome of these calculations is summarized in Scheme 7.6. We were able to locate a transition state for the formation of the two carbon–boron bonds that indicate the occurrence of a concerted, yet asynchronous mechanism with a free energy barrier of 30.8 kcal·mol⁻¹ (Figure 7.3). As the nucleophilic diazo carbon attacks at the electron deficient boron of the Bpin moiety, the 1,2-boron migration of the Bdan moiety occurs to yield the 1,1-diboron intermediate and concomitant release of the dinitrogen. A similar mechanism has been postulated for the metal-free insertion of diazoalkanes into HBpin, Me₂PhSi–Bpin and Bpin–Bpin.^[26,27]



Scheme 7.6. Proposed mechanism for diazo compound type insertion of CH₃(H)CN₂ into Bpin–Bdan. Calculated free energies (and electronic energies in brackets) in kcal·mol⁻¹.

In those cases, the authors proposed a process that may initiate with the formation of a Lewis acid-base interaction between the diazoalkanes and the Bpin moiety, prior to the 1,2-migration of the H, Me₂PhSi, or Bpin fragment. To further analyze the diboron addition and the possible formation of a stable Lewis acid-base adduct, we performed a relaxed potential

surface scan along different values of the C–Bpin bond. Starting at the transition state, only in the free-energy curve, we could observe a very shallow minimum when the C–B distance was increased (at ~ 1.83 Å), and its estimated free energy barrier for dissociation was very low, ~ 1 kcal·mol⁻¹. Thus, we can conclude that the nucleophilic attack and the 1,2-boron migration occurs in a concerted but asynchronous manner.

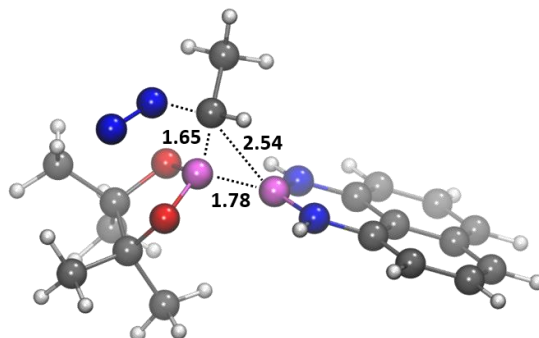


Figure 7.3. Molecular structure and main geometric parameters of the transition state for diazo compound type insertion into the Bpin–Bdan molecule. Distances in angstroms.

For comparison, we analyzed the diazoalkane insertion into symmetric Bpin–Bpin (Figure 7.4 and 7.5B), finding the same concerted, yet asynchronous, mechanism and a very similar free energy barrier (Figure 7.5). In the Bpin–Bdan, we have also characterized an analogous pathway in which the diazo carbon attacks at the other boron of the Bdan moiety (Figure 7.5A). As expected,^[30,31] the lower Lewis acidity of the Bdan fragment increases the energy barrier by ~ 2 kcal·mol⁻¹.

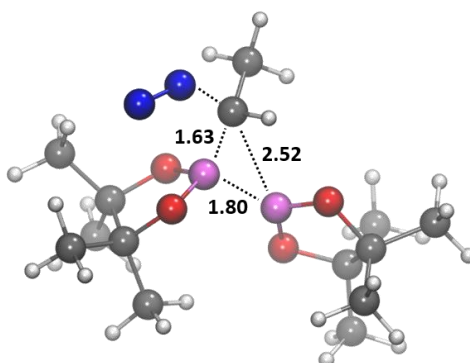


Figure 7.4. Molecular structure and main geometric parameters of the transition state for the diazoalkane insertion into the Bpin–Bpin molecule. Distances in angstroms.

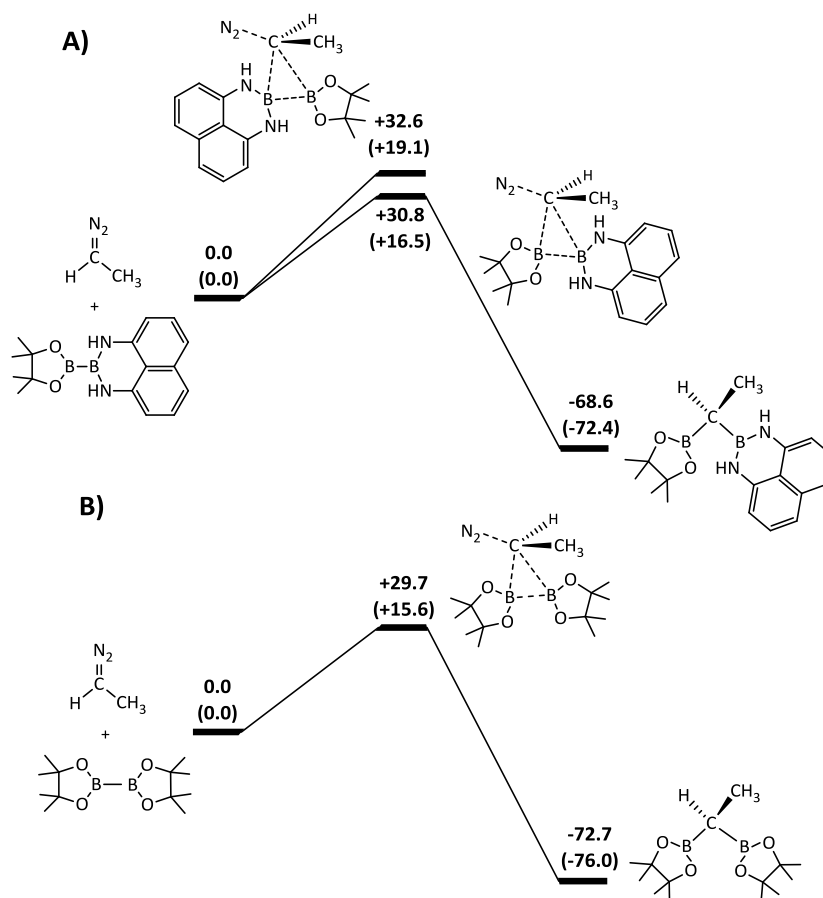
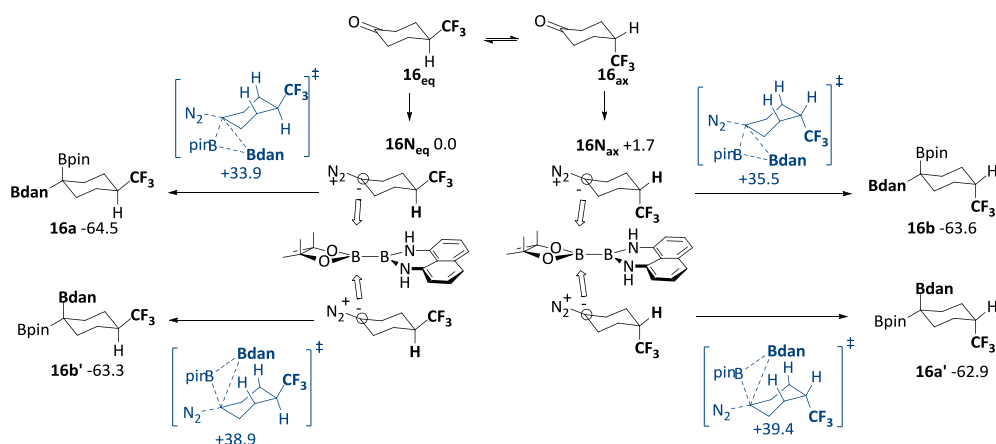


Figure 7.5. Calculated free-energy profiles for the diazo compound type insertion of CH₃(H)CN₂ into Bpin–Bdan (A) and Bpin–Bpin (B). Calculated free energies (and electronic energies in parenthesis) in kcal·mol⁻¹.

The DFT analysis of the origin of diastereoselective preferences is summarized in Scheme 7.7 and Scheme 7.8. For 4-(trifluoromethyl) cyclohexanone (**16**), we considered two possible chair conformations with the CF₃ substituent in the equatorial or axial position, being the equatorial conformer (**16N_{eq}**) 1.7 kcal·mol⁻¹ lower than the axial one (**16N_{ax}**). The more stable species **16N_{eq}** can attack at the Bpin–Bdan substrate through its two diastereofaces (Scheme 7.6, left) and the computed free energy barriers are 33.9 and 38.9 kcal·mol⁻¹. The latter path, leading the Bdan in the axial position (**16b'**) is higher in energy (~5 kcal·mol⁻¹) due to the destabilizing 1,3-diaxial interactions with a cyclohexane structure (see Scheme 7.7 and Figure 7.6). Thus, the computed lowest energy path conducts the experimentally obtained diastereoisomer with Bdan and CF₃ substituents in the equatorial position and *trans* to each other (**16a**, see the X-ray structure in Figure 7.1).



Scheme 7.7. Proposed diastereoisomeric pathways for the 1,1-diboration of 4-CF₃-cyclohexanone with Bpin-Bdan. Relative Gibbs free energies in kcal·mol⁻¹. X-Ray structural determination for major product **16a**.

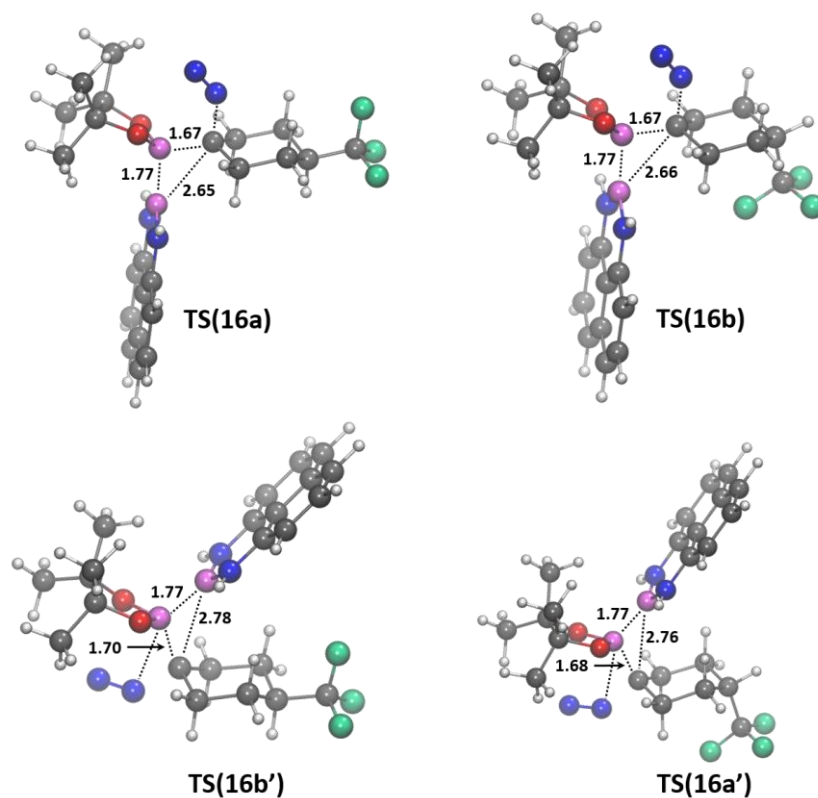
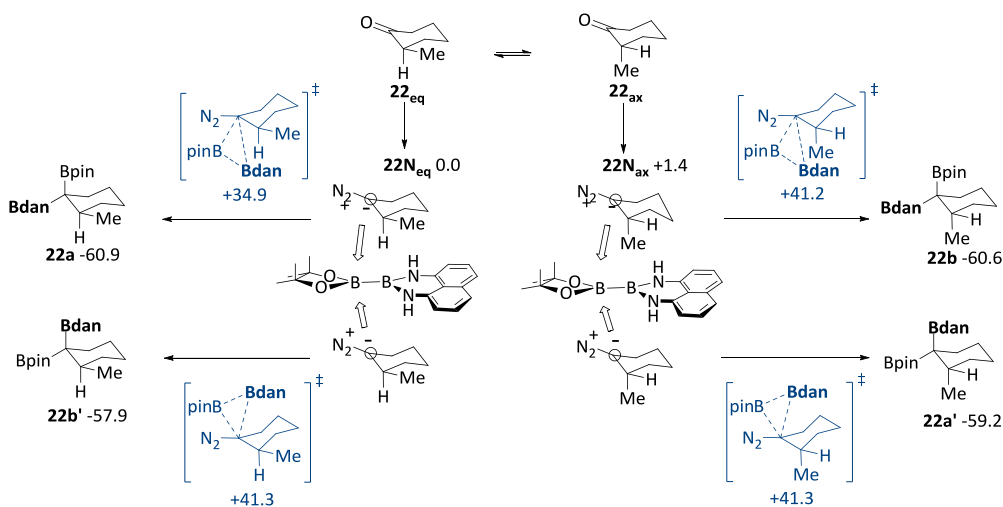


Figure 7.6. Molecular structure and main geometric parameters (in Å) of the transition states structures for all possible diastereoisomeric paths in 1,1-diboration of 4-CF₃-cyclohexanone.

Starting at the diazo conformer with an axial CF₃ (**16N_{ax}** in Scheme 7.7, right), we observed similar free energy barriers to those from **16N_{eq}**, 33.8 and 37.7 kcal·mol⁻¹ for Bdan addition in equatorial (**16b**) and axial positions (**16a'**), respectively. This indicates that the substituent in the para position has little influence on the reaction center. However, the axial CF₃ shifts up the energy of both paths and the approach of Bdan through the less hindered equatorial channel (**16b**) becomes 1-2 kcal·mol⁻¹ higher than the path conducting to **16a**. Since the energy difference is not too large, we expect a non-negligible formation of diastereoisomer **16b** with Bdan and CF₃ substituents in *cis* that agrees with the observed diastereoisomeric ratio 70/30.



Scheme 7.8. Proposed diastereoisomeric pathways for the 1,1-diboration of 2-Me-cyclohexanone with Bpin-Bdan. Relative Gibbs free energies in kcal·mol⁻¹.

For 2-Me-cyclohexanone (**22**) the DFT analysis of the diastereoisomerism shows a similar pattern to **16** (Scheme 7.8), but bringing the substituent from the para to the ortho position has a direct influence on the reaction center. Thus, the path leading to the minor diastereoisomer (**22b**) is destabilized by the *cis*-1,2 interactions of Bdan and methyl substituents in ~5 kcal·mol⁻¹ (Figure 7.7), resulting in a significant increase of diastereoselectivity for *ortho*-substituted cyclohexanones.

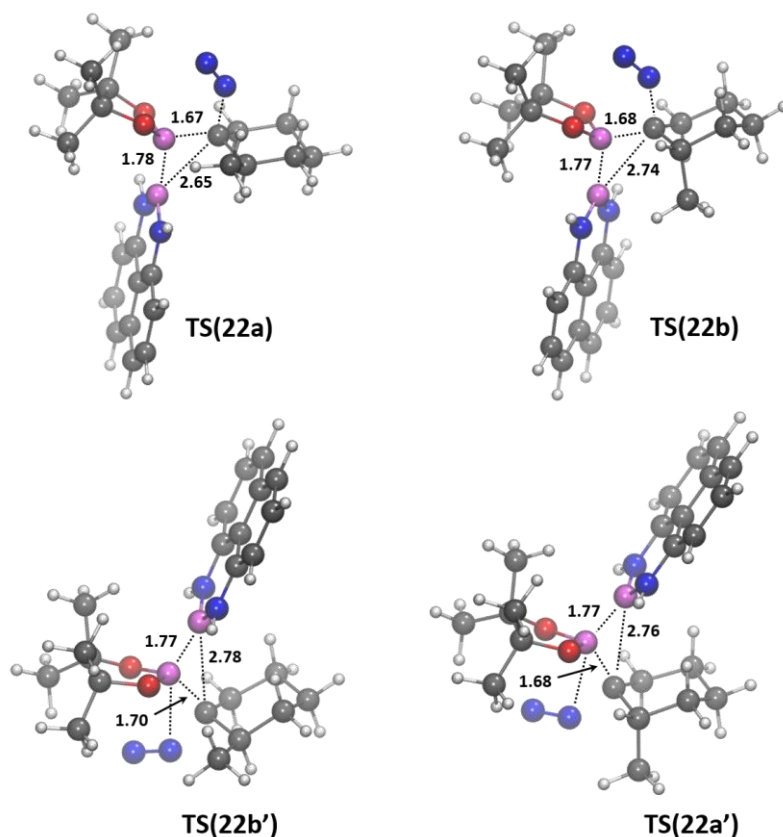


Figure 7.7. Molecular structure and main geometric parameters (in Å) of the transition states structures for all diastereoisomeric possible paths in 1,1-diboration of 2-Me-cyclohexanone.

Concerning the protodeboronation process, we analyzed computationally the reactivity of 1,1-diborylalkanes with alkoxides using $\text{CH}_3(\text{H})\text{C}(\text{Bpin})(\text{Bdan})$ and MeO^- as model substrates (Scheme 7.9). As determined previously,^[30,31] the methoxy group interacts preferentially with the Bpin moiety forming a stable Lewis acid-base adduct. From this adduct, the deborylation to give the carbanion occurs with a moderate free energy barrier ($21.9 \text{ kcal}\cdot\text{mol}^{-1}$). Moreover, the stabilization of the carbanion using the α -Bdan moiety is reflected in the HOMO orbital, which shows strong delocalization of the carbanion p-type electron density into the π -channel of the Bdan moiety (Figure 7.8, left). Analogously, the Bdan could be also activated but the reaction path is shifted up in energy by $\sim 4 \text{ kcal}\cdot\text{mol}^{-1}$, and the resulting α -(pinacolato)boronate carbanion is less stable than the α -(1,8-naphthalenediaminato)boronate by $12.3 \text{ kcal}\cdot\text{mol}^{-1}$. According to NBO analysis, the Bpin fragment supports a less negative charge ($-0.14e$) than the Bdan fragment ($-0.21e$), as inferred from the corresponding HOMO orbitals (Figure 7.8). Thus, selective functionalization of the Bpin position is expected.

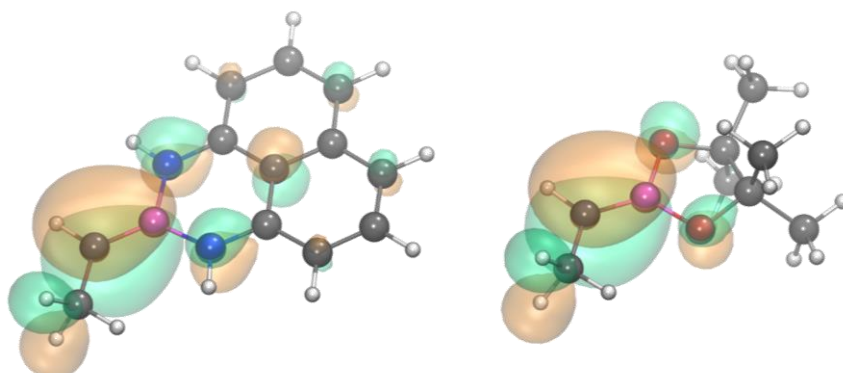
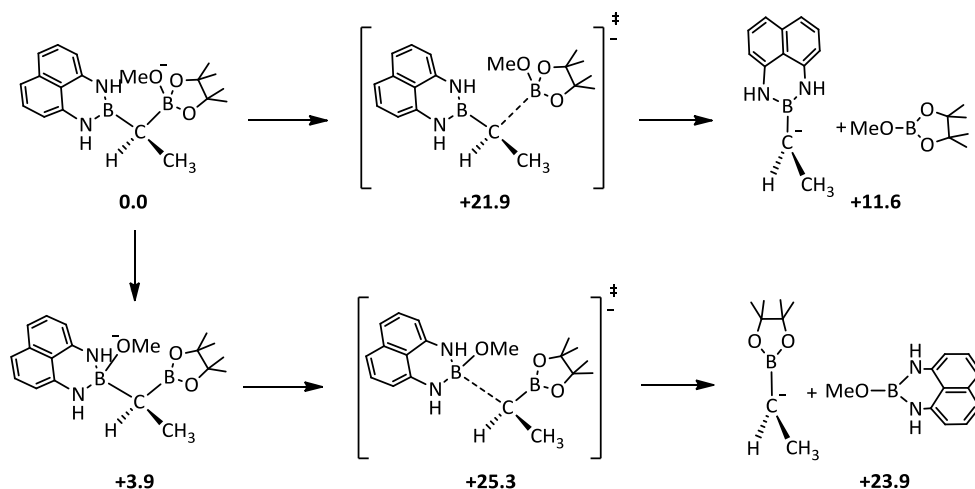


Figure 7.8. Representation of HOMO orbitals, formally corresponding to carbanion lone pair, for α -(1,8-naphthalenediaminato)boronate anion (left) and α -(pinacolato)boronate (right).

7.4. Computational details

All calculations were carried out employing Gaussian09 series of programs.^[32] Full quantum mechanical calculations on model systems were performed within the framework of density functional theory (DFT)^[33] by using the B3LYP functional.^[34–36] All the atoms were represented

by means of the 6-31G(d,p) basis set^[37,38] and geometry-optimizations were full, with no restrictions. Both minima and transition state structures were characterized with a frequency calculation, finding a unique negative frequency mode in the transition states geometries. The fragment charges of Bpin and Bdan carbenoids were analysed by using the NBO method.^[39]

7.5. Conclusions

The observed transition metal-free unsymmetrical 1,1-diboration of aldehydes and ketones by Bpin–Bdan has been analyzed by DFT calculations. In the proposed mechanism, the addition occurs in a concerted, yet asynchronous manner. The distereoselectivity observed in *ortho*-substituted cyclohexanones can also be predicted and interpreted with computational modeling. The combination of repulsive 1,3-diaxial and 1,2-*cis* interactions with the diboron reagent is the key factor determining such diastereoselectivity. Finally, the subsequent and selective deboration of the Bpin group achieved *via* protodeboration in the presence of bases can be rationalized since Frontier Molecular Orbital analysis show that the Bdan moiety stabilize better the transient carbanion species.

7.6. References

- [1] K. Endo, T. Ohkubo, M. Hirokami, T. Shibata, *J. Am. Chem. Soc.* **2010**, *132*, 11033–11035.
- [2] K. Endo, T. Ohkubo, T. Shibata, *Org. Lett.* **2011**, *13*, 3368–3371.
- [3] K. Endo, T. Ohkubo, T. Ishioka, T. Shibata, *J. Org. Chem.* **2012**, *77*, 4826–4831.
- [4] C. Sun, B. Potter, J. P. Morken, *J. Am. Chem. Soc.* **2014**, *136*, 6534–6537.
- [5] B. Potter, A. A. Szymaniak, E. K. Edelstein, J. P. Morken, *J. Am. Chem. Soc.* **2014**, *136*, 17918–17921.
- [6] K. Endo, T. Ishioka, T. Ohkubo, T. Shibata, *J. Org. Chem.* **2012**, *77*, 7223–7231.
- [7] S. H. Cho, J. F. Hartwig, *Chem. Sci.* **2014**, *5*, 694–698.
- [8] J. C. H. Lee, R. McDonald, D. G. Hall, *Nat Chem* **2011**, *3*, 894–899.
- [9] X. Feng, H. Jeon, J. Yun, *Angew. Chemie Int. Ed.* **2013**, *52*, 3989–3992.
- [10] A. J. J. Lennox, G. C. Lloyd-Jones, *Chem. Soc. Rev.* **2014**, *43*, 412–443.
- [11] H. C. Brown, G. Zweifel, *J. Am. Chem. Soc.* **1961**, *83*, 3834–3840.
- [12] P. Binger, R. Köster, *Angew. Chemie* **1962**, *74*, 652.
- [13] D. S. Matteson, J. G. Shdo, *J. Org. Chem.* **1964**, *29*, 2742–2746.

- [14] G. Cainelli, G. Dal Bello, G. Zubiani, *Tetrahedron Lett.* **1965**, *6*, 3429–3432.
- [15] G. Zweifel, H. Arzoumanian, *Tetrahedron Lett.* **1966**, *7*, 2535–2538.
- [16] D. S. Matteson, J. R. Thomas, *J. Organomet. Chem.* **1970**, *24*, 263–271.
- [17] H. C. Brown, E. Negishi, P. L. Burke, *J. Am. Chem. Soc.* **1972**, *94*, 3561–3567.
- [18] R. C. Larock, *J. Organomet. Chem.* **1973**, *61*, 27–31.
- [19] H. C. Brown, C. G. Secuten, R. Liotta, *J. Am. Chem. Soc.* **1979**, *101*, 96–99.
- [20] D. S. Matteson, R. J. Moody, *Organometallics* **1982**, *1*, 20–28.
- [21] R. Soundararajan, D. S. Matteson, *Organometallics* **1995**, *14*, 4157–4166.
- [22] H. Li, Y. Zhang, J. Wang, *Synthesis* **2013**, *45*, 3090–3098.
- [23] H. Abu Ali, I. Goldberg, M. Srebnik, *Organometallics* **2001**, *20*, 3962–3965.
- [24] H. Abu Ali, I. Goldberg, D. Kaufmann, C. Burmeister, M. Srebnik, *Organometallics* **2002**, *21*, 1870–1876.
- [25] A. J. Wommack, J. S. Kingsbury, *Tetrahedron Lett.* **2014**, *55*, 3163–3166.
- [26] H. Li, L. Wang, Y. Zhang, J. Wang, *Angew. Chemie Int. Ed.* **2012**, *51*, 2943–2946.
- [27] H. Li, X. Shanguan, Z. Zhang, S. Huang, Y. Zhang, J. Wang, *Org. Lett.* **2014**, *16*, 448–451.
- [28] K. Hong, X. Liu, J. P. Morken, *J. Am. Chem. Soc.* **2014**, *136*, 10581–10584.
- [29] S. Nave, R. P. Sonawane, T. G. Elford, V. K. Aggarwal, *J. Am. Chem. Soc.* **2010**, *132*, 17096–17098.
- [30] J. Cid, J. J. Carbó, E. Fernández, *Chem. - A Eur. J.* **2014**, *20*, 3616–3620.
- [31] N. Miralles, J. Cid, A. B. Cuenca, J. J. Carbo, E. Fernandez, *Chem. Commun.* **2015**, *51*, 1693–1696.
- [32] M. J. Frisch, G. W. Trucks, H. B. Schlegel, G. E. Scuseria, M. A. Robb, J. R. Cheeseman, G. Scalmani, V. Barone, B. Mennucci, G. A. Petersson, H. Nakatsuji, M. Caricato, X. Li, H. P. Hratchian, A. F. Izmaylov, J. Bloino, G. Zheng, J. L. Sonnenberg, M. Hada, M. Ehara, K. Toyota, R. Fukuda, J. Hasegawa, M. Ishida, T. Nakajima, Y. Honda, O. Kitao, H. Nakai, T. Vreven, J. A. Montgomery, Jr., J. E. Peralta, F. Ogliaro, M. Bearpark, J. J. Heyd, E. Brothers, K. N. Kudin, V. N. Staroverov, R. Kobayashi, J. Normand, K. Raghavachari, A. Rendell, J. C. Burant, S. S. Iyengar, J. Tomasi, M. Cossi, N. Rega, J. M. Millam, M. Klene, J. E. Knox, J. B. Cross, V. Bakken, C. Adamo, J. Jaramillo, R. Gomperts, R. E. Stratmann, O. Yazyev, A. J. Austin, R. Cammi, C. Pomelli, J. W. Ochterski, R. L. Martin, K. Morokuma, V. G. Zakrzewski, G. A. Voth, P. Salvador, J. J. Dannenberg, S. Dapprich, A. D. Daniels, O. Farkas, J. B. Foresman, J. V. Ortiz, J. Cioslowski, D. J. Fox, *Gaussian 09, Revis. A.02, Gaussian, Inc., Wallingford CT* **2009**.
- [33] R. G. Parr, W. Yang, *Density-Functional Theory of Atoms and Molecules*, Oxford University Press, **1994**.
- [34] C. Lee, W. Yang, R. G. Parr, *Phys. Rev. B* **1988**, *37*, 785–789.
- [35] A. D. Becke, *J. Chem. Phys.* **1993**, *98*, 5648–5652.
- [36] P. J. Stephens, F. J. Devlin, C. F. Chabalowski, M. J. Frisch, *J. Phys. Chem.* **1994**, *98*, 11623–11627.
- [37] M. M. Francl, W. J. Pietro, W. J. Hehre, J. S. Binkley, M. S. Gordon, D. J. DeFrees, J. A. Pople, *J. Chem. Phys.* **1982**, *77*, 3654–3665.

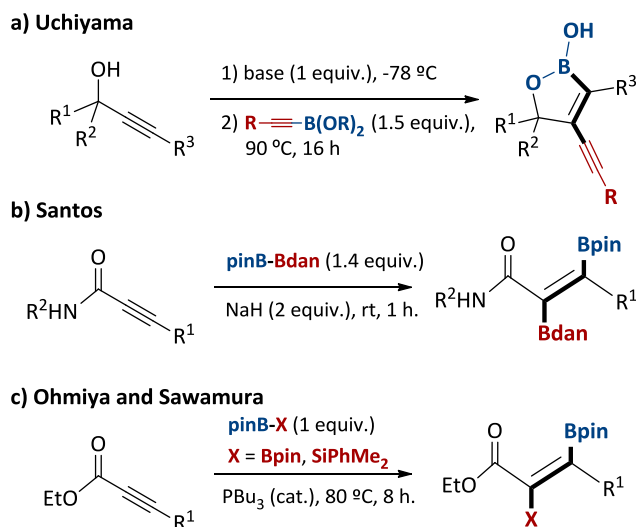
- [38] W. J. Hehre, R. Ditchfield, J. A. Pople, *J. Chem. Phys.* **1972**, *56*, 2257–2261.
[39] A. E. Reed, L. A. Curtiss, F. Weinhold, *Chem. Rev.* **1988**, *88*, 899–926.

8. Unraveling the mechanism of selenoborane *anti*-addition to alkynes

8.1. Introduction

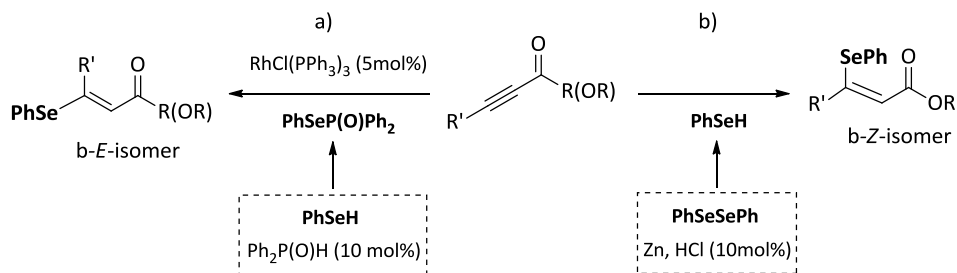
The reactivity of diboron reagents and B-interelement systems with organic molecules has become an important source of selective functionalization.^[1] The addition of these reagents to C–C triple bonds provides an attractive method for the regio- and stereoselective synthesis of functionalized alkenes *via* the formation of C–B and C–interelement bonds. Much effort has been devoted to transition metal catalysis, which generally generate 1,2-*cis*-addition products selectively.^[2] However, some outstanding examples of stereoselective *trans*-hydroboration of terminal and internal alkynes were achieved by copper^[3] and ruthenium^[4] catalysts, respectively. Also, Miyaura *et al.* developed the hydroboration of terminal alkynes by Rh and Ir complexes leading to *Z*-alkenyl boranes selectivity^[5] that occurred *via gem*-addition of B–H bond through a vinylidene intermediate.^[6,7]

In recent years several transition metal-free approaches have appeared that obtain *anti* addition products using special substrates or introducing directing groups (Scheme 8.1).^[1] Uchiyama *et al.* utilized propargyl alcohol substrates to provide access to the selective *anti*-diboration^[8] and *anti*-alkynylboration^[9] of the triple bond through the intramolecular reaction of an alkoxide and selective delivery of the nucleophilic boryl unit (Scheme 8.1a). DFT calculations proposed a mechanism involving deprotonation of propargylic alcohols by ⁿBuLi, coordination of the resulting alkoxide to activate the B–X bond, stereoselective migration of the boron or allynyl group and the Li to form the *anti*-alkenyllithium intermediate, and final intramolecular capture of the boron atom.^[8,9] Santos *et al.* reported the substrate-assisted *anti*-diboration of alkynamides using strong bases which deprotonates the amide group (Scheme 8.1b).^[10] The DFT-derived mechanism indicates that the generated alkoxide activates the diboron reagent intramolecularly resulting in α -addition of one boron, similar to that found for propargyl alcohols, and then a rapid carbon-carbon bond rotation leads to the thermodynamically favored *anti* product.^[10] Alternatively, Sawamura *et al.* has achieved *anti*-selective carboration,^[11] silaboration, and diboration^[12] of alkynoates using catalytic amounts of PBu₃ (Scheme 8.1c). The proposed mechanism involves the rotation of an enolate *double* bond as the key step for selectivity-determining, although in this case, it was not supported by computational studies.^[11] The comparison of Sawamura's reactions with those of Uchiyama and Santos suggests that in the absence of acidic protons alkynoates can be activated by basic phosphines instead of Brønsted bases to produce the alkoxy group, which in turns activates the boron reagent.



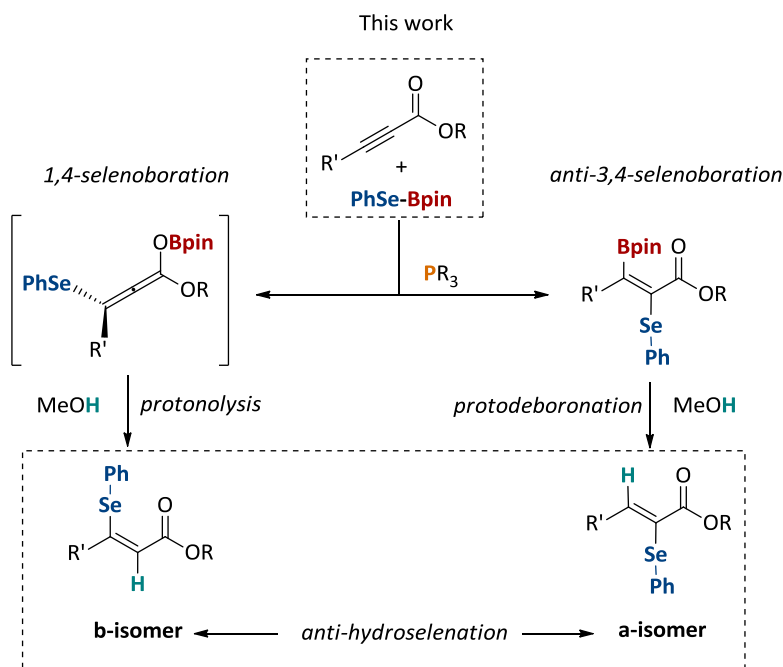
Scheme 8.1. Stereoselective transition metal-free anti addition of diboron and B–interelements reagents to activated alkynes.

Among the potential applications of B–interelement additions to alkynes, processes for the selective synthesis of vinyl selenides, which are important biological scaffolds, are challenging targets.^[13–15] The β -vinyl selenides can be obtained from α,β -acetylenic esters and ynones by means of rhodium-catalyzed *syn*-hydroselenation to generate principally β -*E*-vinyl selenides (Scheme 8.2a)^[16] or *via anti*-addition of organoselenols, formed *in situ* from the corresponding diselenides and Zn in acidic media, to provide the β -*Z*-vinyl selenides (Scheme 8.2b).^[17–22] Alternatively phenylselenoborane^[23] can efficiently be added to alkenes,^[24] in a transition-metal-free context, taking advantage of the “push-pull” effect of B in the B–interelement reagent.^[1] In a previous work, it was proved that stereodefined *Z*-alkenylselenides can be directly formed through the Lewis acid interaction of the carbonyl unit from ynones and the Bpin moiety on PhSe–Bpin, throughout 1,4-selenoborated intermediates.^[25]



Scheme 8.2. Regioselective transition metal-free synthesis of α - and β -seleniated α,β -unsaturated esters.

Herein we aim to understand the mechanism of the transition metal-free addition of boron-interelement systems to alkynoates catalyzed by phosphines in collaboration with the experimental group of Dr. Fernández. To this end, the experimental selenoboration work to electron-deficient α,β -acetylenic esters was extended by adding catalytic amount of phosphine, as in Sawamura's reports.^[12] It came across a stereodivergent synthesis of β -vinyl selenides and α -vinyl selenides, depending on the mode of activation of the phenylselenoborane (Scheme 8.3). These experimental observations were used to perform detailed DFT study of the reaction mechanism, including the understanding of the role of the heteroelement nature.



Scheme 8.3. *Syn*- and *anti*-hydroselelenation towards β -vinyl selenides.

8.2. Experimental background

The β -selenation of α,β -acetylenic esters with representative substrates that combines aryl and alkyl groups in the β -position, as well as sterically differentiated esters groups, was carried out. Table 8.1 shows the moderate to high conversions observed for all the substrates tested, and in particular for methyl-2-nonenato (**Z-9**) (Table 8.1, entry 2), working at 50° C. Lower temperatures provided only small amount of desired products. The steric and electronic

changes introduced in the substrates did not influence significantly the 1,4-selenoboration followed by protonolysis towards the β -selenated α,β -unsaturated esters. The exclusive formation of the *Z*-isomer was confirmed by spectroscopic data and the full characterization of product **Z-8** by X-ray diffraction (Figure 8.1), and contrast with the *Z/E* mixture observed in the β -selenation of α,β -acetylenic ketones.^[25]

Table 8.1. β -Selenation of α,β -acetylenic esters, *via* 1,4-selenoboration.^[a]

Entry	Substrate	Product	NMR Yield (%) ^[b]	Isolated Yield (%)
1			82	74
2			90	79
3			89	78
4			75	72
5			88	69
6			89	76
7			75	68

^[a]Reaction conditions: α,β -acetylenic esters or ynamides (0.2 mmol), PhSe-Bpin (1.1 eq), MeOH (0.15 mL), at 50°C for 16h. ^[b]Yields were determined by ¹H NMR analysis of the crude reaction mixture with naphthalene as an internal standard, which was added after the reaction.

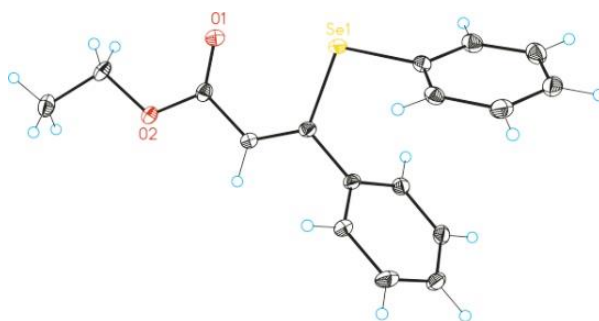


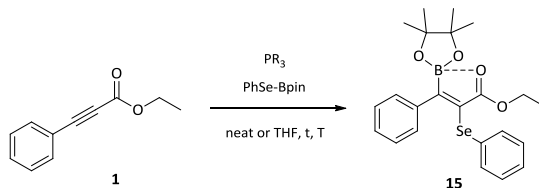
Figure 8.1. X-ray diffraction structure of product (*Z*)-3-phenyl-3-(phenylselanyl)acrylate (**Z-8**), confirming the *Z*-isomerism.

The study was extended to the β -selenation of ynamides 3-(4-methoxyphenyl)-*N,N*-dimethylpropiolamide (**6**) and 3-(4-methoxyphenyl)-1-(pyrrolidin-1-yl)prop-2-yn-1-one (**7**), and in both cases the conversion was comparable (Table 8.1, entries 6 and 7) to the β -selenation of α,β -acetylenic esters, proving the generality of the method despite the functional group.

In the next step, catalytic amounts of phosphine were introduced in order to switch the selenoboration of alkynoates and ynamides towards the formation of α -vinyl selenides with *anti* stereoselectivity, as Sawamura *et al.*^[12] observed for the diboration or silaboration of α,β -acetylenic esters with PBU_3 . The addition of 10 mol% of PBU_3 or PPh_3 did not convert substrate **1** into any selenated or borylated product, working at 50°C with 1.1 equiv. of PhSe-Bpin (Table 8.2, entries 1,2). However, the use of PCy_3 provided the formation of 61% (NMR yield) of a new product identified as the corresponding *anti*-3,4-addition product (Table 8.2, entry 3). The same NMR yield was observed working at room temperature (rt), for 8h, and using 1.5 eq of PhSe-Bpin up to 1.5 mol%, as the optimized reaction conditions (Table 8.2). Although the reaction works efficiently under neat conditions, the addition of 0.15 mL of THF was required to solubilize the Se-B reagent.

Product **15** was not able to be isolated as pure product from the reaction media, however, the transformation of substrates **3**, **4**, and **5** into the corresponding *anti*-3,4-selenoborated addition products **16**, **17** and **18** allowed their isolation (Scheme 8.4). The addition of the Bpin moiety at the β -position of the substrate is confirmed by NMR data and in particular by the interaction between the O from the carbonyl group and the B, with a shifted ^{11}B NMR signal to higher field (δ : 27-29 ppm). Two interesting points have to be addressed at this moment: *i*) while the addition of PhSe-Bpin takes place at room temperature, the addition of B_2pin_2 and $\text{PhMe}_2\text{Si-Bpin}$ requires up to 80°C; *ii*) while the addition of PhSe-Bpin involves PCy_3 as additive, the addition of B_2pin_2 and $\text{PhMe}_2\text{Si-Bpin}$ requires the most basic phosphine PBU_3 .

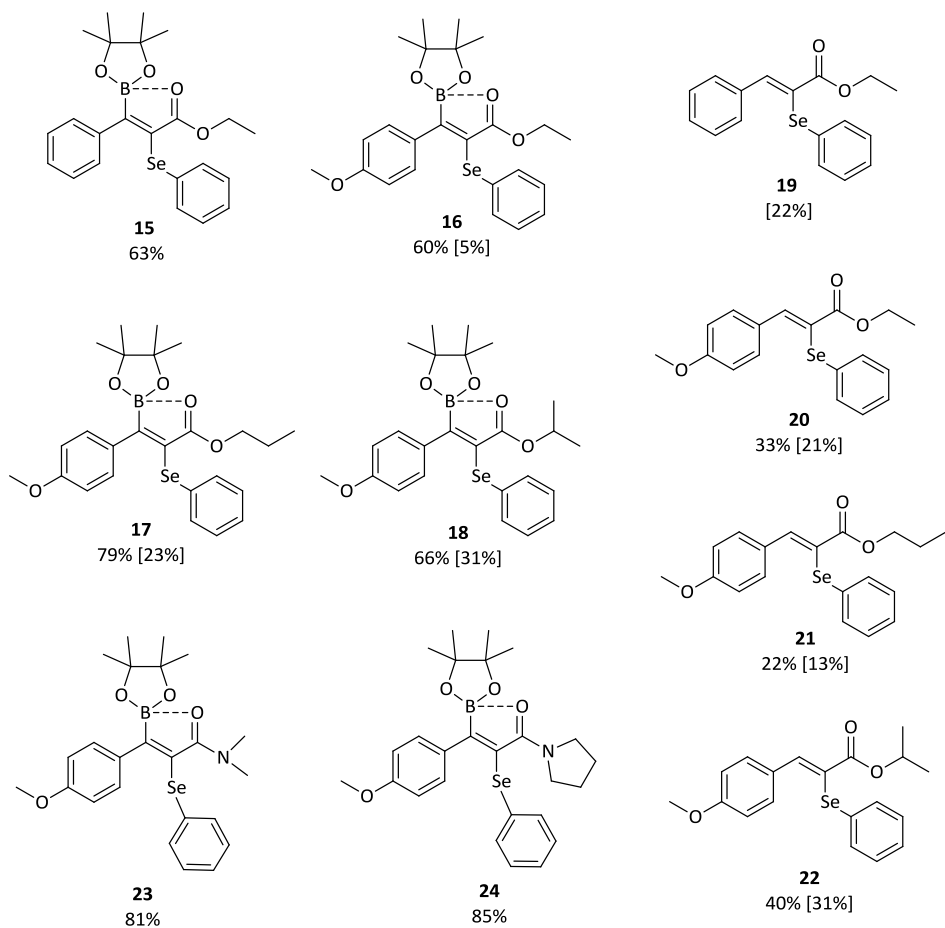
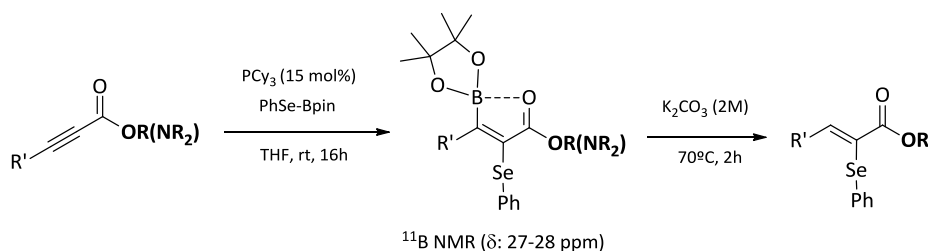
Table 8.2. Optimization of reactivity between of α,β -acetylenic esters, *via* 1,4-selenoboration.^[a]



Entry	PR ₃ (mol%)	PhSe–Bpin	T(°C)	t(h) / solv.	NMR yield (%) ^[b]
1	PBu ₃ (10mol%)	1.1 eq	50°C	16h / neat	-
2	PPh ₃ (10mol%)	1.1 eq	50°C	16h / neat	-
3	PCy ₃ (10mol%)	1.1 eq	50°C	16h / neat	61
4	PCy ₃ (10mol%)	1.1 eq	50°C	8h / neat	60
5	PCy ₃ (10mol%)	1.1 eq	rt	8h / neat	62
6	PCy ₃ (15mol%)	1.1 eq	rt	8h / neat	62
7	PCy ₃ (15mol%)	1.5 eq	rt	8h / THF	63
8	PCy ₃ (15mol%)	2.0 eq	rt	8h / THF	65

^[a]Reaction conditions: **1** (0.2 mmol), PhSe–Bpin, neat or THF (0.15 mL). ^[b]Yields were determined by ¹H NMR analysis of the crude reaction mixture with naphthalene as an internal standard, which was added after the reaction.

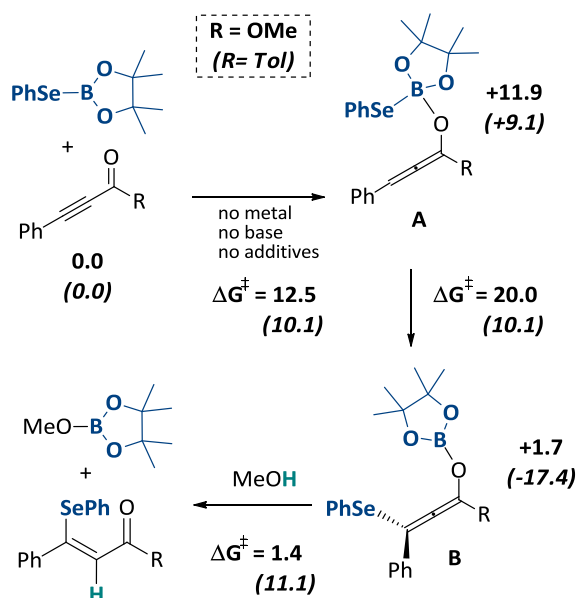
Any attempt to perform the 3,4-addition of PhSe–Bpin, B₂pin₂ and PhMe₂Si–Bpin to α,β -acetylenic ketones proved unsuccessful. The products derived from the *anti*-3,4-selenoboration were further transformed into the corresponding α -hydroselenated compounds, *via* protodeboronation process with K₂CO₃^[26] at 70°C, delivering compounds **19–22** in moderate values (Scheme 8.4), representing the first attempt to obtain those high valued products. Similarly, we conducted the same selenoboration to ynamides **6** and **7**, and although the *anti*-3,4-selenoborated products **23** and **24** were quantitatively determined by NMR yield, their isolation was not successfully accomplished.



Scheme 8.4. α -Selenation of α,β -acetylenic esters and ynamides *via anti*-3,4-selenoboration. Reaction conditions: α,β -acetylenic esters or ynamides (0.2 mmol), PhSe-Bpin (1.1 eq), PCy₃ (15 mol%), THF (0.15 mL), rt for 16h. Yields were determined by ¹H NMR analysis of the crude reaction mixture with naphthalene as an internal standard, which was added after the reaction. Isolated yield in brackets.

8.3. Results and discussion

The previously determined mechanism for the 1,4-selenoboration of ynones^[25] is illustrated in Scheme 8.5. The activation of the boron atom with the oxygen of the carbonyl group in a model substrate leading to intermediate **A**, enhances the nucleophilic attack of the –SePh moiety on the β carbon of the triple bond yielding the 1,4-selenoborated allene intermediate **B**, which in turn undergoes subsequent protonolysis with methanol. Before experimentation, we had analyzed computationally whether this process could be extended to α,β -acetylenic ester 1-(4-methylphenyl)-3-phenyl-2-propyn-1-one, although the ester functional group is expected to be less efficient than the ketone in activating the B–Se bond through the “push-pull” effect. To evaluate the feasibility of the reaction, we compared the potential free-energy profile for the α,β -acetylenic ester with that previously reported for α,β -acetylenic ketones at the same computational level^[25] (R = OMe vs. Tol in Scheme 8.5).

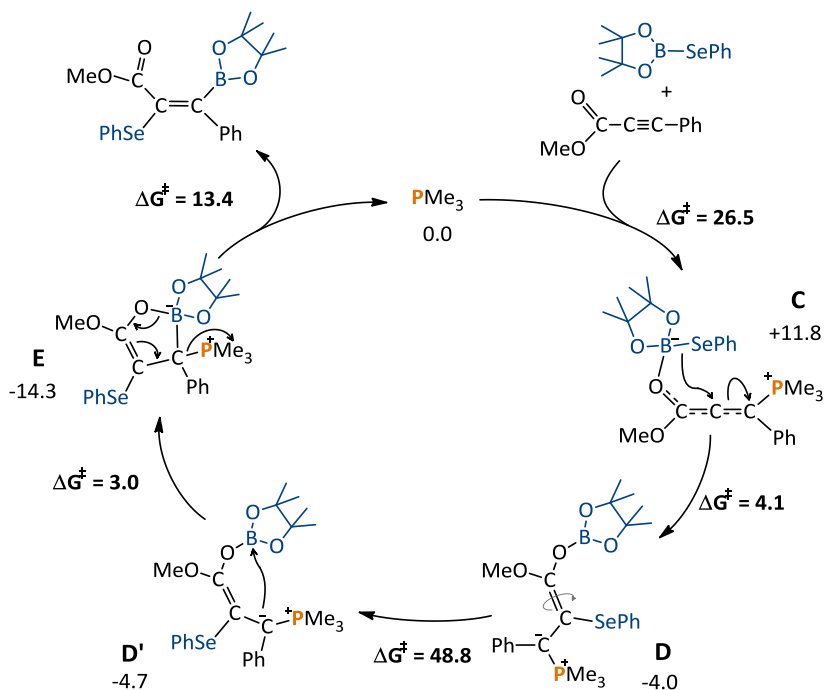


Scheme 8.5. Comparative of relative free-energies and barriers ($\text{kcal}\cdot\text{mol}^{-1}$) for reaction mechanism of β -selenation of α,β -unsaturated ester and ketone (in parenthesis, values taken from ref. [25]).

In the initial activation of the boron atom with the oxygen of the carbonyl group leading to intermediate **A**, the free-energy barrier and the relative energy of **A** are slightly higher (~ 2 $\text{kcal}\cdot\text{mol}^{-1}$) for the ester (R = OMe) than for the ketone (R = Tol). Nevertheless, the lesser activation ability of the ester group is mainly manifested on the nucleophilic attack of the SePh moiety on the β carbon of the triple bond yielding the 1,4-selenoborated intermediate **B**, for

which the energy barrier increases by 10 kcal·mol⁻¹. Finally, the computed free-energy barrier for the protonolysis of the resulting allene intermediate **B** inverts the trend, lowering by 10 kcal·mol⁻¹. Thus, although the overall computed free-energy barrier is relatively high (31.9 kcal·mol⁻¹, from the reactants to the transition state **TS_{A-B}**) for the α,β -acetylenic ester, the value is still feasible for a reaction occurring at the working temperature, 50°C; and therefore, there was enough theoretical support to attempt experimentally the reaction described in previous section.

In order to understand the mechanism of the *anti*-addition to alkynoates using catalytic amounts of phosphines and the switch-like behavior of selenoboration, we also carried out a systematic DFT study. We initially explored a catalytic cycle where the phosphine acts as a catalyst, based on previous mechanisms proposed by Sawamura *et al.*^[11,12] for *anti*-selective carboboration, silaboration and diboration (Scheme 8.6). The phosphine catalyst initiates the reaction by conjugative addition to the alkynoate with the assistance of the Lewis acidic boron, which activates the carbonyl group, yielding the zwitterionic allenolate intermediate **C**. Then, the terminal selenyl undergoes 1,3-migration to form the ylide intermediate **D**, in which the enolate double bond has to rotate (**D'**) to allow the attack of ylidic carbon to the boron atom and to reach the *anti*-stereochemistry. Finally, from the cyclic borate **E**, the B–O bond cleavages and the phosphine eliminates to yield the product.



Scheme 8.6. Possible mechanism for *anti*-3,4-addition of PhSe-Bpin to α,β -acetylenic ester adapted from the proposal for analogous *anti* selective carboboration, silaboration and diboration (ref. [11] and [12]). Relative free-energies and barriers in kcal·mol⁻¹.

We have computed the free-energy profile for the α -addition of PhSe-Bpin to the α,β -acetylenic ester 1-methyl-3-phenyl-2-propyn-1-one catalyzed by PMe_3 as model phosphine assuming a Sawamura-type mechanism. The main energy values are depicted in Scheme 8.6, and the details are provided in Figure 8.2.

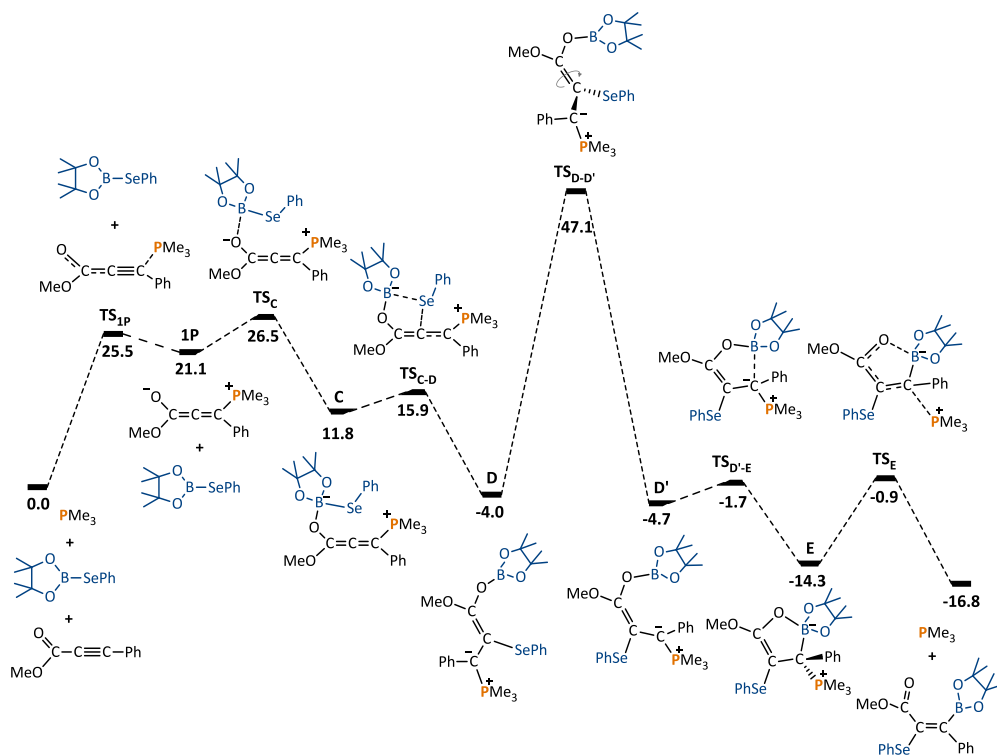


Figure 8.2. Computed Free Energy profile for Sawamura *et al.* (ref. [12]) proposed mechanism for *anti* 3,4-selenoboration of α,β -acetylenic ester. Energies in $\text{kcal}\cdot\text{mol}^{-1}$.

According to our calculations, the overall free-energy barrier for the formation of intermediate (**C**) is about $26.5 \text{ kcal}\cdot\text{mol}^{-1}$, which is mainly associated to the entropic cost of the two consecutive additions to the alkynoate. In intermediate **C**, the phosphine addition changes the polarity of the triple bond making α -position the most electrophilic, while boron coordination to the carbonyl oxygen activates selenium nucleophilicity *via* a “push-pull” effect.^[21,22] As a result, the 1,3-migration of the selenyl to produce **D** is computed to be a fast process with a low barrier, $4.1 \text{ kcal}\cdot\text{mol}^{-1}$. The formation of ylide intermediate **D** is thermodynamically favored, the structure laying $1.2 \text{ kcal}\cdot\text{mol}^{-1}$ below reactants. Then, in order to yield the observed stereoisomer, the bond between the carbonylic and the α -carbon should rotate 180° . However, the computed free-energy barrier for rotation is as high as $48.8 \text{ kcal}\cdot\text{mol}^{-1}$. The **D** species has the typical structure of α -stabilized phosphonium ylides,^[23] in which the P–C bond is covalent yet has significant polar interaction and its ylidic substituent

preserves the double bond character. Thus, the Sawamura-type mechanism is less likely for selenoboration due to the kinetic hindrance associated with carbon-carbon bond rotation.

There are two novel mechanistic proposals in the recent literature for related *anti* selective additions of boron compounds to alkynes. Nevertheless after close examination, none of them can be used to explain the results of selenoboration. According to the calculations by Santos *et al.*,^[10] the stereoselectivity of the transition-metal-free *anti*-diboration of alkylamides is due to a rapid carbon-carbon bond rotation process (Figure 8.3a), which is thermodynamically favored. However, in that case the use of strong bases deprotonates the original amide group generating an intermediate in which the rotating carbon-carbon bond has single bond character ($d_{C-C} = 1.49 \text{ \AA}$) instead of the double bond character in **D** ($d_{C-C} = 1.34 \text{ \AA}$). Alternatively, Zhang, Chung, Wu *et al.*^[27] characterized computationally the mechanism of *anti* selective hydroboration of alkyne catalyzed by Ru complexes, showing that the formation of a stable metallacyclopropene intermediate, after hydrogen migration to the alkyne, explains the selectivity (Figure 8.3c). Such an intermediate is not possible in our metal-free context. Thus, we propose a novel mechanism, in which the selenoborane auto-catalyzes the reaction.

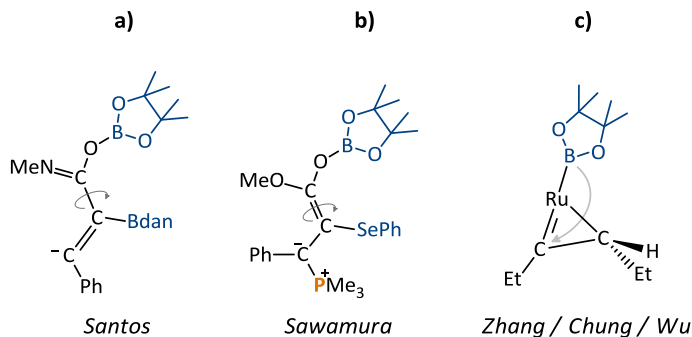
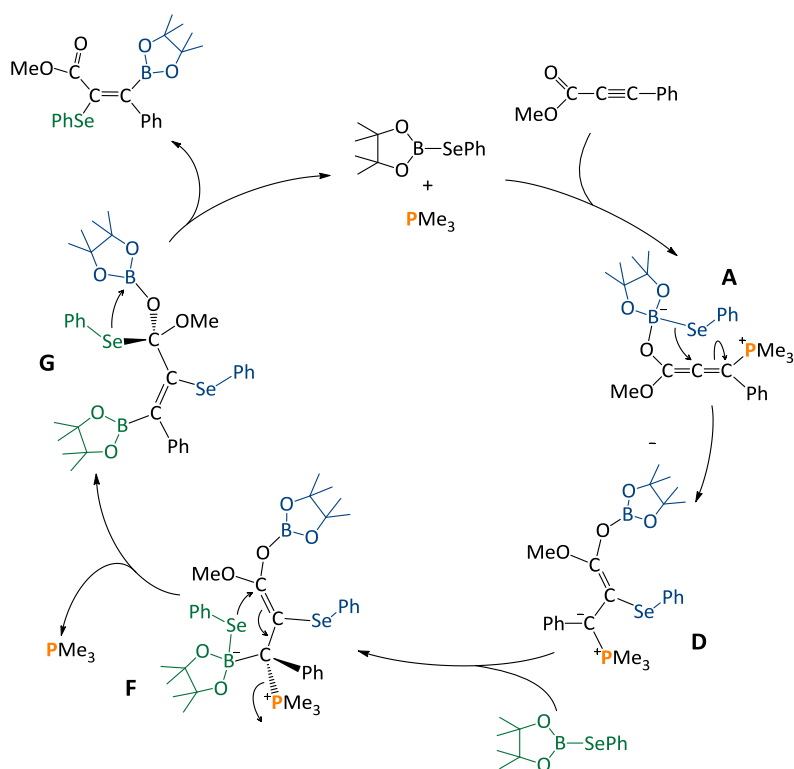


Figure 8.3. Comparison of key stereodetermining intermediates of different mechanistic proposals for *anti*-selective addition of borane compounds to alkynes.

The new mechanism is schematically presented in Scheme 8.7, while Figures 8.4 and 8.6 show the free-energy profile and the key intermediates and transition states, respectively. The first part of the mechanism is analogous to Sawamura's proposal. Then, once the intermediate **D** is formed, the catalytic process could be completed in three new steps: (i) the ylidic carbon of **D** acts as Lewis base and coordinates a second selenoborane molecule to yield intermediate **F**, (ii) the terminal selenyl undergoes 1,3 migration to stereoselectively form intermediate **G**, and (iii) the 1,2-elimination of PhSe–Bpin occurs at the carboxylic group to yield the final product and regenerate PhSe–Bpin species.



Scheme 8.7. Novel mechanistic proposal for *anti*-3,4-addition of PhSe–Bpin to α,β -acetylenic ester implying autocatalysis of one of the selenoborane substrate.

As shown in Figure 8.4, the coordination of the second PhSe–Bpin molecule to the ylidic carbon of **D** yielding intermediate **F** is somewhat endergonic ($+9.4 \text{ kcal}\cdot\text{mol}^{-1}$) and it has moderate free-energy barrier, $23.0 \text{ kcal}\cdot\text{mol}^{-1}$. Analogous to the first selenyl migration, the boron coordination enhances the nucleophilic character of $-\text{SePh}$ moiety *via* a “push-pull” effect and it promotes the selenyl 1,3-migration to the electrophic carboxylic carbon resulting in intermediate **G** and the concomitant release of the phosphine. Thus, the migration of the activated selenyl group has an accessible free energy barrier ($20.6 \text{ kcal}\cdot\text{mol}^{-1}$ from **F** to **TS_{F-G}**). This step is exergonic by $17.1 \text{ kcal}\cdot\text{mol}^{-1}$, laying the intermediate **G** $11.7 \text{ kcal}\cdot\text{mol}^{-1}$ below reactants.

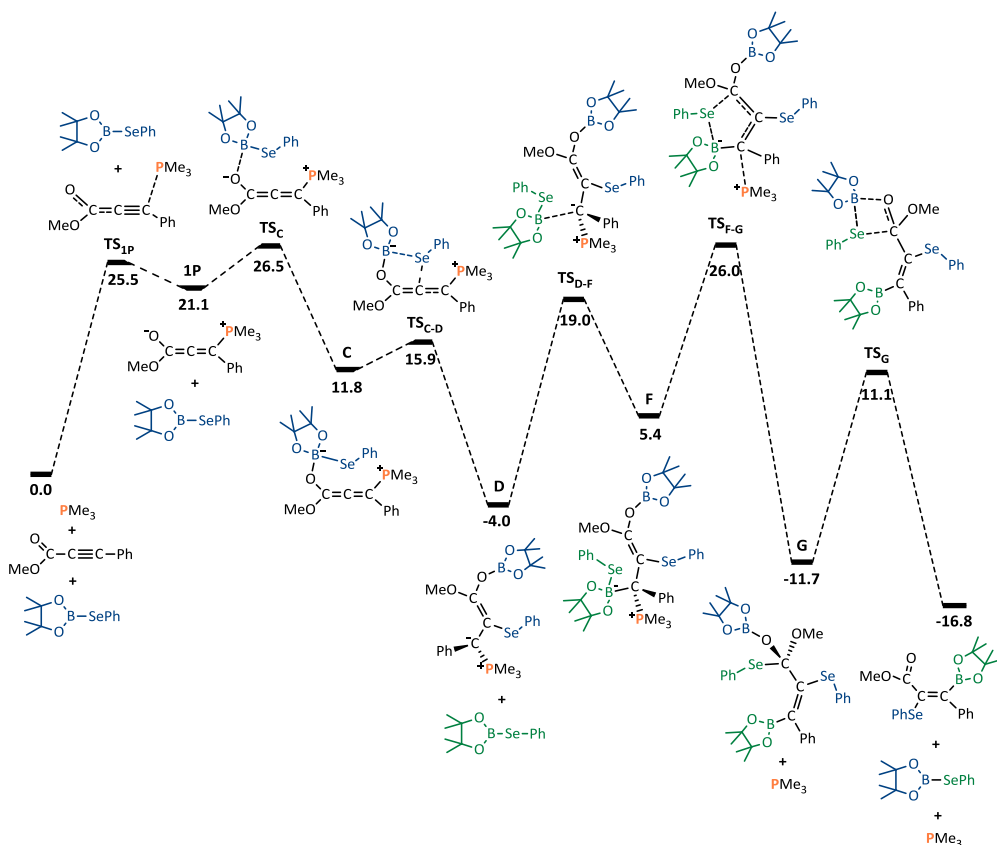


Figure 8.4. Free-energy profile (kcal·mol⁻¹) for the *anti*-3,4-addition of PhSe–Bpin to α,β -acetylenic ester *via* autocatalysis of selenoborane.

More interestingly, the overall reaction leads to the *anti*-addition of selenyl and boryl moieties to the triple bond of the substrate (see Figure 8.6). The stereoselectivity can be explained by analyzing the conformations of the species involved in the $F \rightarrow G$ transformation (see Figure 8.5). Note that several conformational and enantiomeric paths can be considered. As illustrated by Figure 8.5, to reach the transition state for the selenyl migration, TS_{F-G} , the PhSe–Bpin moiety coordinated to the ylidic carbon and the carboxylic group need to be *syn* to each other, forcing the initially added selenyl moiety (blue colored) and the subsequent added boryl moiety (green colored) to be *anti* to each other. Thus, although coordination of PhSe–Bpin through transition state TS_{D-F} can yield different conformers of **F** species, only those with *syn* carboxyl–PhSeBpin arrangement would be reactive, and consequently, the formation of products with *cis* arrangement of selenyl and boryl moieties is not possible (Figure 8.5). In this path, structure **F** results from conformational equilibria either before or after the attack of the second PhSe–Bpin molecule (bold arrows). We have found another conformational path for selenyl migration, $TS_{F'-G}$, but it lays higher in energy respect to reactants than TS_{F-G} by 2.8

(2.6) kcal·mol⁻¹ (dashed arrow). Finally, intermediate **G** undergoes 1,2-elimination of a PhSe-Bpin, which is built from the fragments of two different molecules of PhSe-Bpin yielding the *anti* 3,4-selenoborated product.

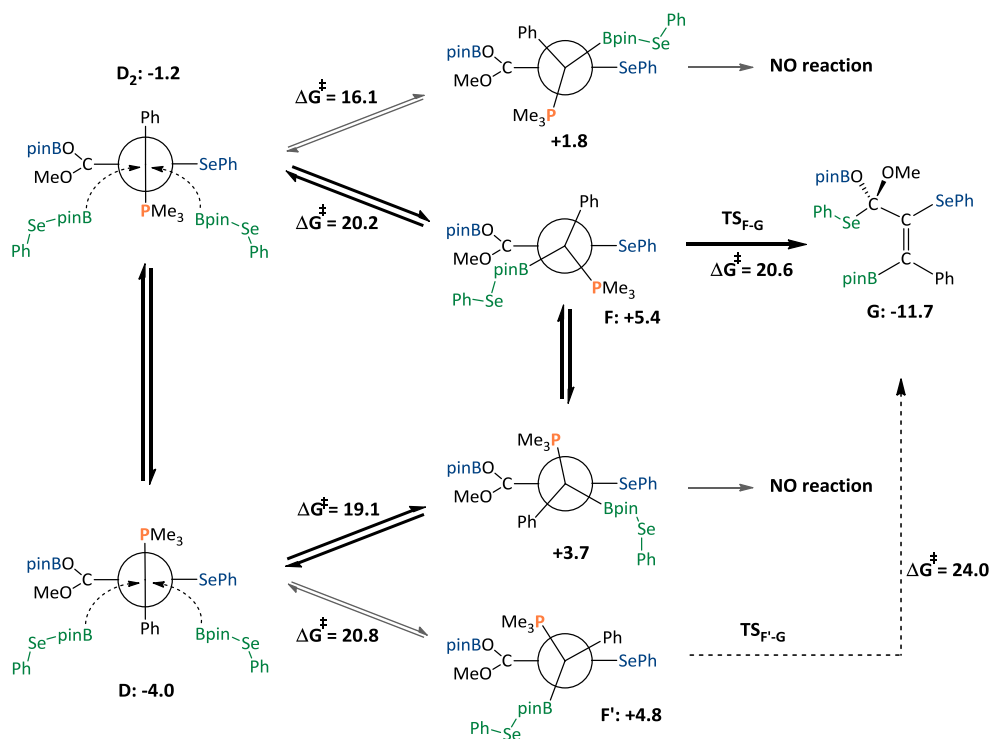


Figure 8.5. Schematic representation of the stereoselectivity-determining step yielding *anti* isomer. Relative free-energies and barriers in kcal·mol⁻¹.

The computed free-energy profile of the overall mechanism in Figure 8.4 indicates that the rate-determining process corresponds to the coordination of the second PhSe-Bpin molecule to the ylidic carbon and subsequent 1,3-migration of the selenyl moiety to the carboxylic carbon (**D** + PhSe-Bpin → **TS_{F-G}**) with an overall computed free energy barrier about 30 kcal·mol⁻¹. This value could be somewhat lower if we discount some amount of free energy corresponding to the overestimation of translational entropy in the associative process. Nowadays there is not a consensus of what correction apply but one of the simplest ones consists of modifying the default thermochemistry expressions from ideal gas standard state of 1 atm to condensate phase 1 mol·L⁻¹. This would yield a corrected free energy barrier of 28 kcal·mol⁻¹. In addition, the model phosphine employed for the computational calculations, PMe₃, is not as basic as the experimental species used, PCy₃. This modification could affect the key steps of the mechanism since the phosphine plays a dual role. First, it coordinates to the β-acetylenic carbon of the alkynoate inverting the polarity of the triple bond and directing the selenyl addition to the α-carbon of the alkyne. Second, it generates a nucleophilic ylide

which is able to coordinate a second PhSe–Bpin molecule through the Lewis acidic boron atom. Interestingly, the PhSe–Bpin acts as autocatalyst allowing the overall *anti* addition of selenyl and boryl units, and regenerating from the fragments of two different PhSe–Bpin species.

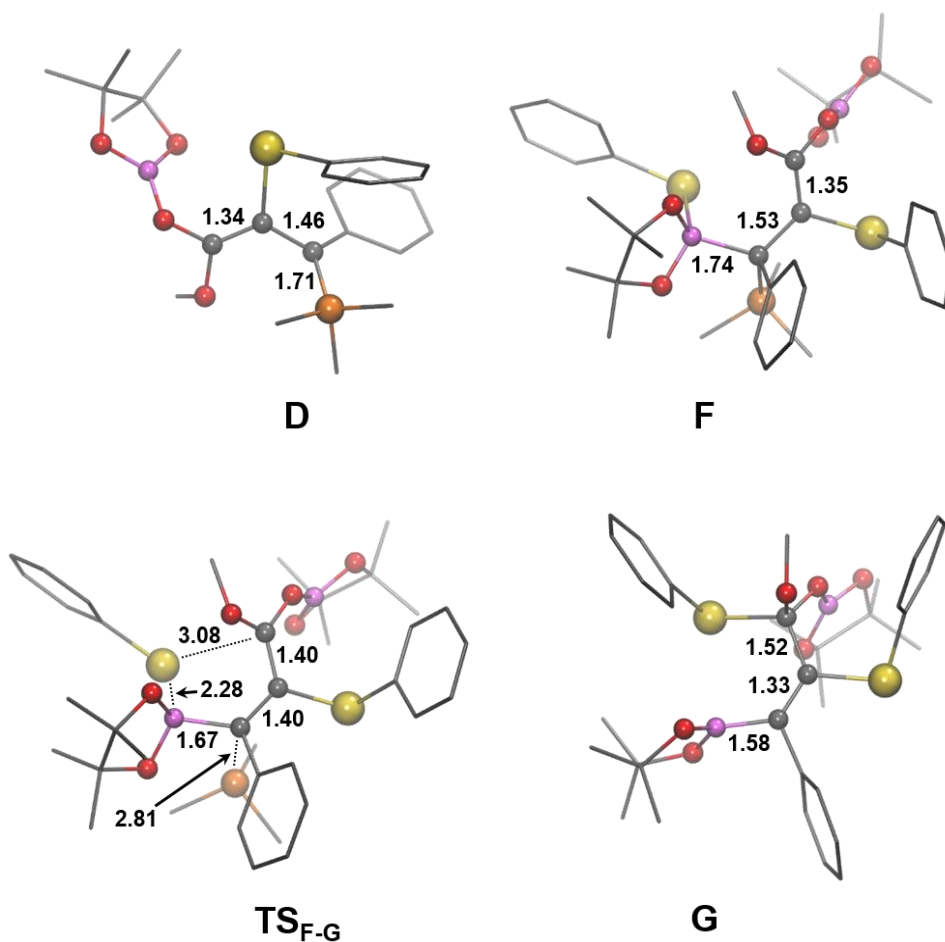


Figure 8.6. Molecular structures and main geometric parameters (Å) of the intermediates and transition states for the novel mechanism of *anti*-3,4-addition of PhSe–Bpin to α,β -acetylenic ester.

Experimentally, while the addition of PhSe–Bpin takes place at room temperature, the addition of B₂pin₂ and PhMe₂Si–Bpin requires up to 80°C. Thus, it would be interesting to rationalize the higher reactivity of selenoborane reagent and to relate this reactivity to its stereoelectronic properties. In the previous Chapter, we identified electronic and steric descriptors of trivalent boron compounds which can be qualitatively and quantitatively related to their nucleophilic reactivity.^[28,29] Similarly, here we compare those descriptors in activated B–interelement compounds using methoxy group as a model of Lewis base:

$\text{MeO}^- \rightarrow \text{Bpin}-\text{X}$ ($\text{X} = -\text{SePh}$, $-\text{Bpin}$ and $-\text{SiMe}_3$). Replacing the interelement fragment from Bpin and SiMe to SePh, its negative charge ($q[\text{X}]$), measured as the sum of all the natural bond order (NBO) atomic charges, increases significantly from 0.00 and -0.12 to -0.56 a.u. Likewise, the interelement p/s population ratio of atomic orbital in the B–X σ bond increases (from 2.1 and 1.1 for $\text{X} = -\text{SiPh}$ and $-\text{Bpin}$ to 5.3 for $\text{X} = -\text{SePh}$), which could indicate that the more p character the more reactive is the fragment as a nucleophile. On the other hand, we did not appreciate significant differences in the measure of the steric bulkiness of the molecular environment using the distance-weighted volume (V_w) parameter.^[30] Thus, both electronic descriptors, $q[\text{B}]$ and p/s , indicate that selenoborane activated *via* a “push-pull” effect has an enhanced nucleophilic character. This might favor key reaction steps such as the 1,3-migration of the selenyl moiety explaining why the reaction can take place at room temperature and discarding this mechanism for $-\text{SiPh}$ and $-\text{Bpin}$ fragments at the same time.

8.4. Computational details

Geometry optimizations and transition state searches were performed with Gaussian09 package.^[31] The quantum mechanics calculations were carried out within the framework of Density Functional Theory (DFT)^[32] by using the hybrid M06-2X functional^[33] and a standard 6-311G(d,p) basis set.^[34–36] Full geometry optimizations were performed without constraints. The nature of the stationary points encountered was characterized either as minima or transition states by means of harmonic vibrational frequency analysis. The zero-point, thermal, and entropy corrections were evaluated to compute Gibbs Free energies ($T=298$ K, $p=1$ bar). The selected method is analogous to that reported in ref. [25] and it allows a straightforward comparison of the results.

8.5. Conclusions

For the observed anti-3,4-selenoboration with delivery of α -vinyl selenides catalyzed by PCy_3 , computational studies discovered a novel mechanism (Scheme 8.7) which differs from previous mechanistic proposals for analogous anti-selective carboboration, silaboration and diboration (Scheme 8.6). The phosphine addition to the β position of the alkynoate modifies the regioselectivity favoring the 1,3-selenoboration and the production of α -selenated phosphorus-ylide intermediate. Then, the autocatalytic action of a second $\text{PhSe}-\text{Bpin}$ substrate determines the stereoselectivity and completes the anti-3,4-selenoboration

reaction. Thus, the ylidic carbon coordinates a second selenoborane molecule, which is activated *via* “push-pull” effect to produce the 1,3-migration of the selenyl moiety to electrophilic carboxylic carbon. The conformational arrangement of the reacting selenyl and carboxyl groups imposes the resulting anti-stereoselectivity of the boryl and the selenyl groups. Finally, the 1,2-elimination of PhSe–Bpin occurs at the carboxylic group to yield the final product and to regenerate PhSe–Bpin. The larger nucleophilic character of –SePh moiety compared to those in related B₂pin₂ and PhMe₂Si–Bpin species allows to perform the reaction under mild conditions.

8.6. References

- [1] A. B. Cuenca, R. Shishido, H. Ito, E. Fernandez, *Chem. Soc. Rev.* **2017**, *46*, 415–430.
- [2] H. Yoshida, *ACS Catal.* **2016**, *6*, 1799–1811.
- [3] W. J. Jang, W. L. Lee, J. H. Moon, J. Y. Lee, J. Yun, *Org. Lett.* **2016**, *18*, 1390–1393.
- [4] B. Sundararaju, A. Fürstner, *Angew. Chemie Int. Ed.* **2013**, *52*, 14050–14054.
- [5] T. Ohmura, Y. Yamamoto, N. Miyaura, *J. Am. Chem. Soc.* **2000**, *122*, 4990–4991.
- [6] C. Gunanathan, M. Hölscher, F. Pan, W. Leitner, *J. Am. Chem. Soc.* **2012**, *134*, 14349–14352.
- [7] J. Cid, J. J. Carbó, E. Fernández, *Chem. - A Eur. J.* **2012**, *18*, 1512–1521.
- [8] Y. Nagashima, K. Hirano, R. Takita, M. Uchiyama, *J. Am. Chem. Soc.* **2014**, *136*, 8532–8535.
- [9] M. Nogami, K. Hirano, M. Kanai, C. Wang, T. Saito, K. Miyamoto, A. Muranaka, M. Uchiyama, *J. Am. Chem. Soc.* **2017**, *139*, 12358–12361.
- [10] A. Verma, R. F. Snead, Y. Dai, C. Slebodnick, Y. Yang, H. Yu, F. Yao, W. L. Santos, *Angew. Chemie Int. Ed.* **2017**, *56*, 5111–5115.
- [11] K. Nagao, H. Ohmiya, M. Sawamura, *J. Am. Chem. Soc.* **2014**, *136*, 10605–10608.
- [12] K. Nagao, H. Ohmiya, M. Sawamura, *Org. Lett.* **2015**, *17*, 1304–1307.
- [13] G. Perin, E. J. Lenardão, R. G. Jacob, R. B. Panatieri, *Chem. Rev.* **2009**, *109*, 1277–1301.
- [14] P. H. Menezes, G. Zeni, in *PATAI'S Chem. Funct. Groups*, John Wiley & Sons, Ltd, **2009**.
- [15] M. Palomba, L. Bagnoli, F. Marini, C. Santi, L. Sancineto, *Phosphorus. Sulfur. Silicon Relat. Elem.* **2016**, *191*, 235–244.
- [16] S. Kawaguchi, M. Kotani, S. Atobe, A. Nomoto, M. Sonoda, A. Ogawa, *Organometallics* **2011**, *30*, 6766–6769.
- [17] B. Battistelli, T. Lorenzo, M. Tiecco, C. Santi, *European J. Org. Chem.* **2011**, *2011*, 1848–1851.
- [18] M. Renard, L. Hevesi, *Tetrahedron* **1985**, *41*, 5939–5954.
- [19] J. V. Comasseto, C. A. Brandt, *Synthesis (Stuttg.)*. **1987**, 146–149.

- [20] O. S. do Rego Barros, E. S. Lang, C. A. F. de Oliveira, C. Peppe, G. Zeni, *Tetrahedron Lett.* **2002**, *43*, 7921–7923.
- [21] G. Perin, R. G. Jacob, F. de Azambuja, G. V. Botteselle, G. M. Siqueira, R. A. Freitag, E. J. Lenardão, *Tetrahedron Lett.* **2005**, *46*, 1679–1682.
- [22] E. J. Lenardão, M. S. Silva, S. R. Mendes, F. De Azambuja, R. G. Jacob, P. C. S. Dos Santos, G. Perin, *J. Braz. Chem. Soc.* **2007**, *18*, 943–950.
- [23] S. A. Westcott, J. D. Webb, D. I. McIsaac, C. M. Vogels, *2006/089402 A1*, **2006**.
- [24] X. Sanz, C. M. Vogels, A. Decken, C. Bo, S. A. Westcott, E. Fernández, *Chem. Commun.* **2014**, *50*, 8420–8423.
- [25] M. G. Civit, X. Sanz, C. M. Vogels, C. Bo, S. A. Westcott, E. Fernández, *Adv. Synth. Catal.* **2015**, *357*, 3098–3103.
- [26] W. Torres Delgado, F. Shahin, M. J. Ferguson, R. McDonald, G. He, E. Rivard, *Organometallics* **2016**, *35*, 2140–2148.
- [27] L.-J. Song, T. Wang, X. Zhang, L. W. Chung, Y.-D. Wu, *ACS Catal.* **2017**, *7*, 1361–1368.
- [28] J. Cid, J. J. Carbó, E. Fernández, *Chem. - A Eur. J.* **2012**, *18*, 12794–12802.
- [29] D. García-López, J. Cid, R. Marqués, E. Fernández, J. J. Carbó, *Chem. - A Eur. J.* **2017**, *23*, 5066–5075.
- [30] M. Álvarez, D. García-López, J. J. Carbó,
<http://rodi.urv.es/~carbo/quadrants/index.html>.
- [31] M. J. Frisch, G. W. Trucks, H. B. Schlegel, G. E. Scuseria, M. A. Robb, J. R. Cheeseman, G. Scalmani, V. Barone, B. Mennucci, G. A. Petersson, H. Nakatsuji, M. Caricato, X. Li, H. P. Hratchian, A. F. Izmaylov, J. Bloino, G. Zheng, J. L. Sonnenberg, M. Hada, M. Ehara, K. Toyota, R. Fukuda, J. Hasegawa, M. Ishida, T. Nakajima, Y. Honda, O. Kitao, H. Nakai, T. Vreven, J. A. Montgomery, Jr., J. E. Peralta, F. Ogliaro, M. Bearpark, J. J. Heyd, E. Brothers, K. N. Kudin, V. N. Staroverov, R. Kobayashi, J. Normand, K. Raghavachari, A. Rendell, J. C. Burant, S. S. Iyengar, J. Tomasi, M. Cossi, N. Rega, J. M. Millam, M. Klene, J. E. Knox, J. B. Cross, V. Bakken, C. Adamo, J. Jaramillo, R. Gomperts, R. E. Stratmann, O. Yazyev, A. J. Austin, R. Cammi, C. Pomelli, J. W. Ochterski, R. L. Martin, K. Morokuma, V. G. Zakrzewski, G. A. Voth, P. Salvador, J. J. Dannenberg, S. Dapprich, A. D. Daniels, O. Farkas, J. B. Foresman, J. V. Ortiz, J. Cioslowski, D. J. Fox, *Gaussian 09, Revis. D.01, Gaussian, Inc., Wallingford CT* **2009**.
- [32] R. G. Parr, W. Yang, *Density-Functional Theory of Atoms and Molecules*, Oxford University Press, **1994**.
- [33] Y. Zhao, D. G. Truhlar, *Theor. Chem. Acc.* **2008**, *120*, 215–241.
- [34] M. M. Francl, W. J. Pietro, W. J. Hehre, J. S. Binkley, M. S. Gordon, D. J. DeFrees, J. A. Pople, *J. Chem. Phys.* **1982**, *77*, 3654–3665.
- [35] W. J. Hehre, R. Ditchfield, J. A. Pople, *J. Chem. Phys.* **1972**, *56*, 2257–2261.
- [36] P. C. Hariharan, J. A. Pople, *Theor. Chim. Acta* **1973**, *28*, 213–222.

Conclusions



"What's the opposite of 'Eureka!'?"

Illustration by Dana Fradon

*For afterwards a man finds pleasure in his pains,
when he has suffered long and wandered far.*

— Homer —

UNIVERSITAT ROVIRA I VIRGILI
COMPUTATIONAL MODELING TO EXPLORE UNCONVENTIONAL REACTIVITY PATTERNS IN C-H ACTIVATION
AND BORON CHEMISTRY
Diego García López

9. Conclusions

This chapter marks the finale of this thesis by summarizing the achievements and conclusions extracted from previous expositions. The combination of both experimental and computational approaches allowed for more specific and precise results. In particular, quantum modeling was supported by the experimental findings in all cases and supplied additional information. This may be seen as a further evidence of the impact achieved by a recently affordable discipline in order to provide deeper insights into chemical systems. Nevertheless, it would be desirable to benchmark computational predictions with experimental outcomes when possible in order to validate them. Therefore, these two areas of chemistry must keep on collaborating to explore uncharted territory.

The conclusions reached in each chapter of this work are condensed below:

- **Chapter 4:** Mechanistic insights in C–H activation involving dimetallic titanium species

By means of DFT calculations, existence of transient alkylidene species were proven to be responsible for the sequential C–H bonds activation observed in a series of dinuclear titanium complexes $\{[Ti(\eta^5-C_5Me_5)R_2]_2(\mu-O)\}$, $R = CH_2SiMe_3$, CH_2CMe_3 , and CH_2Ph) by the experimental group of Dr. Santamaría, at the University of Alcalá. The mechanistic proposal determined that the generation of such alkylidene intermediate occurred through α -H abstraction on the ligands attached to the same titanium atom, which is the determining step. Subsequent β - and γ -H abstractions take place between ligands of different metallic centers in a cooperative manner, allowing the selective activation of the distal C–H bonds. Computational results are in accordance with the experimental selectivity outcome and established a reactivity order for the different ligands involved in the reactivity: $CH_2SiMe_3 > CH_2CMe_3 > CH_2Ph$.

- **Chapter 5:** Unraveling the agostic interaction of arene $C(sp^2)$ -H at a nickel pincer complex

Topology analysis of the electron density was carried out in two $[NiBr(\kappa^3-P,N,(C-H)-L^H)]BF_4$ complexes, synthesized by the experimental group of Prof. van der Vlugt, at the University of Amsterdam, to elucidate a proposed $Ni-(C_{Ph}-H)$ agostic interaction. Employing geometrical, QTAIM and ELF parameters this bond interplay was demonstrated to be a *bona fide* albeit weak (an)agostic coordinative interaction, with predominant $Ni-(\eta^1-C_{Ph})$ character.

- **Chapter 6:** Tracing a nucleophilic map for trivalent boron compounds

A QSAR model was generated for predicting the nucleophilicity of trivalent boron compounds using a varied dataset that includes boryl moieties bonded to alkali and alkaline-earth metals,

to transition metals, and to sp^3 -hybridized boryl units. The optimal predictive model ($r^2 = 0.88$, $q^2 = 0.83$) was obtained by using the computed free-energy barrier (ΔG^\ddagger_{Nu}) as a response variable and three molecular descriptors, namely the p/s orbital population ratio (p/s), the charge of the boryl fragment ($q[B]$), and the steric bulk evaluated with the distance-weighted volume (V_w) parameter. This yielded a three-term easy-to-interpret QSAR equation that showed good predictive abilities establishing a direct connection between the nucleophilicity and the properties of bonded metal fragments.

The use of chemically meaningful descriptors provided insight into the factors governing the nucleophilicity. Thus, the metal fragments that most effectively promote nucleophilic activity are those that polarize the B–M bond to yield negatively charged boryl moieties. Moreover, reducing the steric bulk on the reaction center would favor substrate coordination and reactivity. This computational methodology was also used to make a priori predictions of experimentally untested compounds, evaluating externally the QSAR model. The predictions showed good precision for boryl fragments bonded to any of the metals used to build the QSAR equation, whereas the model had screening ability when the nature of the metal bonded to the boryl is outside the training dataset.

- **Chapter 7:** *Gem*-additions of unsymmetrical diboranes to ketones and aldehydes

The mechanism of transition-metal-free unsymmetrical 1,1-diboration of aldehydes and ketones by pinB–Bdan, observed by the experimental group of Dr. Fernández, at the Universitat Rovira i Virgili, was elucidated by DFT calculations to occur in a concerted, yet asynchronous manner. The distereoselectivity observed in *ortho*-substituted cyclohexanones was also predicted and interpreted with computational modeling, being the diboron reagent as the key factor for the combination of repulsive 1,3-diaxial and 1,2-*cis* interactions. Furthermore, the subsequent and selective deboration of the Bpin group achieved *via* protodeboration in the presence of bases was rationalized from a Frontier Molecular Orbital perspective, which showed that the Bdan moiety stabilize better the transient carbanion species.

- **Chapter 8:** Unraveling the mechanism of selenoborane *anti*-addition to alkynes

Computational studies performed on the *anti*-3,4-selenoboration with delivery of α -vinyl selenides catalyzed by PCy_3 , reported by the group of Dr. Fernández, at the Universitat Rovira i Virgili, discovered a novel mechanism which differs from previous mechanistic proposals for analogous *anti*-selective carboboration, silaboration and diboration. The phosphine addition to the β position of the alkynoate modifies the regioselectivity favoring the 1,3-selenoboration and the production of α -selenated phosphorus-ylide intermediate. Then, the autocatalytic action of a second PhSe–Bpin substrate determines the stereoselectivity and completes the *anti*-3,4-selenoboration reaction. Thus, the ylidic carbon coordinates a second selenoborane molecule, which is activated via push-pull effect to produce the 1,3-migration of the selenyl moiety to electrophilic carboxylic carbon. The conformational arrangement of

Conclusions

the reacting selenyl and carboxyl groups imposes the resulting anti-stereoselectivity of the boryl and the selenyl groups. Finally, the 1,2-elimination of PhSe–Bpin occurs at the carboxylic group to yield the final product and to regenerate PhSe–Bpin. The larger nucleophilic character of –SePh moiety compared to those in related B₂pin₂ and PhMe₂Si–Bpin species allows to perform the reaction under mild conditions.

Acknowledgements

To be honest the performance of this work has been a great delight and a big torture in equal proportions. All in all I don't regret a thing. I had the opportunity to learn a lot, to think in a pseudo-independent way and to meet a fair amount of admirable and charming people. This section is for them, because without their help and support this thesis would not have been possible. I will be switching between different languages depending on the person I am referring since that is how we speak to each other. Let's start:

En primer lloc, m'agradaria agrair el meu director de tesi, en Jordi, el fet de donar-me l'oportunitat de començar un doctorat ara ja farà uns anys. He après moltes coses de tu i crec que el balanç ha estat positiu. Una peça importantíssima d'aquest treball ha estat l'inestimable ajuda dels tècnics que tenim al departament, sense ells la lluita constant amb els ordinadors seria molt desnivellada (les màquines sempre guanyen si no les saps tractar com cal). Així doncs, el meu agraïment cap al Jose, l'Elisenda i el Moisés per fer-nos la vida més fàcil. També voldria mencionar a tots els membres de la unitat de química física de la facultat. L'ambient dins del departament sempre ha sigut excepcional, i amb aquest entorn de treball és molt senzill arribar cada dia a la universitat i continuar la teva baralla personal amb la recerca. Haguem coincidit en més o menys mesura, vull donar les gràcies a la Rosa, el Coen, el Toni, el Josep Maria, la Mar, l'Anna i el Xavi.

Torn ara pels companys de feina amb qui he tingut l'oportunitat de coincidir durant aquests anys. Començaré pels veterans que ja són doctors. Jess, la meva mentora del bor, espero haver estar a l'alçada com a alumne. Gràcies per tots els consells i per tots els "zascas" que em vas regalar, en certa manera crec que em van curtir l'esperit. Pablo A., fue un placer haberte conocido. Eres una persona formidable i te mereces todo lo bueno que te pase. Pedro, mi primer compañero de despacho, gracias por las charlas para desconectar que teníamos, fueron muy necesarias. Qué pena descubrir tan tarde que eres el discjockey de la Isla del Mojito... Marc M, el yanqui, ja saps què tinc ganes de fer amb tu, però ara que estàs muntat en el dòlar ho tindrem més difícil per estovar-nos. Espero que tot et vagi genial. Gian, el mero hecho de que te diera cobijo en mi casa ya era sinónimo de peligro. Cuánto lo disfrutaba... Núria, no se si he après a combinar colors però sí que valoro moltíssim les xerrades que hem tingut i tots els consells que m'has anat donant. Molta sort en la teva nova aventura, estic convençut de que ho petaràs perquè ets una gran investigadora. Pablo J., no creo que muchos echaran de menos tus chistes, pero créeme que a mi me gustaban. Ximo, veure la teva cara sempre en dóna bones sensacions. Crec que tenim un gust molt semblant per l'humor, per la qual cosa he gaudit molt amb tu quan rèiem, pel que fos, era igual el motiu. Zhongling, congratulations for your pregnancy, I'm sure that you will be a great mother, all the best. Magda, hem compartit moltes estones, la gran majoria amb una copa a la mà. No se si això diu molt o poc de nosaltres, però ho trobo a faltar. Sergi, has estat un amic incondicional, amic amb totes les lletres, en majúscules, subratllat i en negreta. És un veritable plaer poder seguir compartint moments amb tu i que siguem comptant l'un amb l'altre, espero que això no canviï mai. Laura, ja fa uns quants anys que ens coneixem, hem viscut moltes experiències plegats i només tinc paraules d'agraïment cap a tu. Des de

que vaig començar a fer el doctorat fins ara que la cosa ja s'acaba he pogut comptar amb la teva ajuda, sempre disposada i amb bona cara. Molta sort en tot allò que et proposis, però crec que no et cal la sort, vas preparada de sobres. No em voldria oblidar d'alguns dels meus companys de màster sense el quals el tràngol de cursar estudis en química teòrica i computacional hagués estat veritablement dolorós. Alberto y Sergi, gracias por hacer que el màster fuera más llevadero. Parece mentira que hayamos llegando donde estamos. Gràcies també als companys de la Universitat Autònoma, sobretot a la inestimable ajuda de l'Andrea. A tots els altres amb qui he tingut menys tracte personal durant el doctorat, Juan Carlos, Mariano i Pep, espero que tot us estigui anat bé

Ara torn pels actuals companys. Albert, també fa uns anys que ens coneixem i des del primer moment ja vaig veure que ets una gran persona. També he tingut el plaer de compartir moltes estones junts i xerrar amb tu del que sigui sempre és motiu per deixar de fer el que estàs fent en aquell moment. Roser, és una pena que no ens puguem acomiadar amb una festa. Sempre recordaré la passió pel menjar que compartim i les competicions per veure qui podia engolir més quantitat d'aliments. Jianfang, best of luck with your doctorate, I am sure that you will end your stay in Tarragona speaking Spanish, don't give up. .Yeamin, muchas felicidades por tu reciente paternidad, te deseo lo mejor para tu familia. Khalid, el mundo de los polioxometalatos está a salvo contigo, mucha suerte en todo lo que te propongas. Marc A., no crec que jo pogués estar investigant el que tu estàs fent mentre ho compagines amb la teva vida nocturna, tens molt de mèrit. Antonio, ha sido de gran ayuda desconectar contigo y compartir memes y chorradas varias, que no te cambie el humor. Almu, els teus sospirs i rialles s'escolten en la llunyania, però sempre preferiré escoltar les rialles. No t'estressis massa amb el doctorat, tot i que això és fàcil de dir. Toni, fa poc que has arribat però ja t'has fet part del grup. No deixis que et portin pel mal camí. No quiero olvidarme de la química orgánica infiltrada en el grupo. Irene, muchas gracias por todos los momentos que hemos pasado y recuerda que siempre estaré de pretemporada, por lo que pueda pasar.

Voldria mencionar també al grup de químics inorgànics liderats per l'Elena. He coincidit amb alguns curretants de laboratori i he pogut aprendre molt de la feina que fan. En especial l'Ana i la pròpia Elena, moltes gràcies per tot el que m'heu ensenyat, ha sigut un autèntic goig haver treballat amb vossaltres. El bor ha estat gran part de la meva tesi i he gaudit molt estudiant la seva versatilitat. No puc oblidar-me tampoc de les altres col·laboracions amb grups experimentals amb qui he compartit feina, a la Universidad de Alcalá i a la Universiteit van Amsterdam. Special thanks to the later ones, Linda and Jarl, whom I had the pleasure to work with in a challenging system, I feel really proud for our publication.

En el desenvolupament d'aquesta tesi també han intervingut persones no relacionades amb el món de la investigació de manera més directa o indirecta. Per tots aquells que ho han fet de manera més indirecta, gràcies per mostrar interès en el que estava fent i preocupar-vos de si estava content amb el que feia. Als que han intervingut de manera més directa donant-me constant suport i ànims, infinites gràcies. A mi canario favorito y compañero de piso durante la última época en Tarragona solo puedo estarle agradecido por las charlas diarias. Iker, gracias por escucharme, hacerme desconectar y sobretodo por hacerme reír. Compañeros de piso he tenido muchos, pero nadie como tú Ann. Eres una persona espectacular y he disfrutado mucho de tu compañía y nuestras charlas. Ich hoffe, eines

Tages mit Ihnen Deutsch zu sprechen (translation sponsored by Google Translator). Danke schön!
Menció especial per als de tota la vida, els que sempre estan allà pel que faci falta. Jan, Tomeu i Xavi, moltes gràcies per interessar-vos per la meva recerca i pel vostre suport. Hem crescut junts i hem viscut aventures plegats que no canvio per res d'aquest món. Sou els millors amics que un podria tenir. Per cert, en Xavi és el dissenyador de la portada d'aquesta tesi, si esteu interessats us puc passar el contacte.

Finalment els més importants, aquells a qui els ho dec tot. Claudia, no només ets admirable com a persona sinó com a treballadora incansable i perfeccionista consumada. Conèixer-nos ha estat de les millors coses que m'han pogut passar a la vida. Necessitaria escriure moltíssimes vegades la paraula "gràcies" per a poder expressar tot el que m'has donat durant aquest temps. Ets la millor companya de viatge que podria tenir. Por último, turno para mi familia. Me lo habéis dado todo, ahora y siempre. Vuestra ayuda y apoyo no solo han sido necesarios sino que han sido vitales. Gracias por haberme convertido en la persona que soy hoy y gracias por estar ahí en los buenos y en los malos momentos, os quiero.

Ja per acabar, només desitjo no haver-me deixat a ningú, tot i que és molt probable perquè tinc moltes persones a qui estar agraït. Aquells que se sentin al·ludits, no m'ho tingueu molt en compte, no esteu veient en quines condicions estic escrivint aquestes línies... En definitiva, moltes gràcies a tots els que heu fet que aquesta tesi hagi estat possible!

UNIVERSITAT ROVIRA I VIRGILI
COMPUTATIONAL MODELING TO EXPLORE UNCONVENTIONAL REACTIVITY PATTERNS IN C-H ACTIVATION
AND BORON CHEMISTRY
Diego García López

List of publications

Related with this thesis:

1. J. J. Carbó, D. García-López, M. Gómez-Pantoja, J. I. González-Pérez, A. Martín, M. Mena, C. Santamaría. Intermetallic Cooperation in C–H Activation Involving Transient Titanium-Alkylidene Species: A Synthetic and Mechanistic Study. *Organometallics* (2017), 36, 3076–3083.
2. D. García-López, J. Cid, R. Marqués, E. Fernández, J. J. Carbó. Quantitative Structure–Activity Relationships for the Nucleophilicity of Trivalent Boron Compounds. *Chem. - A Eur. J.* (2017), 23, 5066–5075.
3. L. S. Jongbloed, D. García-López, R. van Heck, M. A. Siegler, J. J. Carbó, J. I. van der Vlugt. Arene C(sp²)-H Metalation at Ni^{II} Modeled with a Reactive PONC_{Ph} Ligand. *Inorg. Chem.* (2016), 55, 8041–8047.
4. A. B. Cuenca, J. Cid, D. García-López, J. J. Carbó, E. Fernández. Unsymmetrical 1,1-diborated multisubstituted sp³-carbons formed *via* a metal-free concerted-asynchronous mechanism. *Org. Biomol. Chem.* (2015), 13, 9659–9664.
5. D. García-López, M. G. Civit, C. M. Vogels, S. A. Westcott, E. Fernández, J. J. Carbó. Understanding the mechanism of transition metal-free anti addition to alkynes: the selenoboration case. (submitted)
6. D. García-López, E. Fernández, J. J. Carbó. Tracing a nucleophilic map for the generation of organoboron compounds in a metal-free context. (in preparation)

Non-related with this thesis:

1. J. Soler, P. Saura, D. García-López, L. Masgrau, J. M. Lluch, À. González-Lafont. How Can Linoleic Acid Be the Preferential Substrate of the Enzyme 15-Lipoxygenase-1? A QM/MM Approach. *J. Phys. Chem. B* (2016), 120, 1950–1960.
2. J. J. Carbó, D. García-López, O. González-Del Moral, A. Martín, M. Mena, C. Santamaría. Carbon-Nitrogen Bond Construction and Carbon-Oxygen Double Bond Cleavage on a Molecular Titanium Oxonitride: A Combined Experimental and Computational Study. *Inorg. Chem.* (2015), 54, 9401–9412.
3. D. García-López, S. Aguado-Ullate, J. J. Carbó. A general stereochemical model to predict the outcome of asymmetric catalysis. (in preparation)

UNIVERSITAT ROVIRA I VIRGILI
COMPUTATIONAL MODELING TO EXPLORE UNCONVENTIONAL REACTIVITY PATTERNS IN C-H ACTIVATION
AND BORON CHEMISTRY
Diego García López

Collaborations



Universidad
de Alcalá



UNIVERSITEIT VAN AMSTERDAM



UNIVERSITAT
ROVIRA i VIRGILI

UNIVERSITAT ROVIRA I VIRGILI
COMPUTATIONAL MODELING TO EXPLORE UNCONVENTIONAL REACTIVITY PATTERNS IN C-H ACTIVATION
AND BORON CHEMISTRY
Diego García López

UNIVERSITAT ROVIRA I VIRGILI
COMPUTATIONAL MODELING TO EXPLORE UNCONVENTIONAL REACTIVITY PATTERNS IN C-H ACTIVATION
AND BORON CHEMISTRY
Diego Garcia López



UNIVERSITAT
ROVIRA i VIRGILI